HYDRODYNAMIC DELIVERY FOR THE STUDY, TREATMENT AND PREVENTION OF ACUTE KIDNEY INJURY

Peter R. Corridon

Submitted to the faculty of the University Graduate School
in partial fulfillment of the requirements
for the degree
Doctor of Philosophy
in the Program of Biomolecular Imaging and Biophysics
Indiana University

October 2013

Accepted by the Graduate Faculty, of Indiana University, in partial fulfillment of the requirements for the degree of Doctor of Philosophy.

Doctoral Committee

Simon J. Atkinson, Ph.D., Chair

Robert L. Bacallao, M.D.

David P. Basile, Ph.D.

Kenneth W. Dunn, Ph.D.

August 12, 2013

Vincent H. Gattone II, Ph.D.

DEDICATION

I dedicate this dissertation to Dr. Vincent H. Gattone II - a valued member of my dissertation committee. The time we spent working side by side on optimizing the hydrodynamic injection process led me to this critical point. Your mentorship, kind consideration and friendship will always be appreciated and remembered.

ACKNOWLEDGMENTS

I would like to thank my mentor Dr. Simon Atkinson for his earnest commitment to my academic and personal development. Since my first meeting with Dr. Atkinson prior to my move to Indianapolis, and until this day, he has been a monumental part of my life. His guidance and support will forever be appreciated and never forgotten.

I would like to the other members of my doctoral committee, Drs. Robert L. Bacallao, David P. Basile, Kenneth W. Dunn and Vincent H. Gattone II. Individually the each imprinted on me their unique approaches biological scientific investigations and afforded me invaluable amounts of time, advice and support throughout my at IUPUI on scientific matters and those that extended beyond the laboratory.

I would also like to thank the existing and past members of the Atkinson lab with whom I have interacted on a near daily basis for the past four years: Dr. Mark A. Hallett, Ms. Shijun Zhang and Dr. Hao Zhang. These individuals gave selflessly to my academic development as they directly aided my experimental work and provide crucial scientific critiques.

I would like to especially thank Dr. George J. Rhodes: you transformed an engineer into a surgeon with your tireless efforts to improve my technique and understanding of each surgical model we investigated, while being a valued friend and confident.

I would like to thank all the members of the Bacallao, Dagher, Molitoris and Sutton labs for the time each member took to assist my training and development in

biochemistry, animal surgeries and intravital microscopy.

I would like to thank Drs. Sherry Queener, Associate Dean of the IU Graduate School and Director, IUPUI Graduate Office; Dr. Kenneth B. Durgans, past Vice Chancellor for Diversity, IUPUI; Dr. Simon J. Rhodes, Dean, School of Science IUPUI; Ms. Monica Henry, Director of Graduate business Programs in Medicine, Kelly School of Business, IUPUI; Dr. Richard N. Day, Professor of Cellular & Integrative Physiology and Director of Biomolecular Imaging and Biophysics Program, IU School of Medicine; Dr. Joseph P. Bidwell, Professor of Anatomy & Cell Biology; Dr. Randy R. Brutkiewicz, Professor of Microbiology & Immunology and Associate Dean for Graduate Studies, Dr. Jonathan D. Tune, Associate Professor of Cellular & Integrative Physiology, and Adam Goodwin, Postdoctoral Fellow of Cellular & Integrative Physiology, for their interests and support in my advancement in research - your patience, advice and support will be cherished for the rest of my life.

Finally, I would like to thank all the members of my family and friends, in particular my deceased father; mother; wife; and daughter – your love, support and appreciation are without a doubt the major elements that have lead me to this point and will help me to succeed in the future.

ABSTRACT

Peter R. Corridon

HYDRODYNAMIC FLUID DELIVERY FOR THE STUDY, TREATMENT AND PREVENTION OF ACUTE KIDNEY INJURY

Advancements in human genomics have simultaneously enhanced our basic understanding of the human body and ability to combat debilitating diseases. Historically, research has shown that there have been many hindrances to realizing this medicinal revolution. One hindrance, with particular regard to the kidney, has been our inability to effectively and routinely delivery genes to various loci, without inducing significant injury. However, we have recently developed a method using hydrodynamic fluid delivery that has shown substantial promise in addressing aforesaid issues. We optimized our approach and designed a method that utilizes retrograde renal vein injections to facilitate widespread and persistent plasmid and adenoviral based transgene expression in rat kidneys. Exogenous gene expression extended throughout the cortex and medulla, lasting over 1 month within comparable expression profiles, in various renal cell types without considerably impacting normal organ function. As a proof of its utility we by attempted to prevent ischemic acute kidney injury (AKI), which is a leading cause of morbidity and mortality across among global populations, by altering the mitochondrial proteome. Specifically, our hydrodynamic delivery process facilitated an upregulated expression of mitochondrial enzymes that have been suggested to provide mediation from

renal ischemic injury. Remarkably, this protein upregulation significantly enhanced mitochondrial membrane potential activity, comparable to that observed from ischemic preconditioning, and provided protection against moderate ischemia-reperfusion injury, based on serum creatinine and histology analyses. Strikingly, we also determined that hydrodynamic delivery of isotonic fluid alone, given as long as 24 hours after AKI is induced, is similarly capable of blunting the extent of injury. Altogether, these results indicate the development of novel and exciting platform for the future study and management of renal injury.

Simon J. Atkinson, Ph.D., Chair

TABLE OF CONTENTS

List of Tables xvi
List of Figures xvii
I. Introduction 1
A. Acute kidney injury 1
1. The growing prevelance of renal injury 1
2. AKI: A significant clinical problem 2
3. Classification and pathogenesis of AKI 3
4. Present management of AKI 5
B. Genetic medicine: a novel alternative for the study and management of AKI 7
1. The promise of genetic medicine 7
2. Efforts to devise effective AKI gene monitoring and treatment strategies 9
a. Recombinant peptides and proteins 9
b. Cell transplantation 11
c. RNAi therapy 12
3. Mechanisms for exogenous transgene expression in mammalian cells 15
4. Key aspects to facilitate advancements in renal genetic medicine 17
a. The development of efficient renal gene delivery techniques 17
b. Exogenous transgene vectors 21
C. Multiphoton microscopy: a novel tool for renal genetic medicine 24
1. Biomedical applications of optical microscopy 24
2. Applications of multiphoton microscopy for monitoring renal gene expression 26
3. Fundamentals of intravital multiphoton fluorescence microscopy 27
a. Fluorescence excitation and emission 27
b. Lasers: practical ways to generate multiphoton excitation fluoresence 30
c. Image formation in multiphoton fluoresence microscopy 32
d. *In vivo*, *ex vivo* and *in vitro* multiphoton imaging of mammalian tissues 34
D. Hypothesis 37
II. Materials and Methods 41
A. Cell culture and live animals 41
1. Cell culture 41
a. Mouse kidney cell culture 41
b. MDCK cell culture 41

2. Live rats 41
3. Live pigs 42
B. Mild, acute and severe models of renal injury 42
1. Gentamicin toxicity 42
2. Ischemia-reperfusion injury 42
a. Bilateral clamp model 42
b. Contralateral nephrectomy and unilateral clamp model 43
c. Ischemic preconditioning 43
C. Serum creatinine measurements 43
D. Cell and tissue markers 44
1. Tolonium chloride 44
2. Fluorescent cell and tissue markers 44
3. X-ray/CT contrast agents 45
4. Plasmid vectors 45
5. Baculovirus vectors 46
6. Adenovirus vectors 46
E. Cell culture transfection and transduction protocols 46
1. Expression of a single transgene vector 46
2. Simultaneous expression of multiple transgene vectors 47
F. Exogenous fluid delivery to the kidneys of live animals 47
1. Jugular vein infusions in live rats 47
2. Tail vein injections in live rats 47
3. Renal capsule injections in live rats 48
4. Hydrodynamic infusions in live rats 48
a. Renal artery catheter-based injections 48
b. Renal artery fine-needle injections (without vascular cross-clamps) 48
c. Renal artery fine-needle injections (with vascular cross-clamps) 50
d. Retrograde renal vein catheter-based injections 50
e. Retrograde renal vein fine-needle injections (without vascular cross-clamps) 50
f. Retrograde renal vein fine-needle injections (with vascular cross-clamps) 51
5. Monitoring vital signs during renal vein hydrodynamic retrograde infusions in live rats 51
6. Critical parameters for retrograde renal vein hydrodynamic injections in live rats 53
7. Hydrodynamic delivery facilitates the endocytic uptake of virions in live rat kidneys 53
8. Hydrodynamic retrograde venous delivery in rats with ischemia-reperfusion injury 54
9. Hydrodynamic retrograde portal vein injections in live rats 54

10. Renal artery and vein infusions in live Ossabaw swine 54
a. Low rate arterial and retrograde venous infusions into the renal vein of Ossabaw swine 54
b. Hydrodynamic retrograde injection into the renal vein of Ossabaw swine 55
11. Monitoring vital signs during renal vein hydrodynamic retrograde infusions in live pigs 56
G. Cell and tissue imaging 57
1. Fluorescence microscopy 57
a. Confocal fluorescence imaging of live cells 57
b. Spectral analyses to identify transgene fluorescence 57
c. Intravital two-photon fluorescence microscopy 57
d. Two-photon imaging of freshly excised tissues 59
e. Texas- red phalloidin and GFP-actin colocalization to verify transgene expression 59
f. Estimations of transgene delivery efficiencies 59
i. *In vivo* renal transgene delivery efficiencies 59
ii. *In vitro* renal transgene delivery efficiencies 60
g. Functional and structural analyses using fluorescent albumin and dextrans following transgene delivery and fluorescent protein expression 60
h. Investigating the correlation between hydrodynamic injection parameters and reliable transgene expression 62
i. Investigating whether hydrodynamic forces facilitate the endocytic uptake of virions *in vivo* 62
j. Estimations of mitochondrial activity in live rat kidneys based on TMRM fluorescence intensities 63
2. Histology and renal injury assessment 63
3. Fluoroscopy/cinematography to monitor uptake of exogenous dyes in live pig kidneys 65
H. Western blot analysis 65
I. Statistical analysis 67
III. Results 68
Chapter 1. The design and characterization of various methods to facilitate and monitor transgene expression in the rat kidney 68
A. Fluorescent protein expression in cultured cells using plasmid, baculovirus and adenovirus vectors 68
B. Rat kidney tissue autoflouresence, structure and function examined with intravital two-photon fluorescence microscope 72
1. Rat kidneys investigated under normal physiological conditions 72
a. Tissue autofluoresence in normal rats visualized Using two-photon excitations wavelengths that range from 800 to 860 nm 72

b. Renal structure and function in normal rats 74
2. Rat kidneys investigated under nephrotoxic and ischemic conditions 74
a. Tissue autoflouresence, structure and function in the setting of gentamicin-induced nephrotoxicity 74
b. Tissue autoflouresence, structure and function in the setting of ischemia-reperfusion injury 78
C. Characterizations of various methods designed to deliver exogenous fluid to the kidney 81
1. Systemic fluid delivery to the kidney in normal rats via jugular and tail vein infusions 81
2. Localized fluid delivery of fluid to the kidneys of normal rats 81
a. Renal capsule infusions in live normal rat kidneys 81
b. Hydrodynamic fluid delivery in live normal rat kidneys 85
i. Catheter-based renal artery infusions 85
ii. Catheter-based renal vein infusions 85
iii. Fine-needle hydrodynamic renal artery injections of fluorescent dextrans with vascular clamps 88
iv. Fine-needle renal vein injections of fluorescent dextrans without and with vascular clamps 88
v. Fine-needle renal vein injections of toluidine blue dye without and with vascular clamps 96
D. Plasmid- and viral-mediated transgene expression in live rats 99
1. Tissue autofluoresence is unalterted by the fluid delivery process 99
2. Systemic transgene delivery did not facilitate renal transgene expression 99
3. Low levels of plasmid expression and significant levels of renalinjury generated from fine-needle renal artery hydrodynamic injections 101
4. Minimal plasmid expression generated from low volume (0.2 ml), fine-needle renal vein hydrodynamic injections conducted without vascular clamps 106
5. Large volume (0.5-1 ml) fine-needle renal vein retrograde hydrodynamic injections, conducted without vascular clamps, into the renal vein improved levels of viral transgene expression in live rats 106
6. Texas red-labeled phalloidin and fluorescent actin colocalization observed *in vitro* verify results obtained from live rats 112

7. Vascular cross-clamping significantly improved plasmid and adenoviral expression in various renal cell types with large volume (0.5 ml) fine-needle retrograde hydrodynamic renal vein delivery 113
8. Simultaneous expression of multiple transgene vectors generated by single hydrodynamic injections augmented with vascular cross-clamps 128
9. Hydrodynamic renal vein injections augmented with vascular cross-clamping can generate efficient levels of transgene expression in mammalian kidneys 130
E. Critical parameters and viable mechanisms to support effective hydrodynamic gene delivery in the rat kidneys 134
1. Rat Vital signs are unaffected by hydrodynamic renal vein injections 134
2. Hydrodynamic retrograde renal vein injections augmented with vascular clamps produces transient changes in renal venous pressure in live rats 134
3. Nephron structure and function appear normal after hydrodynamic delivery and transgene expression using plasmid and adenovirus vectors 136
4. Hydrodynamic delivery facilitates robust cellular internalization of low-, intermediate-, and high-molecular-weight exogenous macromolecules, which are comparable in size to transgenes vectors, throughout live kidneys 141
5. Serum creatinine levels are unaffected by fine-needle retrograde hydrodynamic renal vein fluid delivery and transgene expression 142
6. Renal histology confirm hydrodynamic-based adenovirus/plasmid delivery and expression do not adversely affect kidney structure 142
7. Hydrodynamic delivery facilitates the endocytic uptake of virions in live rat kidneys 143
8. Transgene expression restricted to kidneys that received retrograde hydrodynamic injections 148
Chapter 2. Hydrodynamic fluid delivery facilitates the live global monitoring of actin cytoskeleton alterations induced by ischemia-reperfusion injury 150
A. Plasmid-derived fluorescent actin transgene expression verified in normal rats 150
B. Actin cytoskeletal alterations visualized in live rats with ischemia-reperfusion injury 150

Chapter 3. Hydrodynamic fluid delivery facilitates reliable transgene expression in live rats with mild and intermediate ischemia-reperfusion injury 157
A. Retrograde hydrodynamic injections facilitate delivery large and low and molecular weight dextrans and toluidine in rats with renal ischemia-reperfusion injury 157
B. Efficient transgene in rats with renal ischemia-reperfusion injury 160
Chapter 4. Hydrodynamic isotonic fluid delivery ameliorates ischemia-reperfusion injury in live rats 170
Chapter 5. Hydrodynamically delivered mitochondrial proteins protect Sprague Dawley rat kidneys against moderate ischemia-reperfusion injury 173
A. Bilateral clamp injury model 173
B. Contralateral nephrectomy and unilateral clamp injury model 176
C. Enhanced mitochondrial activity observed in rats treated with IDH2 and SULT1C1 plasmids, and ischemic-preconditioning 176
Chapter 6. Hydrodynamic fluid delivery facilitates efficient exogenous macromolecule uptake in large animals 189
A. Fluid delivery into live normal Ossabaw swine kidneys 189
1. Low rate renal vein infusions are unable to facilitate the efficient delivery of exogenous macromolecules to Ossabaw swine kidneys 189
2. Low rate renal artery infusions facilitates off-target delivery of exogenous macromolecules in various organs of Ossabaw swine 189
B. Critical parameters and mechanisms to support effective renal transgene delivery in live pigs 191
1. Pig vital signs are unaffected by retrograde hydrodynamic renal vein injections 191
2. Hydrodynamic retrograde renal vein delivery facilitates the atypical internalization of macromolecules in live pigs 191
IV. Discussion 198
A. Summary 198
B. The effect of hydrodynamic delivery on exogenous macromolecule uptake in normal rats 200
C. The effect of hydrodynamic delivery on transgene expression in live normal rats 204
D. Cytoskeletal dysregulation monitored in live rats with ischemia-reperfusion injury 210
E. The effect of hydrodynamic delivery on transgene expression in rats with ischemia-reperfusion injury 210
F. The effect of hydrodynamic isotonic fluid delivery on ischemia-reperfusion injury 212

G. Hydrodynamic-based IDH2 or Sulfotransferase transgene expression enhances mitochondrial activity and blunts serum creatinine increases in rats with moderate IRI 214
H. Fast rate infusions are essential for fluid delivery to live pig kidneys 217
I. Hydrodynamic delivery also facilitates widespread proximal tubule epithelial cell internalization of exogenous macromolecules in live pigs 218
V. Conclusions 220
VI. Future Studies 223
VII. References 224
Curriculum Vitae

LIST OF TABLES

Table 1 23
Table 1 175

LIST OF FIGURES

Figure 1 49
Figure 2 52
Figure 3 61
Figure 4 69
Figure 5 70
Figure 6 71
Figure 7 73
Figure 8 75
Figure 9 76
Figure 10 79
Figure 11 82
Figure 12 83
Figure 13 84
Figure 14 86
Figure 15 87
Figure 16 89
Figure 17 90
Figure 18 92
Figure 19 93
Figure 20 94
Figure 21 95
Figure 22 97
Figure 23 98
Figure 24 100
Figure 25 102
Figure 26 103
Figure 27 104
Figure 28 105
Figure 29 107
Figure 30 108
Figure 31 109
Figure 32 111
Figure 33 114
Figure 34 116
Figure 35 118
Figure 36 119
Figure 37 121
Figure 38 122
Figure 39 123
Figure 40 125
Figure 41 127
Figure 42 129

Figure 43 131
Figure 44 132
Figure 45 133
Figure 46 135
Figure 47 137
Figure 48 138
Figure 49 139
Figure 50 140
Figure 51 144
Figure 52 145
Figure 53 146
Figure 54 149
Figure 55 151
Figure 56 152
Figure 57 153
Figure 58 154
Figure 59 155
Figure 60 158
Figure 61 161
Figure 62 163
Figure 63 164
Figure 64 166
Figure 65 168
Figure 66 171
Figure 67 174
Figure 68 177
Figure 69 178
Figure 70 179
Figure 71 181
Figure 72 182
Figure 73 183
Figure 74 184
Figure 75 185
Figure 76 186
Figure 77 187
Figure 78 190
Figure 79 192
Figure 80 193
Figure 81 195
Figure 82 196
Figure 83 197
Figure 84 207

I. INTRODUCTION

A. Acute kidney injury (AKI)

1. The growing prevelance of renal injury

It appears that we have advanced well beyond Byzantine medical practices of uromancy with respect to the ways we manage renal injury. However, our present day understanding of the kidney in various disease states is still quite limited. This has made it difficult to assist the growing global population in maintaining proper renal health. Thus renal dysfunction is now a common and progressive problem affecting millions[1].

Renal dysfunction can manifest in several forms, yet the most prevelant forms result from the following cases: (1) inherited and congential diseases; (2) nephrotoxicity that results from accumulated broad-spectrum antibiotics, chemotherapeutic drugs and radiocontrast agents; (3) ischemia; (4) major blood loss; (5) trauma; (6) high blood pressure; and (7) diabetes[2-10]. Additionally, the latter two sources of renal injury are poised to generate kidney disease at pandemic proportions.

For instance, in 2007 the National Institute of Diabetes and Digestive and Kidney Diseases of the National Institutes of Health declared that diabetes (types 1 and 2) accounts for virtually 44% of new cases of irreversible kidney injury, making it the most common cause of renal failure[11]. Even when a patient's diabetic syndrome is at a controlled level, it can still lead to chronic renal injury, which again may ultimately progress to renal failure. It is also envisioned that 40% of the existing type 2 diabetic

population will develop long-term renal injuries[12]. Thus, the present 240 million diabetic population worldwide, which is expcted to almost double within the coming 20 years[13], will remain a key demographic driving the need for enhanced renal interventions.

Comparably, the existing billion individuals across the globe that suffer from high blood pressure are anticipated to further drive these statistics to enormous levels by the year 2025, as another 0.5 billion are set to develop high blood pressure[13]. Overall, these incidences will further increase this population's risk of cardiovascular disease and ultimately enhance the total progression of renal insults.

2. AKI: A significant clinical problem

From a clinical persepctive, most forms of significant renal damage result in impaired nephron function[14]. Such damage can occur rapidly, with sudden blood loss and trauma, or steadily from toxin intake, diabetes or hypertension. These injuries are categorized by time-dependent reductions in renal clearance or glomerular filtration rate (GFR), and rises serum createnine (S_{Cr}) levels: (1) early stage injury: 25% decrease in GFR and an increase in S_{Cr} by a factor of 1.5; (2) acute kidney injury (AKI): 50% decrease in GFR and increase in S_{Cr} by a factor of either 2 or 3; (3) acute renal failure (ARF): 75% decrease in GFR and S_{Cr} greater than 4.0 mg/dl; (4) chronic kidney disease (CKD): persistent AKI and complete loss of kidney function for more than 4 weeks; and (5) end stage renal disease (ESRD) - loss of renal function for more than 3 months[2,15].

Serum creatinine clearance is at present the *gold standard* biomarker used to gauge renal function[16]. This method is derived from the fact that creatinine is a by

product of normal muscle metabolism and should be generated and excreted by the kidney at a relatively constant rate. However, with renal injury, nephron capacity is altered substantially to limit renal clearance. Such an event can eventually reduce the excretion of compounds like creatinine, thereby often decreasing urinary creatinine excretions[17], while increasing serum creatinine levels[16].

Among the abovementioned four injury categories, AKI is generally considered as a critical stage within the course of renal dysfunction. This is because renal dysfunction categorized to the point of AKI may be reversed, allowing a patient to either maintain or regain essential renal functiona, a patient's treatment options are limited to renal replacement therapy once the dysfunction progresses to either ARF[7] or ESRD[18].

AKI remains a significant clinical problem, as approximately 25% of ICU patients and 5-15% of all hospitalized patients are diagnosed with this injury[19]. Patients afflicted with this form of injury are likely to endure lengthy periods of hospitalization that accompany high costs[20]. These patients also encounter substantial risks of having their injury progress to renal insufficiency, and ultimately dying during their hospitalization[7], as mortality rates have ranged between 50 to 80% for the past several decades[20].

3. Classification and pathogenesis of AKI

AKI is historically regarded as a myriad of complex disorders[2,6,15]. This definition dates back to it's original classification used to describe injuries crush victims sustained during World War II[15]. These victims had renal injuries characterized by patchy tubular necrosis. This histological characterization paved the way for the clinical definition of

moderate forms of renal injury as acute tubular necrosis (ATN)[15]. However, today ATN, AKI and ARF are often used interchangably to define sudden losses in renal filtration function[21]. This interchangable usage may have orignated from the degradation in proximal tubular epithelial cell integrity that is common to each injury classification[7,22,23].

Classically, ATN is defined as the most common cause of AKI[23], while the ability for acute renal injury reversal give its distincton from ARF. There is much debate over a unified definition of AKI, due to low createnine specificities and sensitivities observed in injury settings and tretment regimes, as a delay generally preceeds rises in serum creatinine[24]. Clinical standards are based on RIFLE[2,25] and Acute Kidney Injury Network[26] criteria, which use serum and urine createnine to define dynfunction severity.

Other biomarkers have been proposed to aid clinicians in providing improved diagnoses[27-32]. For example, serum cystatin C and cytokines have been identified as possible enhanced biomarkers of AKI. Cystain C has desirable measurement characteristics, such as its ability to be freely filtered by the glomerulus, reasborbed and catabolized, but it is also secreted by the tubules[24]. It has also shown promise in its use as a non-invasive estimator of GFR in patients with normal and impaired renal function[24,33]. In similar studies, rapid and significant increases in levels of serum interlukens IL-6[34], IL-8[34] and IL-18[35] correlated with the developoment of AKI in patients that underwent cardiac surgery. These characteristics identify the possible role of cytokines as potential early indicators of AKI, perhaps may augment the diagnostic *gold standard* - 1.5 fold increases in serum createnine and oliguria extending beyond 6 hours[7].

The etiology of AKI can be subdivided into three main categories: prerenal, intrinsic and postrenal. First, prerenal AKI is generated from systemic reductions in renal flow that result from decreases in blood volume/pressure and heart failure, which frequently stem from microvascular alterations. These debilitating vascular modifications may be produced from either renal artery stenosis[36] or renal vein thrombosis[37]. Prerenal mechanisms are the most common causes of AKI[3]. Second, intrinsic AKI is produced by direct kidney damage that can occur during accidents and surgery. Third, postrenal AKI occurs as a consequence of uniary tract obstructions resulting from renal casts and tumors, as well as tumors and retroperitoneal fibrosis originating externally to kidney[38].

4. Present management of AKI

The management of AKI depends on the identification and treatment of its underlying causes. Current treatment regimens are mainly supportive and include fluid, electrolyte and acid-based balance[39]. These methods are employed to prevent/eliminate volume depletion, remove tubular blockages, weaken toxin concentrations, facilitate diuresis and reinstate normal GFR levels[40,41]. Such methods are widely employed to treat patients with prerenal AKI, but further studies are needed to determine exact fluid quantities and infusion endpoints for maximum interventional benefit[40].

Beyond fluid administration, diuretics[42], steroids[43] and inotropes[44] may be employed to indirectly regulate renal function by mainpulating cardiac output, and thus renal blood flow. These approaches are generally used to treat patients with intrinsic AKI[7]. Even though these forms of treatment are commonly utilized, they are closely

monitored, and retracted if necessary, as they can often generate hamful side effects that aid the progression of a patient's renal impairment[45]. Some of these harmful side-effects are metabolic acidosis, hyperkalemia and pulmonary edema. Subsequently, sodium bicarbonate, antihyperkalemia agents, and diurectics may be used in conjunction with these treatments in order to counteract the respective side effects[46].

It may be necessary to employ invasive techniques for post renal AKI cases. In such cases, physicans can first attempt to remove urinary blockages by exogenous fluid delivery or generate bypass channels, and reduce harmful elevated pressures. A bend of steriods, fluids and inotropes can then be used to improve or reinstate renal function[46].

In the event that all previosly mentioned attempts fail to improve renal function, a form of renal replacement therapy will generally be used as the last resort. For example, hemodialysis and peritoneal dialysis are forms of replacement therapy that can be utilized once a patient's sustained injury transitions to a chronic injury[47]. Between these two forms of treatment, peritoneal dialysis offers significant advantages in cost and administration[48]. However, it is less commonly used because of its likelihood to produce infections from the permanent insertion of an abdominal catheter[49]. Even though, such artificial renal systems are known to enhance and prolong patient life, the best long-term solution is renal transplantation if the dysfunction persists and escalates beyond an acute injury. Unfortunately, low organ availability[50-52]; stringent transplant requirements[53]; high rates of organ rejection[54]; and rare chances of reproducing AKI during renal replacement therapy[55], complicate this ultimate option and further limit positive patient prognoses.

B. Genetic medicine: a novel alternative for the study and management of AKI

1. The promise of genetic medicine

The scientific and technological advancements brought about by the Human Genome Project have provided us with a greater understanding of human biology. In particular, it has equipped us with a method to identify genetic variations that occur in the settings of various diseases. This fundamental ability to successfully define genotype-phenotype relationships has accelerated scientific development in the subspecialty field of medical genetics, through which physicians and scientists aim to revolutionize the existing state of human medicine.

Dating back to its emergence in the mid-20th century, scientists envisioned that genetic medicines could facilitate the wide scale implementation of individualized medical diagnostics and therapeutics[56]. Specifically, this new era in medicine was expected to provide innovative methods for the detection, treatment and prevention of incurable diseases; the regeneration of damaged and lost body parts; and the reduction of existing human health vulnerability thresholds. Owing to this, scientists worldwide are now focused on realizing this promise.

During the initial phases of the past century, researchers were focused on the design and development of treatments for disorders that result from single genetic aberrations, such as a mutation, truncation or deletion. The first successful study within this research campaign provided clinical evidence that genetic medicines may be used to treat patients with single genetic abnormalities, like adenosine deaminase (ADA)

deficiency. In that 1990 clinical study, a four year old patient with the aforesaid immunodeficiency received repeated doses of lymphocytes carrying the normal ADA genes that she lacked[57]. This treatment gave her defenseless immune system the ability to temporarily combat infections, and it was heralded as a medical breakthrough.

Thereafter, various efforts were launched to extend this treatment method to other monogenic disorders and a wider platform of ailments. Moreover, research was also directed to provide a fundamental understanding of the major global causes of morbidity and mortality, namely vascular disorders, infectious disease and cancers. Emphasis was given to study of renal injury, as it is closely linked with the previously listed ailments.

The increased interest in gene therapy applications produced pivotal clinical trials that explored ways to boost cellular immunity against cancers and viruses[58,59], and destroy cancer cells by transfecting them with suicide genes[60]. These studies uncovered the fact that most monogenic disorders and diseases with more complex genetic abnormalities may not be simply treated by the approach used to address ADA deficiency. Nevertheless, this identified key challenges related to gene delivery methods and vectors that must be addressed before the renal, as well as the overall medical community, may be able to transform the promise of tailored therapies into a reality[61].

Historically, another significant challenge that has halted interests in genetic medicine is the difficulty in reliably and routinely facilitating targeted gene transfer to various cells and tissues[62,63]. These obstacles hindered the progress of gene medicine until studies conducted during the period 2000 to 2002 spawned its resurgence[64,65]. Since

then several research efforts have been directed towards improving gene delivery methods and vectors in an organ-specific manner. This is because the intricate structures within organs, like the kidney, have traditionally provided distinct challenges to generating reliable renal gene delivery strategies[66,67]. Nevertheless, recent reports on gene therapy have outlined that this form of treatment may yet provide an alternative to existing, and mainly supportive AKI management strategies.

It has been suggested that renal gene therapy may be used to improve AKI patient prognoses, by enhancing transplantation outcomes[68-71], treating and possibly preventing underlying causes and results of AKI[22,72,73]. Continued and complimentary research to identify new key genetic targets, and better examine existing ones while improving gene delivery, will further enhance the utility of genetic medicine as we envision its promise.

2. Efforts to devise effective AKI gene monitoring and treatment strategies

a. Recombinant peptides and proteins

To date, numerous methods have been proposed to deliver exogenous genes to mammalian cells for the study and treatment of human disease[74]. With specific regard to the kidney, attempts have been made to protect and repair renal function using recombinant DNA strategies[75]. In one approach, recombinant growth factors were been used in experimental and clinical AKI settings to both preserve renal function and accelerate tissue repair. These studies have suggested that hepatocyte growth factor (HGF) may have a significant role in the management of AKI. HGF has been shown to have diverse functions in kidney repair following acute injury, as it can act as both a

renotropic and anti-fibrotic agent[76,77]. Parallel studies have shown that HGF may also be used to prevent cyclosporin-induced tubulointerstitial fibrosis, indicating its additional renoprotective capacity[77]. Similarly, other studies have shown that exogenous vascular endothelial growth factor (VEGF-121) was capable of preserving renal microvascular morphology and reducing secondary renal disease following AKI[78].

Further developments in genetic engineering have extended gene therapies to include purified protein products, plasmids and viruses encoding peptides/proteins. The therapeutic potential of recombinant interleukins (IL-18BP) was investigated in an established ischemia AKI rat model. An intravenous dose of IL-18BP was shown to improve renal function and tubule morphology, and reduce tubular necrosis and apoptosis[79]. Recombinant uteroglobin treatment also prevented glomerulonephritis by reducing proteinuria and pathogenic globulin-glomerular binding[80].

Using plasmids vectors, studies have confirmed the renotherapeutic potential of HGF as it mediated tissue regeneration and protected tubular epithelial cells from injury and apoptosis during ARF. These results were obtained using single intravenous injections of plasmids encoding HGF[76]. However, the following factors may limit the clinical benefit obtained from systemic-based therapies: 1) half-life of HGF is quite short; 2) recombinant HGF treatment requires very large doses; and 3) this form of therapy requires frequent injections of the recombinant protein[77,81]. Altogether, these factors outline a basis for the generation of adverse side effects that can result from administering supraphysiologic doses of costly recombinant proteins.

In contrast, vector-based gene transfer procedures can be simple, safe and potentially cost effective, as they require less frequent dosing[81]. Researchers have also utilized adenovirus vectors to deliver immunomodulating genes like interleukin-13[82] (a known potent anti-inflammatory agent) and 2,3-indoleamine dioxygenase[83] (a stimulator of regulatory T cell production) that improved renal transplant outcomes in models of acute rejection. These findings are significant, since both repair of ischemic and toxic renal injury are critically dependent on the regulation of a redundant, interactive network of cytokines and growth factors[79]. Thus, it would be valuable to devise a system that could modulate gene expression levels in an attempt to return kidney function to near normal baseline function[79], in a reliable fashion without inducing harmful viral-derived toxicity. However, viral vector use may ultimately be confined to experimental gene therapy applications unless we overcome obstacles that limit their widespread use[84,85].

b. Cell transplantation

Cell therapy is another form of genetic medicine that is being developed for the prevention and treatment of renal diseases. Original applications of cell transfer were geared towards bone marrow and organ transplantation[86,87], blood transfusion[88] and *in vitro* fertilization[89]. Emphasis was shifted to include research on ways to repair/replace damaged and lost compartments of organs. Such work has also targeted individual components of the nephron that have resisted traditional AKI management regimens[90].

This regenerative strategy relies on the transplantation of exogenous cells into the target organ. Cell therapy utilizes various cell types (stem/progenitor cells; mature

functional cells from humans/animals; genetically altered cells; and transdifferentiated cells) that are manipulated in tissue culture[90], and then implanted into patients[73]. This method is expected to spawn an industry distinct from pharma, biologics and devices[91].

An example of such a therapeutic strategy was presented in a study where mesenchymal stem cells (MSC) facilitated recovery from AKI. Repeated MSC treatments directly reduced the extent of renal fibrosis, and aided kidney tissue remodeling and regeneration in rats with AKI [92]. While, in another investigation, rats given intravenous infusions of relatively undifferentiated NRK52E cells, which were reprogrammed to generate sera amyloid A proteins, had accelerated renal recovery from gentamicin, cisplantin and ischemia-reperfusion derived acute injury[93]. Likewise, for the purposes of aiding existing AKI management standards, transformed mesothelial cells were used to repopulate peritonea denatured by dialysis-derived acute and chronic inflammation[94].

Beyond the clearly outlined potential that this form of therapy may provide, many ethical issues regarding biological and medical applications still thwart progress in the field. Nevertheless, it is apparent that the ability to culture human stem cells on an indefinite basis, while simultaneously governing their differentiation characteristics, offers great possibilities for the future of medicine[95].

c. RNAi therapy

Another option within the growing arsenal of applications being developed for genetic medicine is RNA interference (RNAi). The discovery of mammalian RNAi is possibly one of the most promising therapeutic strategies, because for the first time, it

enables the silencing of any gene[96]. This may be crucial for the development of clinical gene therapies, as research has shown that it may be easier to silence deficient and non-functional genes than replace them[97]. Moreover, RNAi is seen as the most practical approach, thus far, capable of ushering in the much anticipated era of genetic medicine by aiding the identification of complex genetic loci that are essential in human pathology.

RNAi is an endogenous process that provides cells the ability to regulate their genetic activity. Such a process remains central to gene expression and the defense against mutagenesis generated from viral genes and transposons[98]. Presently, main methods used for exogenous RNAi-based gene silencing utilize micro RNA (miRNA), small interfering RNA (siRNA), and small hairpin RNA (shRNA) technologies.

Since its discovery within the past ten years, there has been a growing interest in utlizing RNAi technology to improve the state of renal health[96]. This interest has directed RNAi-based renal research focused on development of the following strategies to improve the the study and management of AKI: 1) identification of miRNA targets and AKI biomarkers; 2) delivery of exogenous silencing mediators; 3) development of siRNA and shRNA targets to either reduce or protect against AKI; 4) determination of *in vivo* silencing efficiencies; and 5) investigation of other small RNAs that can affect post-transcriptional gene silencing[99].

From a diagnostic viewpoint, several research projects have provided insight on renal injury biomarkers. For instance, Valadi *et al*. showed that miRNAs recovered from urinary exosomes provide characteristic information about the kidney in normal and

injury settings[100]. Moreover, Zhou *et al.* showed levels of miR-27b and miR-192 in these urinary vesicles could be used to differentiate between glomerular and tubular damage[101].

Likewise, with regard to therapeutics, exosomes containing miRNAs can enter recipient cells upon their recognition by membrane surface proteins. This phenomenon offers a new mechanism for cell-to-cell communication, and possibly gene delivery[101]. For example, microvesicles derived from endothelial progenitor cells have been shown to protect the kidney from acute ischemic injury. Intravenously delivered microvesicles, enriched with pro-angiogenic miR-126 and miR-296, that localized to tubular and capillary cells, enhanced tubular cell proliferation, and reduced apoptosis and leukocyte infiltration[102].

To further outline the possible broad spectrum of RNAi applications, this technique is being considered as a viable way to combat AKI by reducing the uptake of nephrotoxins, amelioriating immunologic response mechanisms, and downregulating harmful disease mediators[22]. Results like these have prompted interest in the knockdown of dynamin-2 (Dyn2) and low-density lipoprotein-related protein 2 (LRP2). Dyn2, is a critical component of the endocytic pathway[103-105], and its knockdown has shown to block both clathrin-coat dependent endocytosis and coat-independent fluid phase probe uptake in a variety of epithelial cell lines[106]. Silencing LRP2 has also reduced gentamicin toxicity in proximal tubule epithelial cells[107]. LRP2 is a multiligan binding receptor that also functions to mediate endocytosis. As a result, examining these RNAi targets may provide a practical means to combat, and possibly inhibit nephrotoxicity *in vivo*.

In yet another study on renotherapeutic potential of siRNA technology, systemically delivered siRNAs provided supressed in ischemia-induced p53 upregulation, and overall attenuation of ischemic and cisplatin-induced AKI[22]. The oligonucleotides used to facilitate RNAi, contained stabilizing modifications that have a relatively low affinity for albumin and other plasma proteins. Such modifications diminished their hepatic distribution and degradation in sera, enabled their renal clearance and robust endocytic tubular uptake[108]. These results may potentially limit the class of therapeutic siRNAs that may be used in the procedure, based on the natural tendency of systemically delivered materials to accumulate within the liver.

Similarly, expression of transgenic shRNA targeting the proapoptotic BIM gene prevented the development of polycystic kidney disease in Bcl-2 deficient mice[109]. Yet, the death of a significant proportion of the transgenic animals in that study is a major source of concern. It is not clear whether this will turn out to be a general problem or one that is linked to the sequence of the particular shRNA. This issue of mortality limits the use of such transgenes in human studies. Alternatively, these transgenes could readily be given to livestock to produce specific viral and pathogen resistant animal strains[110].

3. Mechanisms for exogenous transgene expression in mammalian cells

Despite the many reports presented on the development of genetic medicine strategies, and their potential to improve AKI management regimens (based on the performance of recombinant peptides, DNA vectors, stem cells and RNAi agents), exact mechanisms related to each approach are still unclear[111]. This fact has made it difficult to

optimize designs for gene-based techniques. Nevertheless, the basic principles for successful transgene expression have been documented throughout scientific literature[112].

All gene therapies rely on the efficient delivery of exogenous genes to specific cellular targets. The techniques discussed earlier achieve this by using either DNA/RNA molecules or DNA/RNA molecules inserted in gene transport vehicles. Once the genetic materials enter the nuclei (specific transport mechanisms/vehicles, which facilitate transgene delivery to and across plasma and nuclear membranes, will be discussed in the subsequent section), they work to either enable or inhibit the expression of the gene product of interest in transformed cells and their progeny.

Similarly, the overall effectiveness of RNAi in inducing gene silencing in any cell depends on the ability of the dsRNA reagent to access the subcellular compartment containing the RNA-induced silencing complex (RISC) and other components of the RNAi machinery[113,114]. This subcelllular compartment is located in the perinuclear region of the cytoplasm[115]. However, with cell transplantation the gene delivery process relies primarily on the integration of the delivered cells, and native cellular division and cell-to-cell communication processes to facilitate sufficient levels of gene expression/inhibition. This is done after the exogenous cells integrate into tissues and organs[92-94,116].

Previous work conducted within our division suggests that the effectiveness of gene therapies, using adenovirus[117] and siRNA[22], depends on the dose and time these transgenes are administered. This reflects variations in drug concentrations at the respective sites of the gene expression and silencing machinery. It is therefore important

to understand how the effective concentration in the cytoplasm relates to the dose and timing of transgene administration as a function of therepautic potency. This is a topic of practical importance, as the mechanism will determine the intracellular fate of exogenous transgenes, from non-viral, viral and cellular sources, and aid the development of novel medical strategies that can control the duration and extent of induced genetic traits.

4. Key aspects to facilitate advancements in renal genetic medicine

a. The development of efficient renal gene delivery techniques

To date, numerous methods have been proposed to deliver exogenous genes to mammalian cells for the study and possible treatment of human diseases[67,74]. These techniques have aimed to provide inexpensive and rapid alternatives to pronuclear microinjection-derived transgenic models[118]. At present there is still need for reliable gene delivery systems, as several reports have indicated mixed views on the effectiveness of existing gene transfer techniques. Such variability has been clearly exemplified amongst reports on renal gene delivery[57,61,67,69-71,73,75,82,119-123].

Generally*, in vivo* gene transfer success is directly influenced by the following phenomena: 1) the ability to deliver vectors to the target cell; 2) the time taken for cells to express the delivered genes; 3) the number of cells that incorporate the exogenous genes; 4) the level of the resulting expression; 5) cellular turnover rates; 6) reproducibility of the process; and 7) the extent and severity of any injury that may result from the gene delivery process[67]. Thus, in order to overcome this delivery challenge, researchers must consider variations in organ morphology and function as crucial elements to potentially

provide efficient rates of transformation, while providing a solution to the problems of mistargeting, limited persistence and/or limited frequency of expression in the target cells.

Efficient gene transfer has been difficult to achieve routinely in the kidney[66,67]. The varied levels of successful transgene incorporation reported within the renal cortex and medulla have illustrated this difficulty[124,125]. The structure of various renal vascular beds and their permeability characteristics present intrinsic challenges to gene transfer processes. For example, proximal tubule epithelial cells have an immense capacity for the apical endocytic uptake of exogenous materials, and thus possible transgene incorporation[66,67,124-126]. Yet, accessibility of the apical domain to exogenously delivered vectors, and accordingly resulting degrees of transgene uptake, are strongly limited by glomerular permeability[66]. The degree to which such cells are accessible for gene transfer at basolateral surfaces, secondary to peritubular capillary leakage, is also unknown.

Independent investigators have such challenges as they observed diverse levels of renal gene expression using adenovirus. This virus was delivered by arterial injections in normal[124,127,128] and cystic rats[127]; pelvic catheter infusions in normal rats[127]; and tail vein[125] and cortical micropuncture[117] injections in uninjured animals.

One group showed intra-arterial injected adenovirions delivered to pre-chilled kidneys, produced transgene expression largely within cortical vasculature[127], whereas combining pre-chilling treatment with vasodilators, gene transfer was observed in both the inner and outer stripes of the outer medulla[127]. Expression in the cystic kidneys was only observed in vasculature, some epithelial cysts and interstitial cells[127].

Another group demonstrated the ability to successfully use adenovirus vectors to transduce rat glomerular endothelial cells by slowly infusing 1.5 ml of a vector solution into the right renal artery, using a 27-gauge needle, for a period of 15 minutes[128]. This technique provided high levels transgene expression, which lasted for at least 3 weeks, without causing significant damage.

To further complicate matters, within the same study, analogous concentrations of the same type of adenovirus vector were suspended in different volumes and delivered to the kidney via arterial injections and pelvic catheter infusions. These methods produced transgene expression in distinct regions of the kidney[124]. The expression generated from the 1 to 2 ml/min rate, 30-gauge needle injection of 2 ml solution into the aorta, at location proximal to the left renal artery, was limited to proximal tubular cells[124], whereas the PE-10 catheter-based retrograde delivery of 300 μl of adenovirus solutions, mediated selective tubular transduction in the medulla and papilla. Expression lasted for two to four weeks using either form of adenoviral delivery.

Comparably, studies using tail vein and retrograde ureteral adenovirus infusions, to target aquaporin water channels also reported varied levels of expression that appeared to be dependent upon the transgene infusion site[125]. This study found aquaporin 1 (AQP1) expression in apical and basolateral membranes of proximal tubule epithelial cells in the renal cortex, but no AQP1 expression was found in glomeruli, loop of Henle, or collecting duct from tail vein infusions of adenovirus vectors. Conversely, through ureteral infusions, significant ureteral and renal papilla transgene expression was

reported. Less intense and patchy expression was observed in cortical collecting ducts. These results indicate the varied nature of renal transgene uptake can be strongly influenced by anatomical obstacles.

Finally, others have explored direct transfer of adenovirus vectors carrying transgenes into individual nephron segments using micropuncture techniques[117]. The results of this study showed site-specific transgene expression within the injected tubules or vascular welling points. These results also demonstrated the utility of intravital fluorescent multiphoton microscopy as a means of directly monitoring protein expression in live animals. One limitation of the approach, however, is that gene expression is restricted to injection sites. Altogether, these studies illustrate that renal gene delivery depends on transgene infusion site, volume and rate, and highlighting the difficult nature of genetically altering multiple cell types, given the intricate anatomy of the kidney.

Clearly, intravenously transgene delivery would be beneficial. However, the effectiveness of this method has so far benefited RNAi, as endocytic uptake of siRNAs by the proximal tubule has shown significant promise. Thus a more direct delivery route may be necessary. This has again been illustarted by the results generated from ureteric introduction that yields expression that is limited to distal tubules and collecting ducts.

As one considers more direct and invasive delivery techniques, from a practical persective the simplest approach is subcapsular gene delivery. Subcapsular injections provide extended expression of a genes in a variety of vectors, albeit the gene expression is limited to the site of injection. This technique is beneficial for *in vivo* imaging studies,

but not for gene therapy. As a result, the majority of gene therapy strategies are thus far confined to laboratory settings as the field progresses[123].

In contrast, hydrodynamic fluid delivery has been proposed to address these challenges by increasing vascular permeability to efficiently deliver exogenous substances throughout the kidney. Specifically, hydrodynamic fluid delivery is aimed at impacting fluid pressures within thin, and stretchable capillaries[121]. The enhanced fluid flow generated from pressurized injections produce rapid and high fluctuations in the blood circulation. This is believed to increase the permeability of the capillary endothelium[121] and epithelial junctions[129] by generating transient pores in plasma membranes that facilitate the cellular internalization of macromolecules of interest[130]. The unique anatomy of the kidney provides various innate delivery paths (renal artery, renal vein, and ureter) that may be ideal for hydrodynamic gene delivery[122].

b. Exogenous transgene vectors

Generally, the gene of interest is infused either systemically or directly into the kidney (Table1). Apart from the artery, vein and ureter, direct infusions into the renal capsule and parenchyma using micro-needles[117] and blunt-tip needles[131] have also been proposed, in conjunction with tail vein[132-134] and peritoneum[22,135,136] infusions.

As indicated before, the success of these methods vary according to the anatomical location of the targeted cells[67], and the types of vectors used to enable genetic expression[67]. These vectors include: PRC-amplified DNA fragments[137]; plasmid DNA[122]; liposomes[67]; polycations[67]; viral vectors (adenovirus[117], baculovirus[138,139],

hemagglutinating virus of Japan (HVJ)[123] and lentivirus[119,140] and stem cells[92-94]. If transgene expression is mediated by using transformed cells as gene vectors, then these cells may be engineered with a variety of anchoring or binding proteins/peptides to assist their integration into the tissue of interest[141]. This process is done to mimic adenovirus[142] and lentivirus[143] endogenous capsid components, which mediate receptor binding and their successful entry into mammalian cells. Alternatively, as is observed only in injured kidneys, there appears to be a process initiated during renal repair that facilitates the incorporation of exogenous renal cells delivered intravenously[93].

Beyond achieving successful genetic modifications, the effects resulting from exogenous transgene delivery and expression need also be considered. Such considerations relate to the levels of cellular toxicity and injury that may result during and after the transfer process. In particular, DNA fragments are aptly degraded by endo- and exonuclueases[137]. However, an overload of exogenous DNA fragmentation may stimulate Ca^{2+} endoclunease activity that may also degrade endogenous DNA, and mediate cell death[144]. Similarly, plasmid DNA, prepared from bacteria, may induce unmethylated CpG motif toxicity that can trigger lower respiratory tract inflammatory responses[67,145]. Oligonucleotides, at doses greater than 10 mg/kg, also stimulate immune system responses, and may induce hepatotoxicity and nephrotoxicity[67].

Virus-induced toxic and immunogenic responses resulting from high titers, protein overexpression and capsid protein infections are also topics of major concern[146]. Mutagenesis derived over a long-term may also be an issue using recombinant

Infusion Site & Method	Gene Expression	Impact
Tail vein Low rate[134,147,148,149,150] and hydrodynamic injections[148,151-157] of plasmid and viral vectors	Low rate injections only produce expression (high levels) in hepatocytes' Hydrodynamic-based plasmid lung, spleen, heart, kidney and liver gene expression; Highest level of expression in liver-specific transfection (~ 40% of the cells in the liver) that persisted for at least 12 weeks	No injury from histology; Transient impact on cardiac function; structural changes in sinusoid/hepatocyte Endothelia with large volume hydrodynamic injections
Renal capsule blunt injections[158-161] or micropuncture[117,157]	Expression was seen in some tubular cells in the adult kidney using plasmids and retrovirus vectors; robust and stable superficial (within 100 μm of the kidney's surface) adenovirus expression; transgenes directly introduced into the lumens of single proximal tubules and vascular welling points of renal cortices	The cells can differentiate into renal tubules when injected under the capsule of an uninjured kidney or intra-arterially after renal ischemia-reperfusion injury; micropuncture-derived expression persisted over a period of two weeks
Renal artery[162, 159,160], pelvis[62,162], vein or ureter[163] injections	Transient transduction of tubules using plasmids; no expression in glomerular, vascular or interstitial compartments; Gene delivery into the renal glomerulus by transfer of genetically engineered cells; expression exclusively in the interstitial fibroblasts near the PTCs of the kidney and collecting ducts; expression limited to collecting ducts with ureteral delivery	Varied review of renal injury/gene expression reported from localized/direct injections to the kidney[63,164-168]

Table 1. An overview of renal gene delivery methods, associated transgene vectors and reported expression.
A review of renal gene delivery method, which highlight the challenge in generating reliable renal transgene expression with minimized injury.

adenovirus[169]. Slow transforming insertional mutagenesis may also arise with retroviruses that incorporate into the genome leading to tumorgenesis[170]. *In vivo* stem cell quiescence can also tamper with DNA repair mechanisms and generate mutagenesis [171].

In sum, there are several challenges to renal transgene delivery. The techniques presented have provided varied levels of success and are capable of inducing harmful side effects. Therefore, there is critical need for the development of safe and efficient transgene delivery options. Such techniques would assist the delivery of clinically relevant genes that can induce transient genetic modifications with minimal physiological interference or damage, and help realize the promise of gene therepy.

C. Multiphoton microscopy: a novel tool for renal genetic medicine

1. Biomedical applications of optical microscopy

Within the last two decades, microscopy has revolutionized our understanding of living systems by providing insight into the dynamics of biological regulatory processes[172]. Amongst all forms of microscopy, optical microscopy has shown substantial value in the study of biological processes. When used in the acquisition of anatomical, physiological, metabolic, and functional data from the living organisms, optical imaging modalities have found widespread utility in the field of biomedicine[173]. Ideally non-invasive or minimally invasive optical microscopy provides high lateral spatial resolution, three-dimensional volume sectioning, and high image contrast[174]. These facts make this system well-suited for studies at tissue, cellular, and molecular levels[173].

The field of optical microscopy can be partitioned into linear and non-linear applications. Traditionally, the most prominent linear microscopy systems include confocal fluorescence and wide-field laser microscopy[174]. Both of these linear approaches are popular choices for cell culture and tissue sections studies. The spatial resolution of these techniques is confined to a useful range of 100 μm from the specimen surface, due to multiple light scattering events blur the image at greater depths, limiting its *in vivo* and thus possible clinical utility[175]. This is a particular problem in confocal microscopy, since the intense degree of light scattering observed in turbid biological media significantly decreases the amount of light that enters the pinhole of the microscope. This in turn results in strong signal attenuations that are highly susceptible to the effects of scattering, which increase with greater tissue depths[176].

By comparison, non-linear microscopy has provided a significant advance in overcoming the barriers to deep-tissue imaging[177]. These methods use higher-order light-matter interactions with multiple photons to generate image-based contrasts. The most widely used application of this principle is in fluorescence excitation by two-photon absorption[177,178]. Two-photon excitation depends on the simultaneous absorption of two-photons to produce fluorescence emissions that vary with the square of the excitation intensity. Consequently, this process is defined by a non-linear (quadratic) relationship between excitation and emission events. This in turn facilitates investigations in tissues at depths that are on the order of a millimeter. These imaging depths significantly exceed those of conventional one photon processes like confocal microscopy.

With enhanced tissue depth penetration comes welcomed benefits that support the use of multiphoton imaging over other light-based microscopy systems for live biological tissue imaging. Such benefits inculude: (1) minimized out-of-focus photobleaching; (2) reduced scattering of infrared-derived excitations; (3) reduced background fluorescence from localized excitations. For these reasons, multiphoton fluorescence microscopy has found widespread application in the intravital imaging of diverse organs, such as the brain, liver, kidney and skin[179,180]. Examples of these applications include analyzing normal renal physiology[176,179,181] and renal pathophysiology[182], rapid diagnosis and quantification of AKI[183], biodistribution and effects of various compounds for drug development[184,185] and monitoring renal genetic alterations.

2. Applications multiphoton microscopy for monitoring renal gene expression

Several methods have been developeed for the study and evaluation of genetic medicine strategies. However, traditional gene transfer and expression assessment methods are known to have limited clinical value[186]. Accordingly, there is ample need to develop gene strategies that could be repeatedly and safely performed in patients[186].

Advancements in pulsed laser systems, image reconstruction software and fluorescent reporters, are making non-linear imaging techniques an increasingly important tool in the field of genetic medicine. These molecular imaging techniques have been successfully used in animal models, but their sensitivity and reproducibility need to be tested and validated in human studies[186,187]. As an example, investigators have utilized

intravital two-photon imaging systems to study genetic alterations that impact renal mammalian cellular structure and function[22,68,117,180].

Using micropuncture injection techniques, studies by Tanner et al. yielded robust and stable superficial (within 100 μm of the kidney's surface) transgene expression from fluorescently tagged chimeric constructs[117]. These transgenes were directly introduced into the lumens of single proximal tubules and vascular welling points of renal cortices, and monitored for a period of two weeks[117,180]. Likewise, multiphoton imaging has been used to track the delivery and localization of genetically altered cells[93] and siRNAs[22] that were used to promote renal recovery following AKI. Such research outlines the importance of non-linear microscopy in the study and development of renal gene therap.

3. Fundamentals of intravital multiphoton fluorescence microscopy

a. Fluorescence excitation and emission

The fundamentals of biological fluorescence date back to the observations presented by Spanish physician and botanist Nicolas Bautista Monardes in 1565[188]. In Monardes' report, he described the visible hues that eminated from different types of wood. As simple as this report may seem, these observations became quite useful as it allowed individuals to distinguish a prized type of wood from its counterfeits. Specifically, coatli, which was then a scarce and costly material known for its diuretic properties, was differentiated from counterfeits by its ability to emit clear blue hues when immersed in water[189]. Such work paved the way for our present technological advances that have spawned from harnessing various forms of emitted visible light.

Two major phenomona that revolve around the emission of visible light are incandesence and photoluminesence. Incandescence is a thermal radiative process in which electromagnetic radiation is generated from thermal motion of charged particles in substances. The electromagnetic radiation generated from incandescence is in the form of visible light, and is emitted in a direct response to heat. This heat provides electronic or charged particles with increased kinetic energy. Charged particles in motion create facilitate radiation emission during such an energy/heat transfer process.

In contrast to incandescence, photoluminesence is used to describe the emission of light that also arises from electronic state transitions, but is independent of heat. This form of *cold light* was the object of an interesting controversy in the 19th century, as scientists argued whether photoluminescence could fit within the field of thermodynamics[189]. Since then, several aspects of this phenomenon have been defined and used daily, which include resonant radiation, phosphorescence and fluorescence.

Resonant radiation is simply the rapid emission of electromagnetic energy produced from the absorption of photons by atoms of gases or vapors. Generally, the incident photon has the same frequency as the resonance frequency (or natural oscillating frequency) of the atoms of the vapor. When these atoms absorb the incident photons, they can transition from lower to higher energy levels. As the atoms transition back to their original state, the will emit photons with energy levels equivalent to those of the incident photons. Thus, there are no significant internal energy transitions or losses occurring between the absorption and emission processes. These discrete energy separations are

characteristic of the atoms involved, and can be used provide an atom with its own signature or unique energy transition marker.

Unlike that of resonance radiation, photons emitted during phosphorescence fluoresence have lower energy levels that the incident photons that induce their excitation. Furthermore, phosphorescence-based radiation emissions also occur on a longer timescale than that of fluorescence. This slower rate process allows phosphorescencent materials to discharge radiaton well after excitations end.

Particularly, the excitation of a fluorophore (or of a luminophore) can occur through either single or multiphoton absorption events. Building on the previously mentioned description provided on resonant radiation, we can first begin to further examine one-photon or conventional fluorescence. In this process, a single photon is absorbed by a fluorophore. Atoms of the fluorophore contain electrons that occupy different electronic states. Each state provides its electrons with a specific energy level, and thus a frequency that defines its perpetual motion. Motion can be in the form of vibrations, rotations or translations, depending on fluorescing compound's physical state.

After a fluorophore absorbs a photon, an electron within a low energy level or ground electronic state can become excited and transition to a state with a higher energy level. Such a fluorophore will collide with surrounding molecules and lose energy until its excited electrons return to their original lower level electronic states in a three-phase process. In the first phase of this process, the fluorophore will utilize some of this absorbed energy for vibrational and rotational motion, and internal conversions through

either radiative decay or radiationless de-excitation process that usually generates heat. Thereafter, the second phase of energy loss or conversion generates a photon. Such a photon, will have less energy (longer wavelength) than the incident photon, as described by the Stokes shift. Finally, during the last phase of energy loss, there is another internal conversion process that occurs within the lower energy states.

In contrast, for multiphoton microscopy, fluorescence is derived from the simultaneous absorption of two or more *low-energy* photons. The energy of each of these photons is insufficient to excite an electron, but when combined is sufficient to faclitate electron excitation/emission. Subsequently, as with single photon fluorescence, de-excitation proceses produce photon emissions and two non-radiative events. These phenomena have been previously well defined in the literature[179].

b. Lasers: practical ways to generate multiphoton excitation fluoresence

In order to generate a multiphoton excitation event, the required photons must be absorbed by the flurorphore within a single attosecond. This constraint drastically minimizes the probability of naturally occuring multiphoton phonemona. In practical terms, a molecule of rhodamine, if exposed to direct sunlight, would experience single photon excitations every second and two photon excitation ever 10 million years[178,179].

Revolutionary work theorized by Marie Groppert-Mayer in 1931, predicted that detectable multiphoton fluorescence could be generated from an enormous incident radiation flux[178,179,190]. This theory laid the foundation for the development of powerful

femtosecond infrared lasers capable of generating energy fluxes needed for multiphoton absorptions. Currently, commercially aviable laser systems, like titanium:sapphire lasers, provide average vast peak photon fluxes that facilitate two-photon excitation.

In practice, the femtosecond pulse durations of these infrared lasers effectively limit incident photon fluxes, from enormous levels of radiation, to those merely capable of raising the temperature of water by 0.2 K/sec[179]. Moreover, these low energy (long wavelegth) photon fluxes are confined within a single volume at a given instant, limiting the exposure and phototoxic effects. This also reduces the effect of scattering and background noise that limit depth penetration and image resolution respectively. These properties support claims that the unique engineering of multiphoton pulsed excitation systems can be both safe and effective for live biological studies. Advancements in pulsed laser technology have also opened the way for three photon fluoresence excitation microscopy. The photon density required for this process is approximately 10 fold that of two-photon microscopy, making this a potentially practical system[191].

By comparison, single-photon excitation is usually generated by exposing tissues to greater levels of higher energy, shorter wavelength visible and ultraviolet radiation, using lasers that cases excite fluorophores throughout substantially larger volumes. This in turn provides single-photon excitation systems with an enhanced capability to generate substantial tissue damage and succumbing to the effects of light scattering in biological media to greater extents than multiphoton excitation systems.

c. Image formation in multiphoton fluorescence microscopy

Once successful multiphoton excitation events are generated, the next step would be to gather photon emissions and convert them into electrical signals. Practical applications of this are presented in various microscopy image acquisition and analysis reports, and he fundamentals of this process have been documented extensively[192]. Thus, for the purposes of this dissertation, the general concept is outlined below.

The major components of a multiphoton fluoresence microscope that enable image formation are the objectives, mirrors and detectors. These components are utilized in the following manner: when incident infrared light is emitted from the pulsed (mode-locked) femtosecond laser, a scanning mirror guides the light towards an objective lens. This lens then focuses the light at a single position within the specimen volume to generate multiphoton excitation and emission events. Emitted fluorescence photons are *in focus* and take either scattered or ballistic trajectories. A greater portion of the emitted light is allowed to reach its designated target, allowing two-photon microscopy to make much better use of the photons generated by dramatically improving signal-to-noise ratio compared with standard confocal microscopy. Objective lens and mode-locking lasers spatially and temporally concentrate emitted photons respectively, to generate the required photon flux for excitation. The low pulse duty cycles limit the average input power to blow 10 mW, which is on the order of powers generated by confocal excitation, despite of the high photon intensities generated by these lasers.

In comparison to confocal fluorescence microspcy, a pinhole is not required for two photon microscopy, allowing greater flexibilty in detection geometry by utilizing descanned and non-descanned dection schemes. For confocal microspcy, emission photons travel the same pathway as excitation photons, as they collide with scanning mirros before they pass through the pin-hole to the detector with descanned geometry. However, for non-descanned systems a dichroic mirror can be placed immediately after the objective lens to direct emitted light to external dectetors without using an objective lens. This non-descanned option allows one to take full advantage of the depth penetration potential of this technique; enables collection of more scattered photons, requires fewer optical elements, such as mirrors and lenses; and reduces the path length, along which dust particles in the air interfere with the fluorescence signal. Consequently, non-descanned detection approaches for two-photon excitation dramatically increases collection efficiency and is essential for maximal depth penetration into living tissue, as the detectors contain highly sensitive photomultiplier tubes capable of detecting low levels of light, and barrier filters that are used to generate red, green and blue pseudo-color images. This process enhances sensitivity without compromising image quality.

In the final generated image, each image point is geometrically related to a corresponding point in the specimen. Additionally, the photons emitted from the specimen originate from the focal point provides a three-dimension (3-D) sectioning characteristic. As the scanning mirror changes its position in the xy-plane, a raster scan process can be used to gather information at various loci within the xy-plane at the same

depth to form a planar image. Beyond the formation of a planar image, one can vary the position of the z-plane or depth within the specimen to acquire 3-D volume data. If this data collection process occurs across a period of time, the data set can be extended to provide timescale or 4-D information.

At present, the fundamental components of multiphoton systems, objectives, mirrors and detectors, are not optimized for biological applications[193]. However, it is hoped that increased demand for this technique could perhaps enhance the development of optimized imaging components for the study of biological specimens.

d. In vivo, ex vivo and in vitro multiphoton imaging of mammalian tissues

In order to answer questions that would aid our understanding of living organisms, scientists have relied on *in vitro, ex vivo* and *in vivo* experimental designs. Historically, such work has facilitated scientific advancements.

For instance, *in vitro* studies allow us to investigate interactions between individual molecules and living cells. This is vital first step that can help us evaluate basic interactions and specific molecular events without having to account for the cascades of intracellular, intercellular, intra-organ and inter-organ events that occur within living organisms. *In vitro* studies also eliminate the need for substantial financial and surgical resources that are needed to conduct *in vivo* studies. Thereafter the simplified experimental model can be scaled accordingly to examine the effects that various compounds may have on the living cells, as well as the effects from potentially

complex molecular interactions. This form of experimentation can also assist the study of various phenomena that may not be approved for animal usage by regulatory boards.

However, in certain cases *in vitro* experimentation has defined either partial or incompatible descriptions of the biological processes[194]. Precisely, *in vitro* models may be unable to account for the aforementioned complex network of cellular interactions that occur *in vivo*. Overall, if this form of experimental design is solely relied upon, we can ultimately generate inaccurate theories on biomedical phenomena. As a result, the utilization of both forms of analyses provides an enhanced arsenal for complementary biological research efforts.

It is from such a perspective that intravital investigations have become increasingly important within the biomedical sciences. Intravital imaging tools like multiphoton fluorescent microscopes, have equipped researchers with extremely powerful ways to uniquely address biologically important questions that can only be accomplished from whole organ investigations[195]. However, this technique's utility is confined to a relatively low penetration depth *in vivo*, and most intravital multiphoton microscopes are experimental systems designed primarily for imaging small animals.

As a result, non-invasive live multiphoton imaging studies are constrained to easily accessible organs like the skin[196-198]. Live investigations in the brain[199-201], liver[202,203] and kidney[195,204-206] of rats and mice are also favorable, using minimally invasive techniques that expose these organs directly to multiphoton excitation light. Thereafter, further *ex vivo* or *in vitro* studies can be done to either verify live findings or

answer questions within deeper tissue structures that are inaccessible with existing intravital multiphoton microscopy systems.

In particular, intravital multiphoton imaging of kidney function and structure has become quite popular, since the kidneys of rats and mice can be easily externalized after anesthesia, and placed in the view of a microscope lens[179,180,207-209]. The preparations made to conduct such imaging studies are crucial in ensuring the generation of useful microscopic data. Below are some essential conditions, related to anesthesia, physiological conditions and surgical environments, which should be considered for an intravital multiphoton imaging study.

The choice of anesthetic is an important factor that must be considered prior to commencing the study. The two main types of sedatives used for small animal research are inhalants and injectable anesthetics. Generally, systemically delivered injectable anesthetics, such as pentobarbital (used in conjunction with analgesics and antiseptics) and thiobutabarbital (inaction) are used for survival and non-survival rat studies respectively. Research within our division has shown that inhalants, like isoflurane, are preferred for relatively short duration studies and procedures on rats, and is generally exclusively used for mice studies. Thiobutabarbital (inactin) has been the preferred anesthetic for non-survival experiments in rats because it provides stable circulatory conditions for long-durations[210]. Furthermore, during such lengthy studies isotonic fluids and serum albumin may be applied to maintain osmotic pressures needed for normal cell and tissue health.

Once the animal is fully sedated, it is important to monitor physiological temperatures, which can be accomplished with an anal probe. Also, heating pads, lamps and blankets can be used to ensure an animal's core temperature stay within normal physiological ranges for all surgical and imaging applications. Blood pressure can also be monitored via carotid or femoral artery access catheter. It is generally recommended to conduct surgical procedures in sterile environments, especially for survival studies. Further safeguards may be taken by sterilizing imaging dish and saline in which externalized kidneys are placed, to limit infection and tissue dehydration/pH alterations.

D. Hypothesis

The overall goal of our research is to test the hypothesis that hydrodynamic retrograde renal vein fluid delivery can be used to facilitate the study and treatment of AKI. In order to achieve this goal we will work towards achieving the following specific aims: (1) to facilitate efficient transgene expression in mammalian kidneys of normal animals and those with ischemia-reperfusion injury; (2) to track functional and structural changes in proximal tubule epithelial cells during AKI, as this is the site of maximal damage observed with this form of injury[22]; (3) to ameliorate, as well as provide protection against, moderate ischemia-reperfuision injury; and (4) to mediate the atypical widespread, robust and organ-specific internalization of exogenous macromolecules in various renal cells of both small and large animals that are standard models for renal and vascular studies. These specific aims will be tested using the following six hypotheses.

In the first case, we hypothesize that hydrodynamic fluid delivery is a robust method to express a variety of exogenous transgenes in live normal mammalian kidneys. We anticipate that a hydrodynamic-based technique will effectively deliver exogenous transgenes in superficial proximal tubules of rat kidneys, with minimal injury, using various non-viral and viral expression vectors. In this work we will characterize transgene expression in live animals using intravital multiphoton fluorescence microscopy, and define optimal parameters for transgene delivery and expression.

In our second study, we will utilize this technique to introduce fluorescent actin plasmid expression vectors in the kidneys of rats, subjected to ischemia-reperfusion injury. We hypothesize that this method can be used to track subsequent structural and functional changes in actin cytoskeleton renal injury initiated by renal pedicle cross-clamp. We predict that this technique will enable us to monitor the loss and remodeling of actin components in live proximal tubule epithelial cells, which is the major site of ischemia-reperfusion injury.

We will then apply this method to investigate the uses of hydrodynamic isotonic fluid delivery for the study of AKI. In particular, our studies will utilize an established rat model for ischemia-reperfusion injury to test the following additional hypotheses listed in the succeeding four studies.

In the third study, we hypothesize that hydrodynamic fluid delivery can be used to efficiently deliver transgenes in live animals with ischemia-reperfusion injury. As before, we anticipate that a hydrodynamic-based technique will effectively deliver exogenous

genes to proximal tubules, the major site of damage with AKI[22], of rat kidneys that are accessible by intravital microscopy. In this work, we will also characterize transgene expression in live animals using intravital multiphoton fluorescence microscopy and define optimal parameters for transgene delivery and expression prior to and at the maximal time of damage with AKI in order to outline a regimen for possible maximal therapeutic benefit.

For our fourth study, we hypothesize that hydrodynamic delivery of isotonic fluid can ameliorate moderate ischemia-reperfusion injury in rats. We predict that this technique can provide substantial reductions in sera creatinine levels with a single retrograde infusion into the renal vein of rats with acute ischemia-reperfusion injury. Here, we will determine the optimal volume and time to generate maximum therapeutic benefit.

For our fifth study, we hypothesize that hydrodynamic retrograde venous injections can be used to effectively deliver mitochondrial specific genes that can protect mammalian kidneys from AKI generated from ischemia-reperfusion injury. Resistance to IR injury can be induced experimentally (e.g., preconditioning) or can be conferred by genetic factors (i.e., as observed in the brown Norway (BN) rat). Little is known about mitochondrial adaptations in experimental or genetic models of resistance. This is an important gap in our knowledge since a variety of organisms and tissues have demonstrable adaptations to ischemia/hypoxia or anaerobic conditions by altering mitochondria protein expression. However, it is our premise that adaptations in

mitochondrial composition can confer protection to ischemia by altering baseline mitochondria function. These adaptations preserve mitochondria integrity in response to injury, leading to cytoprotection and preservation of renal hemodynamics. In this case, we predicted that genes that have been reported to be upregulated in kidneys of rats that are resistant to moderate ischemia-reperfusion injury could be used to protect kidneys, which are incapable of innately initiating this upregulation event. Specifically, we anticipate that the transfer of physiologically relevant concentrations of these genes via hydrodynamic delivery can adequately mimic this renal regulatory and protective process in kidneys that do not naturally exhibit this phenomenon.

In the sixth and final study, we hypothesize that hydrodynamic fluid delivery is capable of facilitating the widespread delivery of various exogenous substances througout the kidneys of small, as well as large animals. We predict that this technique will enable us to effectively deliver exogenous macromolecules of interest to various proximal tubule epithelial cells in the kidneys of live Ossabaw swine.

II. MATERIALS AND METHODS

A. Cell culture and live animals

1. Cell culture

a. Mouse kidney cell culture

We used S3 segment of the proximal tubule epithelial cells[211] cultured in a mixture of 500 ml of essential media with, 7.5% of sodium bicarbonate, 7% of fetal bovine serum (FBS), and 1% of Penn-Strep (streptomysin) (Fisher Scientific, Pittsburgh, PA and grown in a 37°C, 5% CO_2-38% CO_2 humid incubator.

b. MDCK cell culture

Madin-Darby Canine Kidney (MDCK) strain II cells previously described[212], were grown in minimal essential media (Fisher Scientific, Pittsburgh, PA) with 8% fetal bovine serum, 1% L-glutamine, penicillin/streptomycin (Fisher Scientific) and hygromycin (Calbiochem, San Diego, CA), and kept in a 37°C, 5% CO_2 humid incubator.

2. Live rats

We used male Sprague Dawley (Harlan Laboratories, Indianapolis, IN), Frömter Munich Wistar (Harlan Laboratories, Indianapolis, IN) and Simonsen Munich Wistar (Simonsen's Laboratory, Gilroy, CA) rats (150 to 450 g). Rats were given free access to standard rat chow and water and experiments were conducted in accordance with the National Institutes of Health Guidelines (NIH) and were approved by the Indiana University School of Medicine Institutional Animal Care and Use Committee (IACUC).

3. Live pigs

Male and female Ossabaw swine[213] that ranged in mass from 50 to 80 kg were used in collaboration with Drs. Michael Sturek and Jonathan Tune (IUSM). The animals were nil per os for 12 hours prior to surgery. Experiments were also conducted in accordance NIH guidelines and with IACUC approval.

B. Mild, acute and severe models of renal injury

1. Gentamicin toxicity

For our gentamicin toxicity experiments, adult male Sprague-Dawley rats weighing 250-350 g were given a daily intra-peritoneal injection of gentamicin (Sigma-Aldrich, St. Louis, MO) at a dose of 100 mg/kg over the course of 2 weeks, as described in a previously established protocol[214,215]. This work was conducted in conjunction with Dr. B. Molitoris (IUSM) and Dr. A. Hall (University of Zurich, Switzerland). AKI was typically observed after daily gentamicin treatments for 7 days.

2. Ischemia-reperfusion injury

a. Bilateral clamp model

Rats were anesthetized with intraperitoneal injections of 50 mg/kg pentobarbital (Hospira, Inc., Lake Forest, IL and CustomMed Apothecary, Indianapolis, IN), and then placed on a heating pad to maintain normal physiological temperature. We utilized a standard model to generate renal ischemia-reperfusion injury, bilateral renal pedicle clamps were applied to occlude blood flow for periods of 10-15, 30-45 and 60 minutes[68].

These clamp periods correspond to mild, moderate/acute and severe kidney injury respectively[22]. At the end of each injury period, the clamps were removed to reinstate renal blood flow and animals were allowed to fully recover.

b. Contralateral nephrectomy and unilateral clamp model

Again rats were anesthetized with intraperitoneal injections of 50 mg/kg Pentobarbital (CustomMed Apothecary, Indianapolis, IN), and placed on a heating pad to maintain normal physiological temperature. Intraperitoneal incission were made and we ligated the right renal artery, renal vein and ureter using 3-0 or 4-0 silk and subsequently removed right kidneys. Incission were closed and each animal was allowed to recover for 2-4 weeks. Rats werethen subjected to unilateral (left) renal pedicle clamps for 30-45 minutes[68], corresponding to acute kidney injury[22]. At the end of each injury period, clamp was removed from the pedicle to restore renal flow and animals were allowed to recover.

c. Ischemic preconditioning

Rats were again anesthetized in the manner described above and subjected to bilateral pedicle clamps for periods of 30-45 minutes[216]. The incissions were also closed during ischemia. The animals were then allowed to fully recover for a period of 7 days.

C. Serum creatinine measurements

Blood samples we obtained from rats after small incisions were made on their tails. The blood was collected in 1 ml heparin-treated Eppendorf tubes. Blood samples were then centrifuged at 100,000-130,000 rpm for 10 minutes. The plasma (supernatant)

was then stored at 4°C. To determine serum we used the creatinine kinase reagent set (Point Scientific, Inc., Canton, MI). Measurements were performed with a Beckman Creatinine Analyzer 2 (Beckman Instruments, Brea, CA) according to manufacturer's specifications and reported values in milligrams per deciliter (mg/dl)[217].

D. Cell and tissue markers

1. Tolonium chloride

We prepared stock solutions by dissolving 50 mg of tolonium chloride dye (Toluidine Blue O, Electron Microscopy Sciences, Fort Washington, PA), in 5 ml of 0.9% saline. Thereafter, 0.5 ml of this mixture was used for each hydrodynamic injection in a rat, while the 50 ml was used for each injection in a pig.

2. Fluorescent cell and tissue markers

The following fluorescent probes were used in our intravital two-photon fluorescent imaging studies: Texas-red-labeled albumin in phosphate buffered saline, PBS, (Invitrogen, Carlsbad, CA); 3 kDa Cascade Blue, and 4 and 5 kDa Fluorescein Isothiocyanate (FITC) dextrans (Invitrogen, CA); and 150 kDa Tetramethyl Rhodamine Isothiocyanate (TRITC) dextran (TdB Consultancy, Uppsala, Sweden). For rat studies, each dextran solution was prepared by diluting 500 μl of a 20 mg/ml stock solution in 1 ml of saline[117]. We also used 30-50 μl of Hoechst 33342 (Invitrogen, Carlsbad, CA) that was diluted in 0.5 ml saline. Similarly for pig studies we prepared 50 ml of 0.9% saline that contained 400 mg of both dextrans. For mitochondrial *in vivo* investigations we

prepared stock solution by suspending 5 μg of Tetramethyl Rhodamine Methyl Ester, TMRM (Invitrogen Molecular probes, Eugene, OR) in 2 ml of saline.

3. X-ray/CT contrast agents

Standard doses that ranged from 500 to 1000 ml of X-RAY/CT grade constrast media (GE Healthcare, Waukesha, WI) were used in our pig imaging studies.

4. Plasmid vectors

We prepared plasmid DNA treatments suspended in saline using Qiagen Maxi Prep systems (Qiagen, Chatsworth, CA, USA). These plasmids encode: enhanced green fluorescent protein (EGFP), EGFP-actin and EGFP-tubulin (Clontech Laboratories, Inc. (Mountain View, CA, USA); EGFP-occludin (a gift from Dr. Clark Wells, IUSM); EGFP-ZO1; and H2B-tdTomato (a gift from Dr. Richard Day, IUSM). We also used non-fluorescently labeled plasmid vectors that encode mitochondrial enzymes isocitrate dehydrogenase [NADP], mitochondrial (IDH2) and SULT1C1, a member of the sulfotransferase family (OriGene Technologies, Inc., Rockville, MD). The IDH2 vector was a Myc-DDK-tagged ORF clone of Homo sapiens isocitrate dehydrogenase 2 (NADP+), mitochondrial (IDH2), nuclear gene encoding mitochondrial protein as transfection-ready DNA. The SULT1C1 vector was a Myc-DDK-tagged ORF clone of Homo sapiens galactose-3-O- sulfotransferase 2 (GAL3ST2) as transfection-ready DNA. For these hydrodynamic injections, we used a dosage range of 1 to 3 μg of plasmid DNA per gram of body weight.

5. Baculovirus vectors

CellLight® GFP, Actin-GFP and Null (control) BacMam 2.0 baculovirus expression vectors were obtained from the Invitrogen Corporation (Carlsbad, CA). The CellLight® Actin-GFP baculovirus vector encodes fluorescent proteins with a mammalian targeting sequence for both filamentous and globular actin. The Null reagent lacks mammalian genetic constituents, and is designed to identify potential baculovirus-mediated effects and distinguish fluorescence signals from innate tissue fluorescence. For all experiments we used doses the ranged from 1×10^5 to 1×10^7 viral particles/ml.

6. Adenovirus vectors

Replication-incompetent EGFP-actin and RFP-actin adenovirus vectors (gift of Dr. James Bamburg, Colorado State University, Fort Collins, CO). These vectors were kept in concentrations of 3 x 10^8 pfu/ml in DMEM at –80°C[218]. For injections, we used suspended 3×10^5 to 3×10^7 pfu of each adenovirus vector in 0.5 ml of 0.9% saline.

E. Cell cultute transfection and transduction protocols

1. Expression of a single transgene vector

Immortalized cell cultures were grown in in 35 mm glass bottom, No. 1.5 coverslip dishes, with standard thickness of 0.17 millimeters (Corning Inc., Corning, NY). We followed the Effectene Transfection Reagent protocol provided by Qiagen (Valencia, CA), for plasmid-based transfections[219]. We transfected cells at a multiplicity of infection (MOI) of 10:1, and a 24 hour incubation period using both types of viral vectors.

2. Simultaneous expression of multiple transgene vectors

We also investigated the ability to simultaneously EGFP-actin and RFP-actin adenovectors, using the viral titers and incubation period previoulsy mentioned.

F. Exogenous fluid delievry to the kidneys of live animals

1. Jugular vein infusions in live rats

For all animal studies, each rat was first anesthetized by inhaled isoflurane (Webster Veterinary Supply, Inc., Devens, MA), 5% in oxygen, and then given an intraperitoneal injection of either 50 mg/kg of pentobarbital or 130 mg/kg thiobutabarbital (non-survival procedures). The rat was then placed on a heating pad to maintain its core body temperature of roughly 37°C (Figure 1A). Once the animal was fully sedated, its neck was shaved and sanitized it with Betadine Surgical Scrub (Purdue Products L.P., Stamford, CT) solution. An incision was made to expose the jugular vein. The vein was isolated with two 3-0/4-0 silk loops. Superior loop was tied and clamped with a pair of hemostats to stiffen and elevate this vein. A minor incision was made in the jugular vein to insert a PE-50 tubing catheter. The other silk loop was used to anchor the catheter in place. This tubing was attached to a 1 ml syringe containing injectate.

2. Tail vein injections in live rats

The tail vein of a sedated rat was either moistened with a warmed sheet of gauze or placed into a warm bath. A 25-gauge butterfly needle was inserted into the dilated vein tail vein. The butterfly needle was attached to a syringe containing injectates.

3. Renal capsule injections in live rats

The left kidney of an anesthesized rat was exposed via a flank incision (Figures 1B through 1D). Thereafter using a 26-gauge needle, we infused 0.5-1 ml of a tissue dye solution to investigate the uptake and distribution characteristics of exogenously delivered materials.

4. Hydrodynamic infusions in live rats

a. Renal artery catheter-based injections

The first step towards the development of our hydrodynamic infusion technique focused on the ligation of the renal artery by the insertion of a PE-50 catheter. For this process, we made a mideline incision exposing the left renal artery, clamped the region directly below the aorta with micro-serrefines, made a small incission into the artery and inserted the catheter. The clamp was applied for approximately 15 minutes. Thereafter, we rapidly infused solutions (0.5-1 ml) into the artery at a rate of approximately 0.1 ml/s.

b. Renal artery fine-needle injections (without vascular cross-clamps)

After isolating the renal artery, it was elevated with either 3-0 or 4-0 silk loop. Saline (0.2-1 ml) containing either tissue dyes or plasmids were infused into the renal artery at an approximate rate of 0.1 ml/s, using a 30-gauge needle. The needle was removed, and hemostasis was induced with a cotton swab after applying pressure to the injection site for a minimum of 10 minutes. After this, the midline incision was closed and the animal was allowed to fully recover.

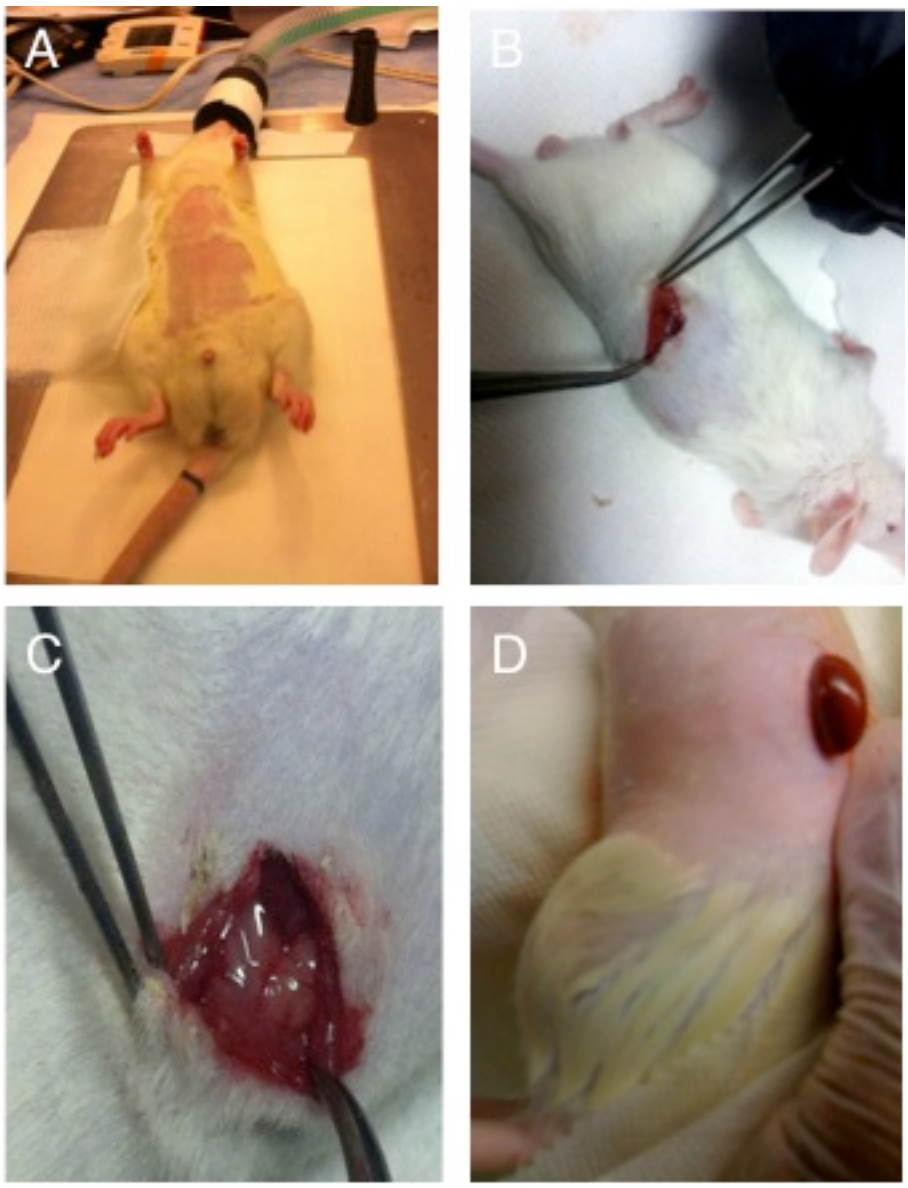

Figure 1. Standard surgery layout and method to exteriorize the rat kidney for intravital imaging

Digital images taken of an anesthetized rat as it was being prepared for surgery (A); and then during the flank incision procedure that was used to exteriorize the left kidney of an anesthetized rat (B through D). Image (C) is a zoom of the field presented in (B) to illustrate the tuft of perienal fat situated at the apex of the kidney, and image (D) is the kidney once it has been exteriorized through the flank incission.

c. Renal artery fine-needle injections (with vascular cross-clamps)

Fine needle injections were performed as described above, except micro-serrefines were used to isolate and occlude both the renal vein and aorta for roughly 5 minutes. During this time we infused saline (0.2-1 ml) containing either tissue dyes or transgene vectors into the renal artery at an approximate rate of 0.1 ml/s, using a 30-gauge stainless steel needle. Again, we removed the needle and applied pressure to the injection site to induce hemostasis. These arterial injections were also prone to failure of timely hemostasis, so pressure was again applied for extended period after injections before the animals were allowed to fully recover.

d. Retrograde renal vein catheter-based injections

As with jugular/arterial cathterization, we inserted a PE-50 tube into the renal vein and prepared the rat for hydrodynamic infusion at an approximate rate of 0.1 ml/s.

e. Retrograde renal vein fine-needle injections (without vascular cross-clamps)

After separating the renal artery and vein as described above, we elevated the renal vein with either 3-0 or 4-0 silk loop and performed a retrograde infusion of a either tissue dye or transgenes at an approximate rate of 0.1 ml/s into the renal vein, using a 30-gauge needle. We then removed the needle and applied pressure to the injection site, with a cotton swab, to induce hemostasis. The animal was then allowed to recover from the effects of the anesthesia. In some cases, we added Optison (GE Healthcare Medical Diagnostics, Princeton, NJ, USA) to the transgene vector solution.

f. Retrograde renal vein fine-needle injections (with vascular cross-clamps)

We adapted the injection process outlined above to incorporate vascular cross-clamping as a means to potentially reduce exogenous substance leakage and renal uptake. For this technique, we first clamped the renal artery, followed by the renal vein, using micro-serrefines. The vein was then elevated with either 3-0 or 4-0 silk loops. At that time either a tissue dye or transgene suspension was infused into the vein as described in Figure 2. The needle was removed and pressure was applied to the injection site using a cotton swab to induce hemostasis. The vascular clamps were removed (venous clamp was removed before the arterial clamp) to restore flow. The total clamping was less than 3 minutes. The midline incision was then closed and the animal was allowed to recover.

5. Monitoring vital signs during renal vein hydrodynamic retrograde infusions in live rats

We made incisions in the legs of anesthetized rats to expose the femoral arteries. The arteries were isolated with two 3-0 or 4-0 silk loops. Using micro-serrefine clamps, we clamped off the artery and tied off the loops as well. Each loop was then clamped with a pair of hemostats to stiffen and elevate each artery. We then made a small incision in the femoral artery and inserted a PE-50 tubing catheter into its lumen. The other silk loop was used to anchor the catheter in place. This tubing was attached to a three-way port that was linked to a PowerLab 8/30 data acquisition system (ADInstruments, Colorado Springs, CO) to record temperature, blood pressure, and heart rate.

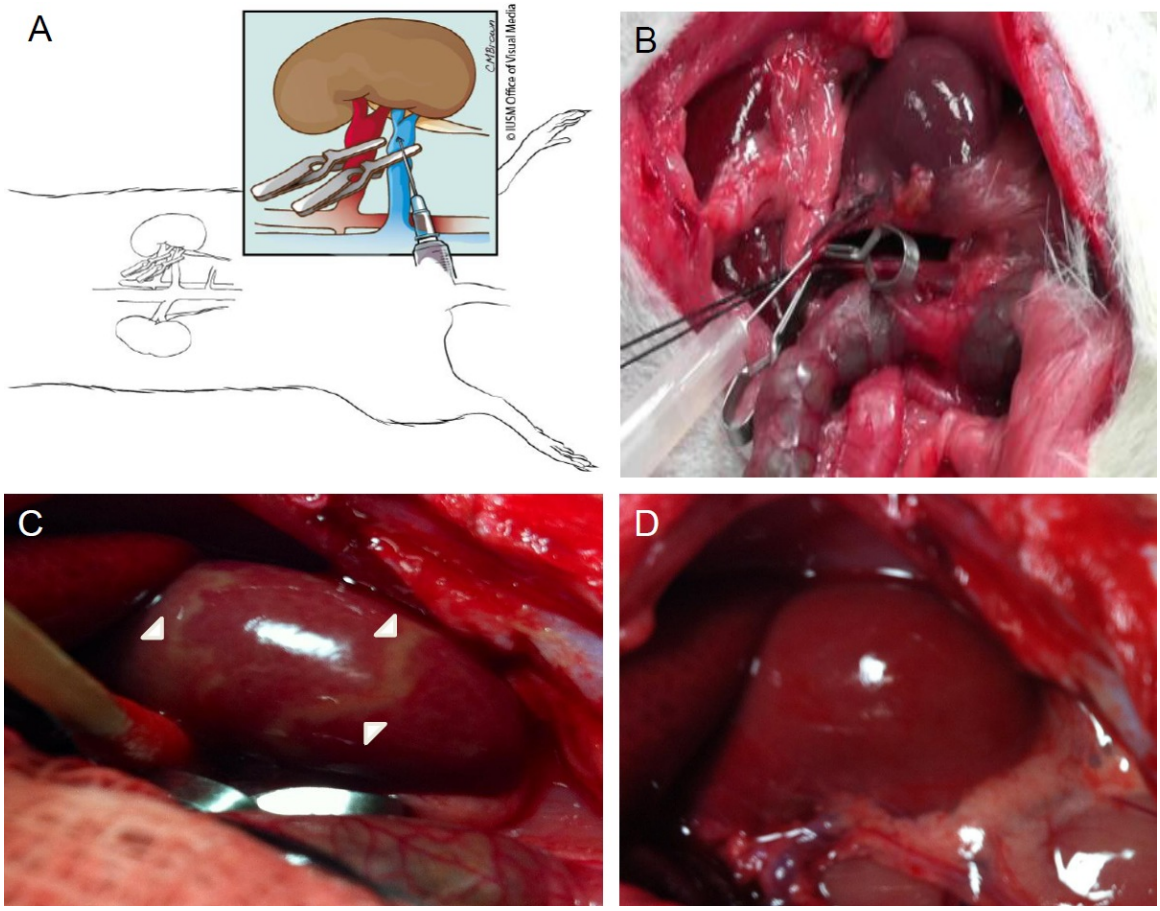

Figure 2. Schematics and live images illustrating the hydrodynamic injection process in the rat kidney

Figure (A) illustrates the retrograde renal vein injection process, and digital images taken of a live rat: (B) directly before hydrodynamic injection, (C) directly after the injection and (D) 3 minutes after the hydrodynamic injection once the vascular clamps were removed. Arrowheads in image (C) show regions where the kidney vasculature which were perfused with saline directly after the injection. Signs of reinstated perfusion were observed once the clamps were removed.

6. Critical parameters for retrograde renal vein hydrodynamic injections in live rats

In order to characterize the hydrodynamic delivery process, we monitored time-dependent pressure profiles during injections. PE-50 polyethylene catheter tubing (Clay Adams, Division of Becton, Dickson and Company, Parsippany, NJ) was introduced into the femoral vein and traversed to the level of the bifurcation adjoining the renal vein and inferior vena cava. Both the vena cava and renal artery were clamped. To monitor renal venous pressure, a three-way stopcock was used to connect the infusion line with a fluid-filled pressure transducer, and data acquired in real time using data-acquisition software (Biopac Systems, Inc., Goleta, CA).

7. Hydrodynamic delivery facilitates the endocytic uptake of virions in live rat kidneys

We attempted to inhibit baculoviral incorporation and expression simultaneously in MDCK cell cultures and in live animals, by incubating the viral particles in sera containing active complement proteins for approximately 90 minutes[220]. Similarly, we attempted to maintain baculoviral-based expression by incubating the viral particles in sera, containing heat-inactivated complement proteins, again for 90 minutes *in vitro* and *in vivo*. The complement proteins were deactivated by heating the sera to 56°C for 30 minutes[221]. For these experiments, the standard dose of $1x10^5$ viral particles.ml^{-1} was used for both the *in vitro* and *in vivo* investigations. This standard viral dosage was also used suspended in the serum sample that was hydrodynamically injected into a given animal

after it was harvested from the same animal. Cell cultures were imaged 24 hours after incubation with baculovirus vectors, and live rats 3 days after hydrodynamic injections to investigate transgene expression.

8. Hydrodynamic retrograde venous delivery in rats with ischemia-reperfusion injury

Rats that were subjected to mild and moderate ischemia-reperfusion injury, as described earlier, received hydrodynamic retrograde injections at either 1 hour or 24 hours after ischemia/reperfusion injury (the 24 hour time point corresponds to the period of maximum damage with AKI[22]).

9. Hydrodynamic retrograde portal vein injections in live rats

After creating intraperitoneal incision, we identified and isolated the portal vein. We then elevated the vein with either 3-0 or 4-0 silk loop. Thereafter, the vein was clamped and we performed a rapid injection of a given transgene solution, described earlier, at a site between the clamp and the liver. Pressure was then applied to this vein as before to induce hemostasis. Again, the total clamping period did not exceed 3 minutes. Finally, the midline incision was closed and the animal was allowed to fully recover.

10. Renal artery and vein infusions in live Ossabaw swine

a. Low rate arterial and retrograde venous infusions into the renal vein of Ossabaw swine

Ossabaw pigs were anesthetized with 5 mg/kg of Telazol (a dissociative anesthetic & benzodiazepine) and 2.2 mg/kg of Xylazine (an $alpha_2$ agonist) and

maintained on isoflurane, between 1 and 5% concentration. Local anesthetic (lidocaine & bupivacaine) was injected subcutaneously at the incision sites. Roughly 10 cm incisions were then made in the right and left inguinal regions to access the right femoral artery and left femoral vein respectively. An 8F-introducing sheath was placed in the right femoral artery, while a 7F-introducing sheath was placed in the left femoral vein, and guiding catheters were inserted into these sheaths and directed to the renal artery or vein. Guidewires, typically 0.014" wires were used to select a specific artery and vein.

Radiopaque contrast media was then injected intravenously and intra-arterially to help select a specific vessel. A 5 mm balloon catheter was placed over the guidewire in the renal artery. An infusion catheter was placed over the guidewire in the renal vein. The 5 mm balloon was inflated in an attempt to occlude either the renal artery or vein. Low rate infusions of contrast media were first utilized to determine whether we could access the kidney from either the venous or arterial lines. Once this was done, we conducted low rate infusions of 50 ml of a mixture containing contrast media, toluidine blue dye, and low and large molecular weight dextrans were infused into either the renal artery or renal vein, and confirmed by angiography to examine the characteristics related to the possible uptake of exogenous materials in live Ossabaw swine kidneys.

b. Hydrodynamic retrograde injection into the renal vein of Ossabaw swine

Several midline incisions were made in pigs, which were anesthetized in the manner described above, to separate the extensive skin, muscle, adipose layers. We then

externalized large and small intestine loops to first identify the spleen and liver. Using these landmarks we then identified the left gonadal vein and ascended the inferior to the common renal vein distal to the left gonadal vein insertion and proximal to anterior branching of the renal vein. We then tied off visible bifurcations of the renal vein, including the branch into to which we made injection, using umbilical cotton tape. This was done in an attempt to temporarily occlude renal blood flow.

Using the umbilical tape looped around this renal vein branch, we extended the vein and delivered 50 ml of saline containing the tissue dye solution (this solution contained equal concentrations of 4 KDa FITC and 150 kDa TRITC dextrans) using a 16-gauge catheter attached to a 60 ml syringe. We then applied pressure to the vein to aid hemostasis. The total time that we occluded renal blood flow did not exceed 8 minutes. It should be noted that the angle from the IVC was quite acute and the anatomy of the length of the common renal vein distal to the left gonadal vein insertion and proximal to anterior branching of the renal vein was quite small, which increased the difficulty to make the injection. Morover, it was difficult to induce hemostasis in this animal because it was given large doses of heparin to aid separate cardiac studies, as well as the complex network of veins intertwined within adipose tissue.

11. Monitoring vital signs during renal vein hydrodynamic retrograde infusions in live pigs

Anesthetized pigs were intubated and ventilated. ECG, Pulse-Oxymetry and Arterial Pressure Line patient monitoring devices were connected to animal's vital signs.

G. Cell and tissue imaging

1. Fluoresence microscopy

a. Confocal fluorescence imaging of live cells

All confocal imaging studies were conducted an Olympus FV 1000-MPE Microscope (Olympus, Tokyo, Japan). Cell cultures were grown in 35 mm glass bottom, No. 1.5 coverslip dishes, with standard thickness of 0.17 millimeters (Corning Inc., Corning, NY). The dishes were placed above the objective and the microscope was set to acquire 512×512 blue-, green- and red-pseudo-color images. To minimize both photoxicity and photobleaching, we reduced both the energy level of the excitation light and the duration of excitation. We also used a Warner DH-35 dish and OW objective warmers to maintain culture temperatures as needed for prolonged imaging sessions.

b. Spectral analyses to identify transgene fluorescence

Using the Olympus Fluoview Ver. 3.1a lambda stack algorithm, which is available with the Olympus FV 1000-MP Microscope, we collected emission spectra, in confocal mode covering major emission spectra of the fluorescent probes used for studies in live kidney and cell culture. Once major peaks were identified, our fluorescent spectra were compared to those of known fluorescent probes, and we noted general factors by which fluorescent signal intensities differed from background intensities.

c. Intravital two-photon fluorescence microscopy

In anesthetized rats, we shaved the left flank and made vertical incisions to externalize the left kidney. The kidney was then placed inside a glass bottom dish

containing saline, which was set above either a 20X or 60X water immersion objective for imaging, with the animal's body acting as weight to stabilize the kidney in this position[207,209] (Figure 4). A heating pad was then placed over the rat to maintain its core temperature. Similarly, for liver imaging, horizontal incisions were made directly under the xiphoid, to facilitate the externalization of the liver lobes using a cotton swab. Lobes were rested in the imaging dish, and the animal was placed on its stomach to provide contact between the lobes and the glass dish, and minimize motion due to respiration.

Fluorescent images were acquired from externalized organ within 800-860 nm excitation wavelength range[207]. Measurements were made with an Olympus FV 1000-MPE Microscope set with a Spectra Physics MaiTai Deep See laser, tunable from 710-990 nm, with dispersion compensation for two-photon microscopy (Olympus Corporation, Tokyo, Japan)[209]. The system is also equipped with two external detectors for two-photon imaging, and dichroic mirrors available for collecting blue, green and red emissions.

The system is mounted on an Olympus IX81 inverted microscope (Figure 5). Emitted light is collected using a 3-fixed band pass filter system: 420-460 nm (blue channel), 495-540 nm (green channel), and 575-630 nm (red channel). It should be noted that as we investigated EGFP-based expression, we merged the pseudo-green and pseudo-red colors to further differentiate between GFP-based fluorescence and endogenous tissue fluorescence. This was done because renal tubules are known to have high levels of green autofluorescence. Such a technique has been presented in the literature to successfully identify positive GFP-based signals *in vivo*[117].

d. Two-photon imaging of freshly excised tissues

Rat and pig tissues were harvested from live animals directly before euthanasia. These tissues were quickly sectioned and placed into imaging dishes for microscopic analyses as previously discussed. Additionally, other tissue sections were fixed with 4% paraformaldehyde, counterstained with Hoechst 33342 and then imaged.

e. Texas-red phalloidin and fluorescent actin colocalization to verify transgene expression

Whole transduced kidneys were either perfusion or immersion fixed with 4% paraformaldehyde solution. Sections (100-200 μm thick) were obtained, then incubated overnight in a phalloidin staining solution. This solution was prepared by diluting Texas-red-phalloidin (Invitrogen Corporation, Mountain View, CA) 1:200 in blocking buffer (2% bovine serum albumin and 0.1% Triton X-100, diluted in phosphate-buffered saline)[117]. The next day the tissues were rinsed three times for two hours in PBS, and then mounted onto slides and analyzed using the aforesaid confocal fluorescence microscope.

f. Estimations of transgene delivery efficiencies

i. In vivo renal transgene delivery efficiencies

We estimated transgene delivery efficiencies for each vector *in vivo* using intravital fluorescent two-photon microscopy. We determined expression efficiencies within live superficial cortex segments of several rats across a 28-day period after transgene delivery. We began our measurements 3 days after delivery, as this was when we could observe signs of stable transformation and renal function after injections.

For these efficiency measurements, we first distinguished transgene expression from autofluorescent backgrounds by conducting spectral analyses. This allowed us to determine that transgene fluorescence signals had intensities at least double those of autofluorescence signals. Using this criterion we then calculated the percentage of nephron cross sections (glomeruli and tubules), which expressed the reporter transgenes within microscopic fields acquired with the 60X objective. Final efficiency value was the average percentage of transformed cross sections in 10 randomly chosen adjacent fields.

ii. In vitro renal transgene delivery efficiencies

Our *in vitro* estimations allowed us to determine the degree of transgene distribution throughout all regions of the cortex and medulla, including those presently inaccessible by intravital two-photon microscopy. For these measurements we acquired a montage of fields using confocal laser-scanning microscopy covering a wedge of the kidney from the cortex to the level of the pedicle. We then estimated the degree of transformation using the same method mentioned for the *in vivo* efficiency measurements, within 100 μm × 1000 μm at various depths from the surface of the kidney (Figure 3).

g. Functional and structural analyses using fluorescent albumin and dextrans following transgene delivery and fluorescent protein expression

After identifying a time-course for renal recovery and viable transgene expression, it was then necessary to investigate whether hydrodynamic delivery process or transgene expression would hinder intrinsic renal structural and functional capacities. For this, we

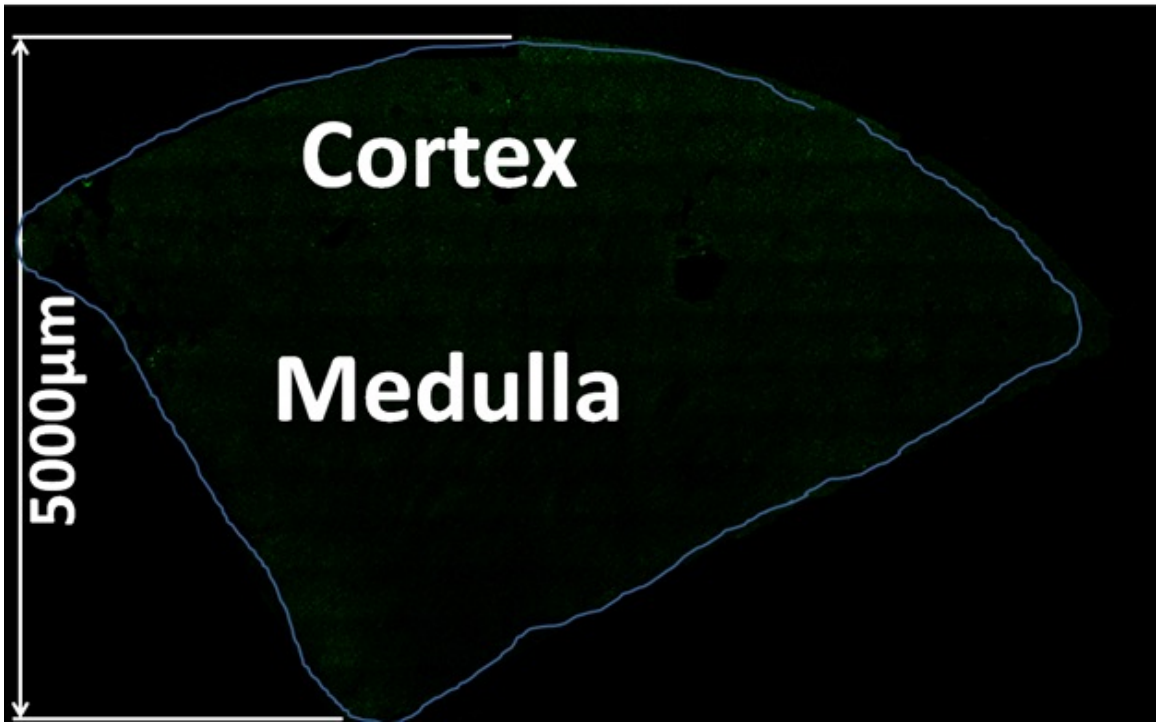

Figure 3. Reconstructed montage of a fixed kidney section
Montage collected from a fixed kidney 3 days following hydrodynamic injection of saline. The montage was reconstructed from a series of confocal laser-scanning micrographs covering a wedge of the kidney from the cortex to the level of the pedicle.

again systemically introduced fluorescent albumin, and low/large molecular weight dextrans to investigate potential uptake and distribution of dyes in superficial nephron cross sections[209], in animals that received hydrodynamic retrograde injections of saline and transgene solutions, throughout a 6-week period after the injection process.

h. Investigating the correlation between hydrodynamic injection parameters and reliable transgene expression

We examined the conditions required to infuse the transgenes at various injection rates. To gain insight into the effectiveness of each infusion rate, we infused the 3 kDa Cascade Blue and 150 kDa TRITC molecular weight dextrans at approximately 0.1 ml/s, 0.008 ml/s and 0.004 ml/s. We investigated the effect each infusion rate had on renal structure and function, and transgene expression as presented below.

i. Investigating whether hydrodynamic forces facilitate endocytic uptake of virions in vivo

We conducted a series of experiments that monitored baculovirus-derived fluorescent protein expression under standard systemic and hydrodynamic renal vein delivery conditions. For systemic baculoviral delivery investigations, we introduced the CellLight® Actin-GFP baculoviral particles through the tail vein and monitored the tissue fluorescence prior to and post transgene delivery.

We next examined the interactions between sera complement proteins and the actin-targeting baculovirus vectors, *in vitro* and *in vivo*, under hydrodynamic conditions. We attempted to inhibit baculoviral incorporation and expression simultaneously in

MDCK cell cultures and in live animals, by incubating the viral particles in sera containing active complement proteins for approximately 90 minutes[220]. Similarly, we attempted to maintain baculoviral-based expression by incubating the viral particles in sera, containing deactivated complement proteins, again for 90 minutes *in vitro* and *in vivo*. We deactivated complement proteins by heating the sera for both *in vitro* and *in vivo* investigations. Note all sera that were re-introduced into a given rat, were originally collected from the same rat.

j. Estimations of mitochondrial potential activity in live rat kidneys based on TMRM fluorescence intensities

We obtained 5-10 adjacent intravital fields that were randomly chosen from each live kidney using a 20X objective, approximately 15-30 minutes after TMRM was introduced into an animal via a jugular vein infusion. We calculated the mean intensity of each tubule in a given intravital fluorescence microscopic field using ImageJ software (National Institute of Mental Health, NIH, Bethesda, MD). Thereafter, a final TMRM intensity value was obtained from the average of all measured intensities. This process allowed us to examine fluorescence intensities from a minimum of 500 tubules per kidney. These kidneys were analyzed from normal and ischemic preconditioned rats, and those that received hydrodynamic treatments of saline, IDH2 and SULT1C1.

2. Histology and renal injury assessment

Biopsies were performed on kidneys 3 days after receiving sham, saline and transgene hydrodynamic retrograde injections. For this process, rats were anesthetized

with pentobarbital and once fully sedated whole kidneys were acquired by clamping each renal pedicle and rapidly excised the kidneys. Once removed, the kidneys were fixed with 4% paraformaldehyde for 24 hours at 4°C. Thereafter the samples were immersed in 10% neutral buffered formalin or 4% phosphate-buffered formalin, again for a minimum of 24 hours at room temperature. The specimens were then rinsed in distilled H_2O and stored in 70% ethanol. For infiltration, the specimens were dehydrated through a graded series of ethanol (70%; 80%, 95%, 100%; two changes each under vacuum for 45 minutes at room temperature). The specimens were cleared in two changes of xylene (under vacuum at room temperature for 45 minutes each), infiltrated with 4 changes of paraffin (under vacuum at 59°C; 45 minutes each), and embedded in fresh paraffin. After which, 4-5 microns thick sections were cut using a Reichert-Jung 820 microtome (Depew, NY).

Sections were flattened on a warm water bath and mounted on coated and charged glass slides. After drying the sections were deparaffinized, rehydrated and stained with hematoxylin and eosin. We then imaged these slides using a Nikon Microphot SA Upright Microscope equipped with a sensitive Diagnostic Instruments SPOT RT Slider color camera (Nikon, Tokyo, Japan) and collected a minimum of 10 randomly chosen adjacent fields with a 20X objective. This generated an approximately 0.24 mm^2 field of view[222].

A blinded reviewer used a method previously described by Kelly et al.[222,223] to assess renal injury by calculating the percentage of damaged tubules: (number of severely injured tubules)/(total number of tubules)×100%. Renal tubules were classified as normal

(showing no evidence of injury); moderately damaged (indicated by loss of brush border staining and simplification void of evidence of necrosis); and severely damaged (indicated by tubules with apparent necrosis, or cellular debris in the lumen). Approximately 500 tubules were scored for such assessments.

3. Fluoroscopy/cinematography to monitor uptake of exogenous dyes in live pig kidneys

Angiograms of live Ossabaw pig kidneys were acquired using a fluoroscopy/cinematography unit. Pigs were anesthetized as described above, and then radiopaque contrast media was injected intravenously and intra-arterially to help select specific vessels. This selection was confirmed by angiography, as we examined characteristics related to possible uptake of exogenous materials in live swine kidneys.

H. Western blot analysis

Immersion fixed kidney samples were homogenized, and we collected protein-enriched fractions. The proteins were separated using sodium dodecyl sulfate (SDS) gel electrophoresis and transferred to membranes for detection. These membranes were incubated with generic proteins to inhibit non-specific binding and primary and secondary conjugations that were used to recognize proteins of interest (such as those expressed by our plasmid and viral vectors). Whole kidneys were harvested from anesthetized rats and were cryofixed by submsersion into liquid nitrogen chambers (no conventional fixatives were used throughout this process). After a minimum of 1 week

cryofixation, the kidneys were taken from the liquid notrogen chamber and we acquired approximately 300 mg tranverse sections that extended from the cortex to the pedicle.

The sections were homogenized in 300 ul RIPA buffer using Dounce homogenizer on ice and spun the lysate at 13,000g for 20 minutes in a 4°C pre-cooled centrifuge. We gently removed the tube from the centrifuge and placed it on ice and transfered the supernatant to a fresh tube (also kept on ice) and then performed a BCA assay to determine the protein concentration. Denatured protein samples were acquired by adding equal volumes of 2X Laemmli Sample Buffer at 70°C for 5 minutes. We then loaded 5 ug of each protein sample into the wells of the 10% SDS-PAGE gel, along with molecular weight markers. We then ran the gel for 50 minutes at 240 V, and the protein was transfered from the gel to the membrane for 36 minutes at 24 V. After wich, we blocked the membrane overnight at 4°C using TBST blocking solution with 3% FBS.

Next we incubated the membrane with 1:1000 dilution of primary antibody (Rabbit PolyAb Anti-IDH2, Novus Biologicals, Littleton, CO) in TBS blocking solution with 0.3% FBS for 1 hour at room temperature and washed it three time with TBS for 5 minutes. The membrane was then incubated with 1:40,000 dilution of secondary antibody HRP D&R in TBS blocking buffer with 0.3% FBS at room temperature for 1 hour, and gel was washed three times with TBS. For signal development, we incubated blots for 5 minutes in the ECL reagents (SuperSignal™ West Pico Chemiluminescent Substrate). After, we removed excess reagent, covered membranes in transparent plastic wrap, and acquired images using chemiluminescence darkroom development techniques.

I. Statistical analysis

We computed the mean and S.E. for all data sets, and evaluated the statistical significance of our results using the Student's *t*-test. All statistical analyses were evaluated with 95% confidence or certainty.

III. RESULTS

Chapter 1. The design and characterization of various methods to facilitate and monitor transgene expression in the rat kidney

A. Fluorescent protein expression in cultured cells using plasmid, baculovirus and adenovirus vectors

We observed non-viral and viral derived fluorescent protein expression in cultured cells using confocal microscopy (Figures 4-6). We analyzed fluorescent protein spectra, and determined that their fluorescence levels were at least double those of autofluorescence in cell culture and tissues. This enabled us to clearly identify transgene expression in cell culture (Figure 5), and fixed (Figure 27) live and tissues (Figure 28).

From our cell culture studies, green florescent proteins appeared throughout the nuclei and the cytoplasm of cells that were infected with EGFP plasmid (Figures 4A and 4B), GFP baculovirus (Figures 5B) and EGFP adenovirus vectors (Figures 6A). Likewise, striking and characteristic filamentous and tubular fluorescent patterns were observed in cells that were infected with non-viral and viral transgene vectors designed to express fluorescent tubulin (Figures 4C and 4D) and actin (Figures 6B and 6C). Cells treated with EGFP-occludin (Figure 5E) and H2B-tdTomato plasmids (Figure 5F) expressed proteins also provided clear signs of anticipated probe localization and morphology. For instance, EGFP-occludin signals ran between adjacent nuclei as punctate fluorescent bands along

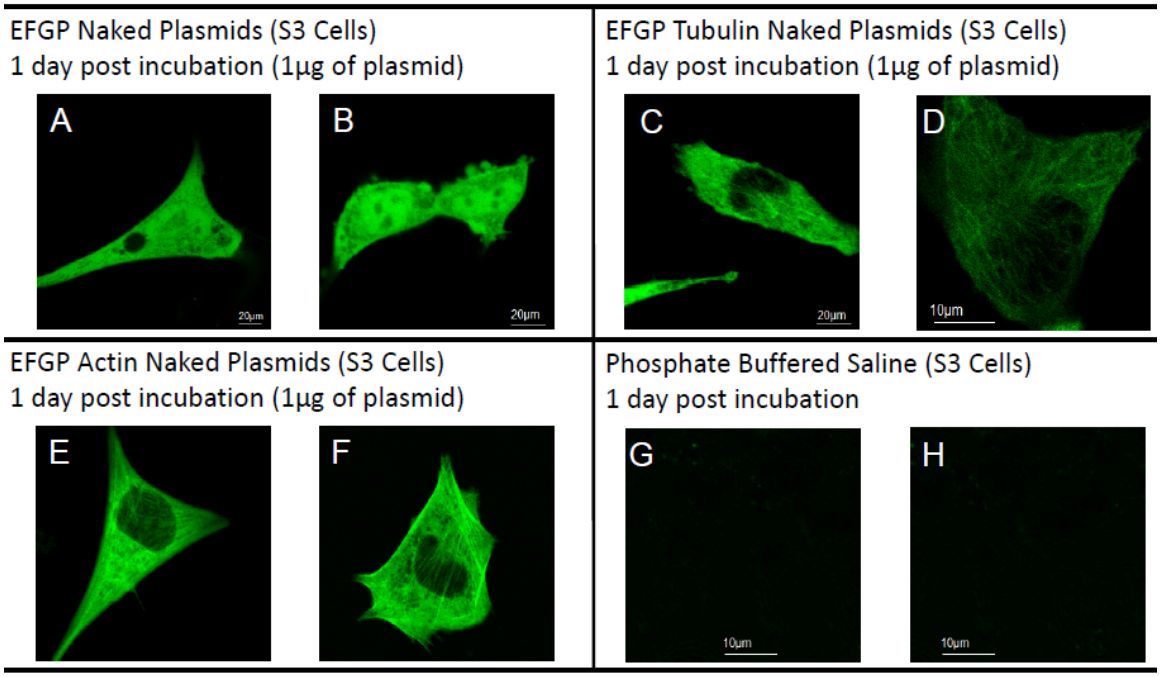

Figure 4. Plasmid-derived fluorescent protein expression in live cells
Confocal micrographs taken of S3 proximal tubule epithelial mouse cell cultures 1 days after they underwent lipofection with EGFP, EGFP Actin and EGFP Tubulin plasmid vectors. Images were taken under 2X or 3X optical zoom to highlight fluorescent structures. Untagged GFPs are expressed throughout the nuclei and cytoplasm observed within images (A) and (B). Cellular nuclei, actin filaments and microtubules are well-defined within images (C and D), and (E and F) respectively. Images G and H were obtained from cells trated with PBS and show a typical lack of fluorescence.

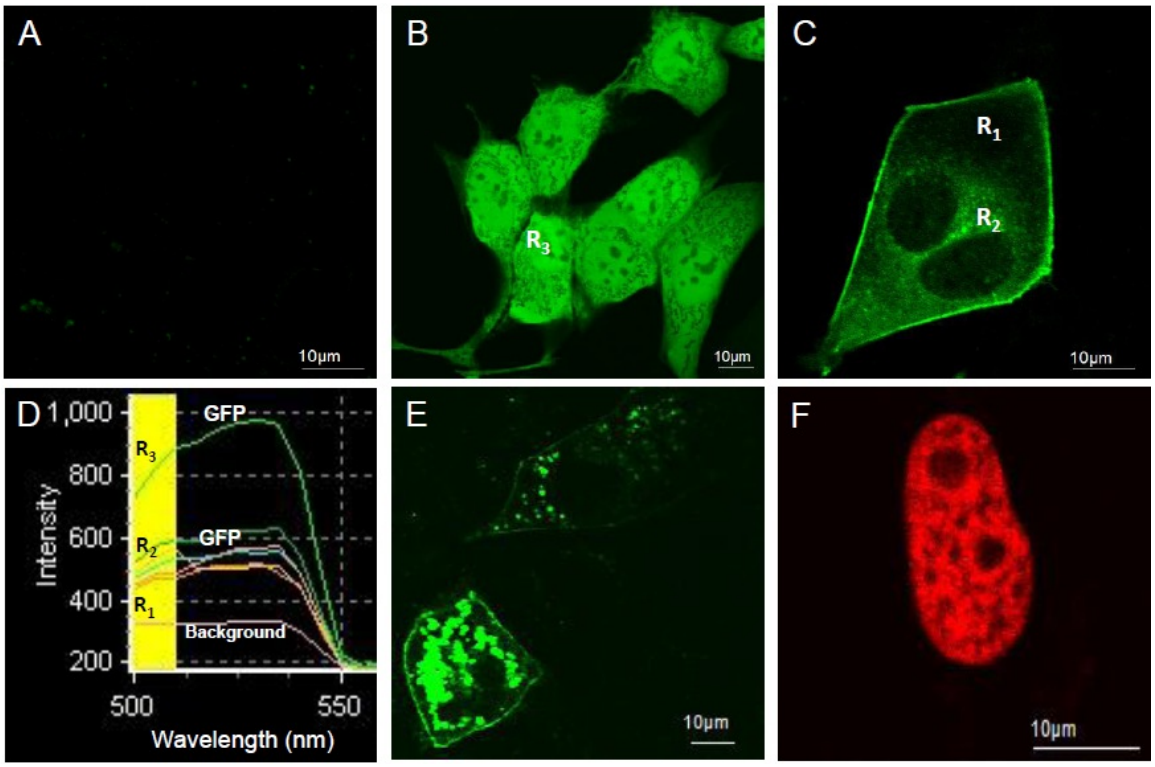

Figure 5. Spectral analyses used to identify baculovirus- and plasmid-derived fluorescent protein expression in live cells

Confocal laser scanning micrographs obtained from MDCK and S3 proximal tubule epithelial mouse cell cultures incubated with: (A) Null baculovirus vectors, (B) GFP baculovirus vectors, (C) Actin-GFP baculovirus vector, (E) EFGP-occludin plasmid vectors; and (F) Histone H2B-tdTomato plasmid vectors. These images were taken 1 day after plasmid and viral transformation. Untagged GFPs are expressed throughout the nuclei and cytoplasm observed within image (B). Within image (C) actin filament staining appears uncharacteristically punctate. Image (E) outlines characteristic plasma membrane-derived tight junction staining and (G) presents typical nuclear and cytoplasmic staining representing histone localization. Spectral analyses presented in (E) identified that transgene-based fluorescence signal intensities were at least double those of the background.

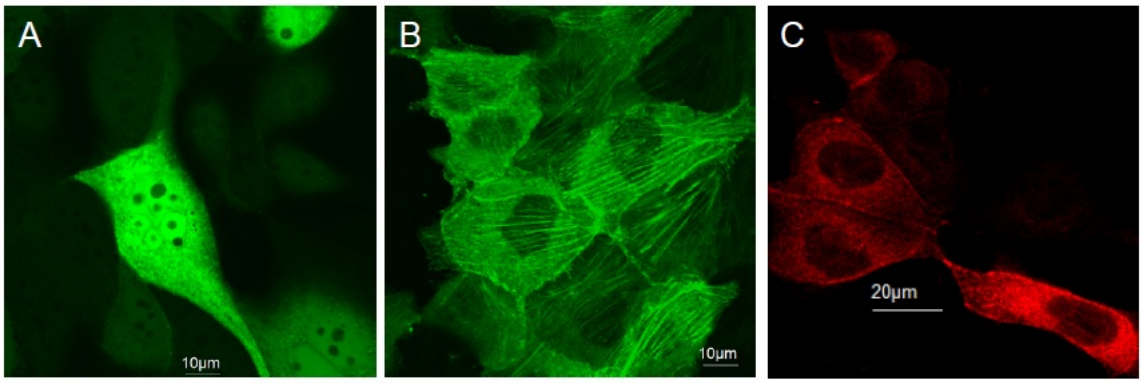

Figure 6. Adenovirus-derived fluorescent protein expression in live cells
Confocal micrographs taken of MDCK cell cultures 1 day after they were incubated with fluorescent adenovirus vectors: (A) GFP, (B) Actin-GFP, and (C) Actin-RFP. Untagged GFPs are expressed throughout the nuclei and cytoplasm observed within image (A). Also, nuclei and actin filaments are clearly defined within images (B) and (C).

regions that would correspond to tight junctions (Figure 5E). Also, fluorescent H2B-tdTomato protein expression was observed throughout the nuclei of transfected cells (Figure 5F). However, fluorescence patterns observed from cells treated with CellLight® Actin-GFP baculovirions (express GFPs that bind to actin filaments) produced punctate fluorescence patterns that deviated from normal cellular morphology (Figure 5C).

B. Rat kidney autofluorescence,structure and function examined with intravital two-photon florescence microscopy

1. Rat kidneys investigated under normal physiological conditions

a. Tissue autofluorescence in normal rats visualized using two-photon excitations wavelengths that range from 800 to 860 nm

We examined innate tissue autofluorescence in various nephron cross sections of live rat kidneys using intravital two-photon microscopy (Figure 7). From the data collected, across this range of excitation wavelengths, we observed that normal proximal tubules had a characteristic punctate autfluorescence pattern. The fluorescence signal levels obtained from proximal tubule epithelial cells were greater than those obtained from distal tubule epithelial cells. In two-photon micrographs, including the images we acquired from normal rat kidneys, distal tubules appear as regions of low fluorescence, as compared to neighboring proximal tubules. The epithelial cells of the proximal tubules have characteristic punctate fluorescence patterns that apprear throughout the cytoplasm (Figure 7). Similalry, Bowman's capsule is the primary visible structure within the

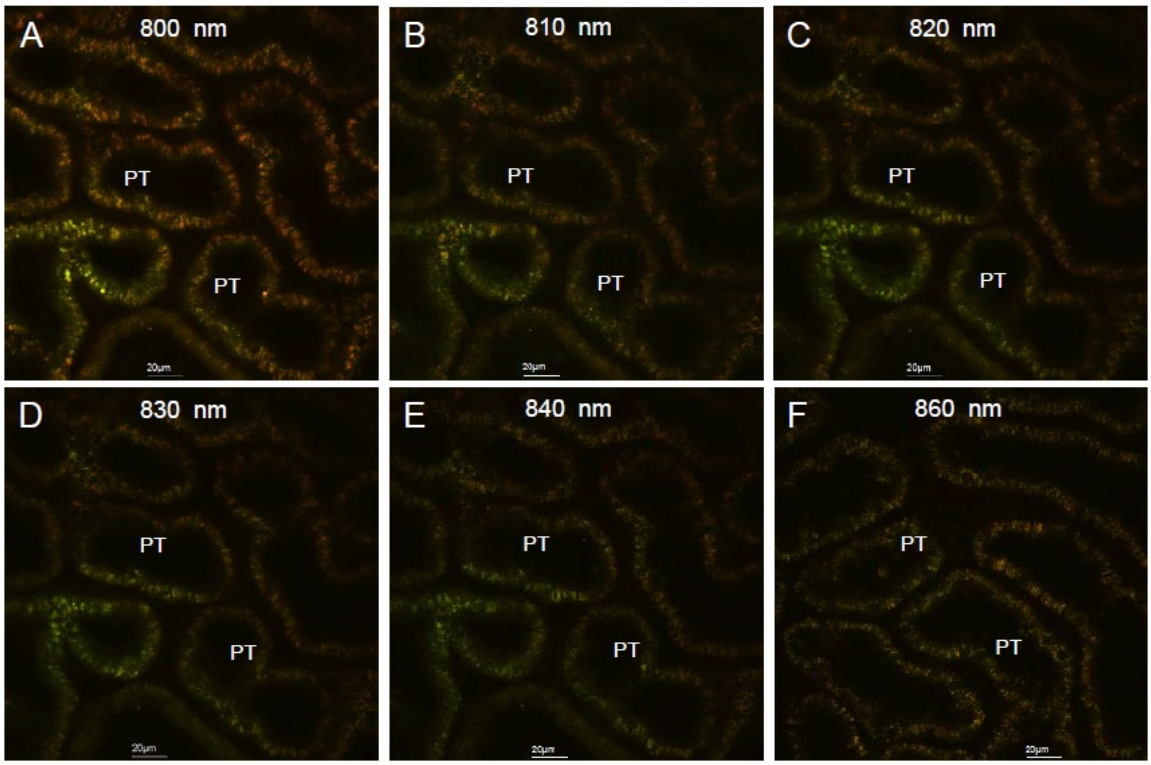

Figure 7. Autofluorescence in the normal rat kidney visualized at excitation wavelentghs ranging from 800 to 860 nm

Intravital micrographs of tissue autofluorescence in normal rat kidneys across excitation wavelength range 800 to 860 μm. These images show the punctate fluorescent patterns characteristic of proximal tubules. In all cases, we merged the red and green pseudo-color channels to form each image.

glomerulus (Figure 8), which gives it a unique appearance when visualized with confocal and multiphoton fluorescence miscroscopy.

b. Renal structure and function in rats

We infused various fluorescent dyes into the jugular veins of live rats to examine key aspects of renal structure and function. This allowed us to visualize peritubular and glomerular capillary integrity, renal microvascular blood flow, glomerular and tubular filtration, and proximal tubular endocytic internalization (Figure 8). These data provided us with a standard by which to identify renal structure and function, as well as to gauge abnormalities in live rat kidneys using intravital fluorescent microscopy.

2. Rat kidneys investigated under nephrotoxic and ischemic conditions

a. Tissue autofluorescence, structure and function in the setting of gentamicin-induced nephrotoxicity

Gentamicin treatments significantly altered normal tissue autofluorescence, structure and function. Specifically, rats that received daily gentamicin injections for 1 and 2 weeks produced acute and severe renal damage respectively. Two days after the treatments began, we observed signs of mild injury in these rat kidneys. The degree of injury escalated as we continuted providing gentamicin treatments. The typical uniform and punctate fluorescence patterns observed in the proximal tubules of normal rat kidneys, were significantly altered in these nephrotoxic rats, as illustrated by regions of clumped and intensified fluorescence (Figures 9B and 9C).

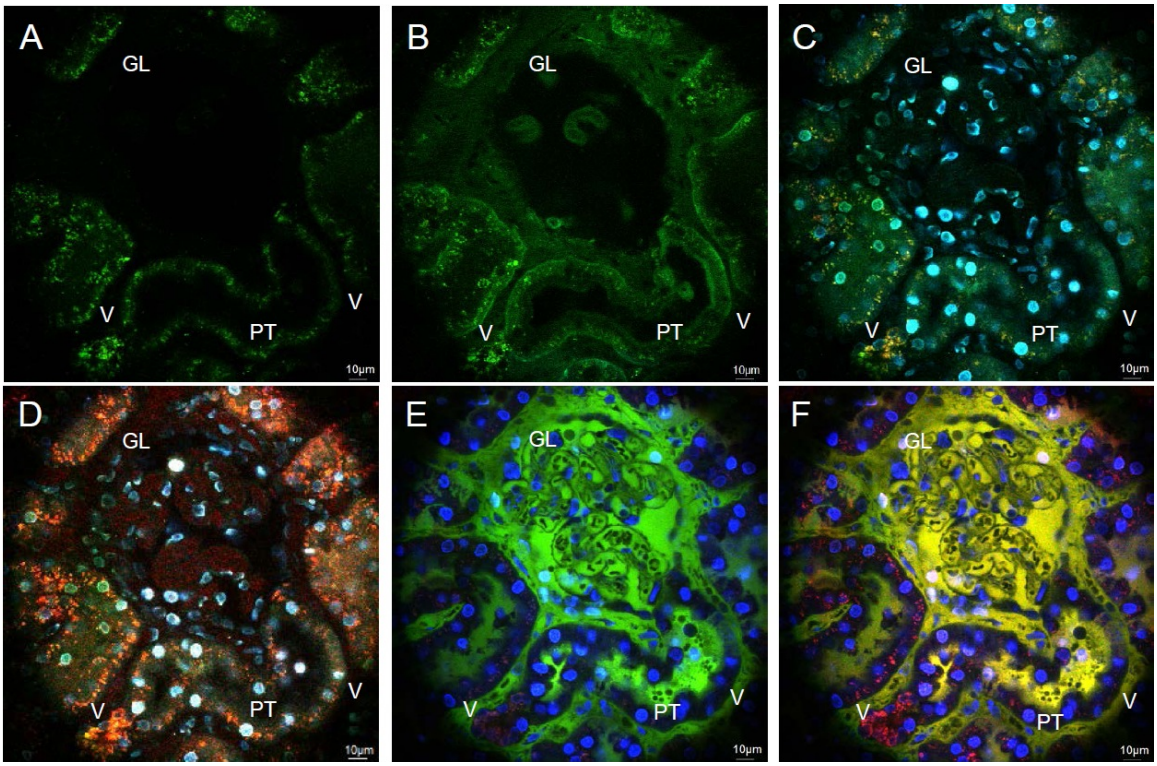

Figure 8. Renal function visualized with intravital two-photon fluorescence microscopy

Glomerular structure and function investigated in live rats that received sequential jugular vein infusions of Hoechst 33342, Texas-red labeled Albumin and 4 kDa FITC dextran solutions : (A) normal glomerulus with non-fluorescent peritubular and capillaries prior to dye infusions; (B) Hoechst is seen filling the peritubular and glomerular capillaries directly after its infusion through the jugula vein; (C) stained nuclei label vascular and tubular cells after the infusion of Hoechst; (D) image taken directly infusing Texas-red labeled Albumin highlights the vascular system and endocytic tubular protein uptake/reclamation; (E) and (F) images taken directly after the infusion of the 4 kDa FITC dextran molecules. These latter images illustrate glomerular filtration, and localization of both the albumin and FITC probes within tubule lumens and as internalized fluorescent puncta with proximal tubule epithelial cells (Glomerulus = GL; proximal tubule = PT; and vasculature = V). The ratio of albumin to dextran is the same in the capillaries as it is in the bowman's space signifying a variation from normal glomerular capillary integrity.

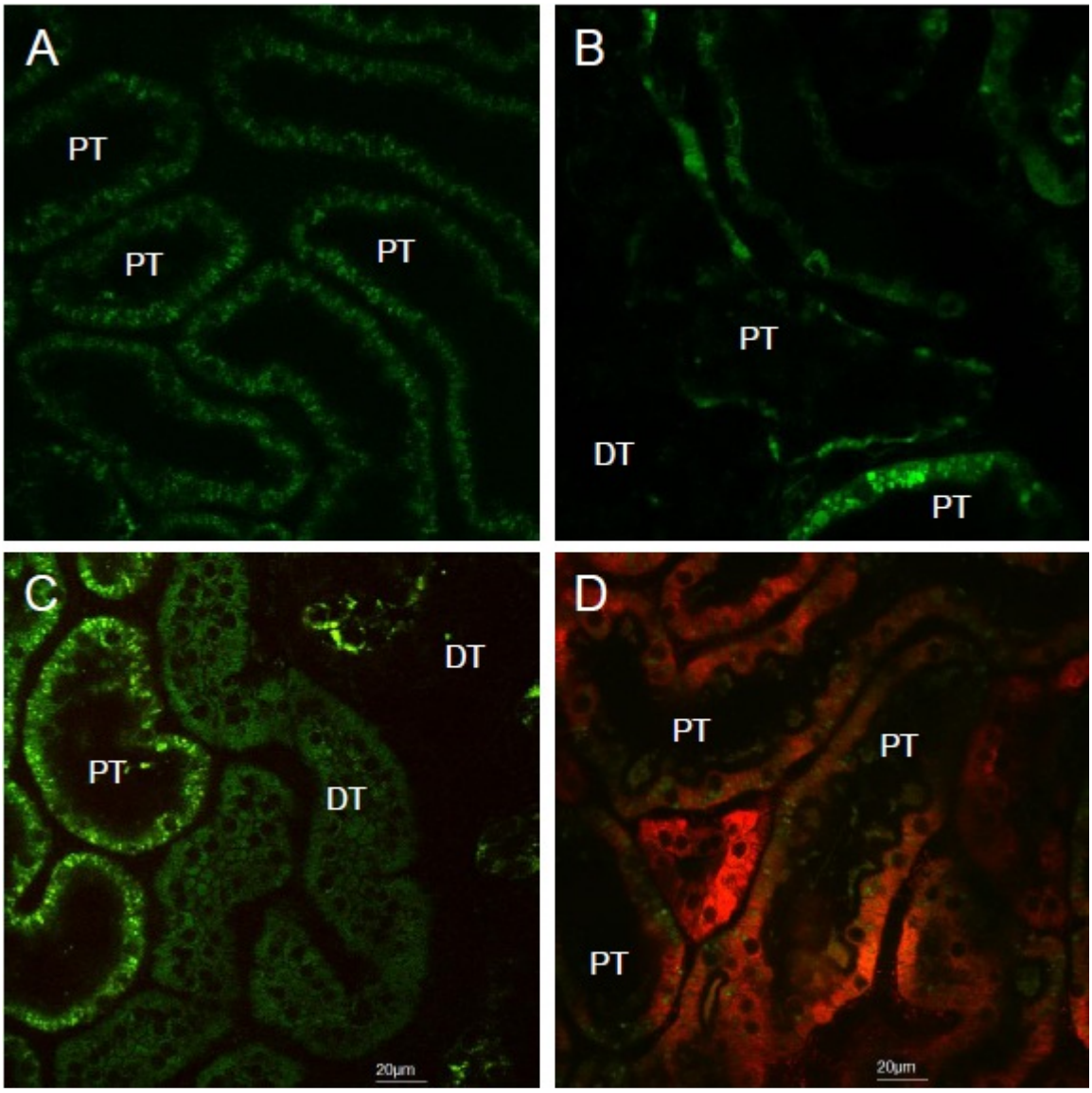

Figure 9. Nephrotoxicity alters normal renal function and structure
An outline of the changes in tissue autofluorescence, structure and function that can be observed from a nephrotoxic kidney when compared to a normal kidney using intravital two-photon microscopy: (A) uniform and punctate fluorescence pattern observed in a normal; (B) through (D) rats treated treated with 100 mg/kg of gentamicin for 2 weeks and imaged 8 days post treatment illustrate signs of patch necrosis, blebs, sloughed cells, casts in lumens, epithelial cells thinning, diminished brush borders, and an overall change

in innate autofluorescence patterns. These changes observed in the injured animal often make it difficult to identify various renal compartments. Moreover, image (D) outlines the reduced levels of proximal tubular endocytic uptake of a low molecular weight mitochondrial marker - Tetramethyl Rhodamine Methyl Ester (TMRM), and varied levels of mitochondrial activity within these cells.

By the eigth day, we observed a large quantity of blebs, sloughed cells and casts within tubular lumens and the supporting vasculature. There was also an overall reduction in proximal tubule brush borders and epithelial thickness (Figure 9D). These alterations are consistent with the documented impact aminoglycosides have on endocytic properties of proximal tubules[224,225]. These changes observed in injured animals often make it difficult to distinguish the various renal compartments.

b. Tissue autofluorescence, structure and function in the setting of ischemia-reperfusion injury

Rats with mild and moderate ischemia-reperfusion injury, generated from 10-15 minute and 30-45 minute bilateral renal pedicle clamps respectively, had microscopic renal damage similar to that observed in the rats with moderate to severe gentamicin-derived nephrotoxicity (Figure 10). The serum creatinine levels in these rats were also significantly elevated (generally greater than 3 mg/dl during the first 24 hours after inducing injury) above the normal baseline. However, the damage observed in the kidneys of rats given mild forms of ischemia-reperfusion injury, generated from 10-15 minute bilateral pedicle clamps, was less severe. Overall tissue fluorescence, structure and function were not significantly altered, and serum creatinine levels remained within a normal measurement range (0.4-0.6 mg/dl).

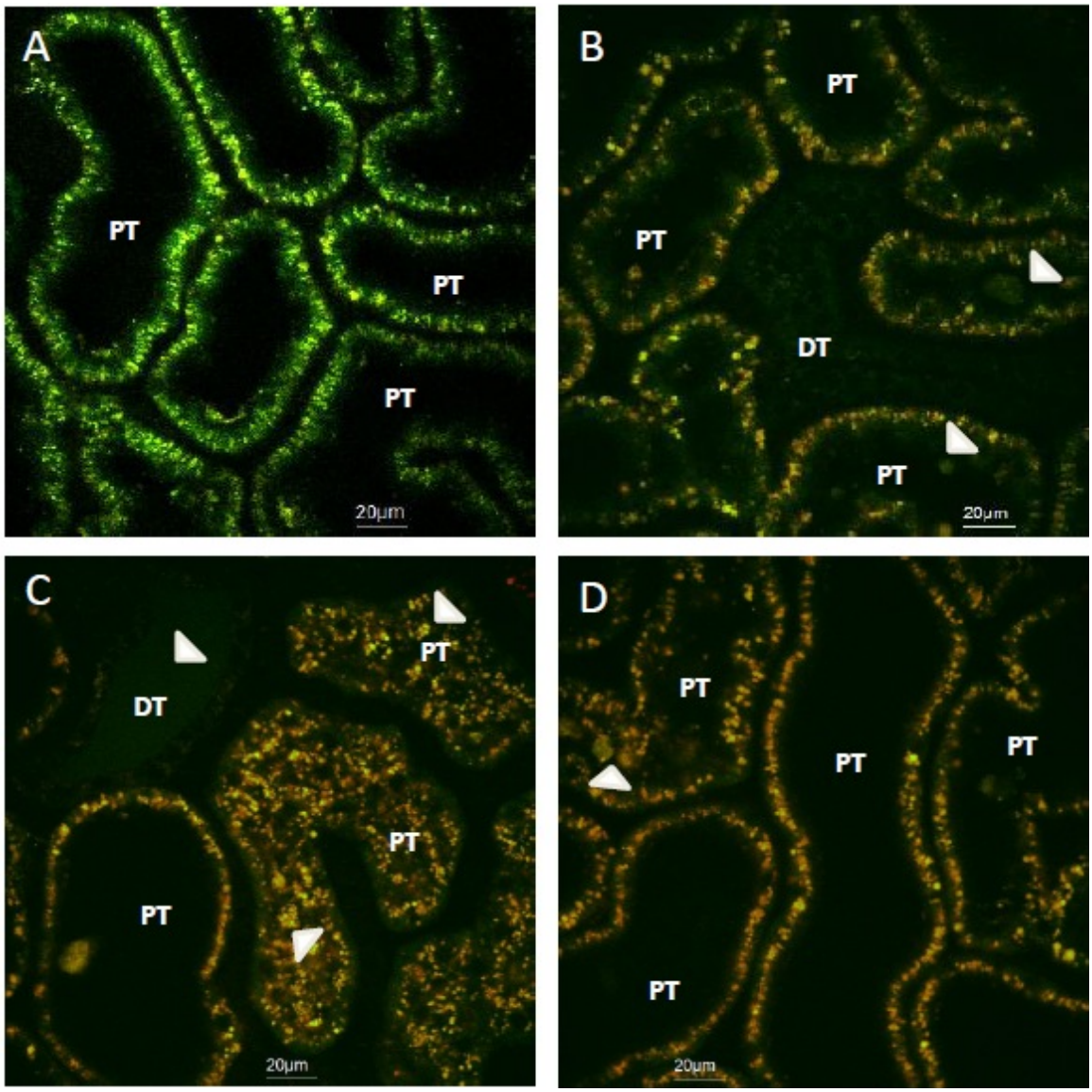

Figure 10. Ischemia-reperfusion injury alters normal renal function and structure
An outline of the changes in tissue autofluorescence, structure and function that can be observed from a kidneys with ischemia-reperfusion injury when compared to a normal kidney using intravital two-photon microscopy: (A) uniform and speckled fluorescent patterns observed in a rat with normal structure and function; (B) rat with mild ischemia-reperfusion injury (15 minute bilateral renal pedicle clamp), and (C) and (D) rats with moderate ischemia-reperfusion injury (30-45 minute bilateral renal pedicle clamp). As

with gentamicin-treated rats, images (B) and C) show blebs, sloughed cells, casts in lumens, epithelial cells thinning, and an overall change in autofluorescence pattern. Red, green and blue pseudo-colors were merged to form these images. Arrowheads indicate cellular debris that filled tubule lumens.

C. Characterizations of various methods designed to deliver exogenous fluid to the kidney

1. Systemic fluid delivery to the kidney in normal rats via jugular and tail vein infusions

High molecular weight (150 kDa) fluorescent dextran molecules delivered systemically through jugular and tail veins were characeristically restricted within the peritubular capillaries that surrounded intact proximal and distal tubules (Figures 11 and 12). This probe was widely distributed within the vasculature of nephron segments that were accessible for imaging by our two-photon microscope independent of the infusion method. This imaging techniuqe allowed us to successfully survey the extensive distribution of the fluorescent dye as a function of renal tissue depth.

2. Localized fluid delivery to the kidneys of normal rats

a. Renal capsule infusions in live normal rat kidneys

After injecting the same dextran used for jugular and tail vein infusions, we examined the renal distribution of this fluorescent probe. In this case, the 150 kDa FITC dextran molecules were again confined within the vasculature, but at a reduced level when compared to the results generated from systemic delivery (Figure 13). Specifically, 150 kDa dextan molecules delivered via renal capsule injections were restricted to narrow regions that surrounded the injection site, within highly superficial cortical zones (region within 20 μm from the surface). Also, this method also did not appear to significantly injure the kidney.

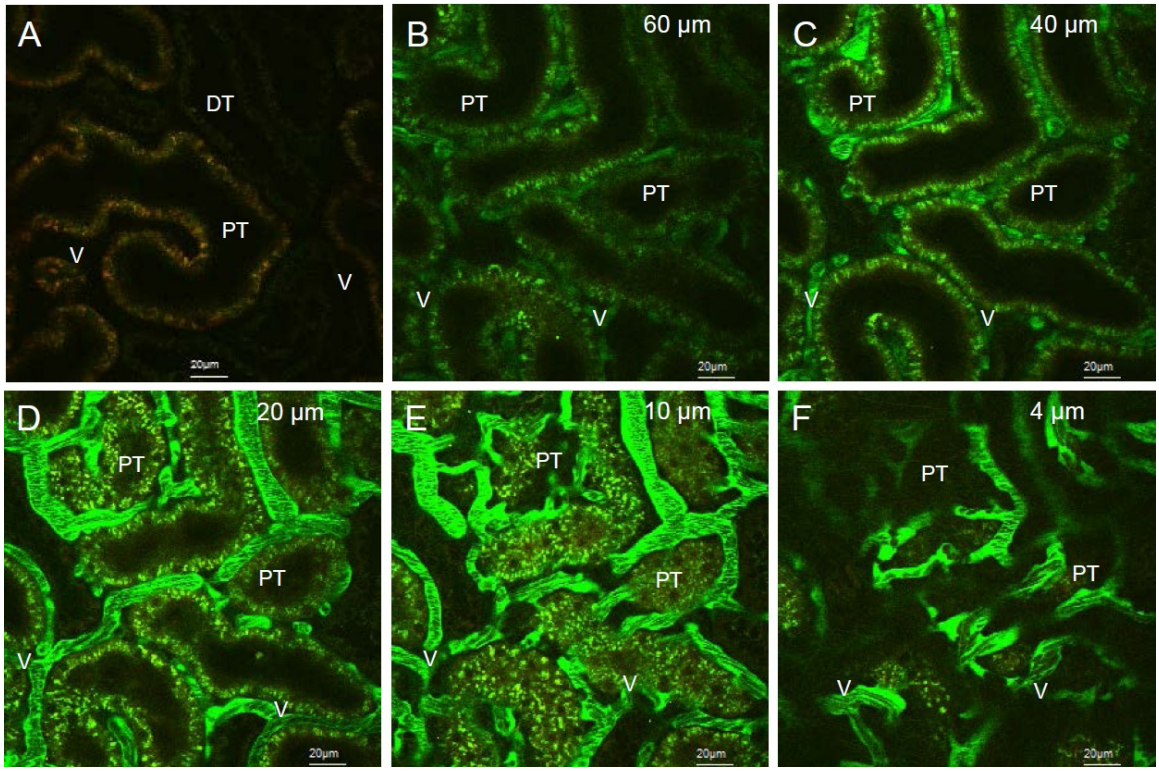

Figure 11. Jugular vein dye infusions used to aid the visualization of live normal rat kidney as a function of tissue depth

Images of normal tubular structure and function in live rats that received jugular vein infusions of a 150 kDa FITC dextran solution. These images were taken at various tissue depths: (A) tissue autofluorescence prior to dextran infusion approximately 40 µm from the capsule of the kidney; (B) approximately 60 µm from the capsule of the kidney; (C) approximately 40 µm from the capsule of the kidney; (D) approximately 20 µm from the capsule of the kidney; (E) approximately 10 µm from the capsule of the kidney; and (F) at the level of the renal capsule. These data show normal vasculature restriction of the large molecular fluorescent dextran. Proximal tubule (PT) and vasculature (V).

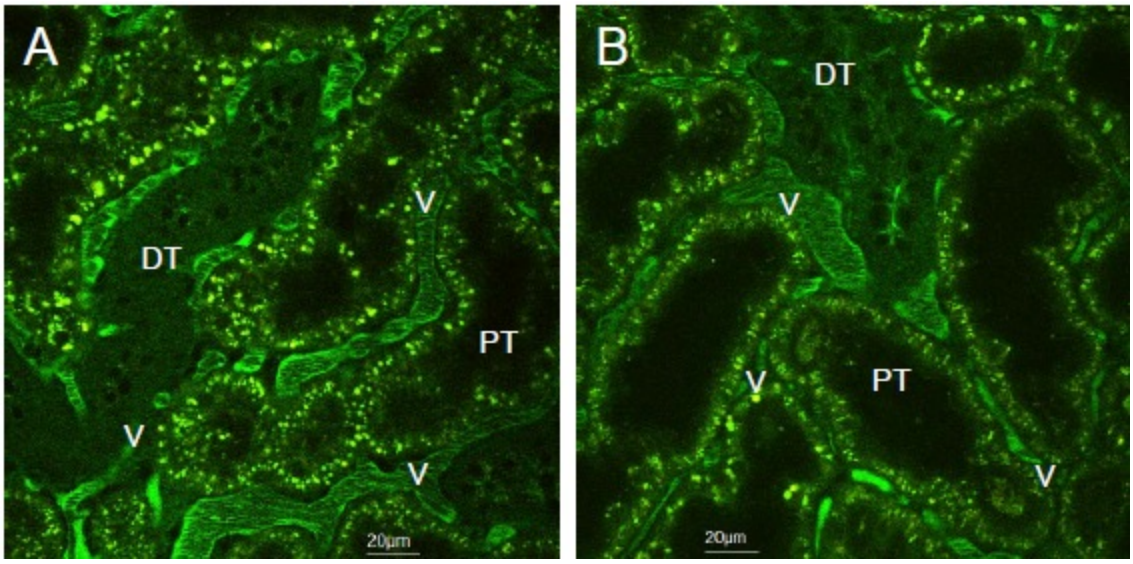

Figure 12. Tail vein dye infusions used to aid the visualization of live normal rat kidney as a function of tissue depth
Intravital micrographs fields taken from a live rat that received a tail vein injection of 150 kDa FITC dextran solution. These data show normal vasculature restriction of the large molecular probe. Proximal tubule (PT) and vasculature (V).

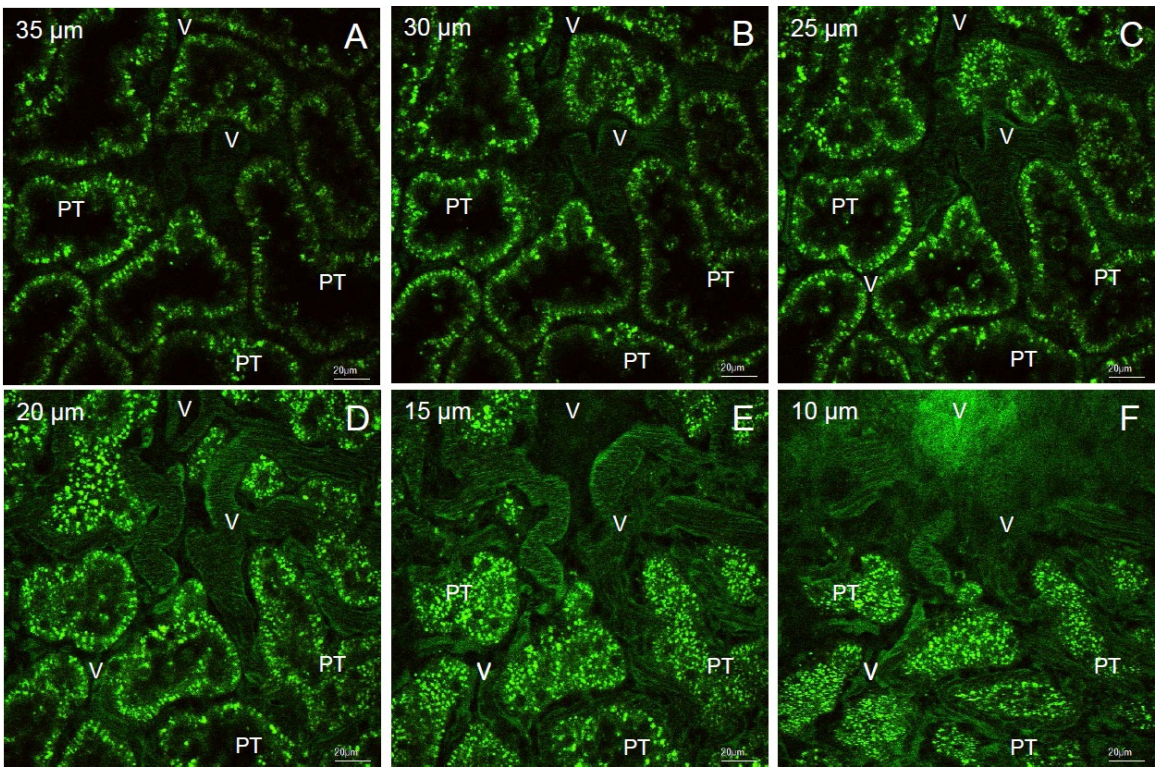

Figure 13. Renal capsule injections faclitate a limited distribution of exogenous probes that are only able to occupy the vasculature
Two-photon micrographs taken at various depths from below the renal capsule to illustrate the limited distribution of 150 kDa FITC dextran molecules injected into the renal capsule: (A) approximately 35 µm from the capsule of the kidney; (B) approximately 30 µm from the capsule of the kidney; (C) approximately 25 µm from the capsule of the kidney; (D) approximately 20 µm from the capsule of the kidney; (E) approximately 15 µm from the capsule of the kidney; and (F) approximately 10 µm from the capsule of the kidney. These data show normal vasculature restriction of the large molecular probe. Proximal tubule (PT) and vasculature (V). These micrographs illustrate significant degree of the large molecular weight dye within the vasculature as anticipated. The dye was not distributed uniformly throughout the kidney and was restricted to a region that surrounded the injection site.

b. Hydrodynamic fluid delivery in live normal rat kidneys

i. Catheter-based renal artery infusions

We utilized the full effect of the pressurized injection system, under conditions of hydrodynamic equilibrium, by inserting PE-50 catheters into renal arteries of live rats and rapidly injected 150 kDa FITC dextran solutions proximal to the point of ligation. After such injections, various microscopic fields that were taken from these live rat kidneys illustrated the widespread distribution of dextran molecules within various nephron cross sections (Figure 14). The dextran molecules accessed the microvasculature, as well as lumens and apical borders of proximal and distal tubules. This in turn facilitated their vesicular internalization by renal tubular epithelia. Unfortunately, this welcomed internalization was accompanied by ample and irreversible injury from arterial ligations.

ii. Catheter-based renal vein infusions

We again investigated the full effect of the pressurized injection system, under conditions of hydrodynamic equilibrium, by inserting a PE-50 catheter into the renal vein. In this case, intermediate molecular weight fluorescent albumin molecules were injected into catheterized renal veins of live rats. Again, as with the renal catheter infusions, this hydrodynamic manipulation resulted in the robust and instantaneous distribution of albumin in vascular and tubular compartments in live animals (Figure 15). The images presented within 20 minutes of the albumin infusion. Additionally, as with the arterial studies, the catheter-induced ligation produced extensive disruptions to renal blood flow, resulting in collapsed vessels and sloughed cells within tubular lumens.

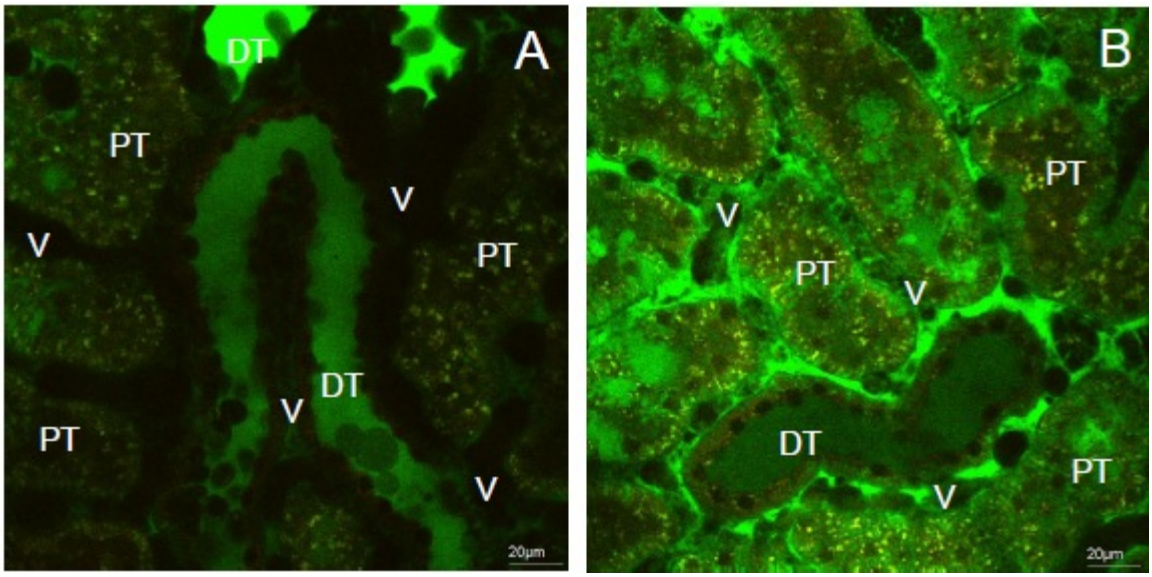

Figure 14. Catheter-based renal artery injections facilitate the widespread delivery of large molecular weight exogenous probes to the tubular epithelia at the expense of significant renal injury

Microscopic fields were taken from a live rat that received a hydrodynamic injection of 150 kDa FITC dextran molecules that were infused through the ligated renal artery, via a PE-50 catheter. There was widespread distribution of dextran molecules throughout the kidneys that appeared within lumens of proximal and distal tubules, and were internalized by proximal tubule epithelial cells. However, we also observed signs of significant renal injury such as constricted vessels, occluded lumens, and lumens that contained a noteworthy concentration of blebs.

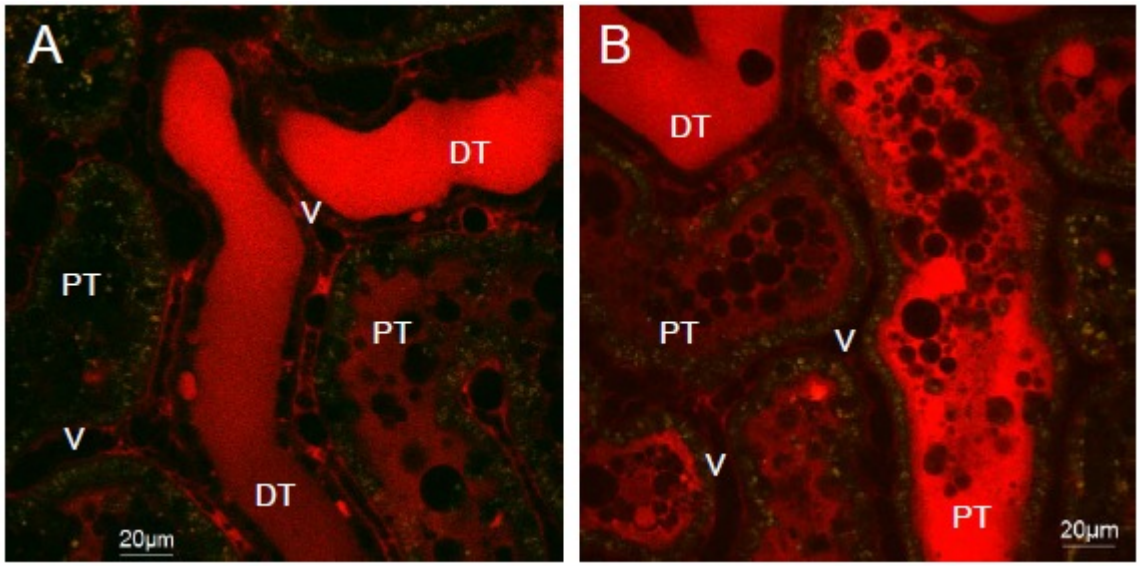

Figure 15. Catheter-based renal vein injections facilitate the widespread delivery of exogenous albumin to the tubular epithelia at the expense of significant renal injury
Intravital two-photon microscopy images illustrating the distribution of Texas red-labeled albumin within a rat kidney generated from a catheter-based hydrodynamic renal vein infusion. The dye was infused into the left renal vein through a PE-50 catheter that completely ligated this vessel. The fluorescent albumin can be seen within the distal tubules (DT), proximal tubules (PT) and vasculature (V). Distal tubules are known to display significantly lower autofluorescence signals that proximal tubules.

iii. Fine-needle hydrodynamic renal artery injections of fluorescent dextrans with vascular clamps

Live rats received fine-needle (30-gauge stainless steel needle) intra-arterial hydrodynamic injections of 5 kDa and 150 kDa FITC dextran molecules. During these injections we either clamped the renal vein for a period of 5 minutes, or both renal vein and aorta for the same period of time. Both cases resulted in simultaneous distribution of low (Figures 16) and large (Figure 17) dextran molecules throughout the kidney.

These pressurized injections, however, did not facilitate robust and widespread vascular distribution of either 5 kDa or 150 KDa FITC dextran molecules. Interestingly, as with catheter-based infusions, the technique faciliated uncharacteristic filtration, and proximal tubular brush border localization and internalization of 150 kDa FITC dextran molecules. However, this was achieved at the expense of significant ischemic injury. This injury was cleary highlihted after infusing 150 kDa TRITC dextrans molecues through the jugular veins of these rats within 30 minutes of them receiving arterial hydrodynamic injections. This venous infusion produced substantial alterations to normal microvascular, glomerular and tubular structure and function similar to the arterial injections.

iv. Fine-needle renal vein injections of fluorescent dextrans without and with vascular clamps

Saline solutions containing both low (3 kDa Cascade Blue or 4 kDa FITC) and large (150 kDa TRITC) molecular weight dextrans were injected into the left renal veins of live rats, at different infusion rates (injections were conducted within 10 seconds, and

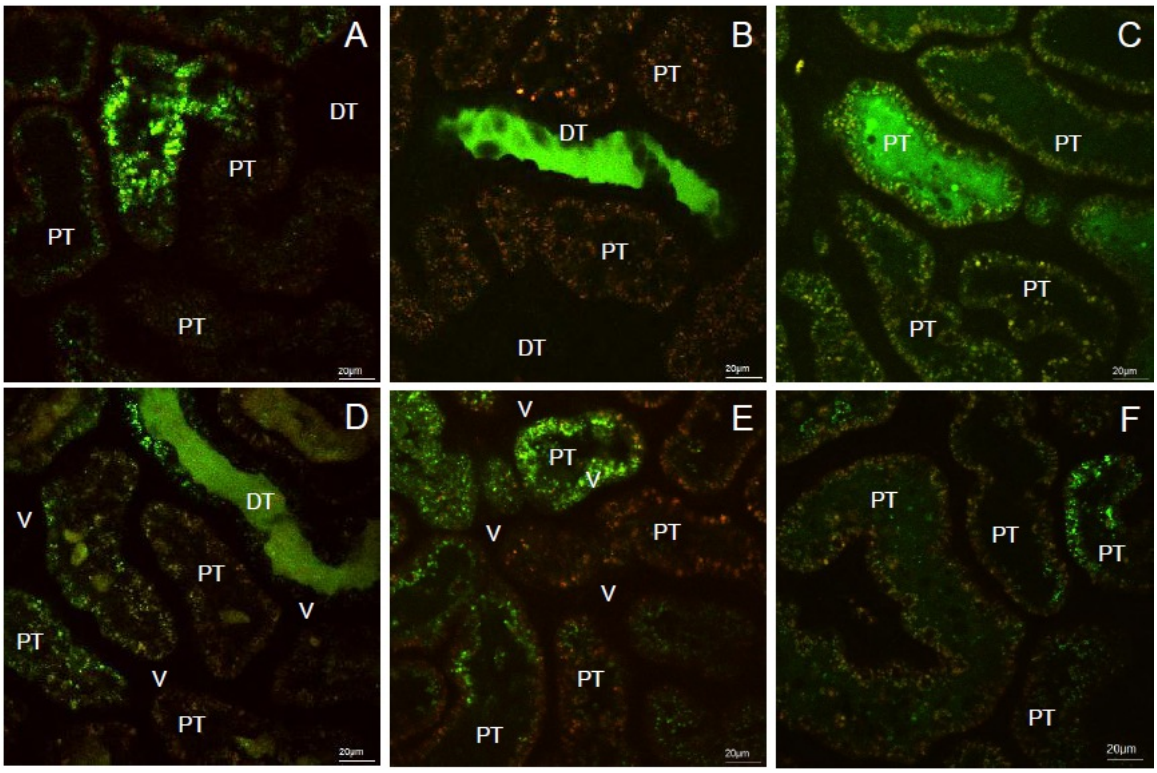

Figure 16. Hydrodynamic fine needle renal arterial injections facilitate the widespread delivery of low molecular weight exogenous probes to the tubular epithelia at the expense of significant renal injury

Various microscopic fields taken from a live rat that received a hydrodynamic injection of 5 kDa FITC dextran molecules infused into the renal artery with only the renal vein clamped for a period of 5 minutes. There was an uneven distribution of dextran molecules throughout the kidney, and a relatively low proportion of these molecules appeared to be endocytosed by proximal tubule epithelial cells. This process generated significant injury illustrated by the patchy distribution of the dextran molecules and fluorescent debris and non-fluorescent blebs within proximal and distal tubule lumens.

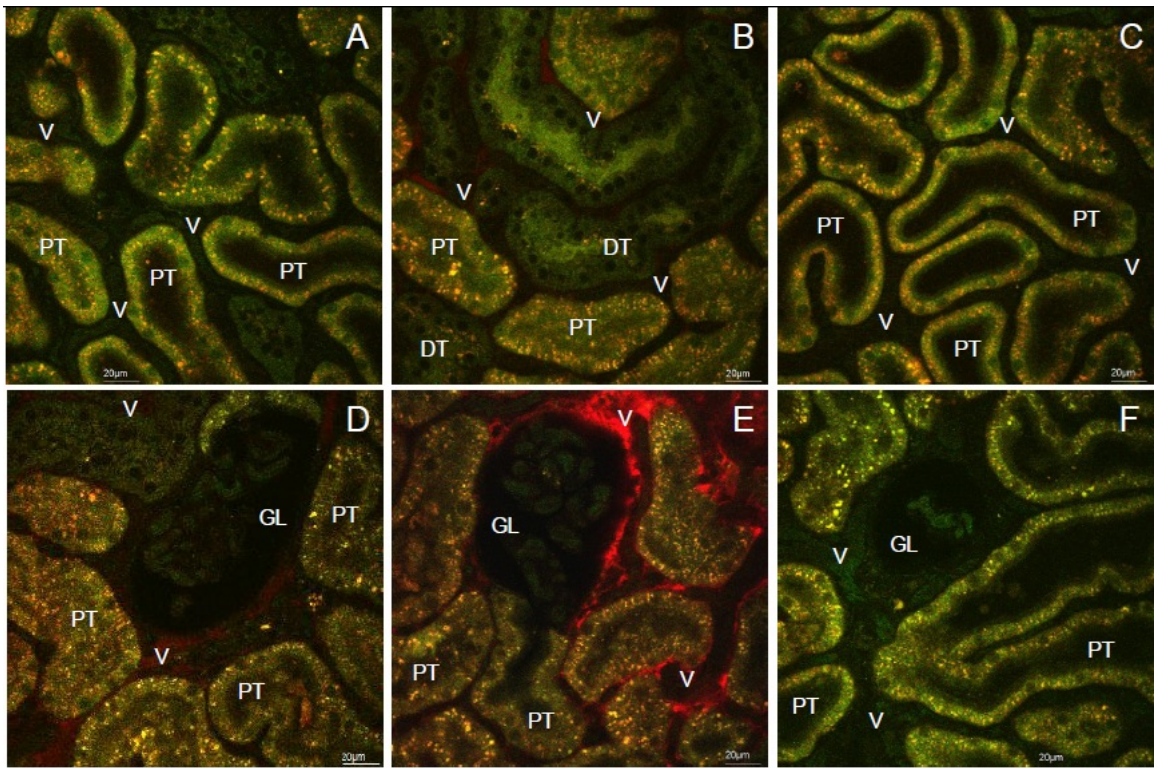

Figure 17. Hydrodynamic fine needle renal arterial injections facilitate the widespread delivery of large molecular weight exogenous probes to the tubular epithelia at the expense of significant renal injury

Microscopic fields taken from a live rat that received a hydrodynamic injection of 150 kDa FITC dextran molecules infused into the renal artery with a single aorta clamp and renal vein clamp, followed by a subsequent (beyond 20 minutes) jugular vein infusion of 150 kDa TRITC dextran. There was a significant amount of blood loss and pressure was applied for period of 10 minutes to the injection site to close the wound. These data illustrate a low and uneven distribution of these large molecular weight dextran molecules throughout the vasculature kidney as observed within glomerular (GL) and peritubular capillaries (V). The combination of hydrodynamic fluid delivery and injury generated from the injection procedure provided these FITC molecules access to tubular lumens. There is a more uniform fluorescent signal, which appeared throughout proximal tubule epithelial cells that may either signify the internalization of these large molecules or injury-based changes in tissue autofluorescence. TRITC dextran was subsequently infused. It also produced and patchy distribution further signifying significant injury.

2 and 4 minutes which corresponded to approximate injection rates of 0.1, 0.004 and 0.008 ml/s), using 30-gauge needles. The kidneys that received hydrodynamic delivery were imaged within approximately 20 minutes of injections. From the 0.1 ml/s rate hydrodynamic injections, conducted with (Figure 18A) and without vascular clamping (Figure 18B), we observed widespread uptake of both dextrans *in vivo*.

As anticipated, intravital micrographs obtained from these rats showed low molecular dextran molecules bound to brush border membranes of the proximal tubular epithelia. We also saw blue and green puncta in these epithelial cells after the internalization of the respective 3 kDa Cascade Blue and 4 kDa FITC dextrans, while concentrated levels in these dextrans appeared within distal tubule lumens. Again, the data are consistent with endocytic uptake of low molecular weight dextran molecules in rat kidneys[195,226]. These observations provided evidence that nephron segments could retain vital functional capacities after rapid fine-needle, hydrodynamic venous delivery.

We also observed that large molecular weight TRITC dextran molecules were widely distributed within the vasculature and internalized by tubular cells across apical and basolateral surfaces as a result of hydrodynamic delivery (Figures 19-21). Large molecular weight dextran molecules were also unexpectedly filtered by renal tubules (Figure 19). Nevertheless, atypical access these large molecular weight dextran molecules had to apical (Figure 20) and basolateral (Figure 21) membranes of proximal tubules was transient and appeared to only occur via the hydrodynamic injection process. In fact, when these 150 kDa molecules were infused through the jugular vein of live rats, they

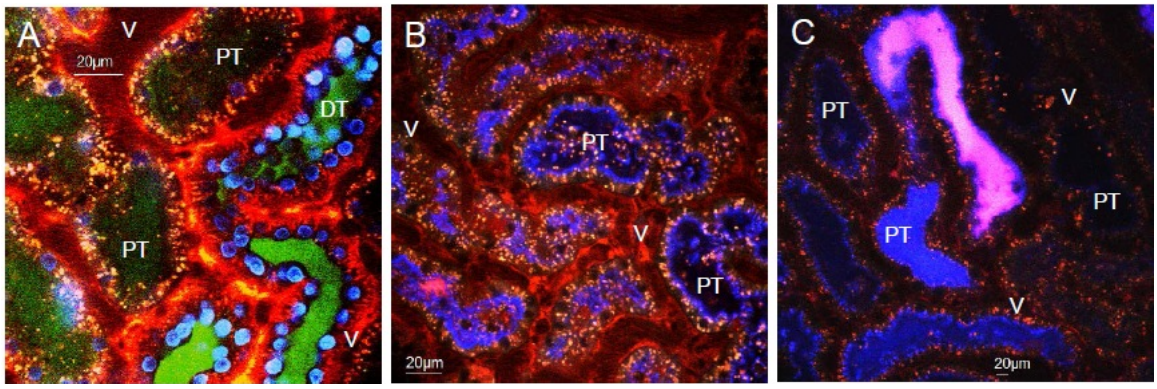

Figure 18. Hydrodynamic fine needle renal venous injections facilitate the widespread delivery of low molecular weight dextrans to the tubular epithelia with minimal renal injury

Intravital two-photon micrographs taken within 20 minutes after the simultaneous infusion of low (either 3 kDa Cascade Blue or 4 kDa FITC) and large (150 kDa TRITC) dextrans. These data illustrate the effects that result from varying the hydrodynamic injection rate and method (lower infusion volume and added vascular clamping). Each retrograde injection was performed using a 30-gauge needle. Signs of intact nephron structure and function are observed from image (A) 10-second long hydrodynamic injections, without vascular clamps, of 1 ml solution containing 3 kDa Cascade Blue and 150 kDa TRITC dextrans, and image (B) 5-second long injections (injection rate 0.1 ml/s), with vascular clamps, of 0.5 ml solution containing 4 kDa FITC and 150 kDa TRITC dextrans (Hoechst was added to label nuclei). In comparison, image (C) outlines that 4-minute long injections (injection rate 0.0042 ml/s), without vascular clamps, of 1 ml saline containing 3 kDa Cascade Blue and 150 kDa dextrans, produce vascular constriction, tubular blockage and irregular filtration of the large 150 kDa TRITC dextran.

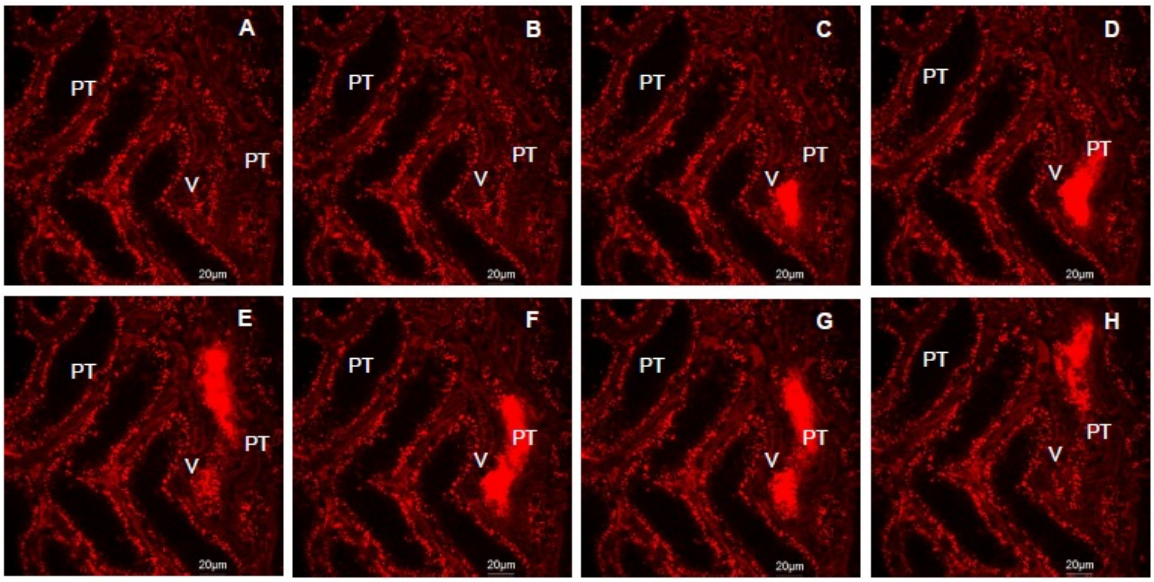

Figure 19. Hydrodynamic fine needle venous delivery facilitates the atypical filtration of large molecular weight dextrans
Intravital two-photon fluorescent micrographs taken from a live rat within 20 minutes of it receiving a hydrodynamic injection of a solution containing 150 kDa TRITC dextran molecules. These images were taken sequentially to outline the dextran molecules being filtered by proximal tubules.

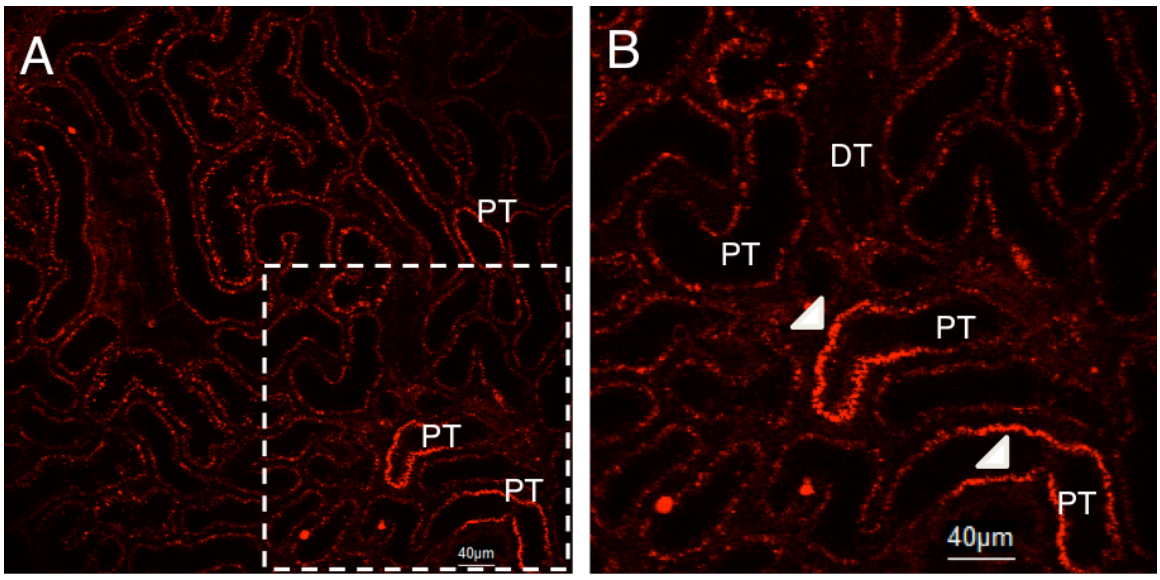

Figure 20. Hydrodynamic fine needle venous delivery facilitates the uncharacteristic internalization of large molecular weight dextrans by the tubular epithelia
Intravital two-photon fluorescent micrographs taken from a live rat within 20 minutes of it receiving a hydrodynamic injection of a solution containing a mixture of 150 kDa TRITC and 3 kDa Cascade Blue dextran molecules. These images outline evidence of the atypical internalization of the large TRITC dextran molecules within proximal tubules (PT). Image (B) through is a magnified image taken from the region highlighted in (A) by the dotted outline. Arrowheads indicate proximal tubule epithelial cells that have incorporated the low and high molecular weight dextrans along apical borders.

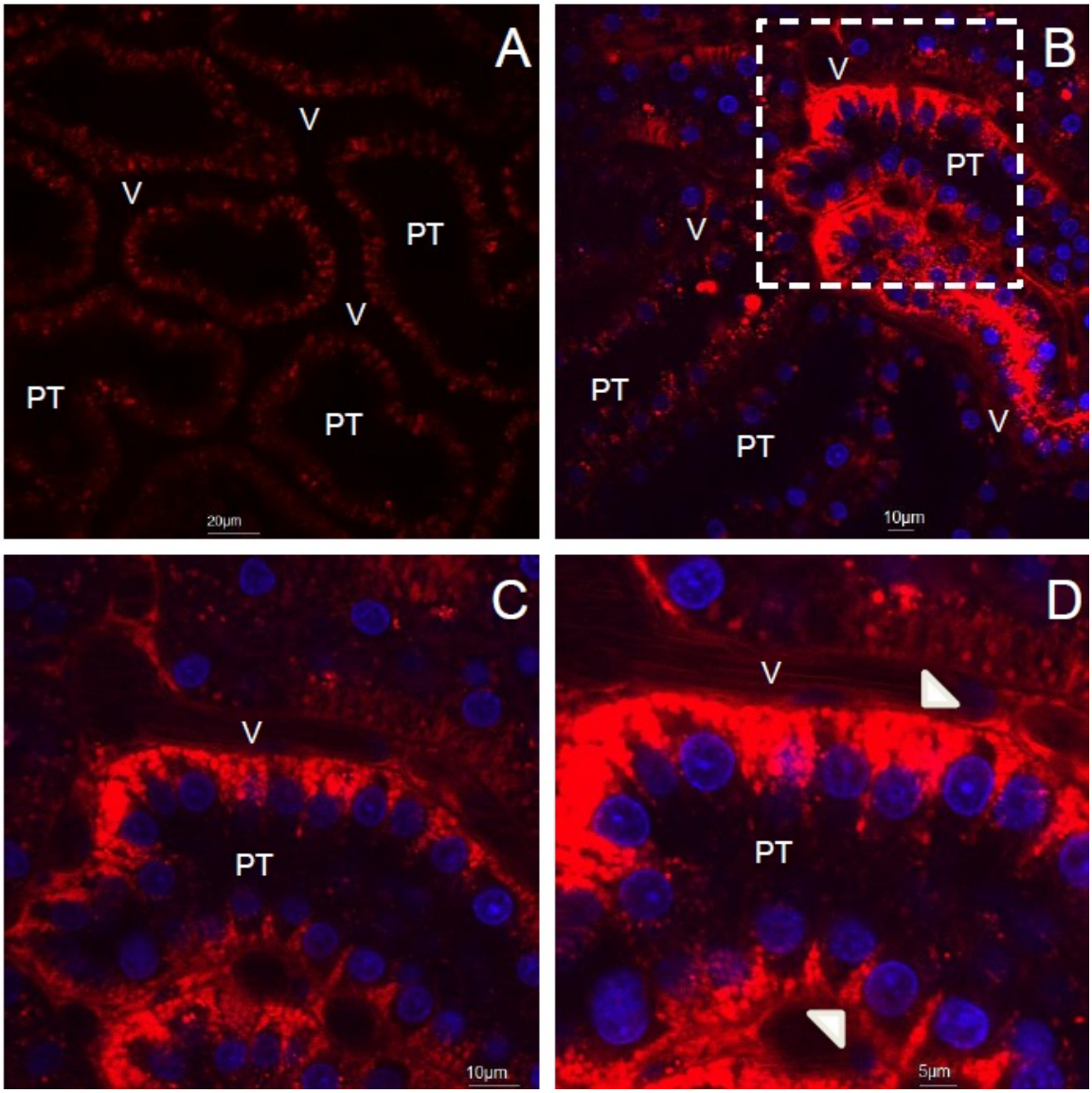

Figure 21. Hydrodynamic fine needle venous delivery facilitates the atypical basolateral uptake of large molecular weight dextrans
Intravital two-photon fluorescent micrographs taken from a live rat before and approximately 20 minutes after it received a hydrodynamic injection of a solution containing 150 kDa TRITC dextran molecules. These images demonstrate that renal tubular cells internalize high molecular weight dextran molecules. Image (D) is a magnified image taken from the region highlighted in (B) by the dotted outline. Arrowheads indicate proximal tubule epithelial cells that have incorporated the low and high molecular weight dextrans along basolateral membranes.

were primarily confined to the vasculature and were not detected at significant levels in the tubule lumen or epithelia when they were injected 5 minutes before hydrodynamic injection of saline into the renal vein (Figure 22A). Similar vascular restriction was observed when 150 kDa dextran molecules were infused through the jugular vein roughly 20 minutes after rats received hydrodynamic saline injections (Figure 22B).

Remarkably, as we decreased the injection rate from 0.1 ml/s to 0.0008 ml/s (10 seconds to 4 minutes) our ability to successfully deliver these large exogenous probes across cell membranes, without generating substantial renal injury, was dramatically reduced. As we decreased our injection rate, the concentration of exogenous large molecular weight dextran molecules that entered renal cells decreased. Furthermore, low rate injections, administered at approximately 0.004 ml/s (total injection period of approximately 4 minutes), produced significant renal damage illustrated by vasculature constriction, reduced blood flow, tubular blockages impeding renal filtration, reduced endocytic uptake of low and large molecular weight dextrans (Figure 18C).

v. Fine-needle renal vein injections of toluidine blue dye without and with vascular clamps

We harvested whole left and right kidneys, hearts, livers, lungs and spleens from rats that received hydrodynamic injections of 0.5 ml of toluidine blue dye to investigate the extent of whole organ uptake that could be attained using these fine-needle injections. Saggital plane sections of these organs revealed robust distribution of the dye within the left (injected) kidney, and no traces within the contralateral kidney and the other organs

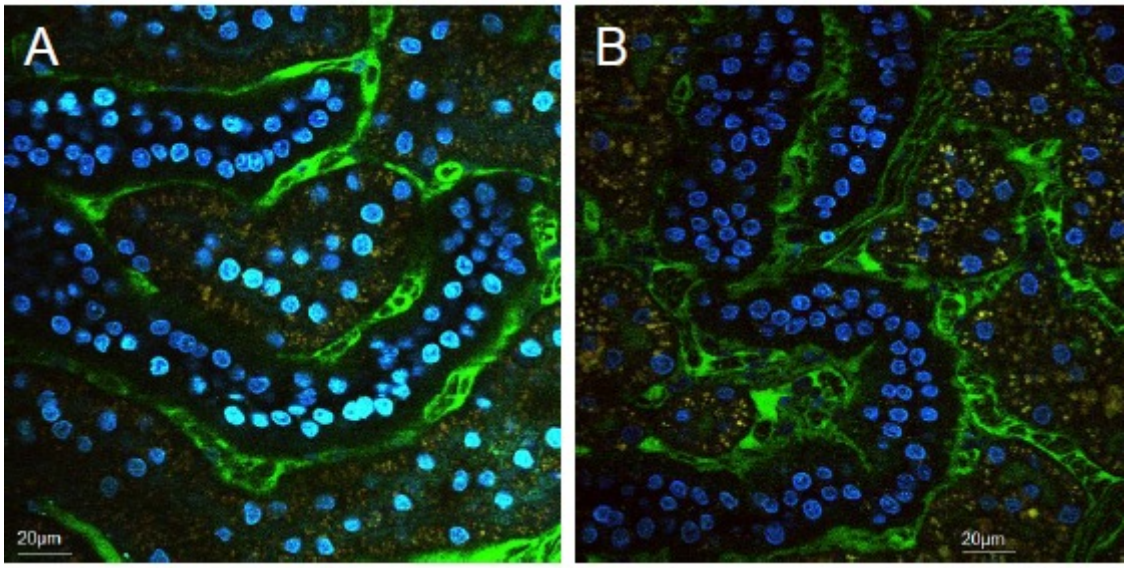

Figure 22. Normal renal tissue integrity is restored after hydrodynamic fine needle venous delivery
Intravital two-photon fluorescent micrographs taken from a live rat after it received a jugular infusion of 150 kDa FITC molecules: (A)immediately and (B) 30 minutes after receiving a renal vein hydrodynamic injection of a saline. These images show evidence of the restriction of the large FITC dextran molecules within the vascular compartments.

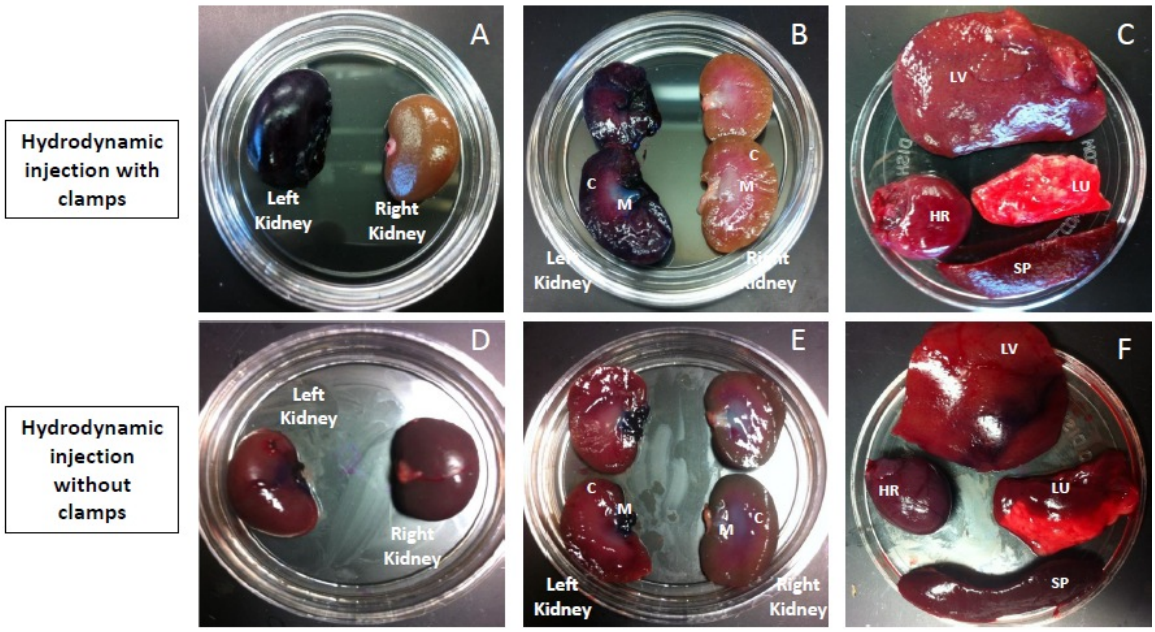

Figure 23. Hydrodynamic fine needle venous injections conducted with vascular clamping is sufficient to limit delivery to the target organ
Digital images of whole kidneys, livers, lungs and spleens were taken from rats that received retrograde hydrodynamic delivery of toluidine blue dye into the left renal vein. These kidneys were harvested and sectioned within 20 minutes of delivering the dye. The dye appears throughout the cortex and medulla of the left kidneys. However, the dye was absent in the contralateral kidneys. Note the following abbreviations: C = renal cortex; M = renal medulla; HR = heart; LV = liver; LU = lung; and SP = spleen.

examined when the injection process was perfomed with vascular cross-clamping (Figures 23A-23C).

In comparison, injections that were conducted without vascular cross-clamping facilitated minimal dye uptake in targeted left kidneys, and significant levels within aforesaid offsite and highly vascular organs (Figures 23D-23F). Overall, these results provided significant evidence that hydrodynamic renal injections, accompanied with vascular cross-clamping, are able to deliver substantial quantities of low, intermediate and large molecular weight substances to various cells throughout the entire kidney.

D. Plasmid- and viral-mediated transgene expression in live rats

1. Tissue autofluorescence is unalterted by the fluid delivery process

We conducted control experiments to determine if modifications in tissue autofluorescence would be mistaken for transgene-derived fluorescence. We thus examined rats that received sham (no injection) and saline injections. Superficial cortices (region within 100 μm of the kidney's surface) were imaged prior to and 3 days after receiving hydrodynamic treatments. From these data, there appears to be negligible differences between tissue fluorescence patterns observed in kidneys before and after receiving sham and saline injections (Figure 24).

2. Systemic transgene delivery did not facilitate renal transgene expression

From a pratical perspective, it would be most beneficial to be able to succesfully deliver trasngene to the kidney intravenously, via a system route. This method would

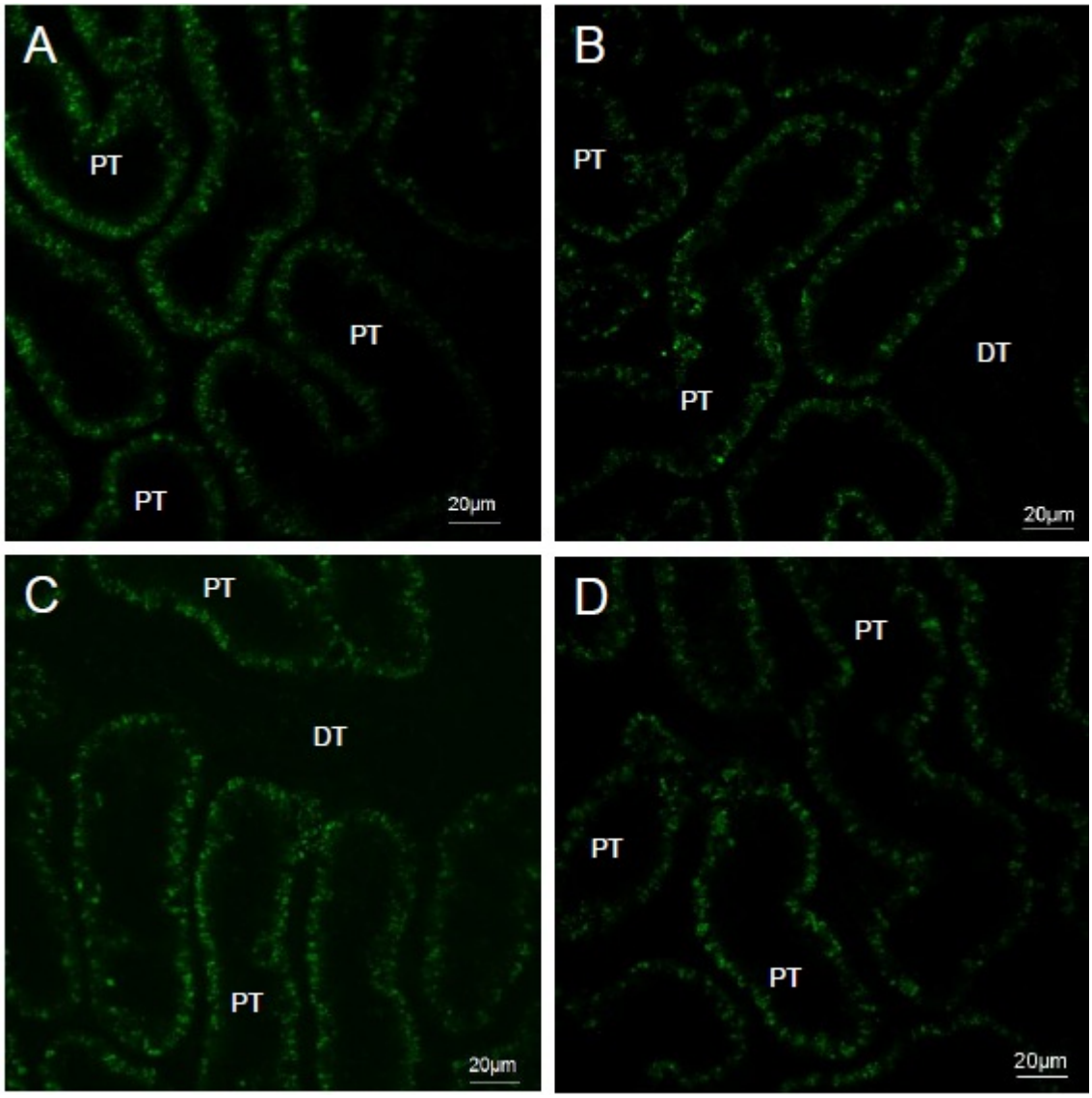

Figure 24. Hydrodynamic delivery does not alter innate tissue autofluorescence
Live rat kidney tubules micrographs obtained from animals prior to and 3 days after they received sham and hydrodynamic injections of saline: (A) rat kidney imaged prior to a sham injection, (B) kidney imaged 3 days after receiving a sham injection, (C) rat kidney imaged prior to a hydrodynamic injection of saline, (D) kidney imaged 3 days after receiving a hydrodynamic injection of saline.

provide the least invasive option. Unfortunely, plasmid, baculovirus and adenovirus vectors delivered via the tail vein did not facilitate transgene expression in rat kidneys (Figure 25).

3. Low levels of plasmid expression and significant levels of renal injury generated from fine-needle renal artery hydrodynamic injections

After realizing that we were incapable of generating effective gene transfer via systemic delivery, we shifted focused to localized gene delivery technique. We thought it possible to improve our chances of eliciting genetic transformation by infusing transgenes directly into the kidney, and first investigated renal arterial injections.

Accordingly, rare transgene expression was observed using arterial injections. The fluorescent protein expression was observed primarily in sloughed cells and casts that occupied tubule lumens (Figure 26). We conducted spectral analyses similar to those conducted to categorize transgene chimeric protein fluorescence in cell cultures (Figure 5F). From these results we again identified that transgene-derived fluorescence signal intensities were at least double those of autofluorescence signal intensities obtained *in vivo* (Figure 27C) and in fixed tissues (Figure 28C). This enabled us to clearly identify and differentiate transgene expression from autofluorescent backgrounds in the rat kidney. Moreover, arterial injections, generated significant periods of ischemia-reperfusion injury. Hemorrhaging was frequent, which complicated our attempts to induce hemostasis at the injection site. As a result of these surgical complications and unreliable renal transduction, we halted further investigations using arterial injections.

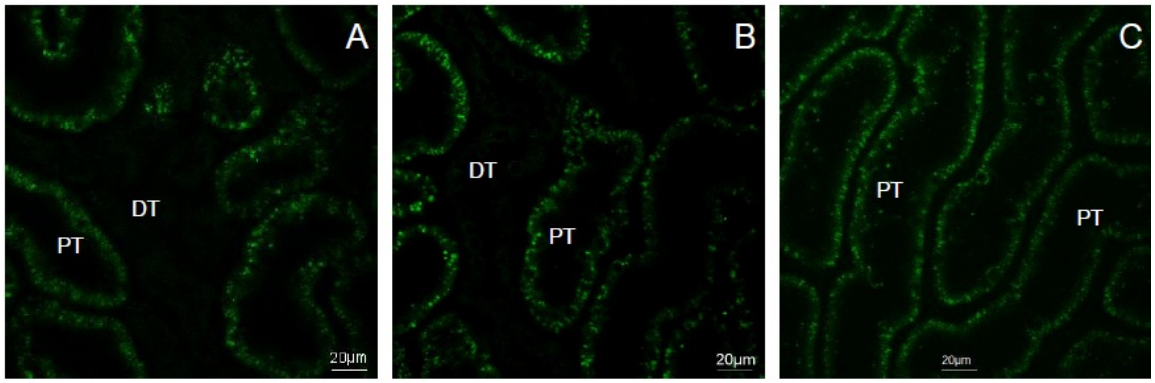

Figure 25. Tail vein injections were incapable of facilitating renal transformation
Intravital two-photon micrographs taken of left kidneys from rats that received transgene treatments via tail vein injections: (A) autofluorescent background before the tail vein injection; (B) image of the same kidney taken 3 days after the tail vein injection of baculovirus vectors; and (C) another image taken from a rat 3 days after it received tail vein plasmid infusion.

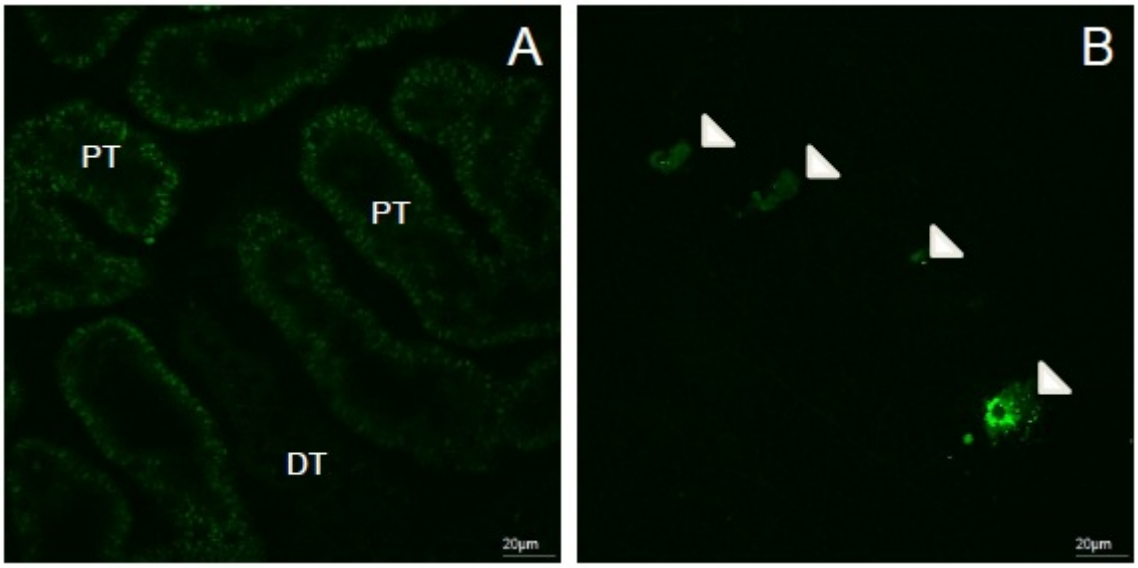

Figure 26. Hydrodynamic renal artery injections of plasmid-DNA rarely facilitated transgene expression within the superficial cortex
Images taken from a rat that received an arterial injection of plasmid EGFP DNA and Optison microspheres. Image (A) was obtained close to the renal capsule and illustrates regions with a fluorescent signal. However, it was not possible to decipher any specific compartment from which these signals emanated. Furthermore, as we imaged deeper into the superficial cortex we were unable to observe any fluorescent signals, but merely innate tissue autofluorescent patterns, as present in (B). Arrowheads indicate regions of transgene expression.

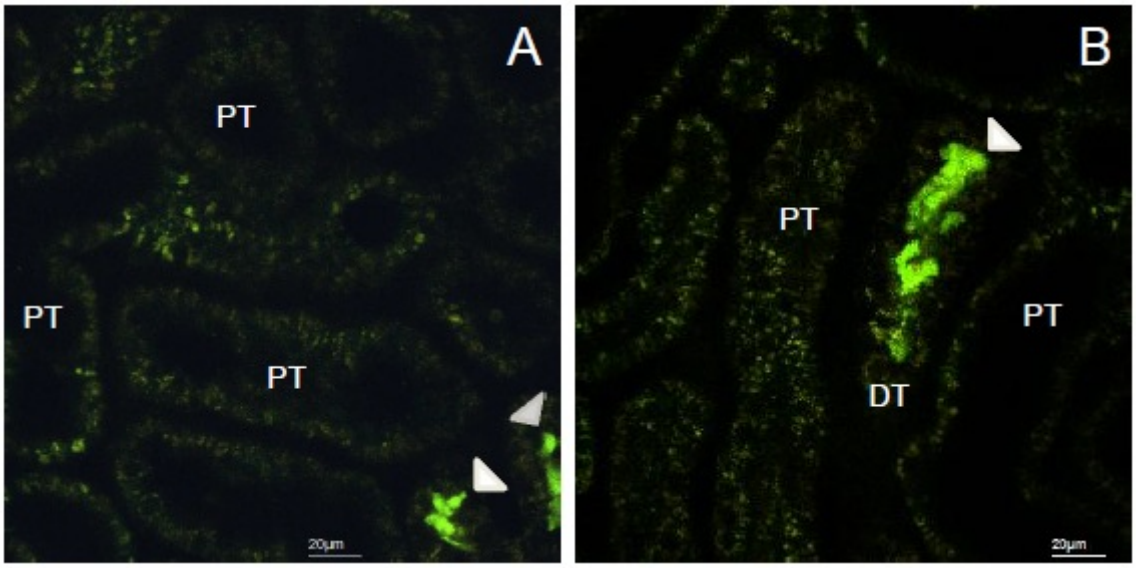

Figure 27. Hydrodynamic renal vein injections of plasmid-DNA conducted without vascular clamps facilitated limited levels of transgene expression within the superficial cortex

Images taken from a rat that received a renal vein injection of plasmid EGFP DNA and Optison microspheres. Image (A) and (B) illustrate regions with transgene-based fluorescence. However, it was not possible to decipher any specific compartment from which these signals emanated. Furthermore, as we imaged deeper into the superficial cortex we were unable to observe any fluorescent signals, but merely innate tissue autofluorescent patterns. Arrowheads indicate regions of transgene expression as sloughed materials occupying tubular lumens.

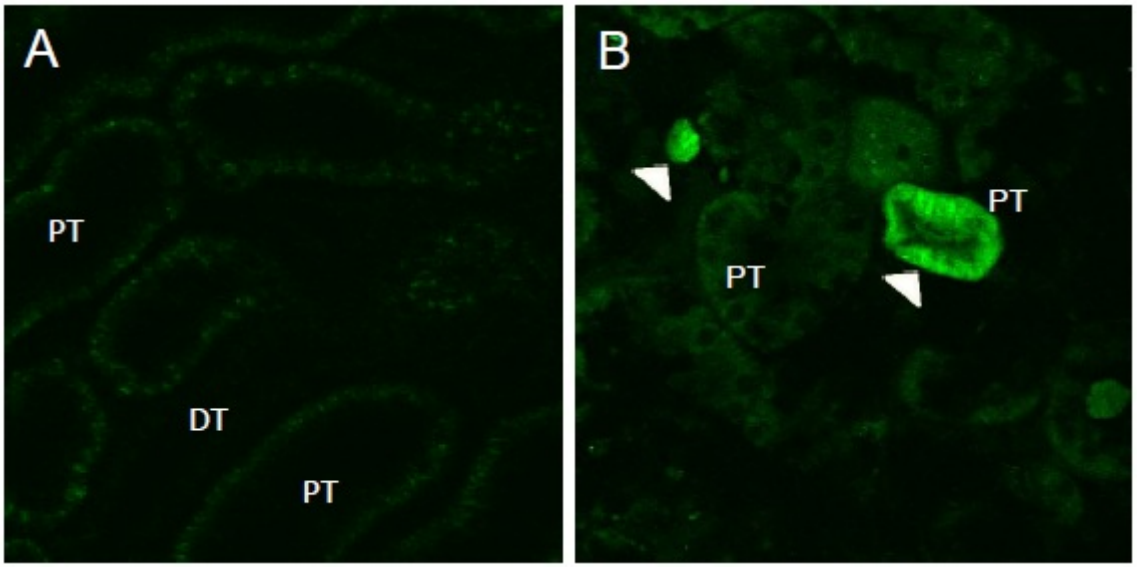

Figure 28. Hydrodynamic renal vein injections of plasmid-DNA conducted without vascular clamps facilitated limited levels of transgene expression within the renal medulla

Images taken from a rat that received a venous injection without clamps of plasmid EGFP DNA and Optison microspheres. Image (A) tissue autofluorescence taken prior to the injection process in the live animal, and (B) an image taken from a kidney section acquired 3 days after transgene delivery. Arrowheads indicate regions of transgene expression that appear within tubular debris and throughout an entire tubule.

4. Minimal plasmid expression generated from low volume (0.2 ml), fine-needle renal vein hydrodynamic injections conducted without vascular clamps

We next attempted to deliver plasmid DNA via the renal vein. Hydrodynamic injections using relatively low fluid volumes, 0.2 ml, conducted without vascular clamps also produced low levels of expression. Particularly, this technique generated rare expression *in vivo* using plasmids. Transgene expression detected in live rat kidneys was observed primarily in sloughed cells and debris that filled tubular lumens (Figure 27).

Realizing our limited *in vivo* imaging depth confines investigations to superficial cortical regions of the kidney, we harvested these rat kidneys and imaged various sections within deeper cortical segments and the renal medulla. From these sections we also observed tubular transgene expression, this time within intact epithelial cells (Figure 28). However, there was no overall significant improvement in the extent of transgene expression observed from these tissue sections.

5. Large volume (0.5-1 ml), fine-needle retrograde hydrodynamic injections, conducted without vascular clamps, into the renal vein improved levels of viral transgene expresion in live rats

Relatively large volume (0.5-1 ml) hydrodynamic renal vein injections significantly improved the extent of transgene expression in live rat kidneys using viral vectors. Baculovirus-based fluorescent protein expression was observed in the glomerulus (Figure 29), and in the proximal and distal tubules of live rats (Figure 31).

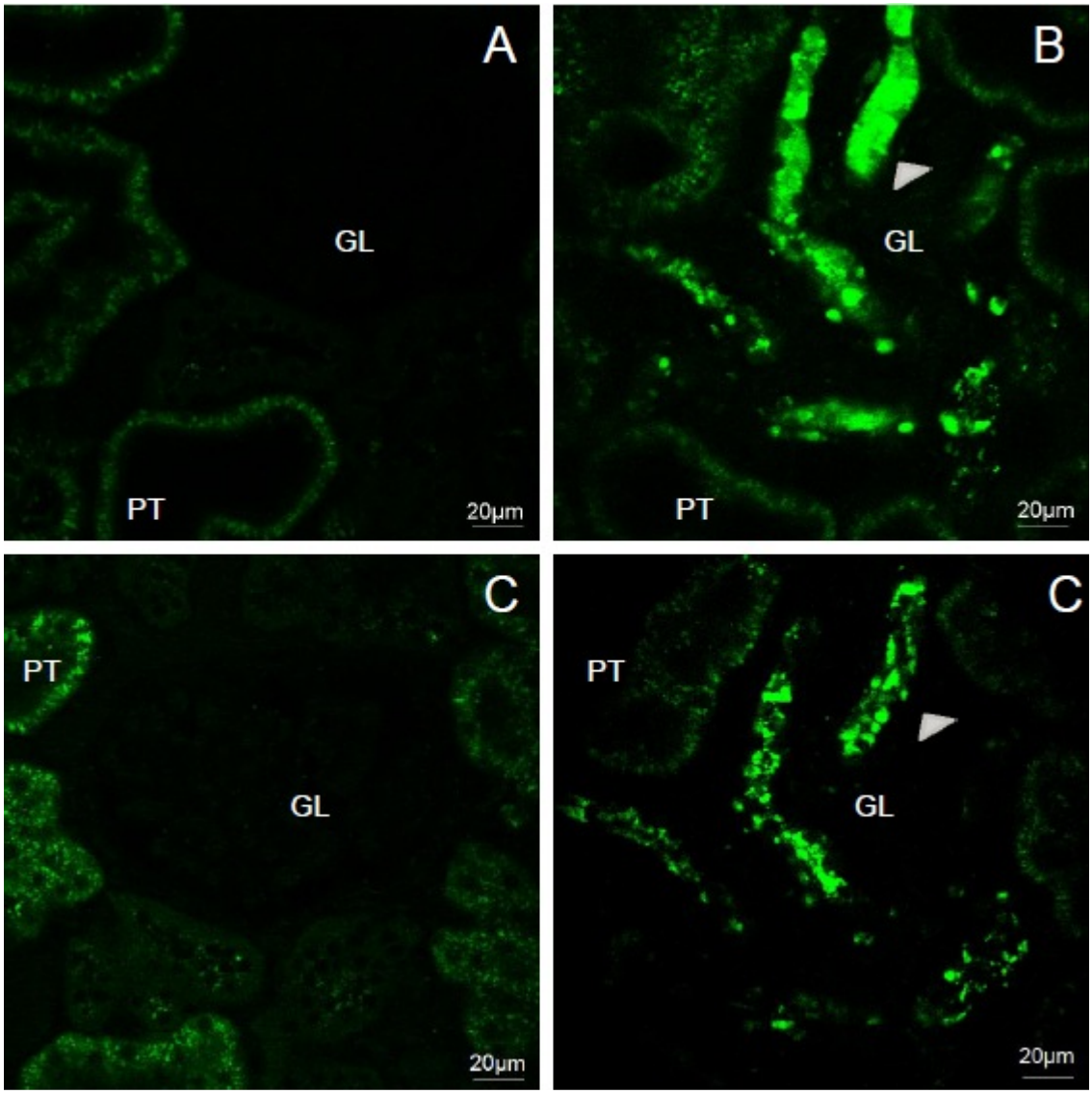

Figure 29. Baculovirus-based fluorescent protein expression within live glomeruli
Intravital two-photon microscopy images taken of live glomeruli in two Munich Wistar rats prior to GFP baculovirus hydrodynamic treatment, images (A) and (C), and 3 days post treatment, images (B) and (D). Images (A) and (B) were both taken from one animal, while (C) and (D) were taken from the another rat using the equivalent data acquisitions settings. Fluorescent transgene expression can be observed within the Bowman's space of the glomerulus (GL) presented in images (B) and (D). The Bowman's space identified by their innate lack of fluorescence. Arrowheads indicate regions of transgene expression.

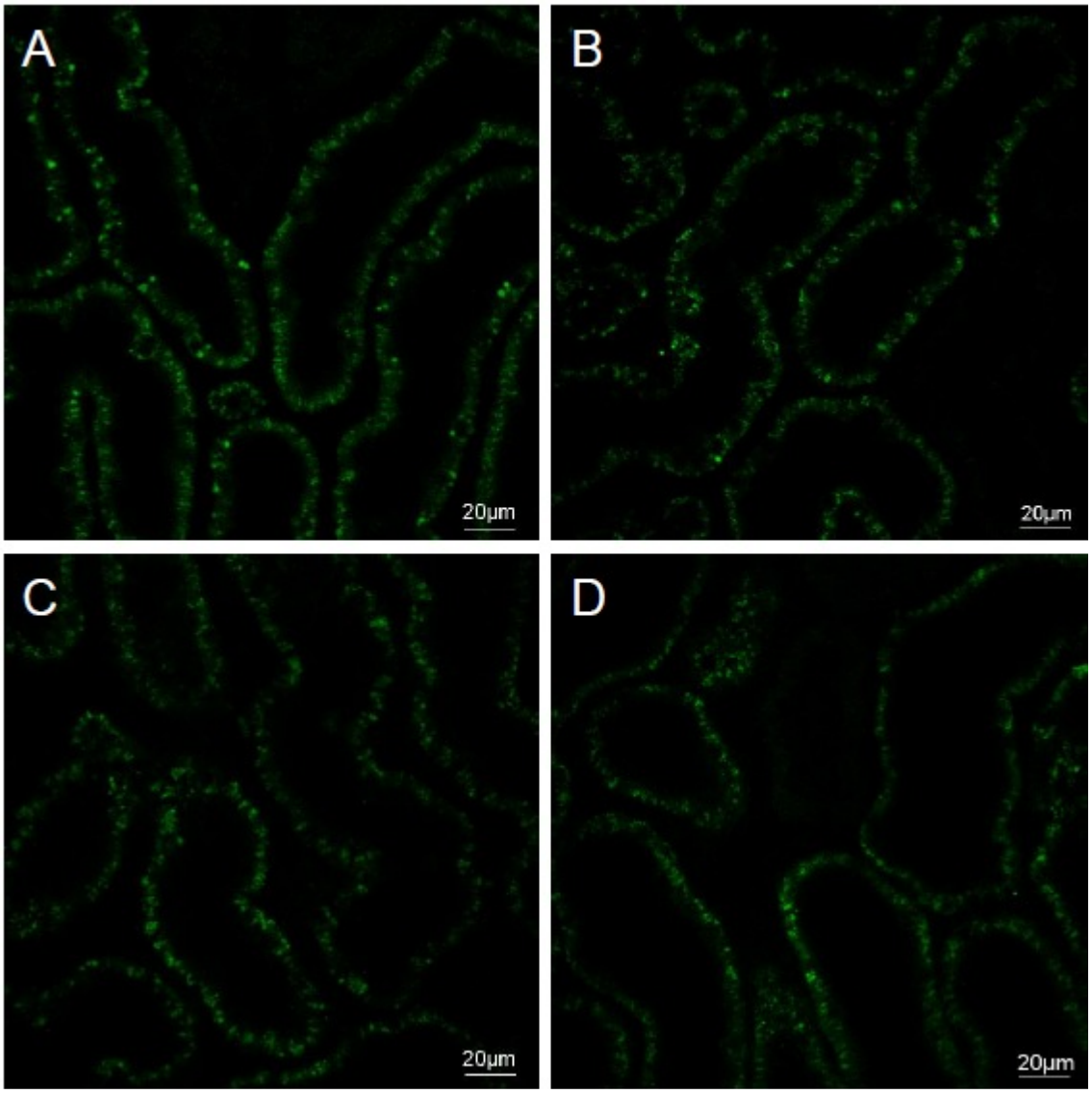

Figure 30. Hydrodynamic injection of saline and null baculovirus vectors do not alter tissue autofluorescence

An investigation of tissue autofluorescence as a direct result of hydrodynamic retrograde injections. These intravital two-photon micrographs outline live rat kidney tubules from animals that received: (A) no injection (innate tissue autofluorescence in the green channel), (B) sham injection, and (C) saline, and (D) null baculovirus vector, via hydrodynamic injections. Images were taken 3 days after all injection-related surgeries.

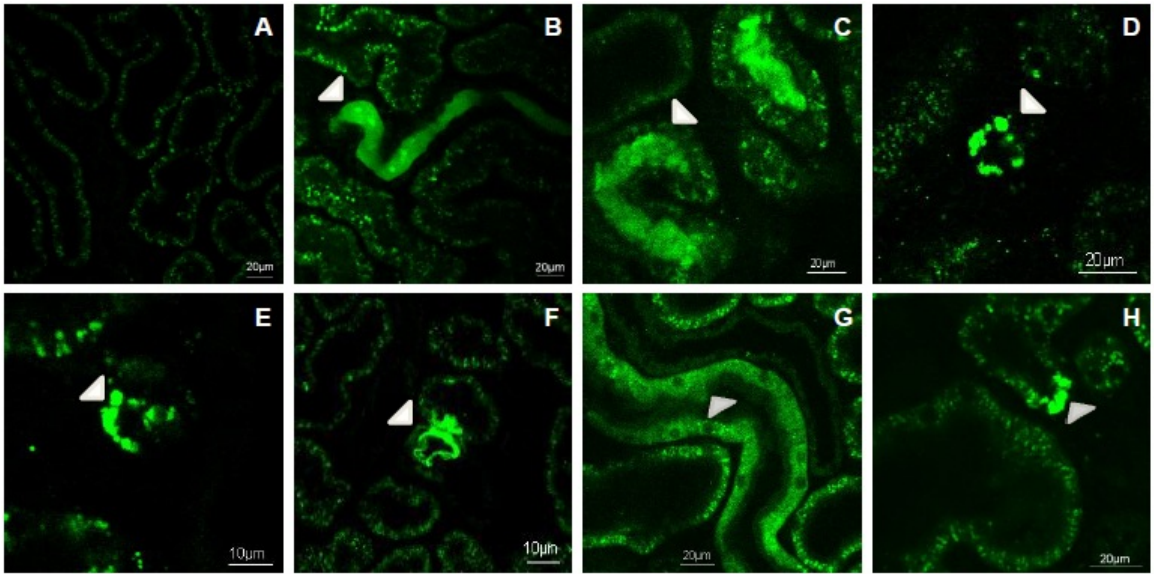

Figure 31. Live baculovirus expression persists up to three weeks in the rat kidney
Data collected using intravital two-photon microscopy from live Sprague Dawley rats injected with Actin-GFP baculovirus. This probe targets incomplete segments of both filamentous and globular actin protein structures. These images were taken from animals across a 3 week time frame, post hydrodynamic viral delivery: (A) tissue autofluorescence, (B) Day 1, (C) Day 2, (D) Day 3 (E) Day 4, (F) Day 5, (G) Day 6 and (H) Day 21. Arrows are used to indicate regions with transgene expression distal tubules (DT) and proximal tubules (PT).

We reconfirmed that the hydrodynamic injection process did not affect tissue autofluorescence, and the increase in fluorescence intensities did not originate from viral vectors lacking the ability to drive fluorescent chimera expression (Figure 30).

For our glomerular investigations we used Frömter and Simonsen Munich Wistar rats, as these strains of rat have superficial glomeruli that are accessible for imaging by two-photon microscopy[227]. Generally, the Bowman's space of normal glomeruli can be identified in fluorescent micrographs as regions absent of fluorescence[209], as observed from images taken from the kidneys of normal Munch Wistar rats (Figure 29A and 29C). In comparison, images collected from the same animals 3 days after hydrodynamically delivering CellLight® GFP baculovirus generated GFP expression within live glomeruli (Figure 29B and 29D). Similarly, fluorescent protein expression appeared in a variety of cortical tubular compartments accessible for imaging with two-photon fluorescence microscopy using CellLight® GFP-Actin baculovirus vectors (Figure 31). This fluorescent protein expression persisted up to 3 weeks after hydrodynamic delivery.

During our two-photon intravital studies we observed initial signs of renal injury, which was identified by fluorescent cellular debris within the tubular lumens (Figures 31B and 31C). Such injury may have resulted from mild ischemia-reperfusion damage generated from the injection process[165], or fluorescent protein over-expression[228]. Nevertheless, these signs of injury subsided 3 days after gene transfer. This indicated a viable time point for long-term renal transduction stability and homeostasis. This transient injury response was also observed using adenovirus vectors (Figure 32).

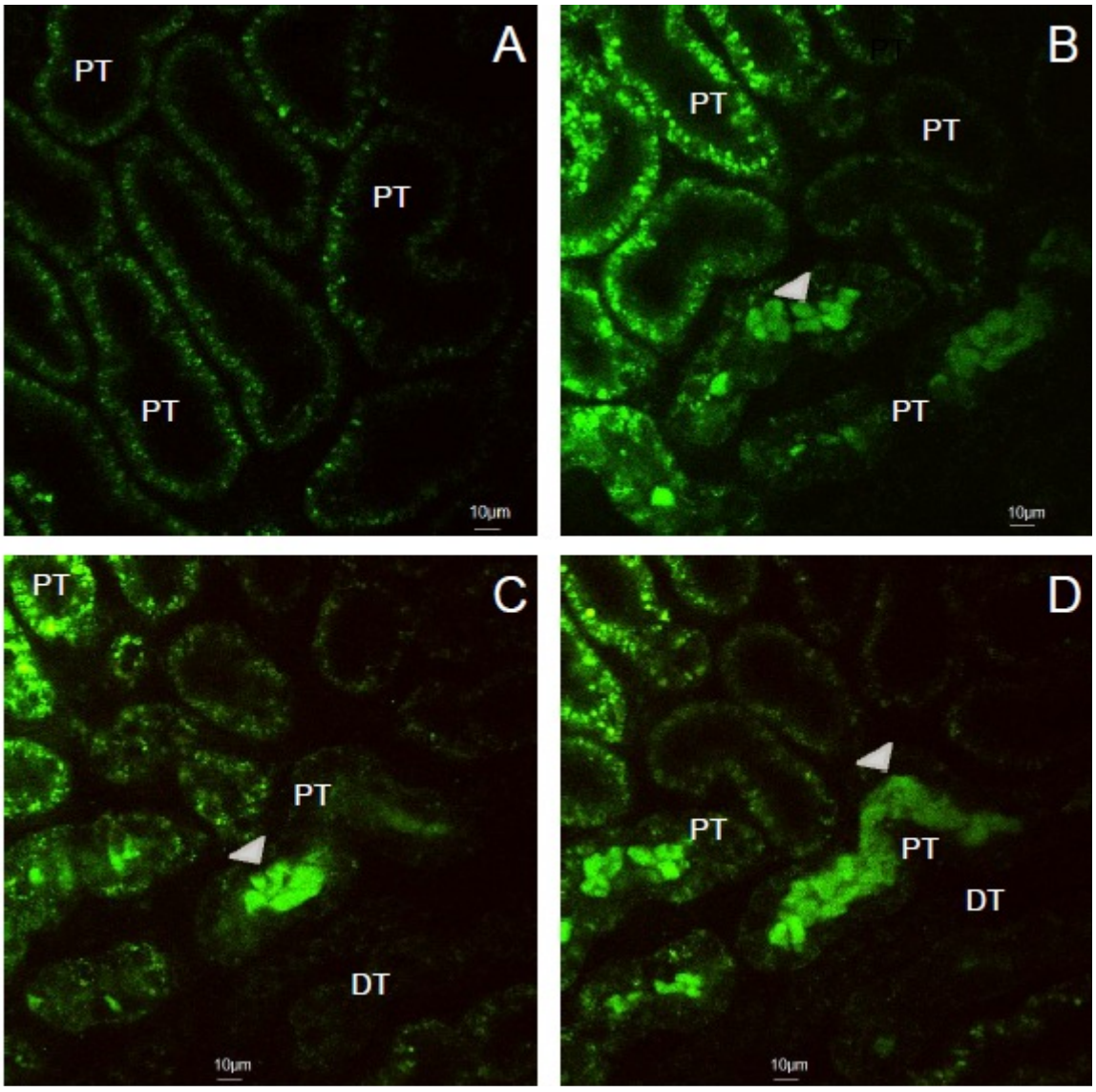

Figure 32. High titers of adenovirus vectors appear to generate an immunological response

Data collected using intravital two-photon microscopy from live a Sprague Dawley rat that received Actin-GFP adenovirus treatment. This probe targets incomplete segments of both filamentous and globular actin protein structure: (A) tissue autofluorescence, (B through D) taken 2 days after this rat received the adenovirus treatments. Arrows indicate regions with transgene expression proximal tubules (PT). Significant levels of sloughed fluorescent cells observed throughout the kidney with viral titers of 3×10^{6} - 3×10^{7} pfu.

Further, even though baculovirus vectors provided a substantial improvement in the extent of transgene expression, their expression patterns generally deviated from endogenous tissue morphology. This may have originated from either fluorescent protein aggregation or an immunological response to the insect-derived viral expression *in vivo*. Finally, it should be noted that this injection process provided a reliable way to facilitate exogenous protein expression using viral vectors. We did not record any improvements in the extent of fluorescent protein expression using plasmid vectors when we conducted the hydrodynamic injections without vascular cross-clamps. At that point, only few studies were done with adenoviral vectors. In those experiments we hydrodynamically injected high viral titers (3×10^6 - 3×10^7 pfu). These titers generated significant levels of fluorescent debris/cast formation (within tubular lumens), which persisted beyond 3 days after their hydrodynamic delivery. This indicated a possible immunological response that could have been generated from the delivery of the higher viral titers.

6. Texas red-labeled phalloidin and fluorescent actin colocalization observed in vitro verify results obtained from live rats

To further support claims of targeted *in vivo* cell transformation obtained, we used a immunohistochemical assay to examine fluorescent actin expression[218]. We counterstained kidney sections taken from rats that received hydrodynamic baculovirus venous injections, with Texas-red-tagged phalloidin to label F-actin filaments.

From these sections we observed increased GFP-based fluorescent intensities from several cell types. Tissues treated with the GFP baculovirus vectors displayed

widespread and non-specific fluorescent labeling of renal cells. Using actin-targeting GFP probes (CellLight® Actin-GFP baculovirus), we observed increased levels of fluorescence intensities emanating from apical brush borders of proximal tubule epithelial cells. These signals coincided with those that originated from the Texas-red-labeled actin cytoskeleton (Figures 33G-33I). Significant spatial overlap of these two fluorescent signals provided further evidence for the potential to target specific cellular components and loci using the hydrodynamic delivery via fine-needle, retrograde renal vein injections.

The morphological structure of renal tissues infected with the baculovirus vectors illustrated in these *in vitro* studies also deviated from normal tissue morphology, as exemplified by kidney sections that received saline hydrodynamic saline injections (Figures 33A-33C). If such variations in tissue condition were not a direct result from tissue processing, then this evidence further supports the possibility that baculovirus vectors may have adversely altered renal tissue structure and function. Moreover, reducing the hydrodynamic injection rate correlated with a reduction in the extent of transgene expression and an increase in the degree of renal injury (Figure 34D-34L), as previously observed *in vivo* (Figure 18C).

7. Vascular cross-clamping significantly improved plasmid and adenoviral expression in various renal cell types with large volume (0.5 ml) fine-needle retrograde hydrodynamic renal vein delivery

In an effort to further improve transgene expression levels and injection efficacy, we performed hydrodynamic injections augmented with vascular cross-clamping. These

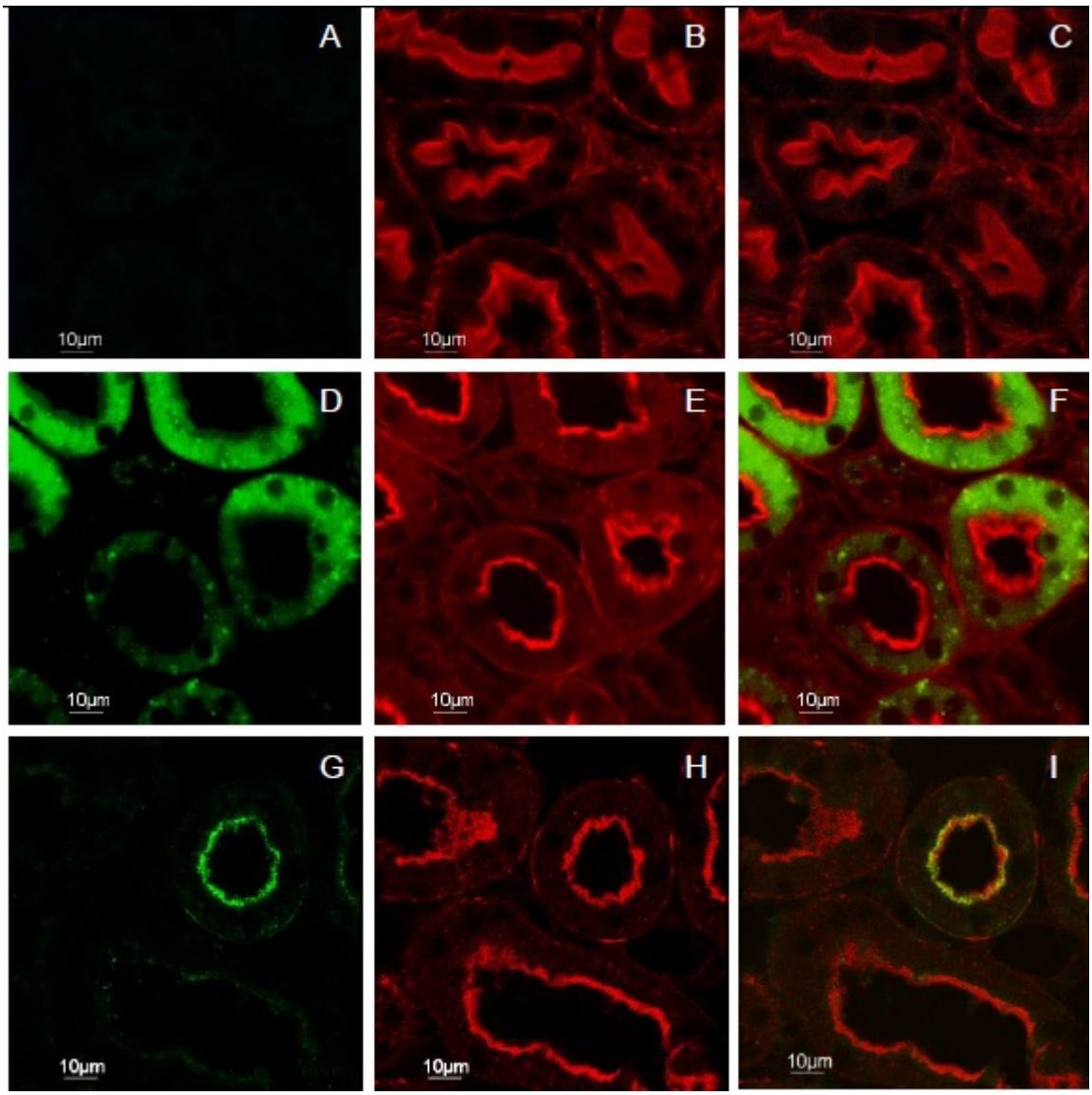

Figure 33. Fluorescent baculovirus expression in proximal tubules observed *in vitro*
Confocal laser scanning micrographs of cortical sections taken from animals treated with saline, GFP baculovirus and Actin-GFP baculovirus that were counterstained with Texas red-labeled phalloidin. Images (A) through (C) were taken form an animal treated with saline: (A) fluorescent signal from the green channel, (B) Texas red-labeled phalloidin signal and (C) merged image of (A) and (B). Images (D) through (F) were taken from an animal treated with the GFP baculovirus: (D) fluorescent signal from the acquired from

the green channel showing GFP expressed in proximal tubules, (E) Texas red-labeled phalloidin signal and (F) the overlay of (D) and (E). Images (G) through (I) were taken from an animal treated with the Actin-GFP baculovirus: (G) fluorescent signal acquired from the green channel showing Actin-GFP signals observed from the brush border regions, (H) Texas red-labeled phalloidin stained actin filaments, (I) overlay of images (G) and (H) illustrating colocalized actin-derived signals from the baculovirus-driven GFP and Texas red labeled phalloidin.

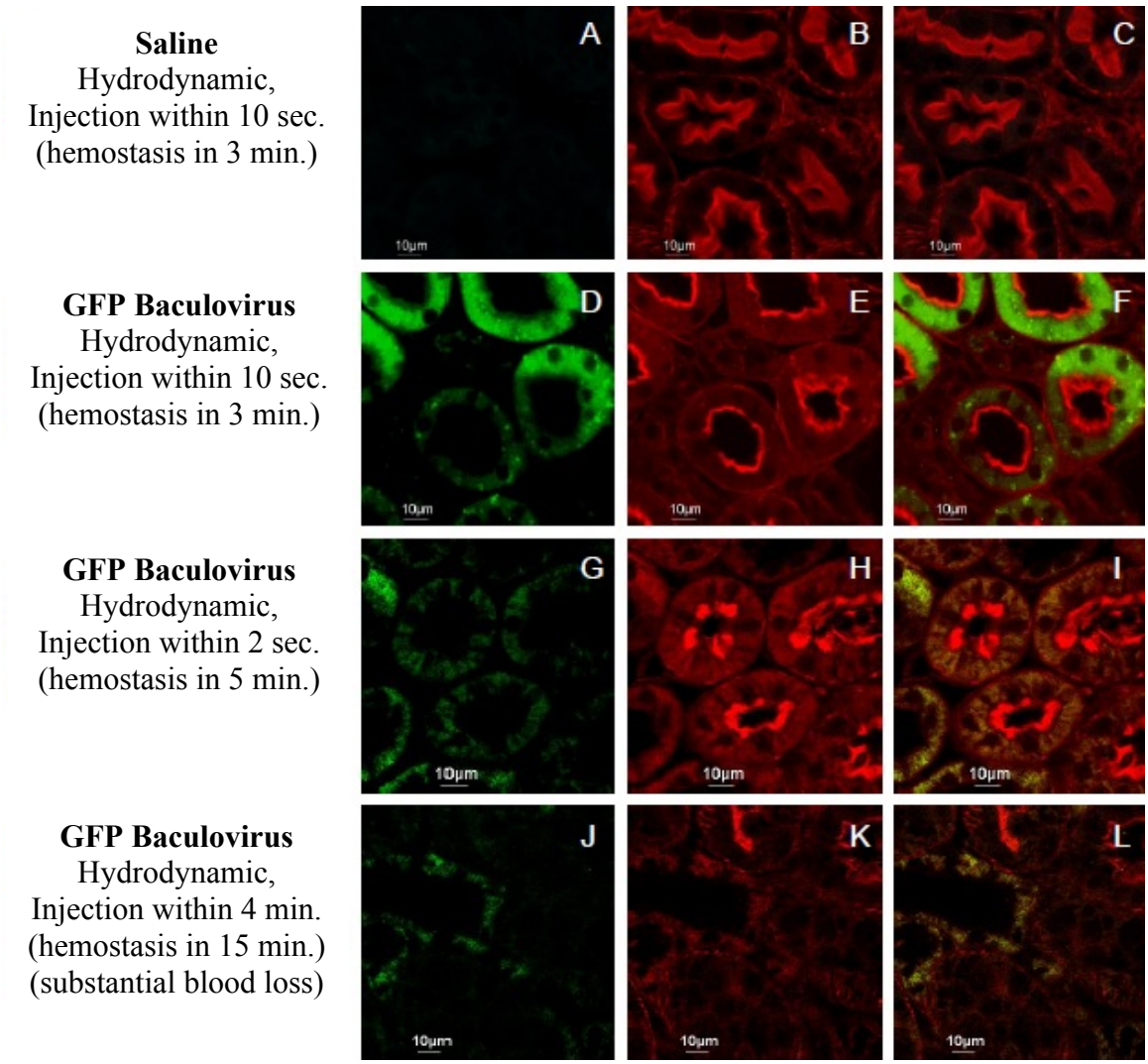

Figure 34. The rate of hydrodynamic injections significantly affects transduction rates and injury levels

Data obtained to correlate transgene delivery and incorporation, with resulting effects on innate tissue conditions 3 days after delivery. Confocal laser scanning micrographs of cortical sections taken from animals treated with saline and baculovirus vectors, and counterstained with Texas red-labeled phalloidin to compare with the effects of varied renal vein injection rates: (A) through (F) rapid hydrodynamic injections; (G) through (I) 2-minute injections; and ((J) through (I) 4-minute injections. Lower rate injections generated significant renal injury.

injections generated widespread fluorescent protein expression lasting over a month after the introduction of non-viral and viral transgenes (we investigated plasmid and adenovirus transgene expression up to 4 weeks in live animals and 6 weeks *ex vivo*). Using plasmids we successfully transfected live rat kidneys with EGFP, (Figures 35B and 35C), EGFP-tubulin (Figures 35E and 35F), EGFP-actin (Figures 36 and 37); EGFP-occludin (Figure 40A), and H2B-tdTomato (Figures 40B and 40C); and transduced with EGP-actin (Figures 38 and 39) and RFP-actin (Figure 39) adenovirus vectors. Fluorescent protein was observed 1) in proximal and distal tubules; 2) within glomeruli; 3) within the peritubular interstitum; 4) within the renal capsule; and 5) within the perirenal fat.

We also visualized intact tissue morphology in nephron cross-sections that were transformed by the plasmid DNA and adenovirions (adenovirus treatments containing 3×10^5 pfu provided stable transgene expression). These improvements in the level and quality of transgene expression were consistent with the use of both plasmids and adenoviral vectors. Once more, injections of higher titers of adenovirus (3×10^6 - 3×10^7 pfu) generated lengthy damage illustrated by persistent cellular sloughing and tubular blockages. We again observed the structure of renal compartments, which expressed baculovirus-derived proteins, generally deviated from normal tissue morphology that accompanied extensive fluorescent protein aggregation (Figures 29 and 31).

In comparison, images obtained from live rats that that expressed EGFP-occludin and H2B-tdTomato plasmid-derived fluorescent proteins provided clear signs of the expected probe localization and morphology. For instance, EGFP-occludin fluorescence

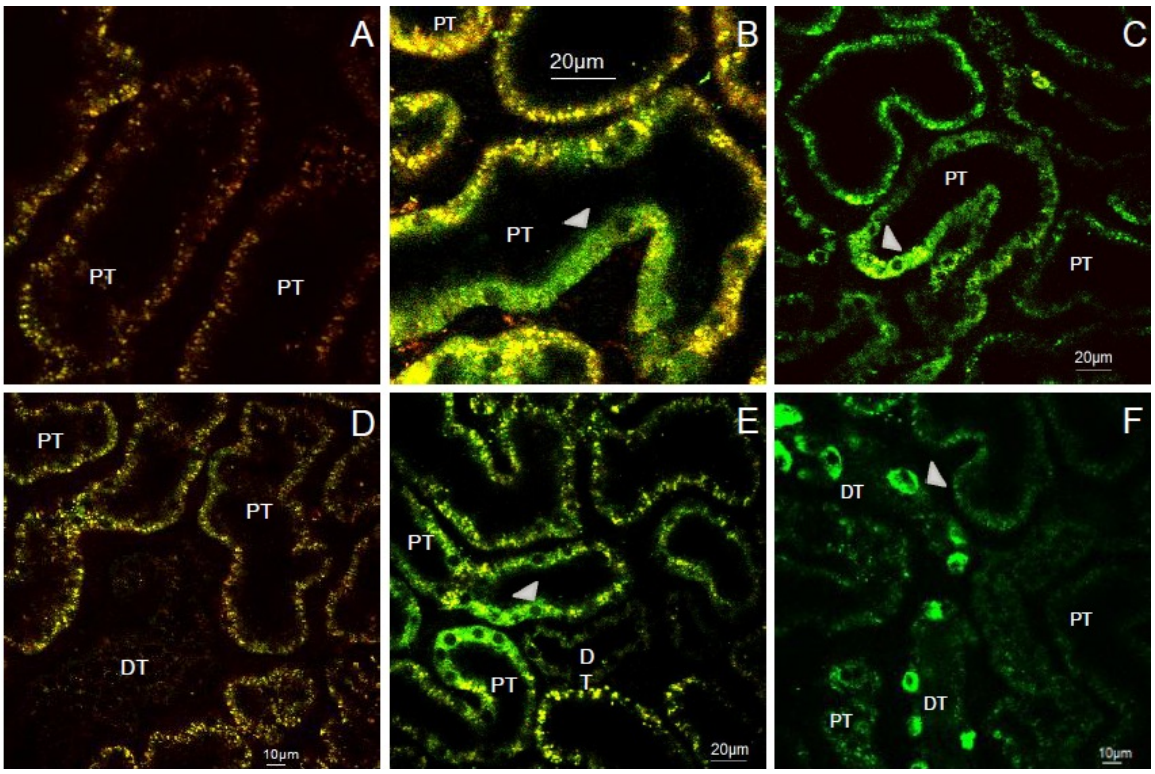

Figure 35. Hydrodynamic delivery conducted with vascular clamps facilitated robust GFP and GFP-tubulin expression in live rat kidneys
Transgene expression recorded in live Sprague Dawley rats that received hydrodynamic injections (augmented with vascular clamps) of EGFP and EGFP-Tubulin plasmid vectors. Image (A), was taken from a rat prior to its treatment with EGFP plasmid vectors, and (B) and (C) were taken from that animal 3 days after it was treated with EGFP plasmid vectors. Similarly, image (D), was taken from another rat prior to its treatment with EGFP-Tubulin plasmid vectors, and (E) and (F) were taken from that animal 3 days after it was treated with EGFP-Tubulin plasmid vectors. Transgene expression can be seen within live distal tubules (DT), image (F), and proximal tubules (PT), images (B), (C) and (E). Red and green pseudo-colors were merged to differentiate between EGFP and autofluorescence signals. Arrowheads indicate regions of transgene expression.

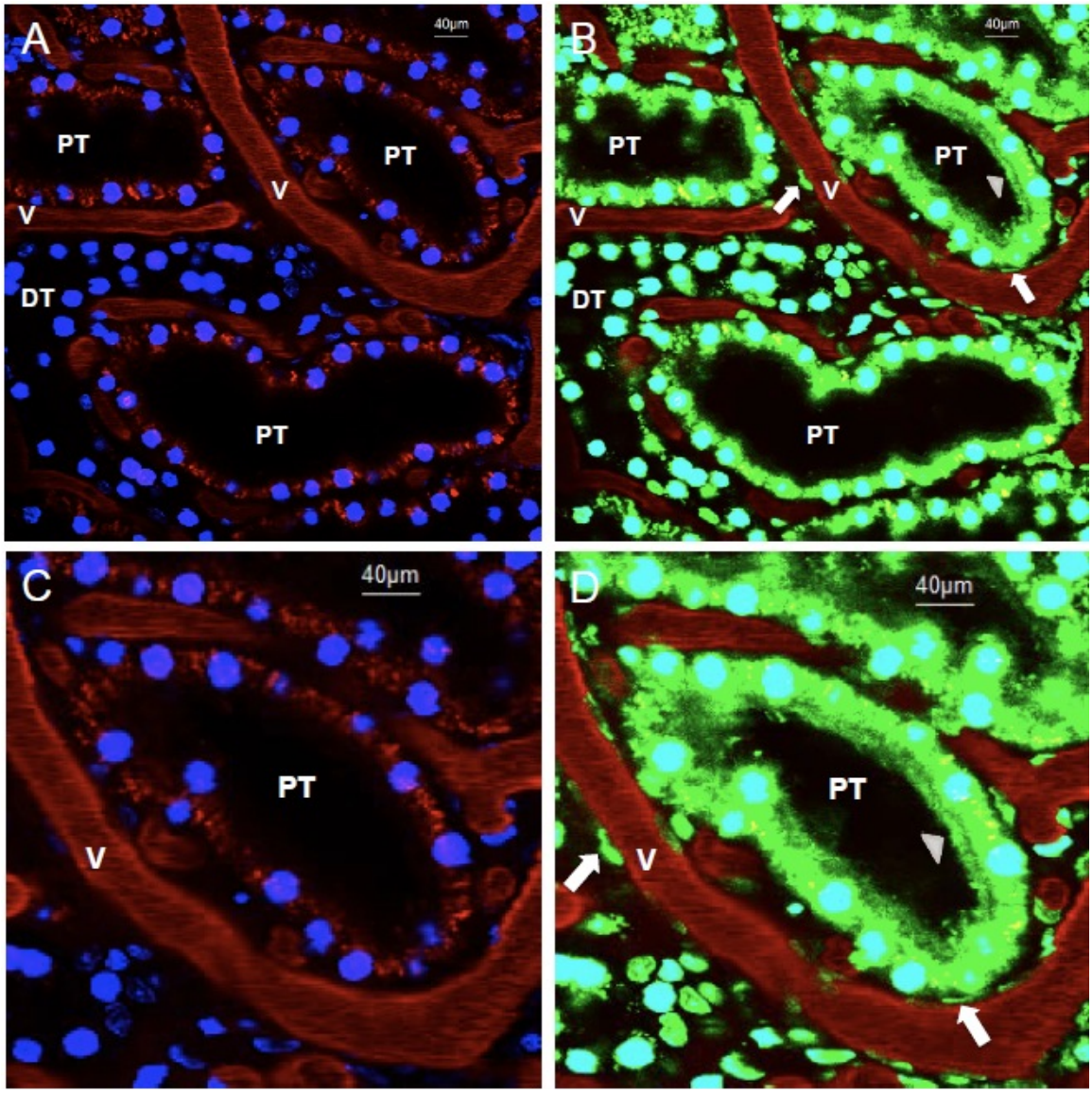

Figure 36. Plasmid-based fluorescent actin expression in live tubular brush borders and interstitium

Transgene expression recorded in a live Sprague Dawley rats that received hydrodynamic injections (augmented with vascular clamps) of EGFP-actin naked plasmid vectors. These images were taken from the rat 2 days after transgene delivery. Prior to acquiring these images, Hoechst 33342 and a 150 kDa Rhodamine dextran were infused through the rat's jugular vein to better outline renal architecture. Images (A) and (C) were formed by merging the blue- and red-pseudo-color channels, and (B) and (D) from merging blue-,

green-, and red-pseudo-color channels. Images (C) and (D) are magnified images obtained from the microscopic field presented in (A) and (B) respectively to highlight fluorescent protein expression in the actin brush border, and endothelial cells of the per tubular vasculature. Arrowheads and arrows indicate regions of EGFP-actin plasmid expression in the brush border and endothelial cells lining the peritubular vasculature respectively. It should also be noted that the teal-colored nuclei don't reflect nuclear EGFP actin, but signal crosstalk.

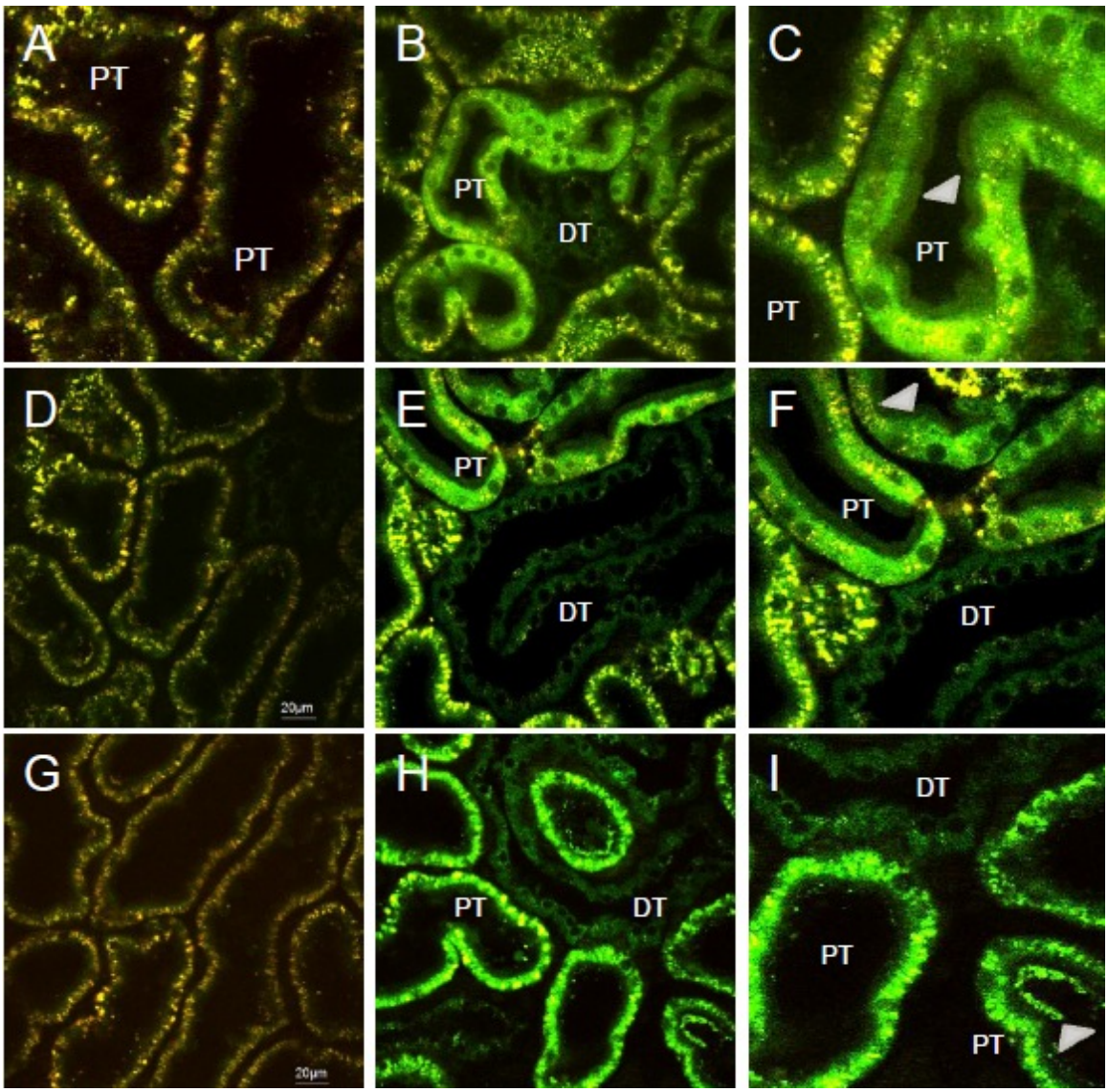

Figure 37. Long-lived hydrodynamic-derived plasmid expression in rat kidneys
Live images were taken from rats that received hydrodynamic injections (augmented with vascular clamps) of EGFP-actin plasmids: (A) a rat prior to plasmid treatment, and (B) and (C) same rat in (A) 3 days post transgene delivery; (D) a rat prior to plasmid treatment, and (E) and (F) same rat in (D) 14 days post transgene delivery; and (G) a rat prior to plasmid treatment, and (H) and (I) were taken in the same in (G) rat 28 days post delivery (Distal (DT); proximal (PT) tubules). GFP-based fluorescence was intensified along the brush border of cells that express the actin transgenes (arrowheads)

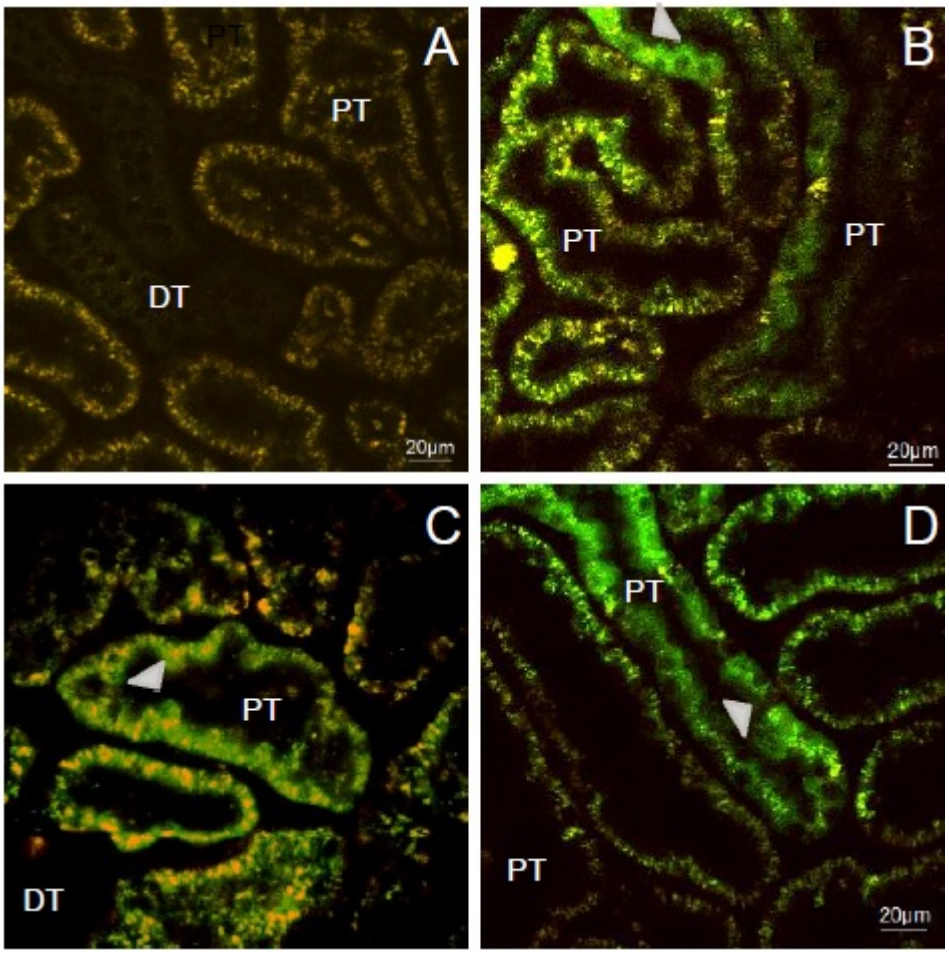

Figure 38. Long-lived hydrodynamic-derived adenovirus expression in rat kidneys
Transgene expression recorded in live Sprague Dawley rats that received hydrodynamic injections of GFP-Actin adenovirus vectors. Image (A) was recorded prior to transgene delivery (innate autofluorescence), and (B) was taken from an animal 3 days post adenovirus delivery, (C) was taken from an animal 7 days post adenovirus delivery, and (D) was taken from an animal 14 days post adenovirus delivery. Adenovirus-based transgene expression can be seen within live distal tubules (DT) and proximal tubules (PT) epithelial cells. Again, GFP-based fluorescence was intensified along the brush border of cells that express the actin transgenes as compared to cells within tubules that do not express the fluorescent proteins these in these images. Red and green pseudo-colors were merged to distinguish between EGFP and autofluorescence signals. Arrowheads indicate regions of transgene expression.

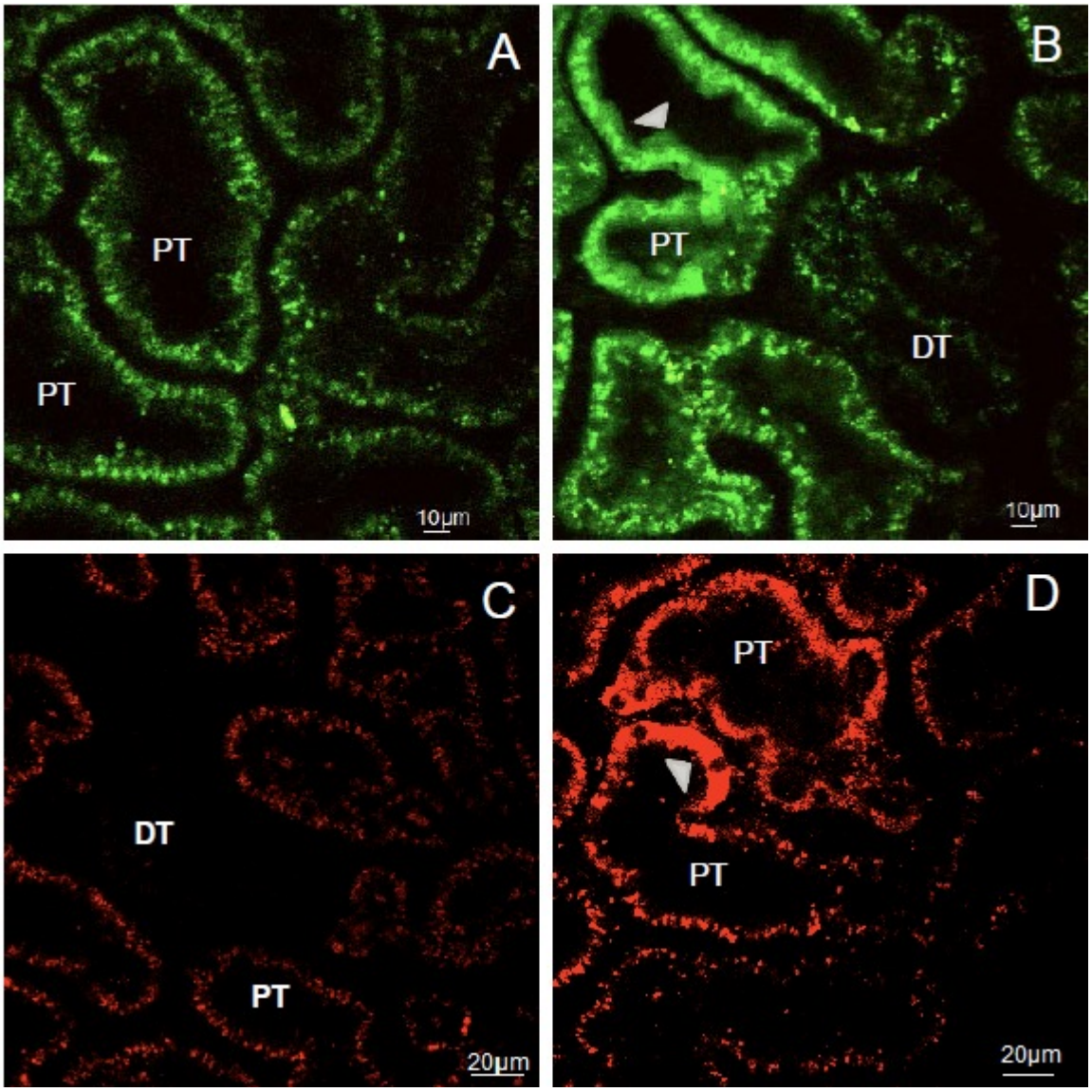

Figure 39. A comparison of fluorescent micrographs taken from live Sprague Dawley rats treated with hydrodynamic injections of EGFP-actin and RFP-actin adenovirus vectors.
Images obtained from rats that received hydrodynamic treatments of EGFP-actin and RFP-actin: (A) was recorded in a rat prior to transgene delivery of EGFP-actin adenovirus vectors; image (B) was taken from the same rat 3 days post the delivery of EGFP-actin adenovirus vectors; image (C) was recorded prior to transgene delivery of RFP-Actin adenovirus vectors; and image (D) was taken from the same rat 3 days post

the delivery of RFP-actin adenovirus vectors. Red and green pseudo-colors were merged to distinguish between fluorescence (GFP and RFP) and autofluorescence signals. Arrowheads indicate regions of transgene expression.

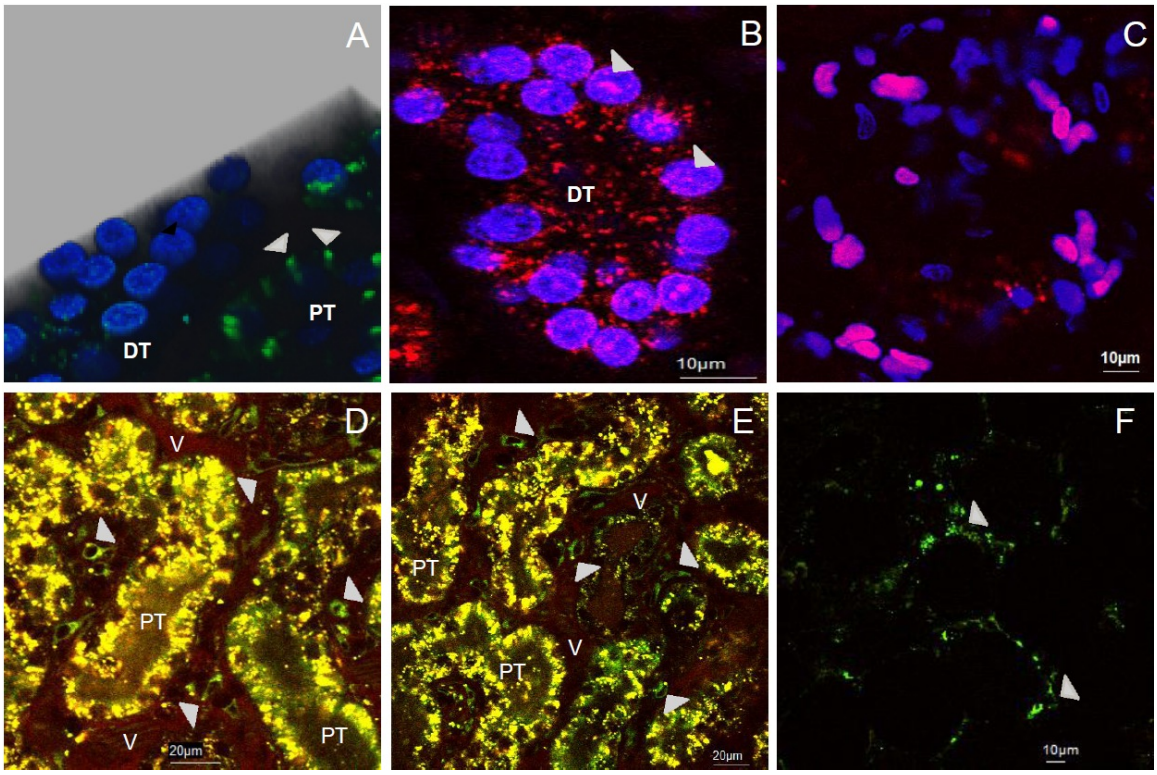

Figure 40. Hydrodynamic delivery facilitates the expression of a variety of plasmid vectors in live rat kidneys
Transgene expression is observed in proximal tubule cells (A), distal tubule cells (B), as well as in interstitial cells surrounding the peritubular vasculature (D) and (E), within the renal capsule (C) and (F) adipose tissue of the perirenal fat. These images were taken from live rats 3 days after receiving hydrodynamic injection of EGFP-occludin (image A), H2B-tdTomato (images B and C) and EGFP-Actin (images D, E and F) plasmid vectors. A 150 kDa TRITC dextran solution was infused through the jugular veins to outline vasculature (V). Arrowheads indicate regions of transgene expression.

signals ran between adjacent nuclei as punctate fluorescent bands along regions that correspond to tight junctions (Figure 40A). Fluorescent H2B-tdTomato signals colocalized with Hoechst counterstained nuclei (Figures 40B and 40C).

Analogously, in fluorescent micrographs taken from live rats that were previously treated with EGFP-actin plasmids (Figures 36 and 37), and EGFP-actin (Figure 38 and 39) and RFP-actin (Figure 39) adenovirus vectors, there were marked increases in fluorescence intensities along brush border of proximal tubules expressing these transgenes, as compared to adjacent tubules that did not express these transgenes. This fluorescence pattern is consistent with prior studies using fluorescent actin reporters[117,180].

As previously mentioned, significant levels of plasmid- and adenovirus-derived fluorescent protein expression were also present in other cells types native to the following renal structures: peritubular interstitium, (Figures 40D and 40E); adipose tissues (Figure 40F); and glomeruli (Figures 41B through 41D). The cells in the peritubular interstitium identified have morphological structure similar to peritubular endothelial cells and monocytes[117]. Glomerular transgene expression was investigated primarily in Wistar rats. We also visualized glomerular transgene expression in a Sprague Dawley rat on the rare occasion that this structure appeared within the range of two-photon imaging in this rat strain. Glomerular morphology was grossly normal in rats that received hydrodynamic saline injections (Figure 41A).

Within non-viral and viral infected glomeruli (Figures 41B and 41C), there appeared to be transgene expression in podocytes, but the resolution limit of light

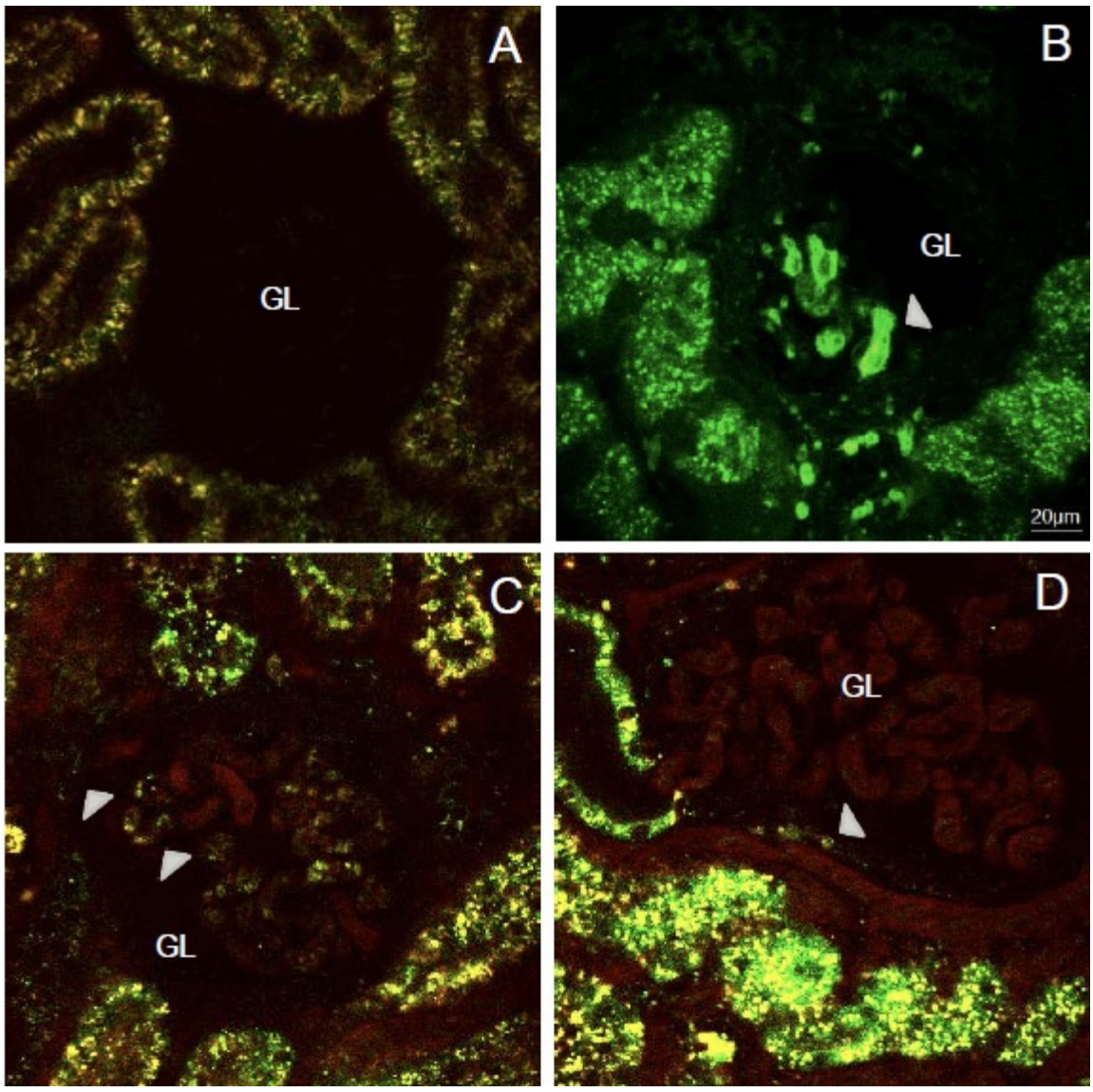

Figure 41. Fluorescent EGFP-actin plasmid expression in live rat glomeruli
Hydrodynamic-based transgene expression (arrowheads) in live glomeruli using adenovirus and plasmid vectors rats 3 and 7 days post transgene delivery: (A) image of a glomerulus taken from a kidney treated with saline (control) 3 days post hydrodynamic injection; (B) image of a glomerulus taken from a kidney treated with GFP-Actin adenovirus vectors 7 days post hydrodynamic injection; and (C) and (D) images of glomeruli taken from kidneys treated with EGFP-actin plasmid vectors 3 days post hydrodynamic injection. Prior to obtaining images (C)and (D), 150 kDa TRITC dextran solutions were infused through jugular veins to investigate renal structure and function.

microscopy does not allow us to state this definitively. Similarly, transgene expression was visualized in S1 segments of proximal tubules (Figure 41D) and parietal epithelial cells of Bowman's capsule (Figures 41B through 41D). Additionally, 150 kDa TRITC dextran molecules, which were introduced via the jugular vein during imaging (Figures 41C and 41D) were confined to the glomerular capillaries and surrounding vasculature. These results provided further evidence that intrinsic nephron structure and function were maintained after hydrodynamic injections and gene expression using plasmids and adenovirus. We must also emphasize that hydrodynamic-based transformation appears to be non-selective relative to cell type and region of the kidney genetically transformed.

8. Simultaneous expression of multiple transgene vectors generated by single hydrodynamic injections augmented with vascular cross-clamps

Realizing it was possible to produce reliable transgene expression from various types of vectors using hydrodynamic delivery, we next considered delivering multiple transgenes in a single hydrodynamic injection. We introduced a mixture of EGFP-actin and RFP-actin adenovirions (10^5 pfu of each vector) in MDCK cells and live rat kidneys. Cells were imaged 1 day after incubation with adenovirions, while kidneys were harvested from rats 3 days after hydrodynamic viral injections. These kidneys were imaged within 5 minutes after their excision. The *in vitro* and *ex vivo* data illustrate regions that simultaneously expressed the EGFP-actin and RFP-actin adenovirus vectors (Figure 42). Interestingly, this result identified the potential to generate multiple renal genetic modifications in live mammalian kidneys by single hydrodynamic injections.

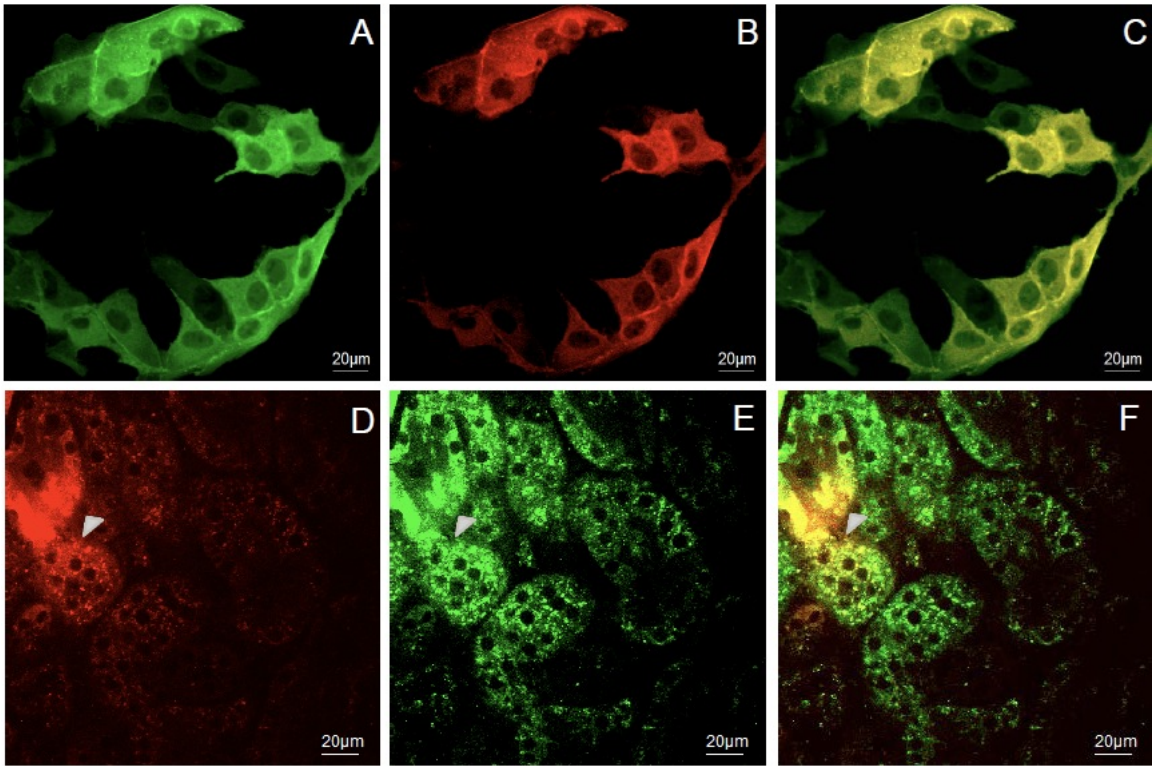

Figure 42. Hydrodynamic delivery facilitates the expression of multiple transgenes simultaneously in renal cells
Simultaneous transgene expression was observed in MDCK cells and Sprague Dawley rat kidneys treated with both GFP-Actin and RFP-Actin adenovirus vectors. The cells were imaged 1 day after incubation with the adenovirus vectors, while the *ex vivo* kidney images were taken from within the superficial cortex of a freshly excised whole kidney. The kidney was harvested from a rat 3 days after it was injected with the adenovirus vectors, and was imaged within 5 minutes after its excision. Red and green pseudo-colors were merged to distinguish between fluorescence (GFP and RFP) and autofluorescence signals, and to highlight regions with co-transgene expression. Arrowheads indicate regions of transgene expression.

9. Hydrodynamic renal vein injections augmented with vascular cross-clamping can generate efficient levels of transgene in mammalian kidneys

We examined tissue sections harvested from rats 3 days after they were treated with plasmids, baculovirus and adenovirus vectors to gain insight into the efficiency of the hydrodynamic delivery for each type of vector. For this work, we again used two-photon (Figures 43) and confocal laser-scanning microscopy (Figure 44) to visualize fluorescence protein expression in freshly harvested whole kidneys and tissue sections respectively throughout the renal cortical and medulla.

We observed widespread transgene expression throughout the renal cortex and medulla in freshly excised kidney sections (Figure 43), and fixed tissue sections (Figure 44). With plasmid and adenovirus vectors, we typically saw that multiple cells (>50%) in a particular tubular cross section simultaneously expressed the fluorescent proteins. However, this was not the case with our baculovirus vectors, as we frequently observed that only single cells in various nephron cross-sections expressed fluorescent proteins.

Baculoviral transformation provided lowest delivery efficiency, ranging from 10 to 50% of nephron cross-sections (Figure 45). Particularly, within most superficial cortical regions, which would be accessible by intravital two-photon microscopy, only approximately 10% of nephron cross-sections were transduced. At depths below 500 μm from the kidney surface, there was a gradual decrease in fluorescent protein expression in regions that would correspond to the deeper cortex, corticomedullary junction and medulla. Much higher levels of protein expression were observed using plasmid and

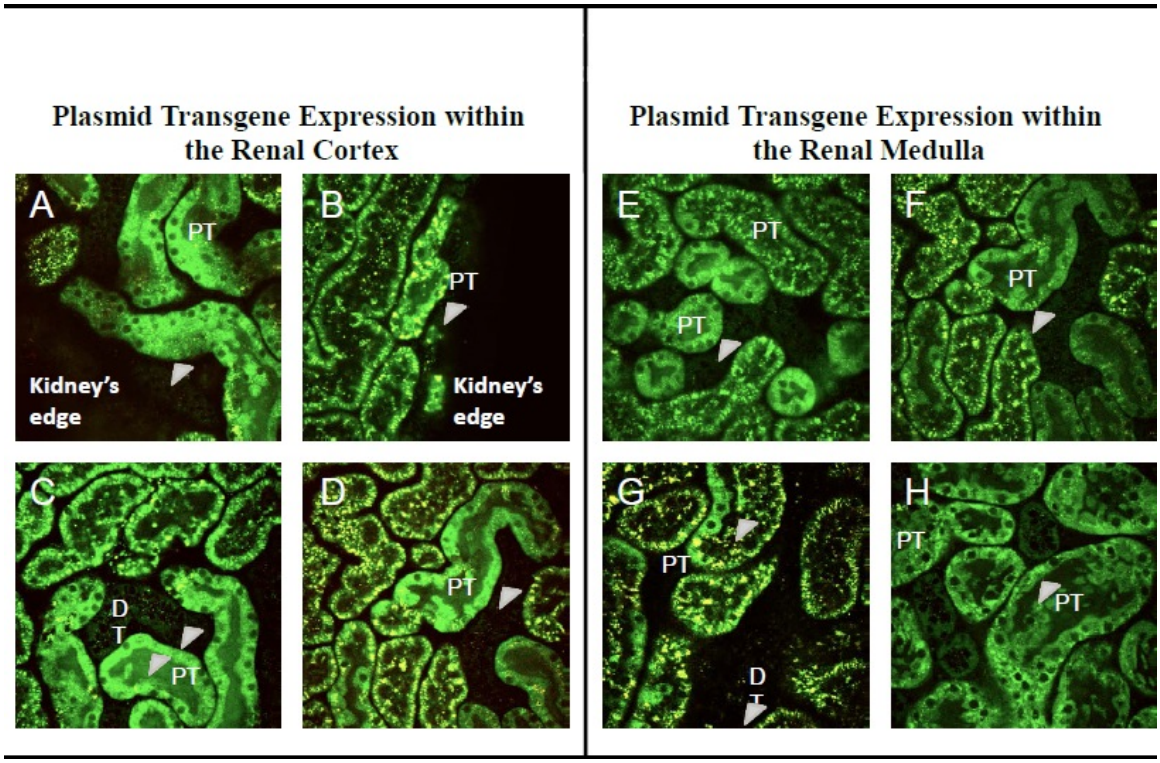

Figure 43. Hydrodynamic injections conducted with vascular clamps facilitates robust plasmid expression in both the renal cortex and medulla
Transgene expression recorded in freshly excised whole kidneys acquired from Sprague Dawley rats that received hydrodynamic injections augmented with vascular clamps EGFP-actin plasmid vectors. Images A through D and E through F were taken from the renal cortex and renal medulla of freshly excised whole kidneys. Extensive transgene expression can be seen within distal tubules (DT) and proximal tubules (PT). Red and green pseudo-colors were merged to differentiate between EGFP and autofluorescence signals. Arrowheads indicate regions of transgene expression.

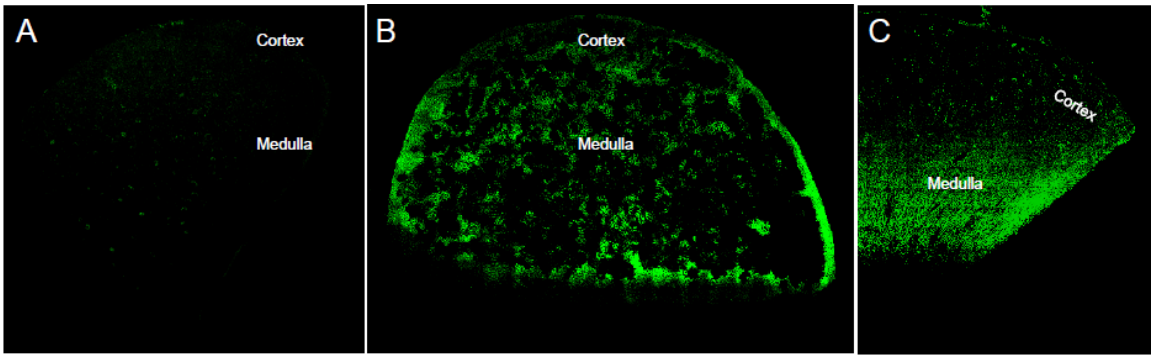

Figure 44. A comparison of baculovirus, plasmid and adenovirus fluorescent protein expression generated from fine needle renal vein hydrodynamic injections
A comparison of hydrodynamic-based transgene expression throughout the cortex and medulla using plasmid and adenovirus vectors: (A) kidney treated with baculovirus vectors, (B) kidney treated with EGFP-Tubulin plasmid, and (C) kidney treated with EGFP-actin adenovirus. Whole kidneys were harvested from these rats 3 days after hydrodynamic transgene delivery and 100µm thick sections were collected and imaged from the cortex to the level of the renal pedicle. Each series of images was then reconstructed to outline entire cross-sections of tissue samples treated with the various agents.

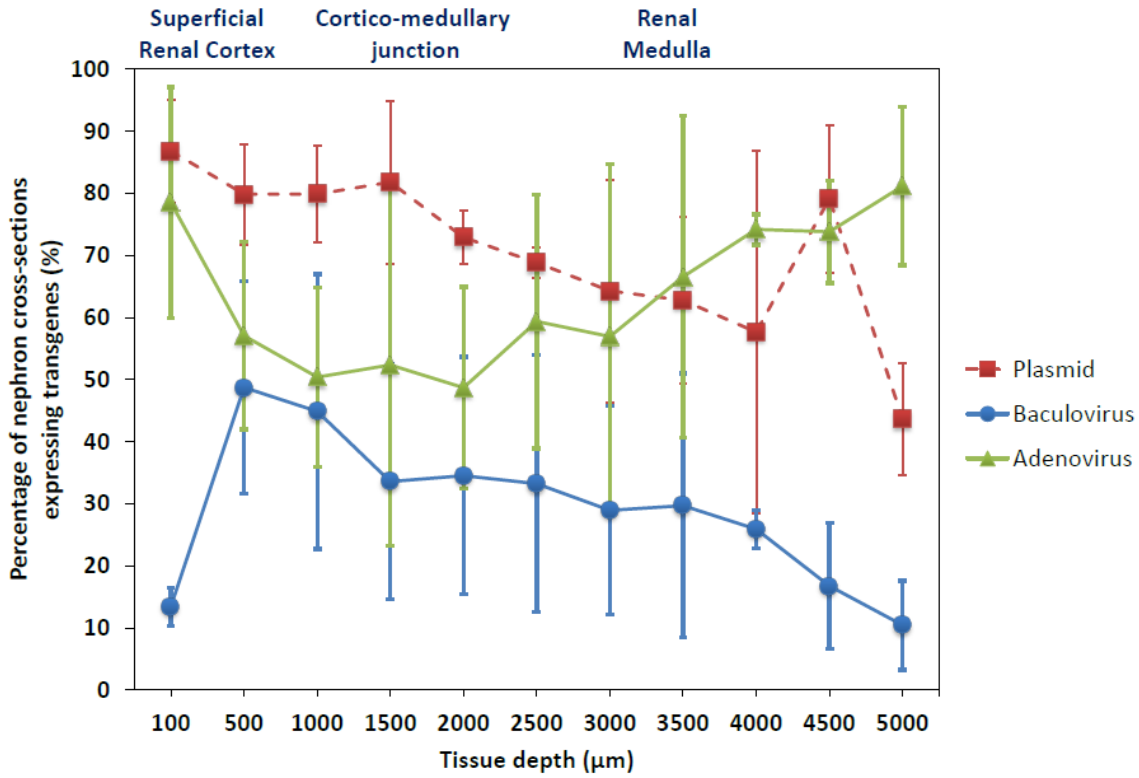

Figure 45. Plasmid and adenovirus vectors generated greater levels of transgene expression throughout the rat kidney

Estimates of hydrodynamic-based transgene delivery efficiencies (3 days after transgene delivery) from kidneys treated with plasmid and adenovirus vectors. These efficiency measurements were computed from various reconstructed like those presented in Figure 48.

adenovirus vectors (Figure 45). Using these vectors, 40 to 86% of nephron cross-sections expressed fluorescent proteins. Within the superficial cortex (<100 μm from the surface of the kidney), we saw that approximately 78-86% of nephron cross-sections expressed fluorescent proteins, explaining the relative ease with which live expression was detected.

The high level of fluorescent protein expression in this superficial region of the cortex permitted us to investigate the level of expression as a function of time by imaging live animals over a period of 4 weeks (Figure 46). During this period, the percentages of nephron cross-sections that expressed fluorescent proteins ranged from 80 down to 14% using adenovirus vectors and 61 down to 28% with plasmid vectors. Thus, transgene expression appears to be relatively long-lived with even the rudimentary vectors we used.

E. Critical parameters and viable mechanisms to support effective hydrodynamic gene delivery in the rat kidneys

1. Rat vital signs are unaffected by hydrodynamic renal vein injections

We recorded vital signs in live rats throughout hydrodynamic injections were conducted with vascular cross-clamps. These measurements showed that hydrodynamic injection process did not alter blood pressure, heart rate and body temperature.

2. Hydrodynamic retrograde renal vein injections augmented with vascular clamps produces transient changes in renal venous pressure in live rats

In order to characterize critical parameters required for effective transformation, we recorded changes in renal venous pressures generated during this hydrodynamic

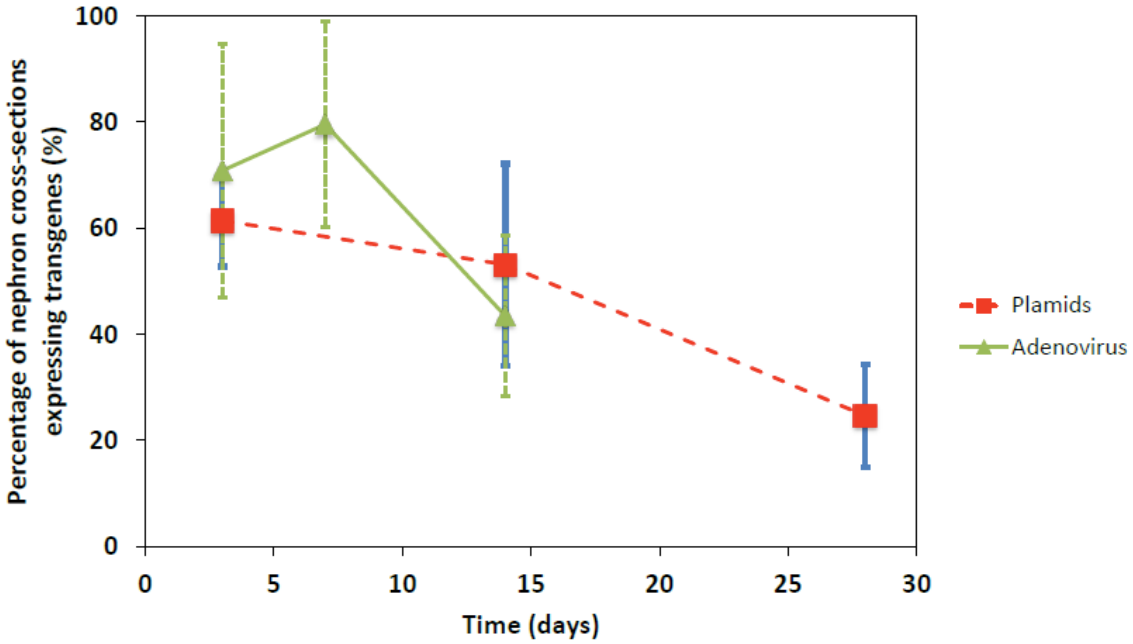

Figure 46. Hydrodynamic based expression levels diminished with time
Estimates of time-dependent hydrodynamic-based transgene delivery efficiencies in live kidneys treated with plasmid and adenovirus vectors.

injection procedure. From these measurements we observed both the application and removal of the vascular clamps produced small and transient changes in renal pressure. Additionally, hydrodynamic fluid delivery produced pressure responses (increase up to 25 mmHg) that generally lasted the duration of the infusions (Figure 47).

3. Nephron structure and function appear normal after hydrodynamic delivery and transgene expression using plasmid and adenovirus vectors

We looked for evidence of injury following hydrodynamic gene delivery by examining kidney structure and function using several approaches. In one approach we utilized intravital two-photon microscopy to determine that rat kidneys retained microvascular integrity and cells of the various nephron segments remained metabolically active after gene delivery and expression. Various animals were injected with high-molecular-weight dextrans (150-kDa) via the jugular vein, after which we observed robust peritubular vasculature perfusion kDa) dextrans labeled with Cascade blue, respectively, and gauged renal filtration and endocytic uptake capacities. This analysis was conducted 3 to 28 days after the non-viral and viral hydrodynamic injections.

In all cases, after infusing the dextrans, we observed the rapid appearance of both dextrans in the kidney by two-photon microscopy. As stated before, large-molecular-weight dextran molecules were restricted to the vasculature. The low-molecular-weight dextran molecules passed the glomerular filtration barrier, and were endocytosed by proximal tubule epithelial cells and concentrated within the distal tubule lumens (Figures 48-50). These results are consistent with normal nephron function in these animals[180].

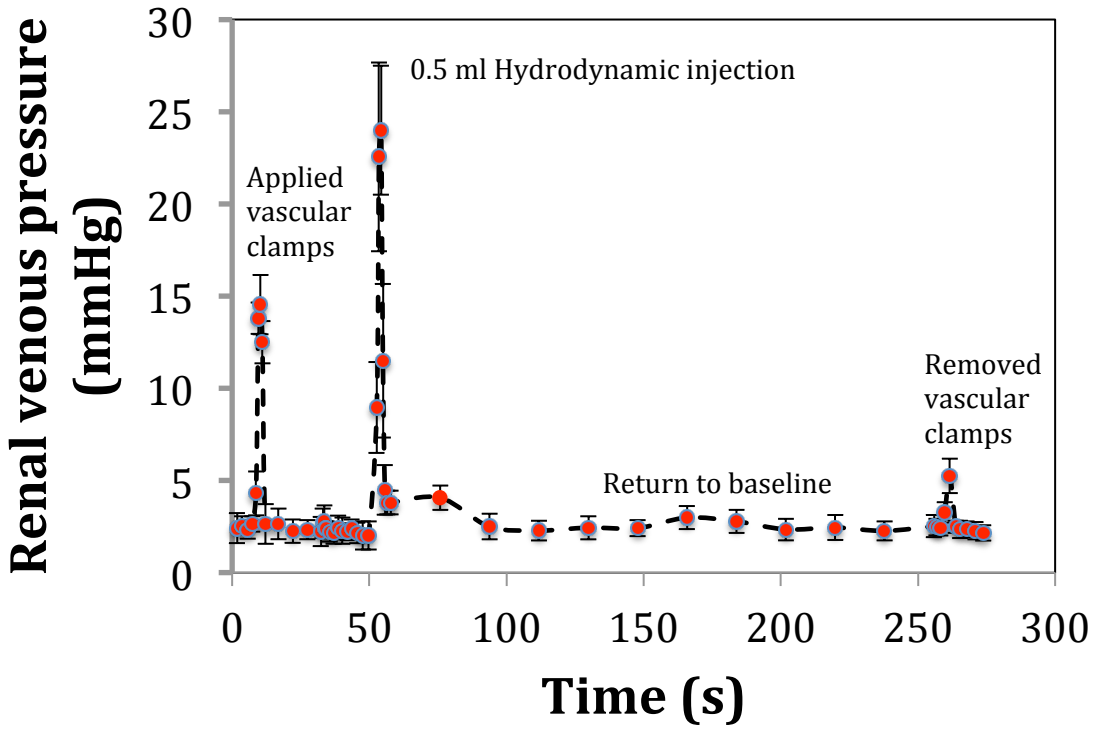

Figure 47. Changes in renal venous pressure recorded during hydrodynamic injections

A measure of the changes in venous pressure that occur throughout a hydrodynamic injection (with vascular clamps) of 0.5 ml solution into the left renal vein of a live rat.

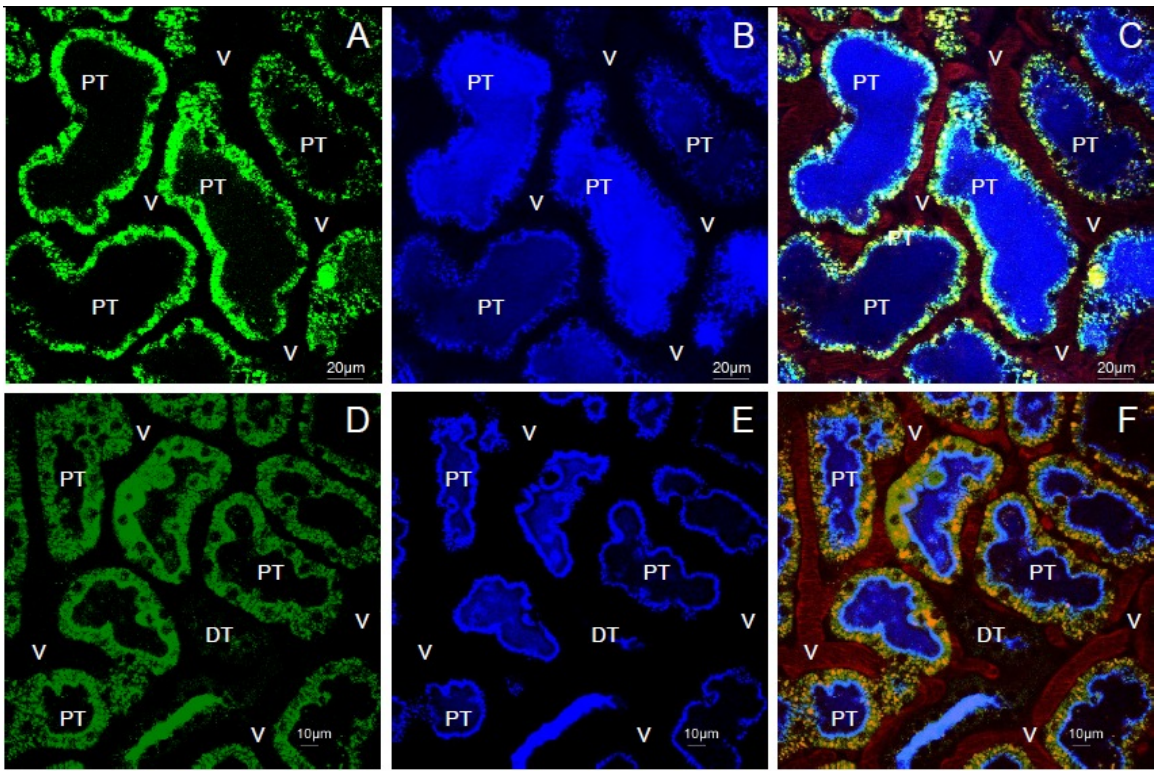

Figure 48. Renal structure and function appeared unaltered by hydrodynamic delivery and expression of plasmids and adenovirus vectors
These data provide signs of intact renal structural and function capacities post hydrodynamic transgene delivery. The data are taken from a live rat 3 days after it was treated with EGFP and EGFP-actin naked plasmid vectors. Images (A-C) outline EGFP and (D-F) outline EGFP-actin transgene expression in proximal tubule (PT) epithelial cells. Solutions containing 3 kDa Cascade blue and 150 kDa TRITC dextrans were infused into the jugular veins of live rats. Robust and widespread uptake of the low molecular weight dextran solutions was observed after dye infusion, presented in images (B) and (E). The Cascade blue dextran was rapidly filtered by glomeruli, and was then endocytosed by into proximal tubule epithelial cells. Additionally, the large molecular weight dextran molecules were restricted to the vasculature as shown in images (C) and (F). Images (C and F) were composed by merging green, blue and red pseudo-colors originating from the EGFP transgenes, and low and large molecular weight dextrans respectively. These data provided evidence that both transformed and non-transformed renal cells retained their functional activity.

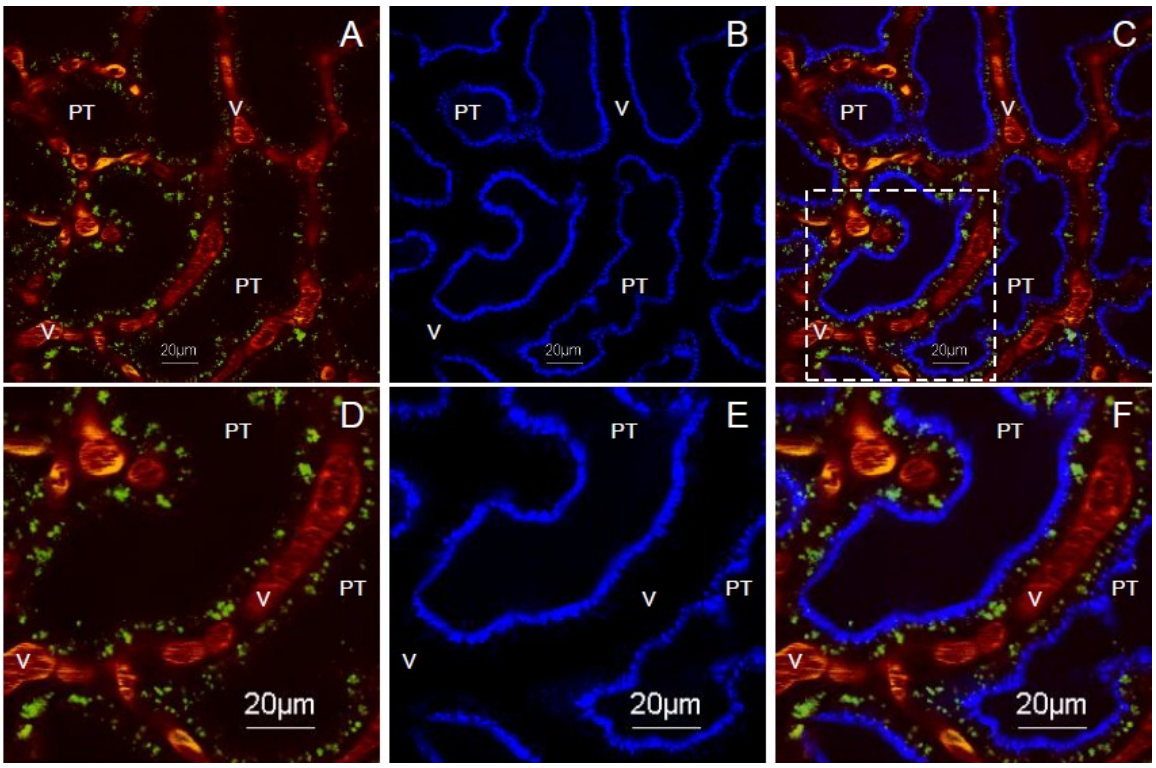

Figure 49. Vascular flow and renal filtration appear to be hindered by hydrodynamic-based baculovirus expression
Monitoring renal function in live animals 3 days after they received hydrodynamic baculoviral treatment. Intravital two-photon micrographs are presented to illustrate the simultaneous filtration and endocytic uptake, and vascular distribution of a low (3 kDa Cascade Blue) and large (150 kDa TRITC) dextrans respectively. The dyes were introduced systemically via a jugular catheter: (A) vascular (V) containment of the red large molecular weight dye and regions expressing the GFP transgenes, (B) robust accumulation of the filtered Cascade blue dye only along the brush borders of proximal tubules (PT) expressing the transgenes and regions absent of the transgene incorporation, (C) overlay of images (A) and (B). Images (D) through (F) present a magnified view of the region highlighted in (C).

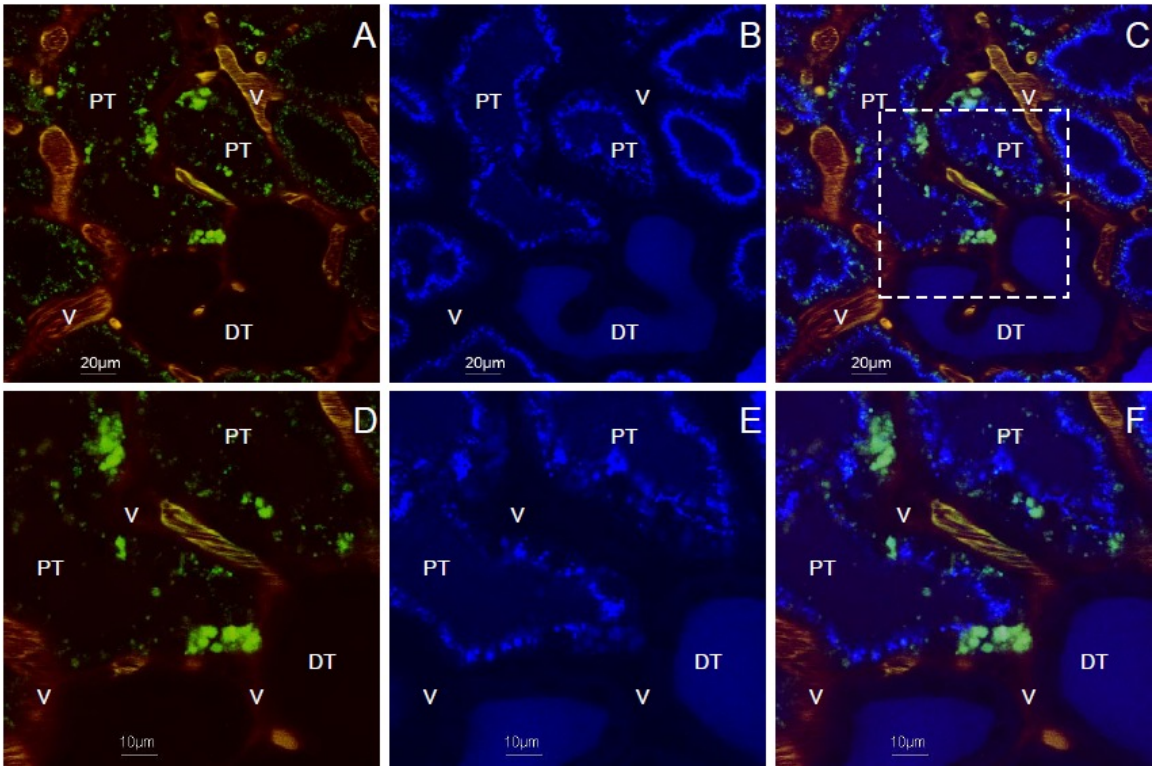

Figure 50. Renal cells functional activity appears to be hindered by hydrodynamic-based baculovirus expression

Monitoring renal function in live animals 3 days after they received hydrodynamic baculoviral treatment. Intravital two-photon micrographs are presented to illustrate the simultaneous filtration and endocytic uptake, and vascular distribution of a low (3 kDa Cascade Blue) and large (150 kDa TRITC) dextrans respectively. The dyes were introduced systemically via a jugular catheter: (A) vascular (V) containment of the red large molecular weight dye and regions expressing the GFP transgenes, (B) limited accumulation of the filtered Cascade blue dye in the brush border regions of proximal tubules (PT) that expressed the baculovirus transgenes and, (C) overlay of images (A) and (B). Images (D) through (F) present a magnified view of the region highlighted in (C). Again, there was no evidence of these low molecular weight dextrans being internalized by vesicles in these epithelial cells.

An important result from these experiments revealed the low-molecular-weight dextran molecules were taken up equally well by cells that either did or did not express fluorescent proteins in rats treated with plasmid and adenovirus vectors. This indicated that these cells retained functional activity. However, baculovirus vectors appeared to alter renal structure and function, beyond the 3-day period, as the endocytic capacity of renal cells that expressed baculovirus vectors appeared to be inhibited. Specifically, 3 kDa Cascade Blue molecules aggregated along proximal tubule brush borders and were not internalized by these epithelial cells as expected (Figures 49 and 50).

4. Hydrodynamic delivery facilitates robust cellular internalization of low-, intermedicate-, and high-molecular-weight exogenous macromolecules, which are comparable in size to transgene vectors, throughout live rat kidneys

We investigated whether hydrodynamic injections augmented with vascular clamps could reliably facilitate cellular uptake of exogenous low, intermediate and large macromolecules in various live nephron segments. Remarkably, this pressurized injection facilitated robust and widespread basolateral distribution (Figure 21), and apical cellular internalization of albumin and large-molecular-weight dextran molecules in a manner similar to the incorporation of low molecules weight molecules (Figures 19 and 20).

We also observed albumin and large molecular-weight dextran molecules were uncharacteristically able to access the tubule lumen at high concentrations after being delivered to the kidney via this hydrodynamic injection technique (Figure 2A). Similarly,

when 150-kDa molecules were introduced into the bloodstream before hydrodynamic injection of saline, they were internalized within tubular epithelial cells (Figure 22). Nevertheless, this atypical access for large-molecular-weight dextrans to tubule lumens and tubular epithelial cells was transient and appeared to only occur for molecules present at the time of the hydrodynamic injection process, as 150-kDa dextran molecules infused via the jugular approximately 20-30 minutes after hydrodynamic pressurized injection of saline remained confined to the vasculature (Figure 22). These results indicate possible routes of transgene entry that may facilitate renal transformation.

5. Serum creatinine levels are unaffected by fine-needle retrograde hydrodynamic renal vein fluid delivery and transgene expression

We monitored creatinine levels in normal rats that received hydrodynamic injections of saline and transgene vectors. Serum creatinine levels in these rats remained within normal baseline levels (0.3 to 0.5 mg/dl) throughout our measurement period (of up to 14 days after hydrodynamic fluid delivery). There was no significant difference between serum creatinine levels in rats that received transgenes and isotonic fluid.

6. Renal histology confirms hydrodynamic-based adenovirus/plasmid delivery and expression do not adversely affect kidney structure

Kidney biopsy was performed on rats 3 days after receiving sham, saline and transgene hydrodynamic retrograde injections applied with vascular clamping. Comparisons were made between these groups of animals demonstrated that the hydrodynamic injection process or the transgene (plasmid and adenovirus vectors)

expression did not adversely affect kidney structure (Figure 51A through 51C). However, studies conducted on tissues obtained from rats that received injections with baculovirus vectors revealed extensive glomerular deformation and disruptions to proximal tubule brush border in integrity (Figure 51D). These data confirmed our intravital two-photon and confocal fluorescence microscopy, and serum creatinine observations.

7. Hydrodynamic delivery facilitates the endocytic uptake of virions in live rat kidneys

As presented earlier, systemic baculovirus delivery did not facilitate transgene expression (Figure 25). This result could be due to baculoviral inactivation by the complement system[229], which would have reduced effective concentrations of viable virions capable of effecting renal transformation. To further investigate this phenomenon, we examined the interactions between serum complement proteins and the actin-targeting baculovirus vectors, *in vitro* and *in vivo*, under hydrodynamic conditions.

In cell culture, we did not observe transgene fluorescence from cells incubated with virus in sera with active complement proteins (Figure 52C). Whereas, intense fluorescent protein expression was recorded from cells treated with standard doses of baculoviral particles (Figure 52B), and those treated with baculovirus vectors incubated in sera containing deactivated complement proteins (Figure 52D). An analogous effect was observed *in vivo*, as presented in (Figure 53). Collectively, these data suggested that rapid and direct introduction of viral particles through the renal vein likely protected baculovirions from complement-based inactivation, and thus facilitated their expression.

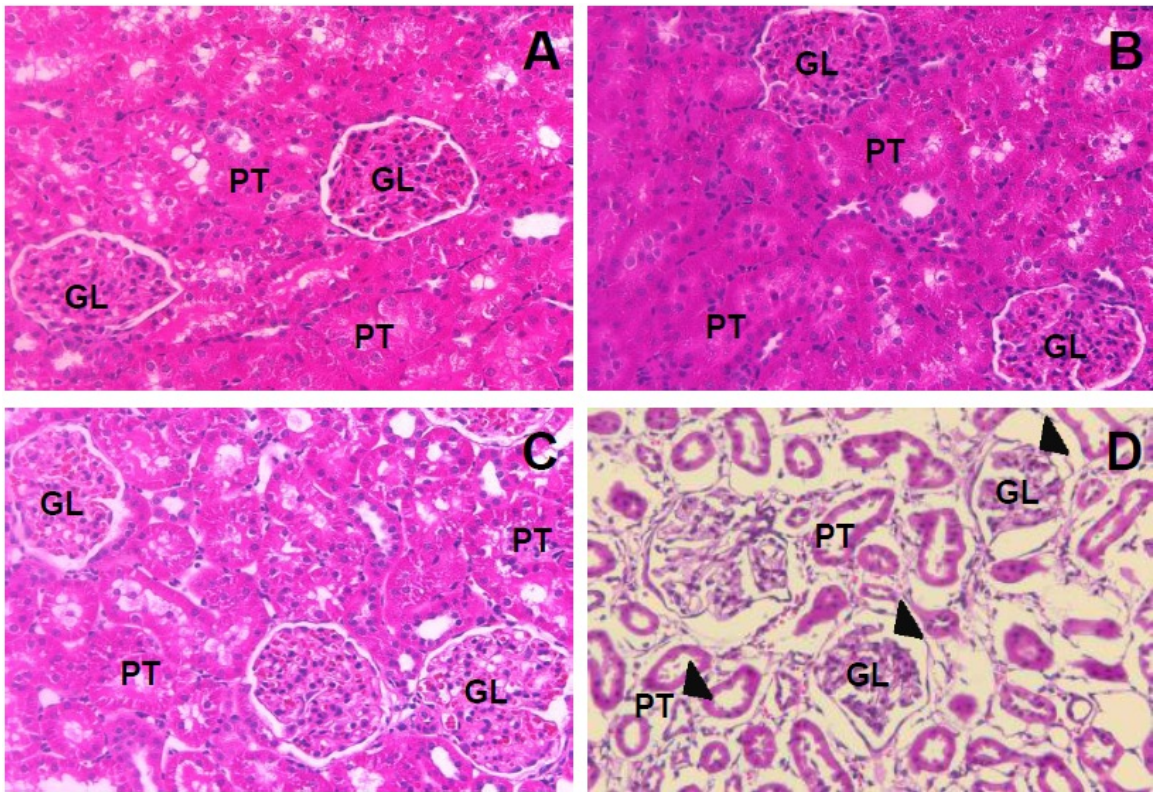

Figure 51. Histology supports claims of hydrodynamic delivery derived injury related only to baculovirus expression
Histology studies conducted on kidney tissues excised from various groups of rats that received: (A) sham injection; (B) hydrodynamic injection of saline; (C) hydrodynamic injection of Actin-GFP plasmid vectors; and (D) hydrodynamic injection of baculovirus vectors. Comparisons were made between these groups of animals illustrating that the hydrodynamic injection process and the transgene (plasmid vectors) expression did not adversely affect renal structure. However, tissues obtained from rats that received injections with baculovirus vectors had shrunken/deformed glomeruli and reduced proximal tubule brush borders (Figure 55D), as outlined by the arrowheads (GL = glomerulus and PT = proximal tubule).

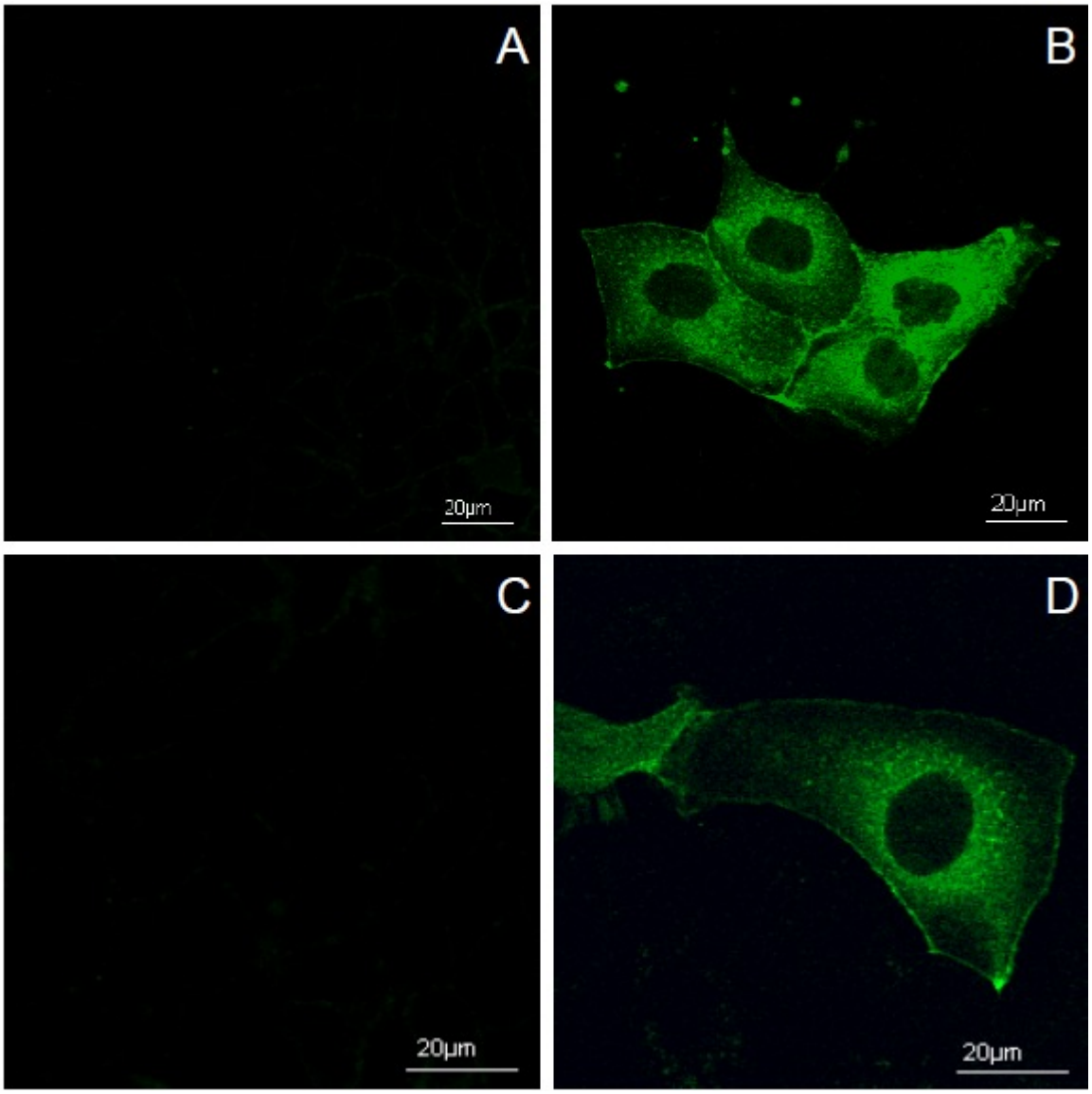

Figure 52. The complement response inhibits viral transformation *in vitro*
Investigating the effect complement immune proteins have on transgene expression (standard dose of the Actin-GFP applied to all cases) using MDCK cells incubated in: (A) Hepes-buffered saline; (B) Actin-GFP baculovirions suspended in Hepes-buffered saline; (C) Actin-GFP baculovirions suspended in blood sera containing active complement proteins; and Actin-GFP baculovirions suspended in blood sera containing deactivated complement proteins. These confocal micrographs were taken 1 day after treatments.

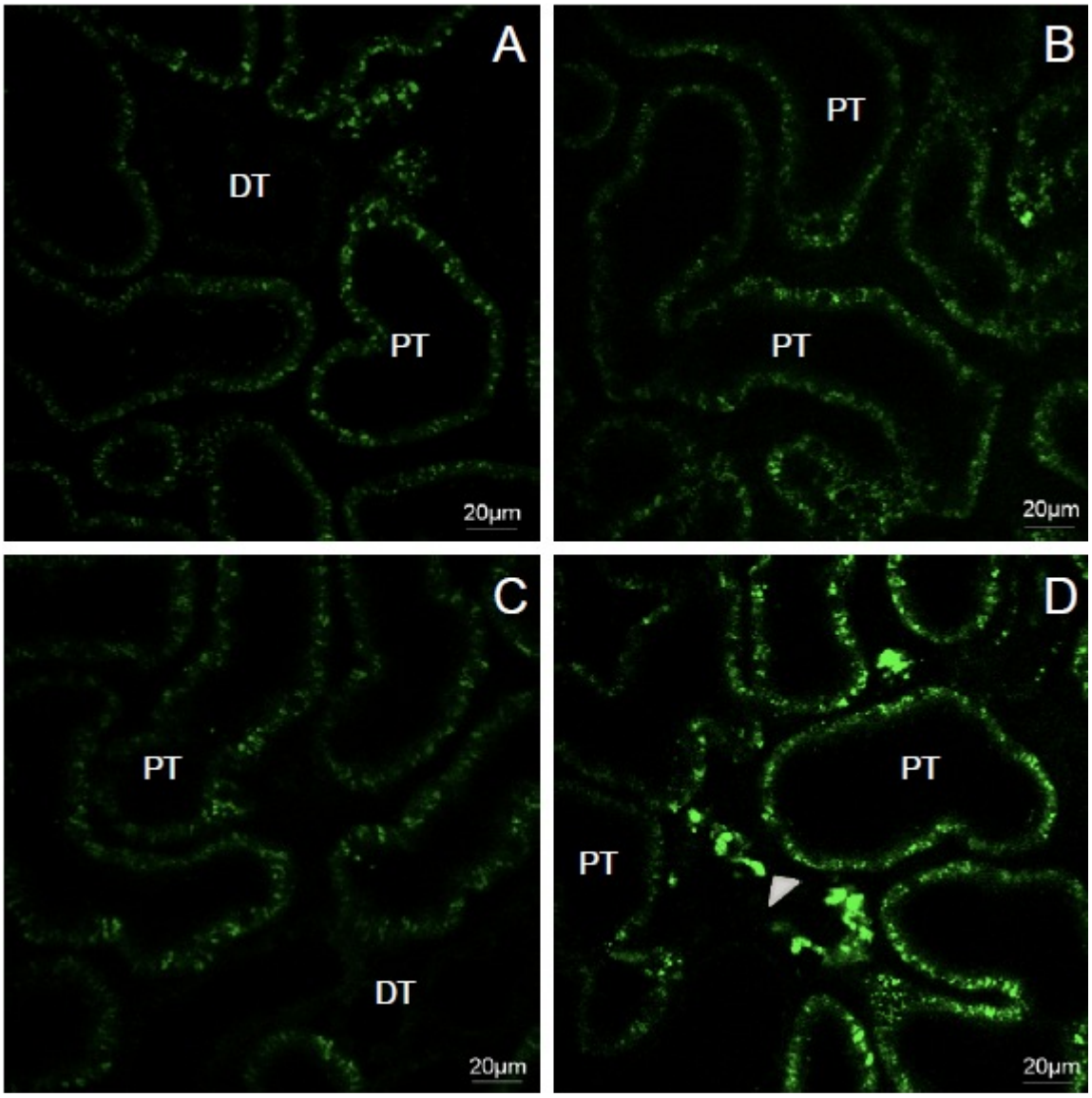

Figure 53. Hydrodynamic delivery provides a way to evade the complement immune response to facilitate exogenous gene expression *in vivo*
Live intravital micrographs illustrate transgene expression mediated by endocytic uptake of baculovirus vectors that were delivered to live rat kidney using hydrodynamic delivery. Using standard 1×10^{5} viral particles.ml^{-1} baculoviral dosage we observed: (A) baseline image taken before treatment viral; (B) image of the rat presented in (A) taken 3 days post treatment with Actin-GFP baculovirions incubated in blood sera containing active

complement proteins; (C) baseline of a 2nd rat prior to viral treatment; and (D) image of the 2nd rat presented in (C) taken 3 days post treatment with Actin-GFP baculovirions incubated in blood sera containing deactivated complement proteins. Each blood sera sample introduced into a given rat was previously drawn from its recipient. Arrowheads indicate regions of transgene expression.

8. Transgene expression restricted to kidneys that received retrograde hydrodynamic injections

No signs of fluorescent protein expression were detected in the contralateral right kidney (i.e. non-injected kidney) or the other highly vascular organs examined (heart, liver, lung and spleen) harvested from rats that previously received viral and non-viral plasmid hydrodynamic or tail vein injections (Figure 54).

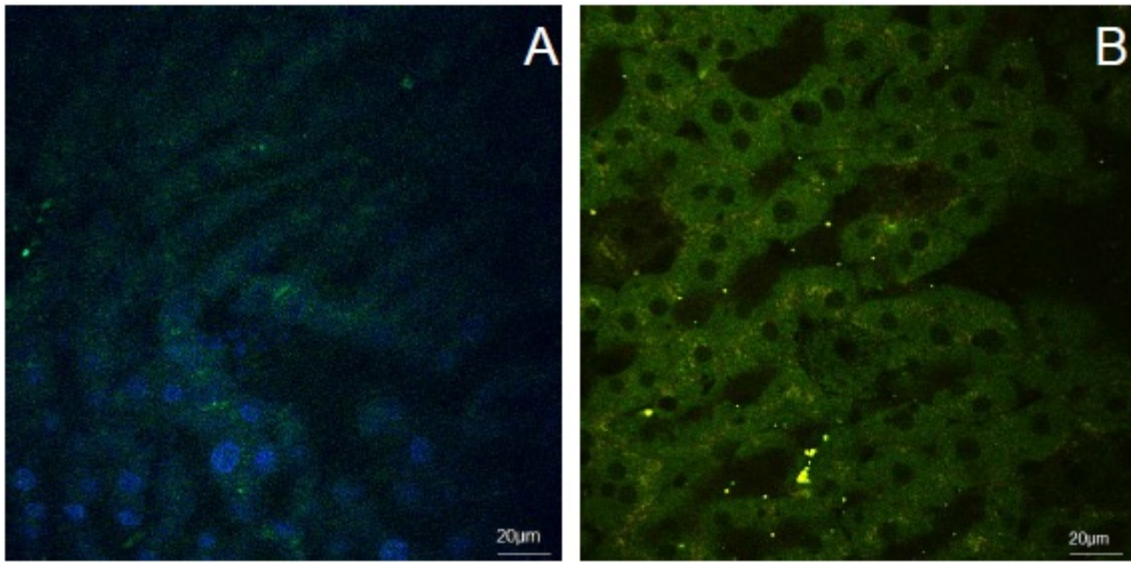

Figure 54. Transgene expression was not generated from tail and portal vein injections of baculovirus vectors
Absence of transgene expression indicating that tail vein baculovirus injections failed to deliver transgenes to live rat livers. Two-photon intravital fluorescent micrographs obtained from live rats 3 days after they received: (A) GFP tail vein injection of GFP baculovirus vectors (Hoechst was added to label nuclei), and (B) portal vein delivery of GFP-Actin plasmid vectors.

Chapter 2. Hydrodynamic fluid delivery facilitates the live global monitoring of actin cytoskeleton alterations induced by ischemia-reperfusion injury

A. Plasmid-derived fluorescent actin transgene expression verified in normal rats

Using hydrodynamic injections we were again able to generate stable plasmid-based, fluorescent actin expression in various renal tubules (Figures 55 and 56). Within these images, we noted enhanced fluorescence signals along brush borders of transformed proximal tubule epithelial cells in live rats, throughout the 2-week measurement period.

B. Actin cytoskeletal alterations visualized in live rats with ischemia-reperfusion injury

After detecting actin-chimeric fluorescent proteins in various renal tubules of rats that received hydrodynamic injections of EGFP-actin plasmid vectors, we subjected these animals to moderate (30-45 minutes of ischemia using bilateral pedicle cross-clamps) and severe (60 minutes of ischemia induced from bilateral renal pedicle cross-clamps) renal injury. We monitored transfected regions throughout the first 60-minutes directly after renal blood flow was reinstated (Figures 57-59).

The intact fluorescent protein morphology observed in these rats prior to inducing ischemia-reperfusion injury (IRI), were transformed into regions of fluorescent clumps and fragments following injury. The lumens of these tubules were in many cases narrowed or filled with fluorescent tissue debris, as expected with such ischemic injury.

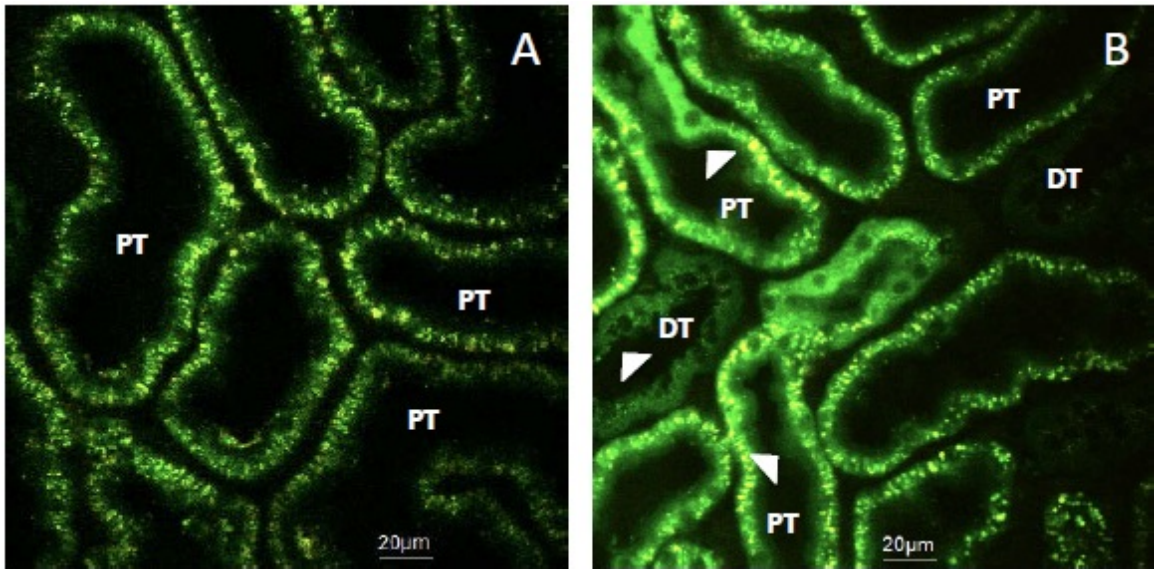

Figure 55. Intravital micrographs of fluorescent actin expression generated 3 days after hydrodynamnic delivery in a rat directly before it was subjected to ischemia-reperfusion injury

Intravital two-photon micrographs taken: (A) before hydrodynamic delivery (tissue autofluorescence), (B) rat in (A) 3 days after hydrodynamic treatment of saline, and (C) 3 days after hydrodynamic delivery of Actin-GFP plasmids in another rat. Arrowheads indicate the regions of enhanced transgene-based fluorescence along the brush border of proximal tubule (PT) epithelial cells and within distal tubule epithelial (PT) cells. Red and green pseudo-colors are merged in these images to differentiate between transgene and innate tissue fluorescence signals.

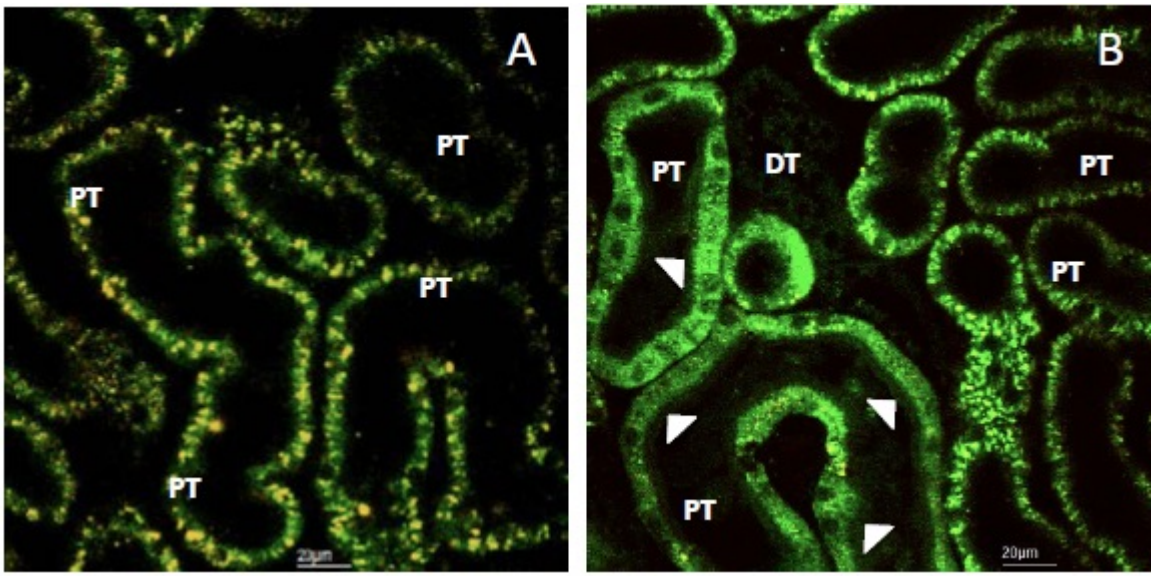

Figure 56. Intravital micrographs of fluorescent actin experssion generated 14 days after hydrodynamnic delvey in a rat directly before it was subjected to ischemia-reperfusion injury

Intravital two-photon micrographs taken from a rat in 14 days after hydrodynamic treatment of Actin-GFP plasmids. Arrowheads indicate the regions of enhanced transgene-based fluorescence along the brush border of proximal tubule (PT) epithelial cells and within distal tubule epithelial (PT) cells. Red and green pseudo-colors are merged in these images to differentiate between transgene and innate tissue fluorescence signals.

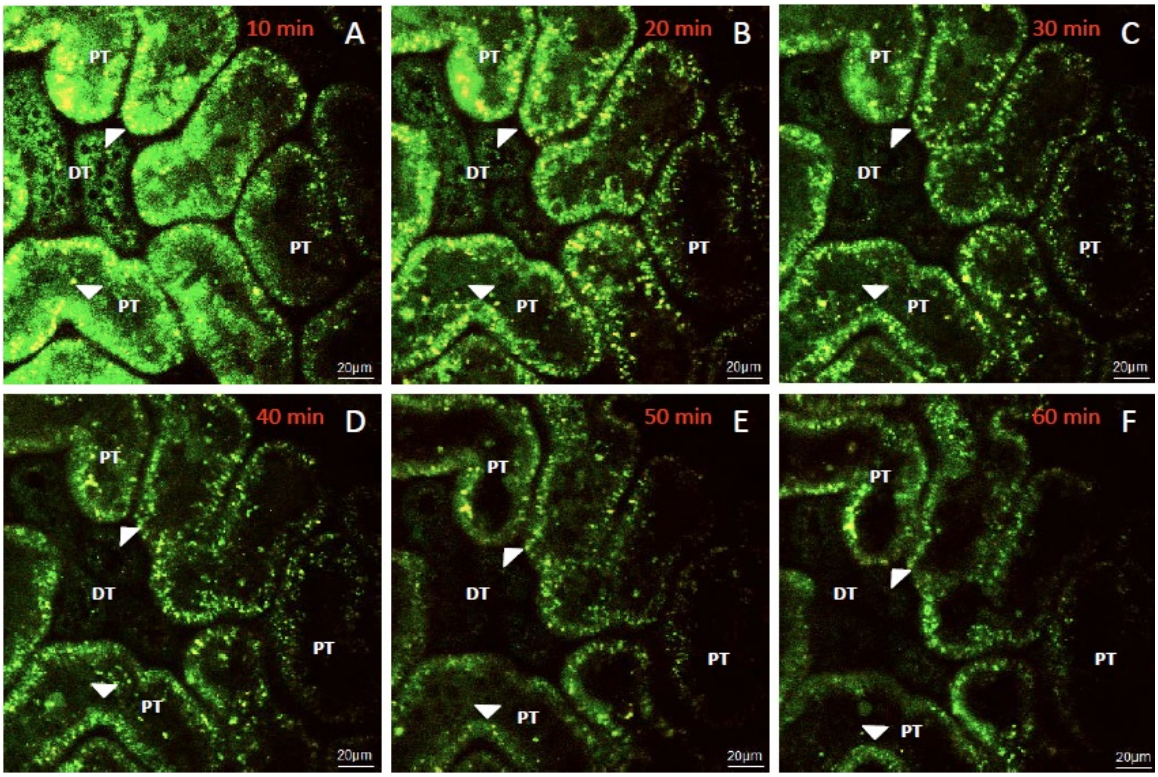

Figure 57. Intravital micrographs illustrating the disruption of cellular and tubular actin-based structures in the setting of severe bilateral ischemia-reperfusion injury on day 3 after transgene delivery

Various intravital two-photon micrographs taken from a rat 3 days after it received hydrodynamic treatment of Actin-GFP plasmids. At that time the rat was subjected to a severe ischemia/reperfusion injury. Transgene expression was first verified in this animal receiving hydrodynamic treatment as shown in Figure 55(B). The animal was then subjected to a severe renal injury (60 minute occlusion of renal blood flow). After which, we monitored the widespread loss and redistribution of fluorescent actin cytoskeletal components (arrowheads) directly after ischemia/reperfusion injury for a period of 60 minutes. Red and green pseudo-colors are merged in these images to differentiate between transgene and innate tissue fluorescence signals.

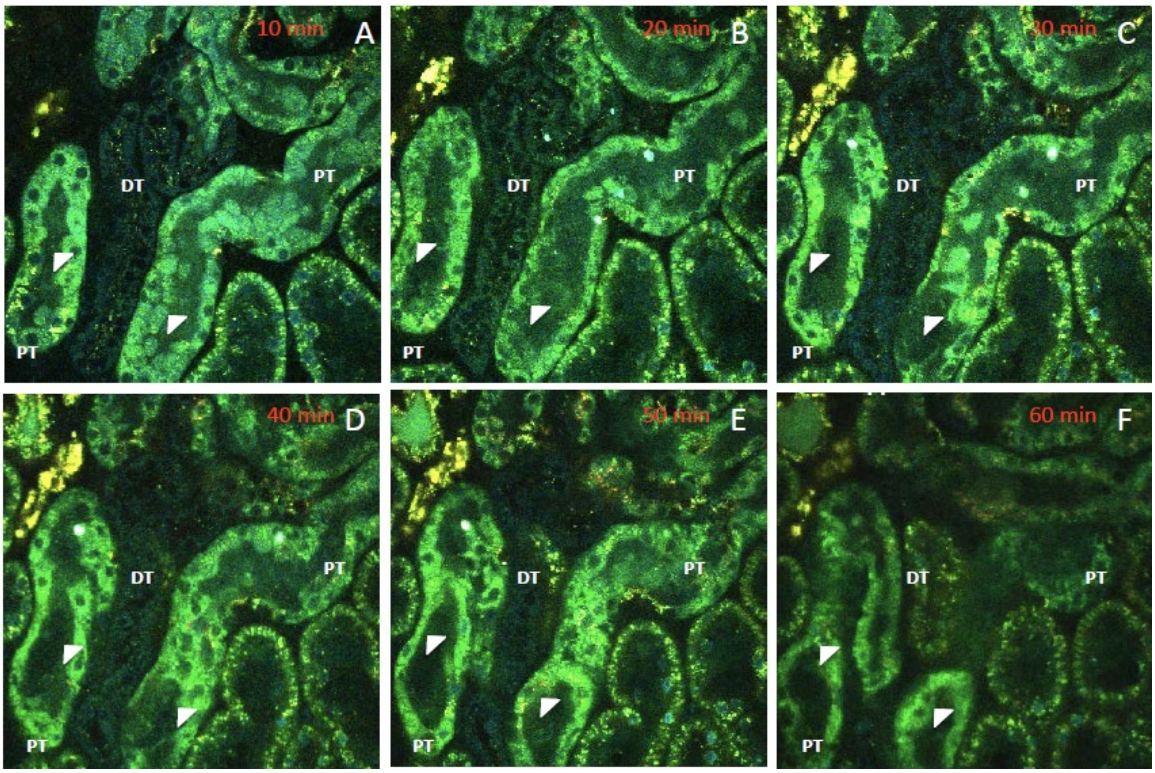

Figure 58. Intravital micrographs illustrating the disruption of cellular and tubular actin-based structures in the setting of severe bilateral ischemia-reperfusion injury on day 14 after transgene delivery

Various intravital two-photon micrographs taken from the same rat 14 days after it received hydrodynamic treatment of Actin-GFP plasmids. At the 14-day mark it was subjected to a severe ischemia/reperfusion injury. Transgene expression was first verified in this animal receiving hydrodynamic treatment as shown in Figure 56(B). The animal was then subjected to a severe renal injury (60 minute occlusion of renal blood flow). After which, we monitored the widespread loss and redistribution of fluorescent actin cytoskeletal components (arrowheads) directly after ischemia/reperfusion injury for a period of 60 minutes. Red and green pseudo-colors are merged in these images to differentiate between transgene and innate tissue fluorescence signals.

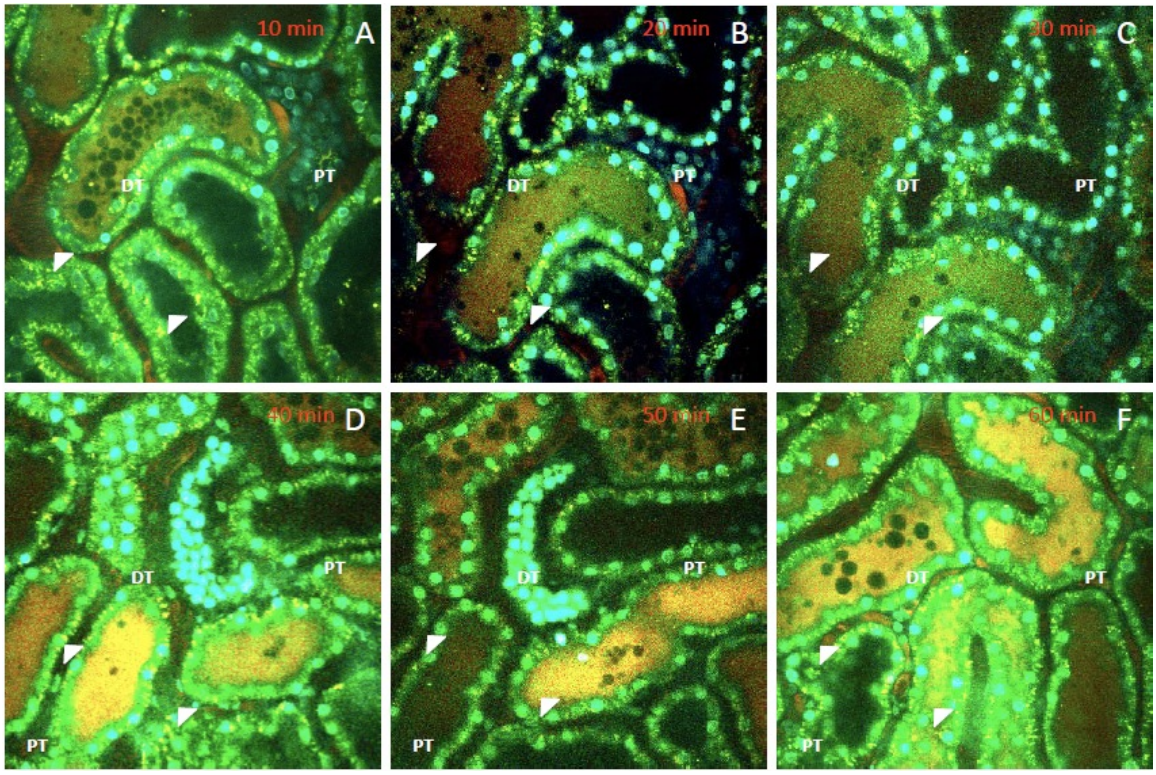

Figure 59. Widespread alterations to fluorescent actin in the setting of severe bilateral ischemia-reperfusion injury on day 3 after transgene delivery
Various intravital two-photon micrographs taken from the same rat 7 days after it received hydrodynamic treatment of Actin-GFP plasmids. The animal was subjected to a severe ischemia/reperfusion injury on the 7th day. The animal was then subjected to a severe renal injury (60 minute occlusion of renal blood flow). After which, we monitored the widespread loss and redistribution of fluorescent actin cytoskeletal components (arrowheads) directly after ischemia/reperfusion injury for a period of 60 minutes. Red and green pseudo-colors are merged in these images to differentiate between transgene and innate tissue fluorescence signals.

These data provide demonstrate that hydrodynamic-based fluorescent protein expression can serve as a good fluorescent cellular marker for in both normal and injury settings.

During the reperfusion phase we observed the real-time break down of fluorescent tubular structures, cell sloughing, an overall progressive loss of tubular florescence, and the migration of fragmented nuclei traveling through tubule lumens and blood vessels (Figures 58 and 59). Sloughed fragments of renal tissues travelled through tubular lumens where they could eventually form debris clusters.

In separate experiments, low and large molecular weight dextrans were infused into jugular veins after initiating IRI. Using these compounds we further monitored structural and functional changes in rats for 60 minutes during reperfusion (Figure 59). These studies also revealed evidence of altered renal vascular integrity, as signified by the filtration of both low and large molecular weight dextrans into proximal tubule lumens.

Chapter 3. Hydrodynamic fluid delivery facilitates reliable transgene expression in live rats with mild and intermediate ischemia-reperfusion injury

A. Retrograde hydrodynamic injections facilitate delivery of large and low molecular weight dextrans and toluidine dye in rats with renal ischemia-reperfusion injury

Prior to attempting hydrodynamic transgene delivery in rats with any form of renal ischemia-reperfusion injury, we first determined whether it was possible to use this injection technique (Figure 2A) to successfully deliver exogenous substances to injured kidneys. To answer this question, we compared the results obtained from hydrodynamic delivery of fluorescent dextrans in injured kidneys to those obtained from normal kidneys.

Intravital two-photon micrographs were taken from both groups of rats, within 20 minutes of them receiving hydrodynamic infusions of 0.5 ml saline containing both 4 kDa FITC and 150 kDa TRITC dextrans. In normal rats (Figure 60A), and rats with mild IRI (Figure 60B), we again observed that hydrodynamically delivered dextran molecules appeared within the vasculature, localized along brush borders of proximal tubules and within vesicles of tubular epithelial cells (Figure 60A). In comparison, images obtained from a rat that received a hydrodynamic injection 1 hour after a 45 minute bilateral renal clamp also showed the widespread distribution of the fluorescent probes within the vasculature, localized along brush borders of proximal tubules and within vesicles that were incorporated inro tubular epithelial cells (Figures 60A through 60D).

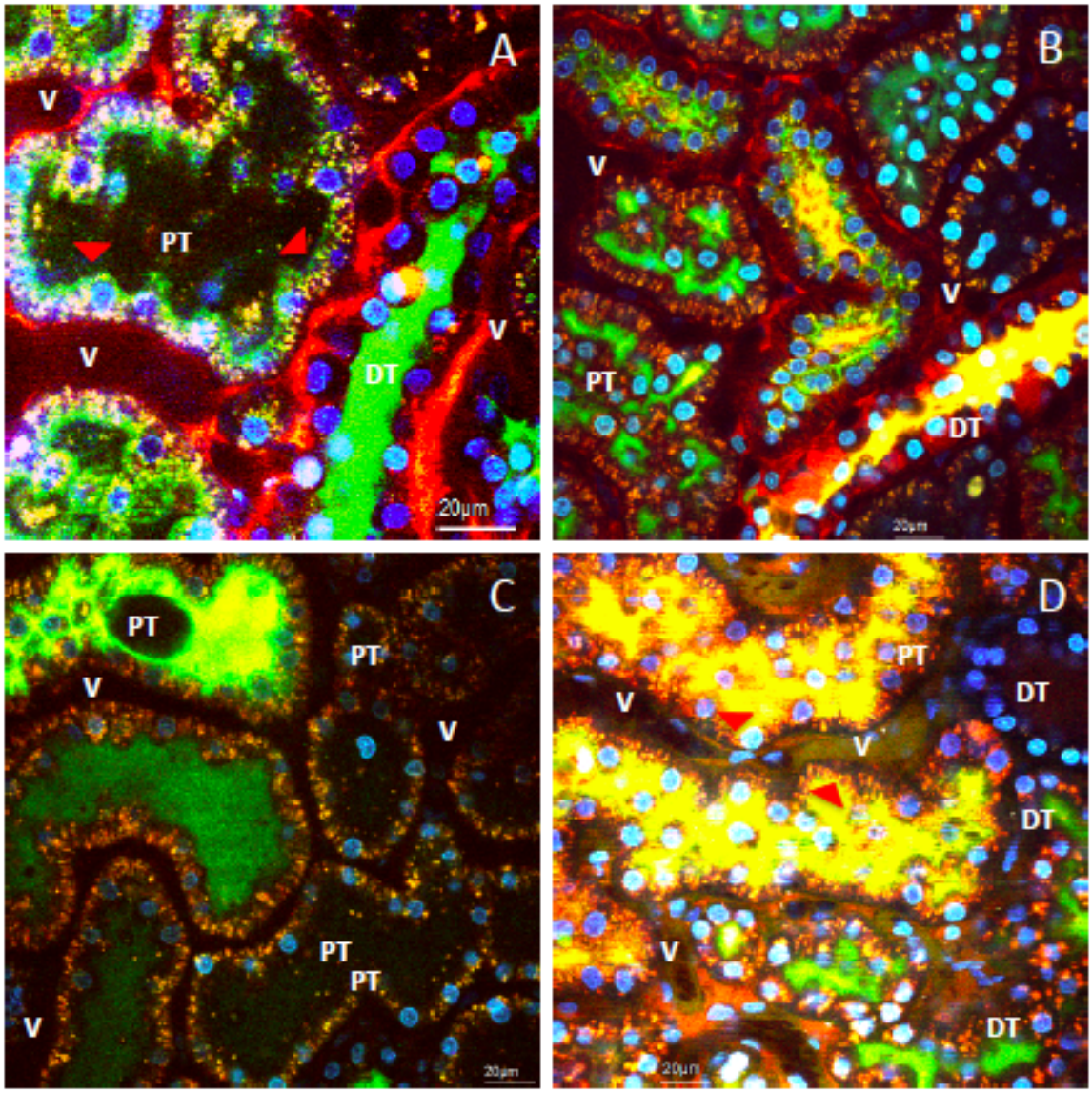

Figure 60. Hydrodynamic fine needle injections, conducted with vascular cross-clamps, facilitate the simultaneous delivery of low and large molecular weight dextrans to proximal tubule epithelia in normal and injured rat kidneys
Hydrodyanmic injections facilitate widespeared deilvery of low and high molecular weight dextrans in kidneys of rats with mild and moderate forms of renal injury. Intravital two-photon micrographs, taken with a 60x objective, from two live rats within 20 minutes of receiving hydrodynamic infusions of 0.5 ml saline containing 4 kDa FITC and 150 kDa TRITC dextrans, and Hoechst 33342 in (A) a normal rat; (B) a rat with mild

renal injury (hydrodynamic injection was given 1 hour after a 15 minute bilateral renal occlusion); and (C) and (D) rats with moderate renal injury (hydrodynamic injection was given 1 and 24 hours after a 30-45 minute bilateral renal occlusion respectively). In Figure (A), 1.5x digital zoom, we observe intense TRITC signals confined to the vasculature, FITC dextran molecules that appear to adhere to brush borders (arrowheads) and as endocytosed puncta within proximal tubule (PT) epithelial cells, and accumulation of the FITC dye within the lumens of the distal tubules (DT). These observations provide evidence of intact structural and functional renal capacities and widespread delivery of exogenous materials. In comparison, the relatively varied and mixed signal from the TRITC and FITC dextrans within the vasculature (V) in (B), (C) and (D) signify a reduction in renal blood flow, deformed and denatured nuclei within PTs, DTs, and the vasculature (arrows) - hallmarks of apoptosis, and reduced level of renal filtration (reduced concentration of FITC molecules and blebs within distal tubule lumens), are characterized by severe ischemia/reperfusion injuries. There is widespread uptake of the exogenous materials in this injury model. Red, green and blue pseudo-colors are merged in show the presence of each probe. All images present a merger of signals derived from Hoechst 33342 labeled nuclei (blue pseudo-color signal) tissue auto fluorescence (green pseudo-color signal) and dye-based fluorescence (red pseudo-color signal). Arrowheads outline regions that incoprated the large molecular weigh dextrans.

We observed deformed nuclei in intact epithelial cells in both distal and proximal tubules, as well as in sloughed cells that occupied tubule lumens and supporting vasculature. Other signs of injury were outlined by varied labeling intensty of FITC dextran and blebs within tubular lumens, consistent with impaired renal filtration. There was also a reduction in TRITC dextran-based fluorescence signals within the vasculature, which could have resulted from the filtration of TRITC dextran molecules generated from the hydrodynamic delivery process, and further enhanced by the induced renal injury.

We again found that hydrodynamic delivery, augmented with vascular clamps, provided significant evidence that this method was capable of delivering substantial quantities of low molecular weight substances throughout the entire kidney (Figure 61). Whole kidneys taken from rats that received hydrodynamic delivery of 0.5 ml of toluidine blue dye into the left renal vein after ischemia-reperfusion injury: mild ischemia and delivery 1 hour after reperfusion; moderate ischemia and delivery 1 hour after reperfusion; and moderate ischemia and delivery 24 hours after reperfusion. These kidneys were harvested and sectioned within 20 minutes of injections. The dye appeared throughout the cortex and medulla of left kidneys and absent in contralateral kidneys.

B. Efficient transgene expression in rats with renal ischemia-reperfusion injury

Based on those results, we examined transfection in injured rats at the 3-day time point. Two-photon fluorescent micrographs were acquired from live rats that received hydrodynamic transgene injections with mild and acute ischemia-reperfusion injury.

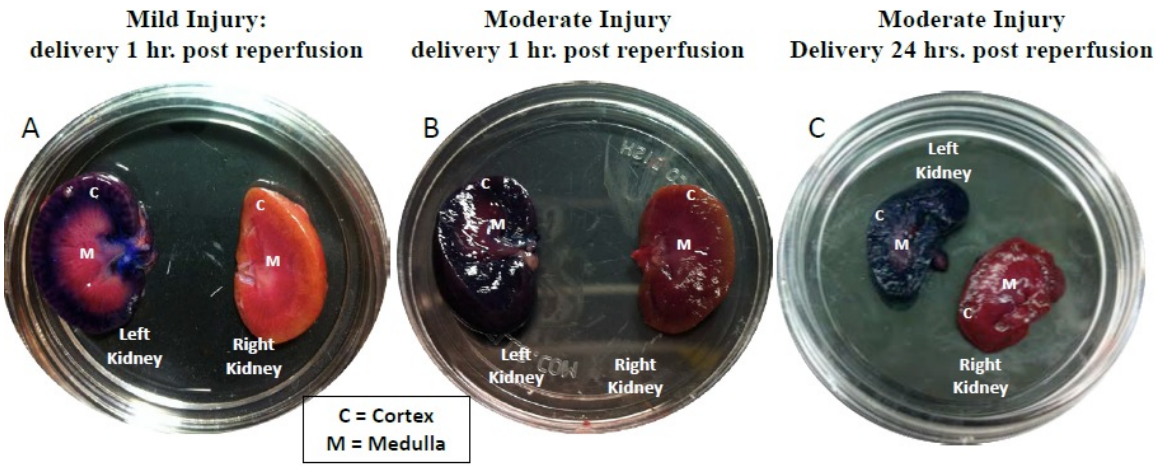

Figure 61. Hydrodynamic fine needle injections, conducted with vascular cross-clamps, limits the delivery of exogenous probes to target kidneys in rats with moderate forms of ischemic injury

Hydrodynamic injections facilitate the delivery of exogenous substances throughout the entire kidney.Whole kidneys taken from rats that received hydrodynamic delivery of 0.5 ml of toluidine blue dye into the left renal vein after ischemia-reperfusion injury: (A) mild ischemia and delivery 1 hour after reperfusion; (B) moderate ischemia and delivery 1 hour after reperfusion; and (C) moderate ischemia and delivery 24 hours after reperfusion. These kidneys were harvested and sectioned within 20 minutes of delivering the dye. The dye appeared throughout the cortex and medulla of the left kidneys and was absent in contralateral kidneys.

In these micrographs, fluorescent expression is observed within proximal tubule epithelial cells and within the lumen of occluded tubules of live rats that received plasmid treatments at both investigated injection time points (1 and 24 hours after establishing IRI). The distinctive fluorescent pattern observed along proximal tubule brush borders in normal rats (Figure 62) was also present in rats, with the mild form of ischemic injury (Figure 63), which received hydrodynamic injections of EGFP-actin plasmids. However, this pattern was absent in rats with moderate ischemia-reperfusion injury (Figures 64 and 65). As expected, there was also a substantial disruption to normal renal architecture in rats that received moderate injury. This made it at times particularly difficult to make morphologic distinctions between proximal and distal tubules (Figure 64D).

Using intravital two-photon microscopy, we estimated a 70-90% transfection efficiency using this injection technique in rats with moderate ischemia-reperfusion injury that received hydrodynamic delivery 1 and 24 hours after establishing injury. These rates were greater than those obtained for normal rats and those subjected to a mild form of ischemia-reperfusion injury, which ranged from approximately 60-70%.

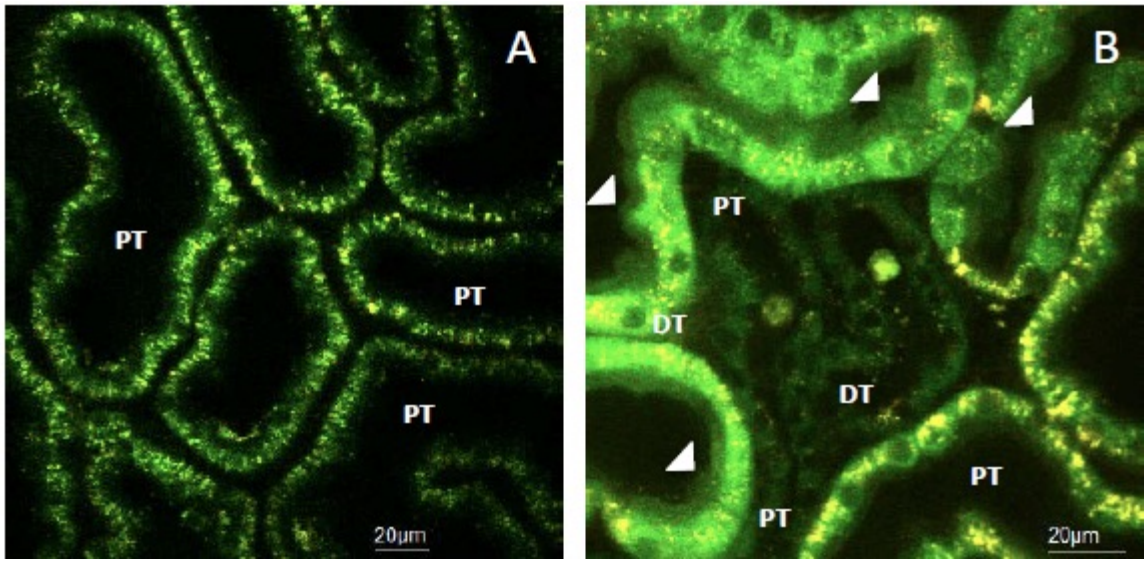

Figure 62. Fluorescent plasmid-derived protein expression in live rat proximal and distal tubules

Gene delivery and expression in live renal tubules. Intravital two-photon micrographs taken: (A) before hydrodynamic delivery (tissue autofluorescence), (B) 3 days after hydrodynamic delivery of Actin-GFP plasmids in the same rat (1.5X optical zoom to highlight transgene expression pattern along brush borders). Arrowheads indicate the regions of enhanced transgene-based fluorescence along the brush border of proximal tubule (PT) epithelial cells and within distal tubule epithelial (PT) cells. Red and green pseudo-colors are merged in these images to differentiate between transgene and innate tissue fluorescence signals.

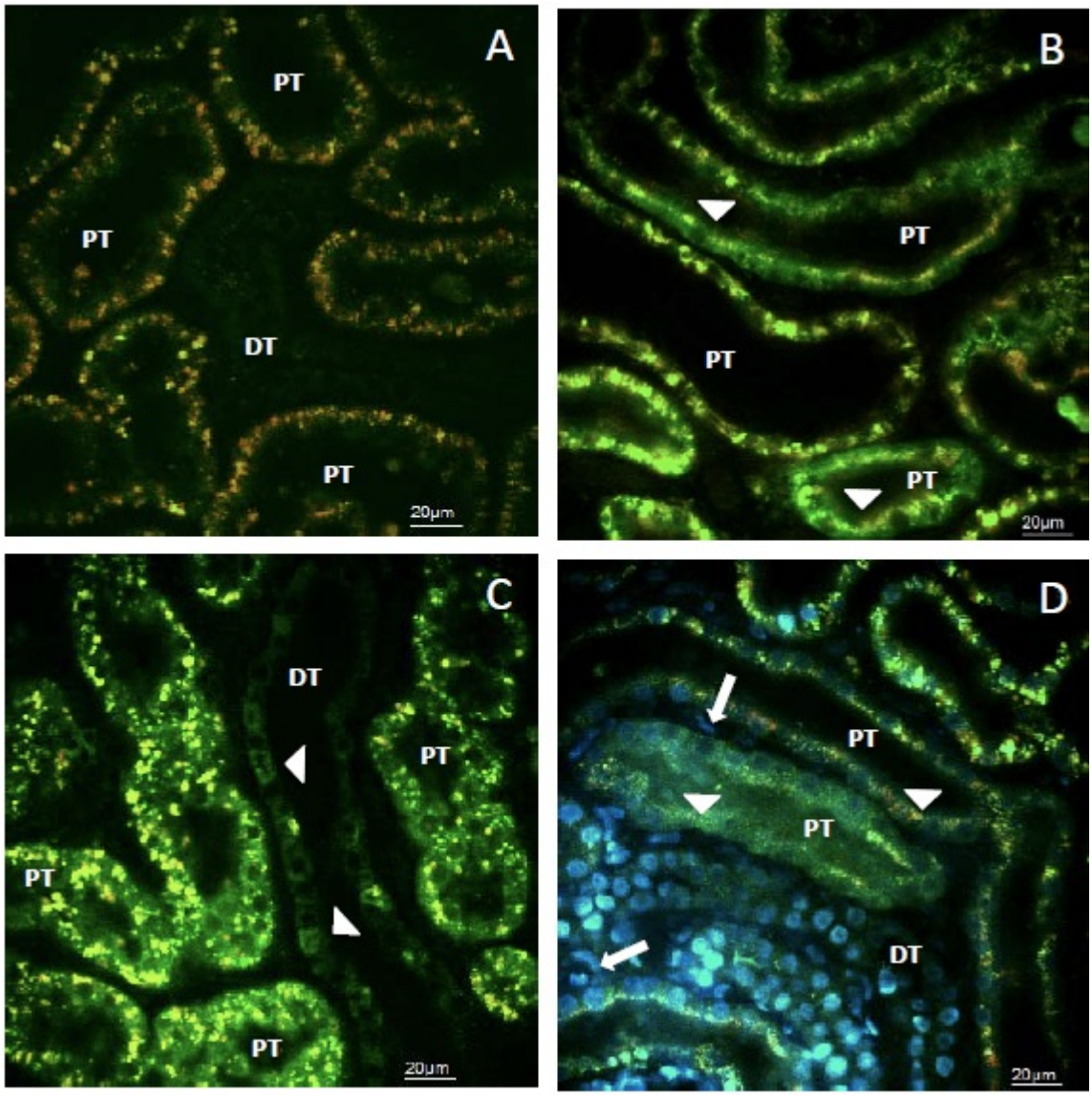

Figure 63. Hydrodynamic delivery facilitates plasmid-based fluorescent protein expression in rats with mild ischemia-reperfusion injury
Two-photon fluorescent microscopic images taken from a live rats with mild ischemia/reperfusion injury 3 days after the initial insult: (A) image taken from a rat that did not receive any transgene or saline treatment. Structural damage can be seen within proximal tubules (PT) by debris within tubule lumens; (B), (C) and (D) images taken from separate rats that were subjected to hydrodynamic transgene delivery of Actin-GFP

plasmids 1 hour after a 15 minute bilateral renal clamp. Enhanced transgene-based fluorescence can be seen within intact proximal tubule (PT) epithelial cells (arrowheads). Again, deformed nuclei within proximal (PT) and distal tubules (DT), and the vasculature (arrowheads) are hallmarks of apoptosis, which are expected with this ischemia/reperfusion injury. Red and green pseudo-colors are merged in these images to differentiate between transgene and innate tissue fluorescence signals.

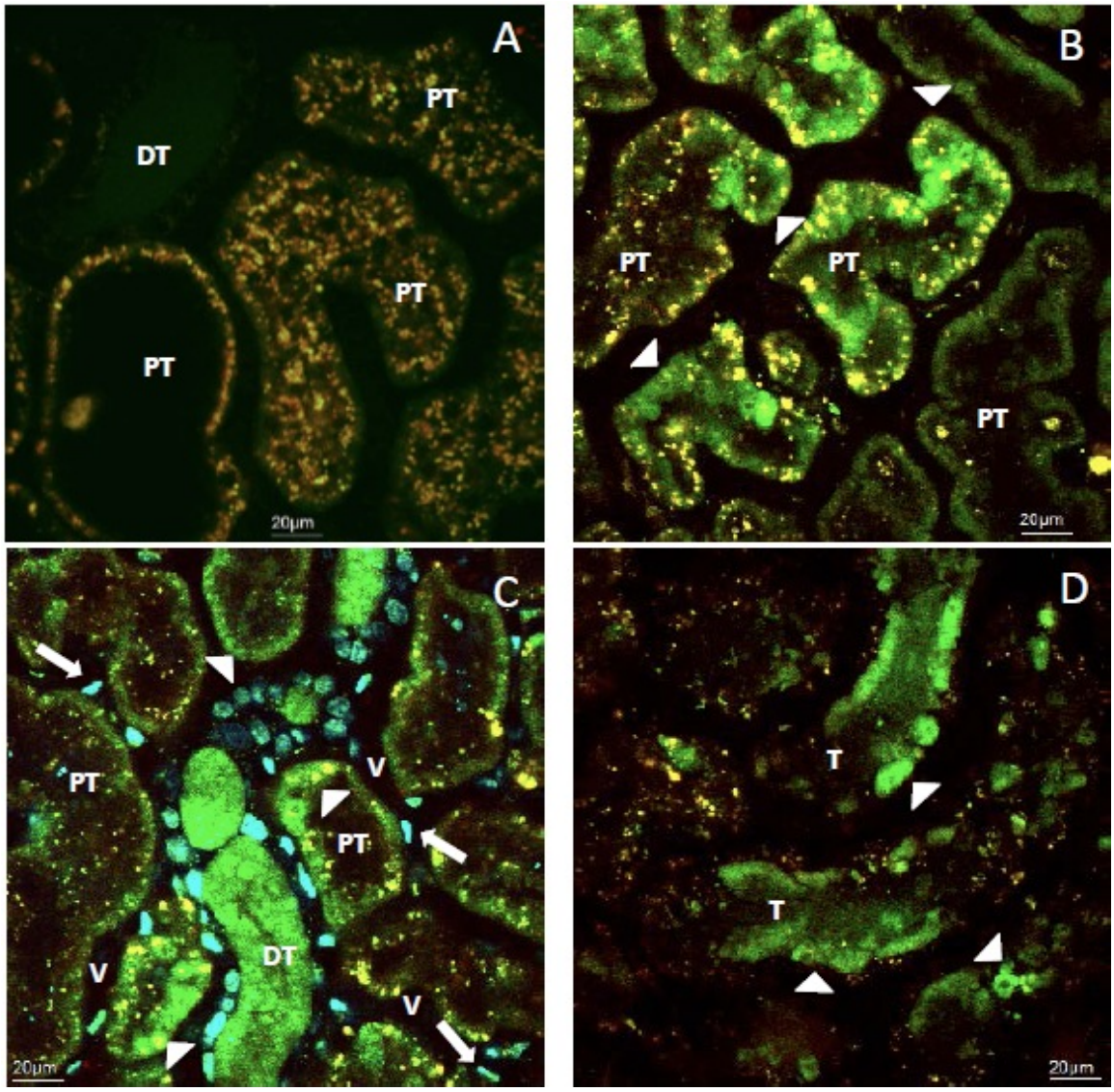

Figure 64. Hydrodynamic delivery facilitates plasmid-based fluorescent protein expression in rats with moderate ischemia-reperfusion injury 1 hour after the injury was established

Fluorescent microscopic images taken from a live rats with moderate ischemia/reperfusion injury 3 days after the initial insult: (A) image taken from a rat that did not receive any transgene or saline treatment. Structural damage can be seen within proximal tubules (PT) by debris within tubule lumens; (B), (C) and (D) images taken

from separate rats that were subjected to hydrodynamic transgene delivery of Actin-GFP plasmids 1 hour after a 45 minute bilateral renal clamp. Enhanced transgene-based fluorescence can be seen within intact proximal tubule (PT) epithelial cells and within the lumens of occluded tubules (arrowheads). In (C) Hoechst 33342 was added to label nuclei. Red and green pseudo-colors are merged in these images to differentiate between transgene and innate tissue fluorescence signals. In certain cases the injury was so severe that it was difficult to identify specific renal segments as seen in (D).

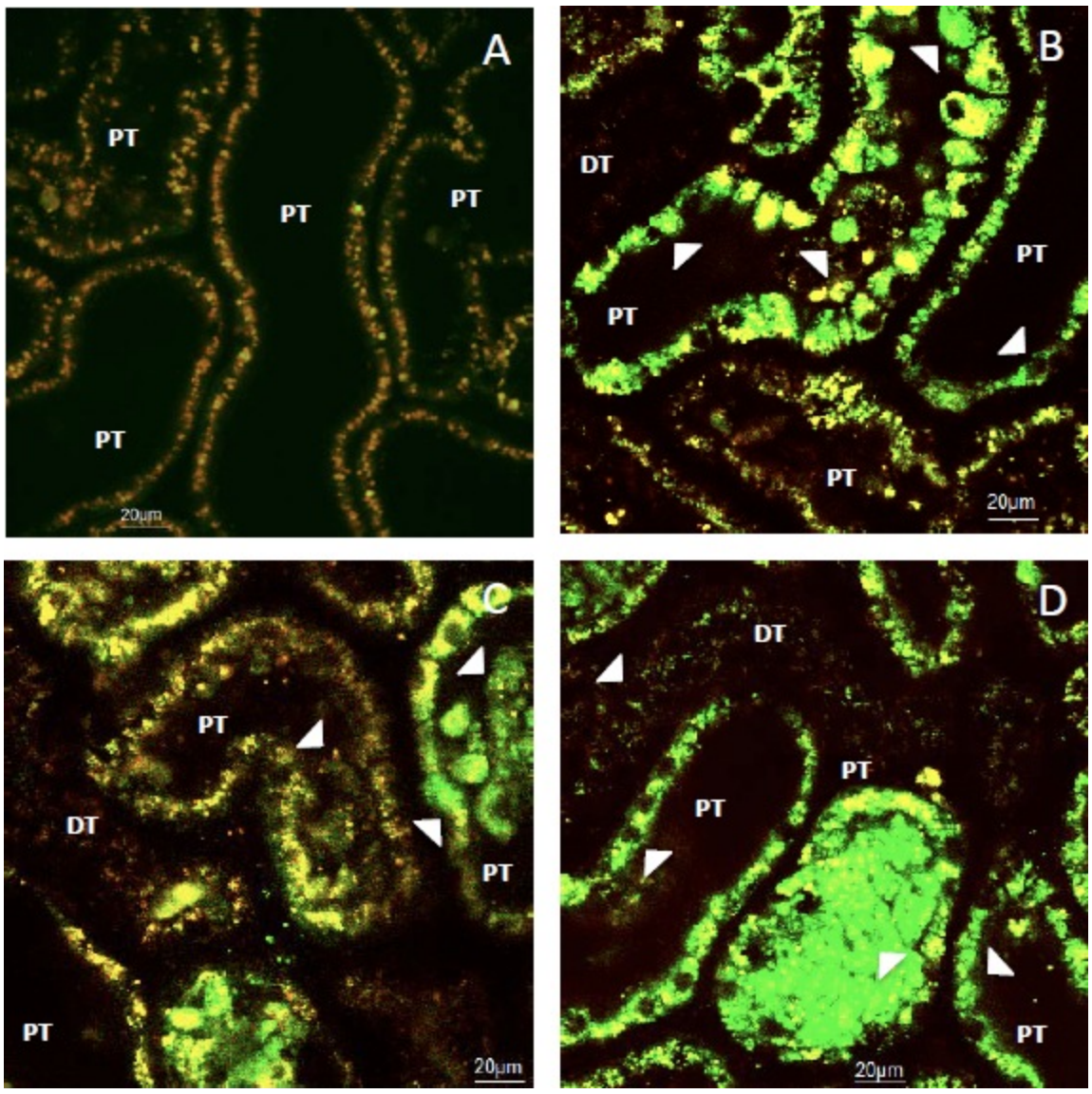

Figure 65. Hydrodynamic delivery facilitates plasmid-based fluorescent protein expression in rats with moderate ischemia-reperfusion injury 24 hours after the injury was established

Fluorescent microscopic images taken from a live rats with moderate ischemia/reperfusion injury 3 days after the initial insult: (A) image taken from a rat that did not receive any transgene or saline treatment. Structural damage can be seen within proximal tubules (PT) by debris within tubule lumens; (B), (C) and (D) images taken

from separate rats that were subjected to hydrodynamic transgene delivery of EGFP-actin plasmids 24 hours after a 45 minute bilateral renal clamp. Enhanced transgene-based fluorescence can be seen within intact proximal tubule (PT) epithelial cells and within the lumens of occluded tubules (arrowheads). Again, deformed nuclei within proximal (PT) and distal tubules (DT), and the vasculature (arrows) are hallmarks of apoptosis, which are expected with this form of ischemia/reperfusion injury. Innate tissue autofluoresence is significantly altered with renal injury, so red and green pseudo-colors are merged in these images to differentiate between transgene-based fluorescence (green) and tissue fluorescence signals.

Chapter 4. Hydrodynamic isotonic fluid delivery ameliorates ischemia-reperfusion injury in live rats

From our serum creatinine measurements we determined that hydrodynamic isotonic fluid delivery significantly reduced rises in serum creatinine when administered 1 and 24 hours after inducing moderate ischemia-reperfusion in live rats. Strikingly animals treated with hydrodynamic saline injections from at the 24-hour mark had substantial and statistically significant (p-value = 0.02) decreases in serum creatinine as compared to control/untreated animals. The creatinine levels in rats that received hydrodynamic injections 1 hour after the injury was established were also significantly lower (p-value = 0.03) than those recorded in control/untreated rats, when measured the 24 hours injury was established. Additionally, hydrodynamic isotonic fluid delivery administered at both the 1 and 24 hour marks resulted in faster returns to normal baseline serum creatinine levels. This return to baseline occurred as early as three days after the initial insult.

In contrast, creatinine levels of injured rats that did not receive hydrodynamic treatments had an extended return to baseline, generally occuring 5 days after inducing moderate IRI (Figure 66). These latter results, which were obtained from the control/untreated group, are consistent with those obtained by Molitoris et al. [217]. Moreover, we monitored serum creatinine in rats where the injection process was not executed well. In those cases hemorrhaging occured at the injection site. Interestingly, the

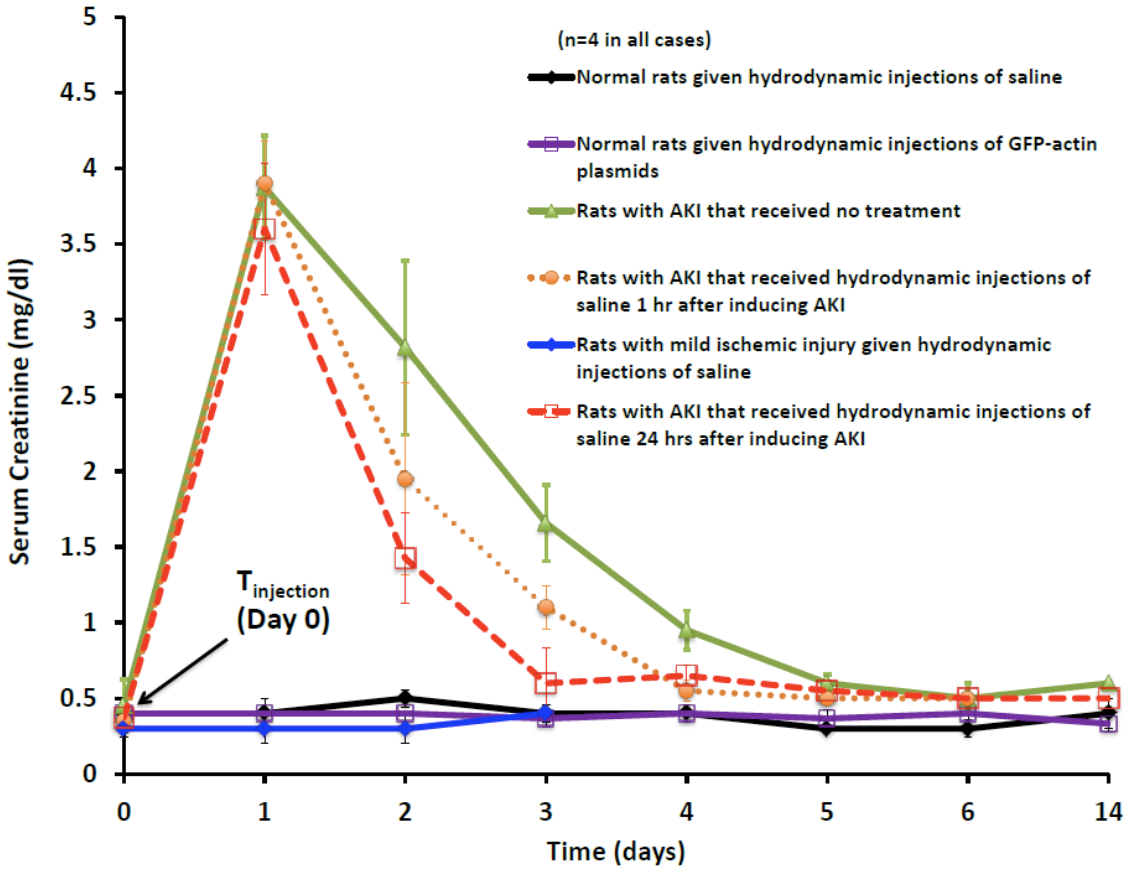

Figure 66. Hydrodynamic isotonic fluid delivery ameliroates moderate forms of renal injury

Influence of hydrodynamic isotonic fluid delivery on serum creatinine levels after ischemia-reperfusion kidney injury in rats. Hydrodynamic fluid delivery does not alter serum creatinine levels in normal rats, but appears to ameliorate serum creatinine changes during bilateral ischemia-reperfusion injury.

serum creatinine levels in these rats remained elevated, nullifying the previously observed therapeutic effect that was provided with the hydrodynamic fluid delivery. Similarly, we also monitored serum creatinine levels in rats with moderate IRI that received tail vein injections of the same volume of isotonic fluid. Systemic delivery of the given volume, appeared to have no therapeutic effect when administered at either the 1 or 24 hour time points.

As a means of further characterizing our delivery process we examined whether the hydrodynamic delivery process can adversely affect renal function. For these studies we monitored the serum creatinine in normal rats that received hydrodynamic injections of either saline or transgene vectors. From our measurements, we observed that hydrodynamic delivery has not effect on creatinine levels in normal rats, as there was no change from baseline (normal) creatinine during the 2 weeks that followed the administration of hydrodynamic fluid injections (Figure 66).

Chapter 5. Hydrodynamically delivered mitochondrial proteins protect Sprague Dawley rat kidneys against moderate ischemia-reperfusion injury

A. Bilateral clamp injury model

Serum creatinine measurements obtained from groups of rats that previously received hydrodynamic injections of saline and plasmids encoding mitochondrial genes (IDH2 and SULT1C1) were monitered across a two week period. On the 7^{th} day after each rat received a hydrodynamic injection containing either saline or a mitochondrial plasmid, they were subjected to moderate ischemia-reperfusion injury (IRI). We monitored serum creatinine levels for a week after inducing IRI and determined that hydrodynamic delivery of IDH2 or SULT1C1 genes was sufficient to blunt the effect of IRI in Sprague Dawley rats. Specifically, serum creatinine levels in these rats remained within normal levels despite being subjected to moderate IRI, when compared to rats that received hydrodynamic or tail injections of saline or fluorescent plasmids (Figure 67).

The basis for these studies were developed upon the fact that resistance to IRI can be induced experimentally (e.g., preconditioning) or can be conferred by genetic factors (i.e., as observed in the BN rat). Using Label-free quantative mass spectroscopy (LFQMS), 13 proteins were identified in a screen of mitochondria preparations obtained from the kidneys of SD rats subjected to ischemia preconditioning and compared to control kidneys (Table 2). From these, we randomly selected sulfotransferase (SULT1C1) and isocitrate dehydrogenase 2 (IDH2) proteins for gene delivery studies.

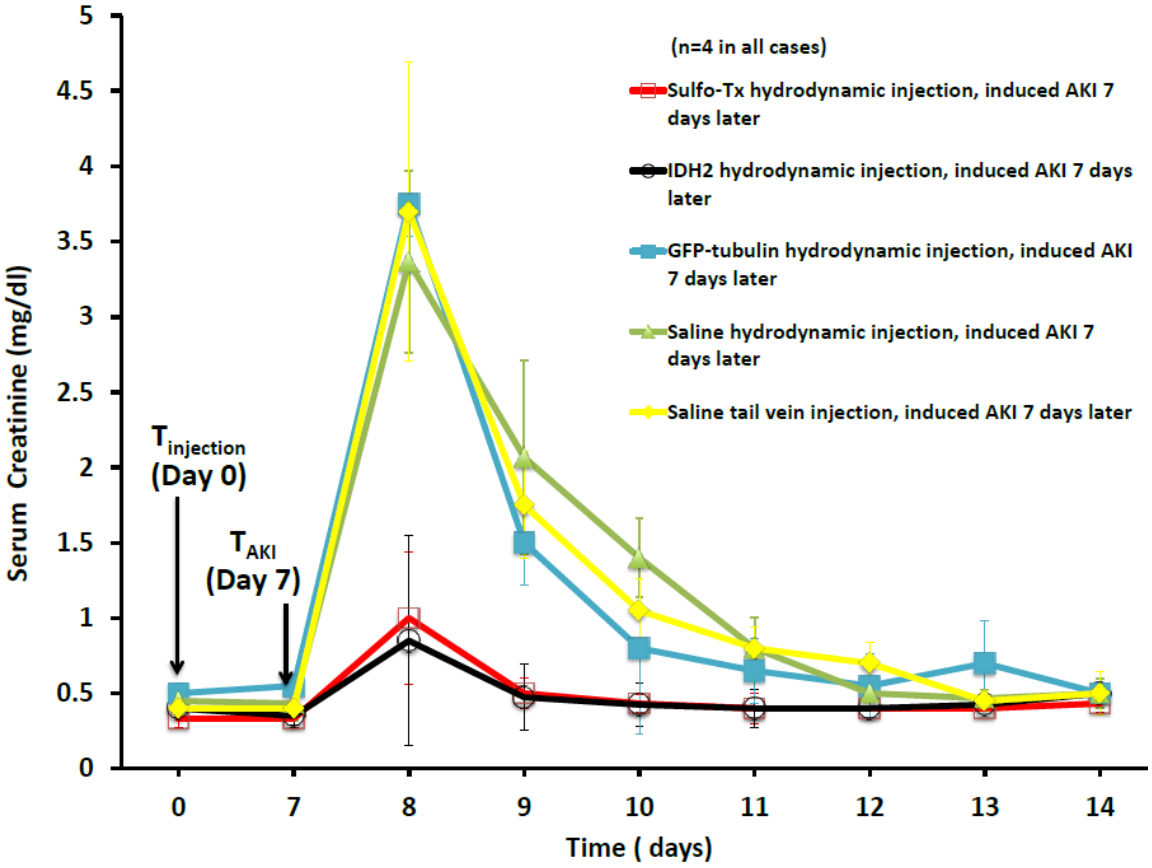

Figure 67. Hydrodynamic-based IDH2 and SULT1C1 (Sulfo-Tx) mitochondrial enzyme upregulation protects the kidney from moderate forms of renal injury
Rats hydrodynamically treated with plasmids encoding mitochondrial proteins seven days earlier, appear less susceptible to moderate ischemia-reperfusion injury.

Gene Symbol	Gene Name	Fold difference	p-value
SULT1C1	Sulfotransferase 1C2-like	2.4	0.40
IDH2	Isocitrate dehydrogenase [NADP] mitochondrial	2.2	0.31
HIST1H2BC	Histone H2B	2.0	0.25
C1QBP	Complement component 1 Q subcomponent-binding protein	1.9	0.26
ACOT2	Acyl-coenzyme A thioesterase 2, mitochondrial	1.5	0.53
ACSL1	Long-chain-fatty-acid--coa ligase 1	1.7	0.29
THUMPD2	THUMP domain containing 2 isoform 1	-3.0	0.09
MTCH2	Mitochondrial carrier homolog 2	-1.9	0.27
HSDL2	Hydroxysteroid dehydrogenase-like protein 2	-1.6	0.37
SLC25A13	Solute carrier family 25, member 13	-1.6	0.13
NDUFA5	NADH dehydrogenase [ubiquinone] 1 α subcomplex subunit 5	-1.6	0.33
SUCLG1	Succinate-coa ligase, alpha subunit	-1.6	0.04
ISCA2	Iron-sulfur cluster assembly 2 homolog	-1.3	0.01

Table 2. List of prominent protein alterations in IPC kidney mitochondria as determined by LFQMS

Using proteomics, 13 proteins were identified in a screen of mitochondria preparations obtained from the kidneys obtained from Sprague Dawley rats subjected to ischemia preconditioning and compared to control kidneys.

B. Contralateral nephrectomy and unilateral clamp injury model

We monitored serum creatinine levels in three groups of uninephrectomized rats that received hydrodynamic injections of saline, and IDH2 and SULT1C1 plasmid vectors. The right kidney was first removed from each animal, and they were then allowed to recover for 26 days. Thereafter, these rats received hydrodynamic injections of saline or plasmids, and were again allowed to recover for a week from the hydrodynamic injection before inducing moderate IRI. Uninephrectomizations and hydrodynamic injections did not alter serum creatinine. Yet, more interistingly, we determined that hydrodynamic delivery of either IDH2 or SULT1C1 plasmid was also able to blunt the effect of IRI in uninephrectomized Sprague Dawley rats (Figure 68).

C. Enhanced mitochondrial activity observed in rats treated with IDH2 and SULT1C1 plasmids, and ischemic-preconditioning

Jugular vein infusions of the mitochondrial membrane potential-dependent dye TMRM were used to gain insight into mitochondria function in various groups of live rats. After the infusion in normal Sprague Dawley rats, we observed instantaneous and non-uniform basolateral TMRM uptake in proximal and distal tubule epithelia cells (Figure 69). We subjected these rats to 30-45 minutes unilateral ischemia, via ligatures placed around left pedicle of kidneys that received hydrodynamic injections. This lead to abrupt decreases in TMRM fluorescent signals, which were drastically reduced within 30 minutes of inducing ischemia illustrating rapid mitochondria depolarization (Figure 70).

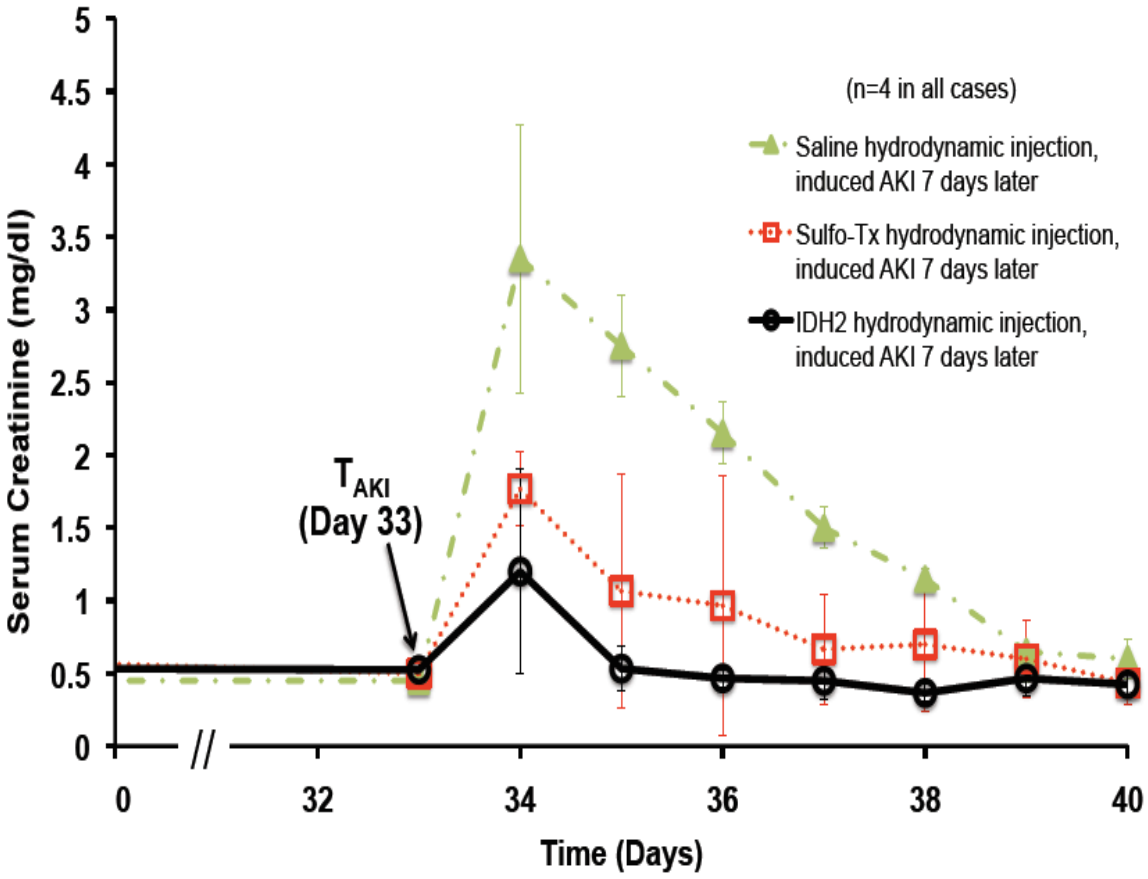

Figure 68. Hydrodynamic-based IDH2 and SULT1C1 (Sulfo-Tx) mitochondrial enzyme upregulation protects the kidney from moderate forms of renal injury in uninephrectomized rats

Uninephrectomized rats hydrodynamically treated with plasmids encoding mitochondrial proteins appear less susceptible to moderate ischemia-reperfusion injury. Normal rats were subjected to right nephrectomies n Day 0 and allowed to recover from this procedure. After which, on Day 26, the rats received hydrodynamic injection of saline or plasmid vector (IDH2 or SULT1C1). The rats then were subjected 7 days after hydrodynamic saline/gene delivery on Day 33 and monitored for serum creatinine seven days thereafter until Day 40.

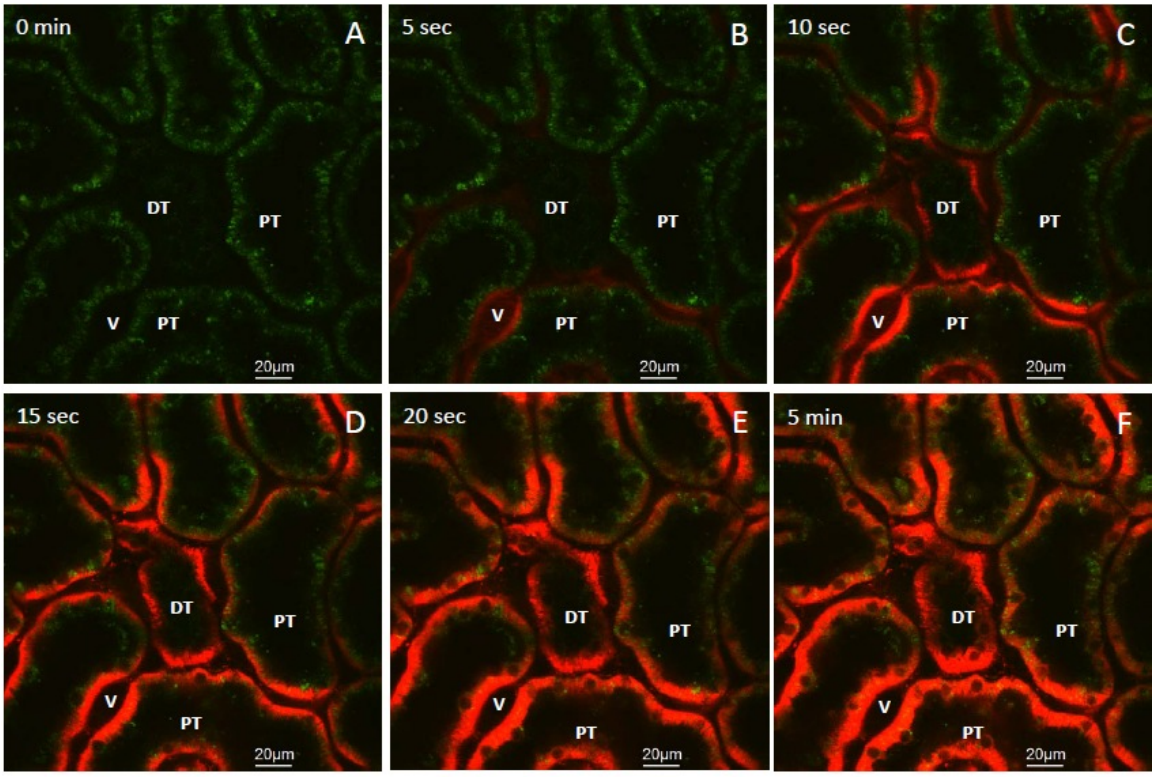

Figure 69. Robust and rapid basolateral uptake of TMRM in a live rat kidney outlining mitochondria membrane potential activity in nephron segments of a live normal rat

TMRM was infused through the rat's jugular vein: (A) before infusion, and at various times (B) 5 seconds, (C) 10 seconds, (D) 15 seconds, (E) 20 seconds and (F) 5 minutes after infusing the dye. These varied levels of fluorescence potentially outline the varied levels of mitochondrial activity in the normal kidney. These images were taken from the same microscopic field.

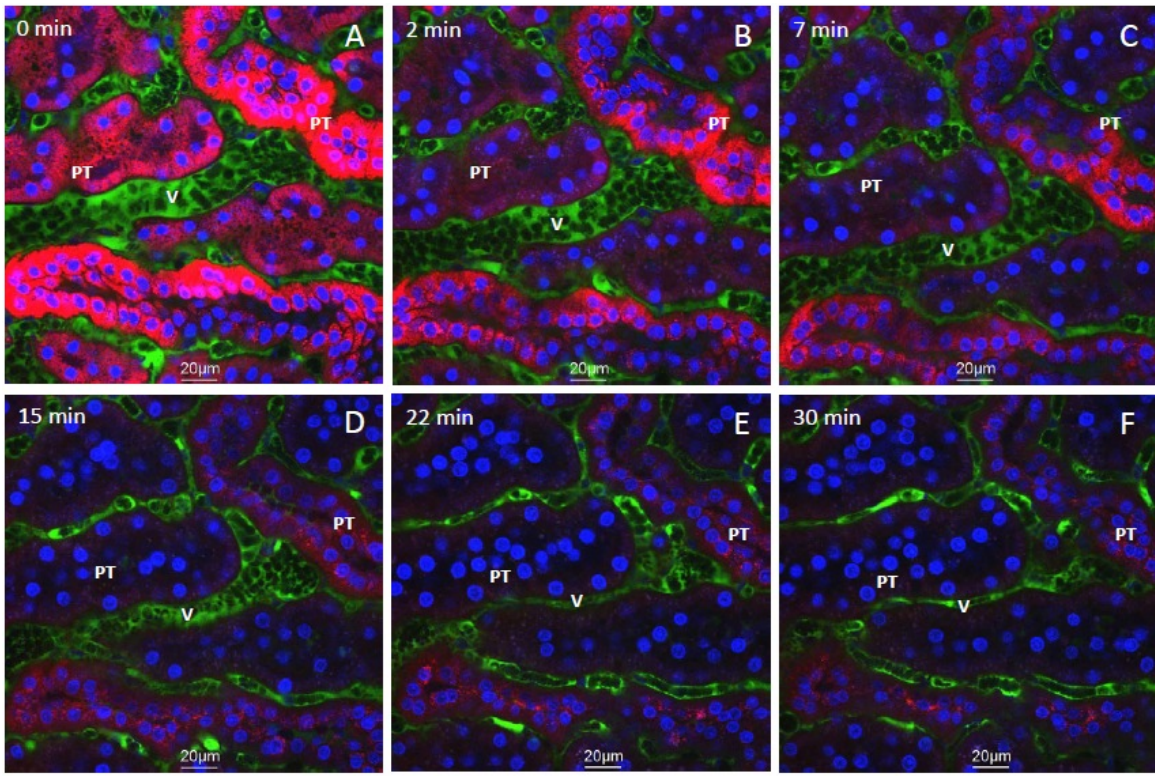

Figure 70. Rapid mitochondria depolarization in live nephron segments as a direct result of ischemia that was induced for 30 minutes
TMRM was infused via the jugular vein approximately 5-10 minutes before the ischemia. Time 0 min and 30 min mark the beginning and end of the ischemic event respectively. 150 kDa FITC molecule weight dextran molecules were infused before inducing ischemia-reperfusion injury to outline the supporting microvasculature, which constricted as blood flow was occluded during ischemia. This dextran enabled us to observe the complete disruption to renal blood flow during ischemia and its restoration during reperfusion. These images were taken from the rat that was imaged in Figure 69.

However, after blood flow was restored, there was a gradual increase in the TMRM signal, signifying mitochondrial repolarization *in vivo* (Figure 71). The TMRM signal returned to its initial elevated levels approximately 15 minutes after blood flow was restored (Figure 72). This increase in the TMRM-based fluorescence signified the regeneration of mitochondrial activity. However, this regeneration was not observed throughout the kidney after reperfusion, implying that moderate IRI was significant enough to grossly impair mitochondrial repolarization/function. These results outline the dynamic depolarization and repolarization of mitochondria as a direct result of significant ischemia-reperfusion injury and compare well to previously reported results[215].

In comparison, TMRM fluorescent signal intensities measured in rats that previously received hydrodynamic injections of either IDH2 or SULT1C1 plasmid vectors, as well as those that received ischemic preconditioning, were significantly greater than those measured in rats that received hydrodynamic saline injections and uninjected normal rats (Figures 73-75). These data outline a possible increase in mitochondrial activity related to the upregulation of the mitochondrial enzymes facilitated by hydrodynamic IDH2 and SULT1C1 gene delivery and ischemic preconditioning (data to support ischemic preconditioning facilitates the upregulation of various mitochondrial enzymes, including IDH2 and SULT1C1, were obtained from proteomic studies conducted by Bacallao, R.L., Basile, D.P. and Witzmann, F.A. these data were the framework upon which we established these studies). This upregulation in mitochondrial enzyme activity was confirmed with Western analysis (Figures 76 and 77).

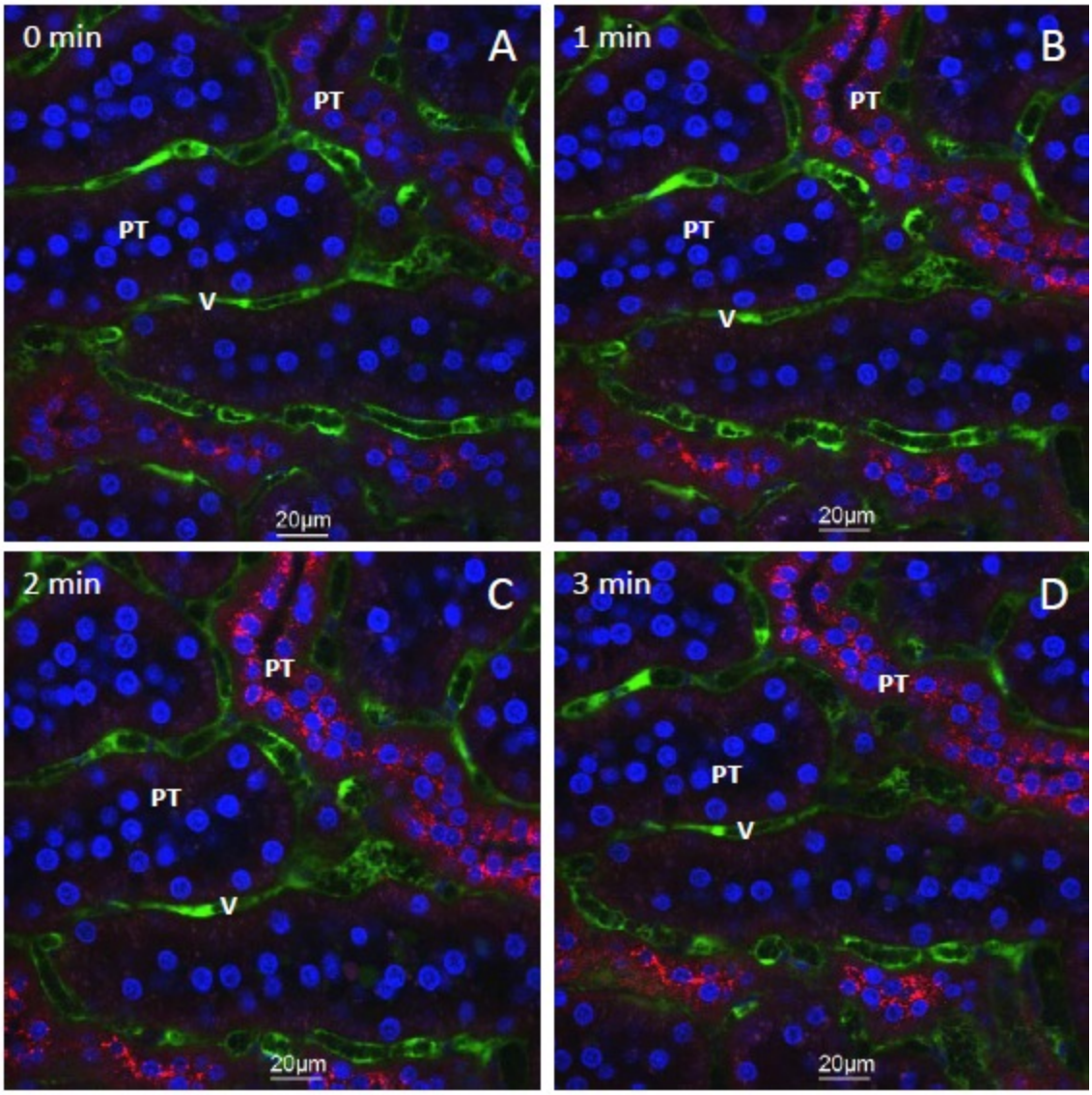

Figure 71. Mitochondria repolarization in live nephron segments when blood flow was restored to the kidney after 30 minutes of ischemia
TMRM was infused via the jugular vein approximately 5-10 minutes before the ischemia. Images were acquired 1, 2 and 3 minutes after renal blood flow restored. These images were taken from the same microscopic field and the rat presented in Figures 69 and 70.

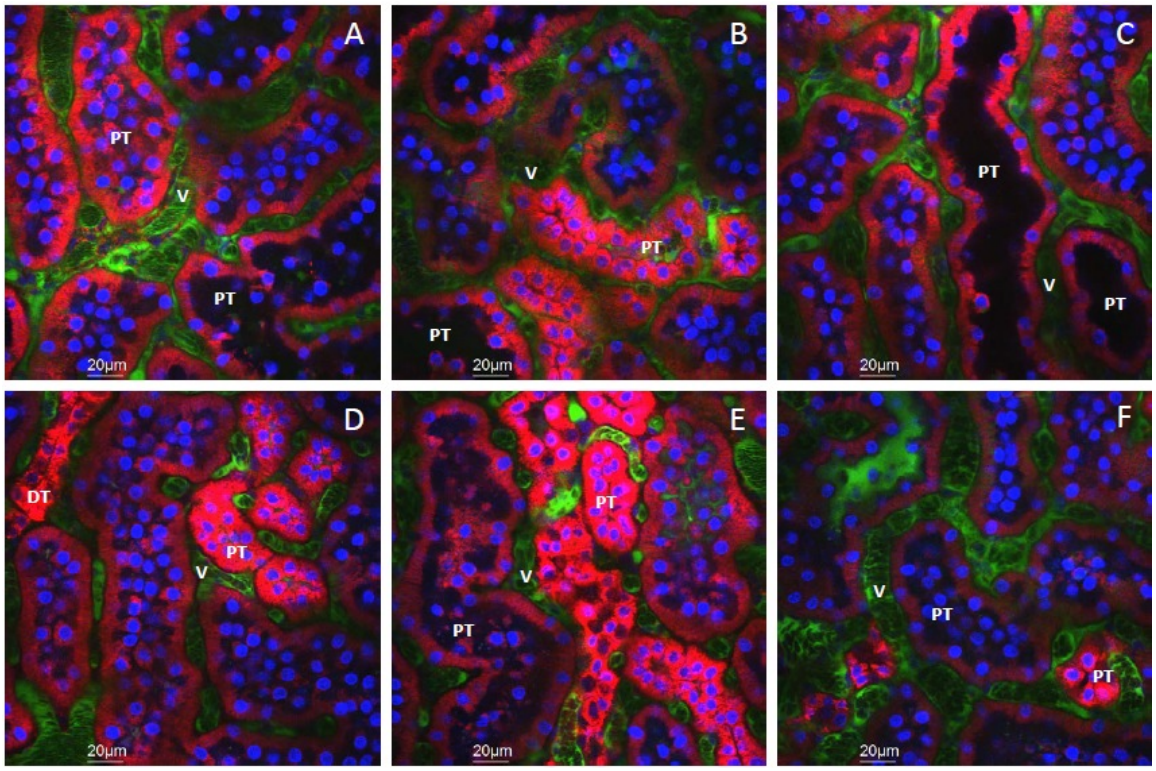

Figure 72. Mitochondria function was restored in various in live nephron segments directly after ischemia-reperfusion injury
Images A through F were obtained from adjacent microscopic fields approximately 15 minutes after renal blood flow was restored. The TMRM and 150 kDa FITC dextran were infused via the jugular vein approximately 5-10 minutes before the ischemia to outline the renal architecture. The TMRM signal returned to elevated baseline levels observed in Figures 69 and 70, before ischemia approximately 15 mutes after reperfusion

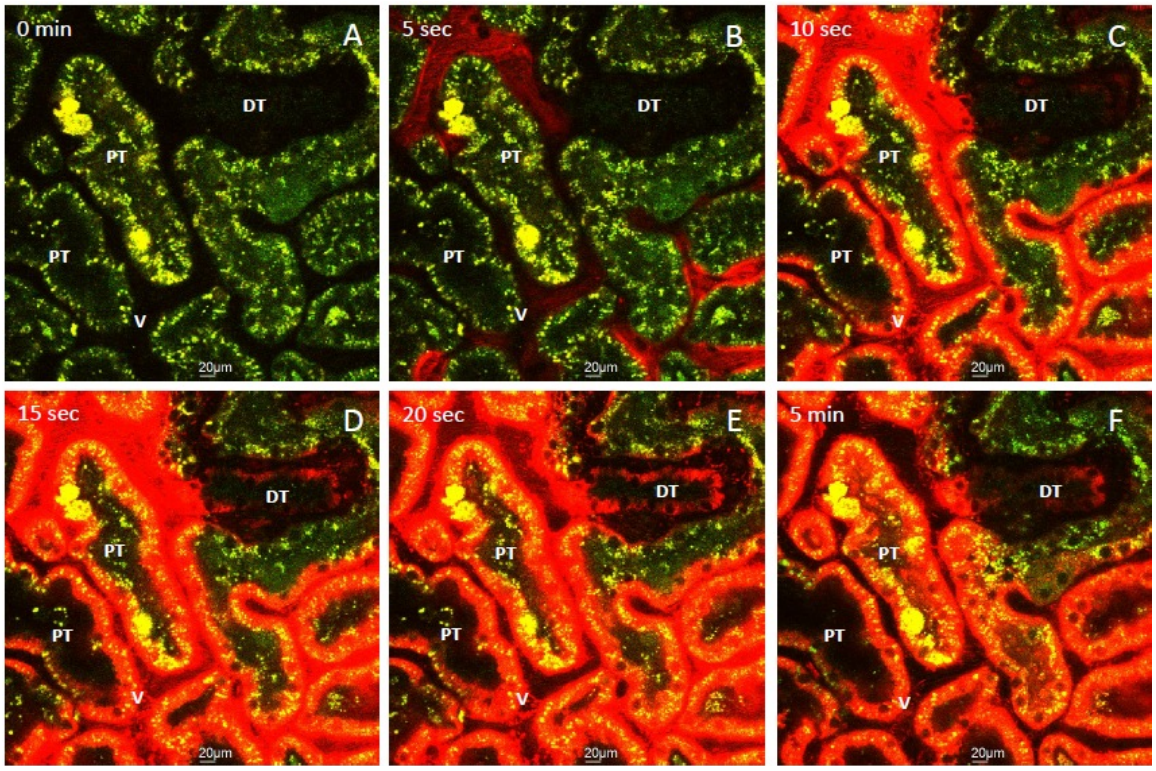

Figure 73. Robust and rapid basolateral uptake of TMRM in a live rat kidney outlining mitochondria membrane potential activity in nephron segments of a live rat that ischemic-preconditioning treatment

TMRM was infused through the rat's jugular vein: (A) before infusion, and at various times (B) 5 seconds, (C) 10 seconds, (D) 15 seconds, (E) 20 seconds and (F) 5 minutes after infusing the dye. These varied levels of fluorescence potentially outline the varied levels of mitochondrial activity in the normal kidney. There is a significant increase the TMRM fluorescence when compared to those generated from a normal rat in Figure 69. These images were taken from the same microscopic field.

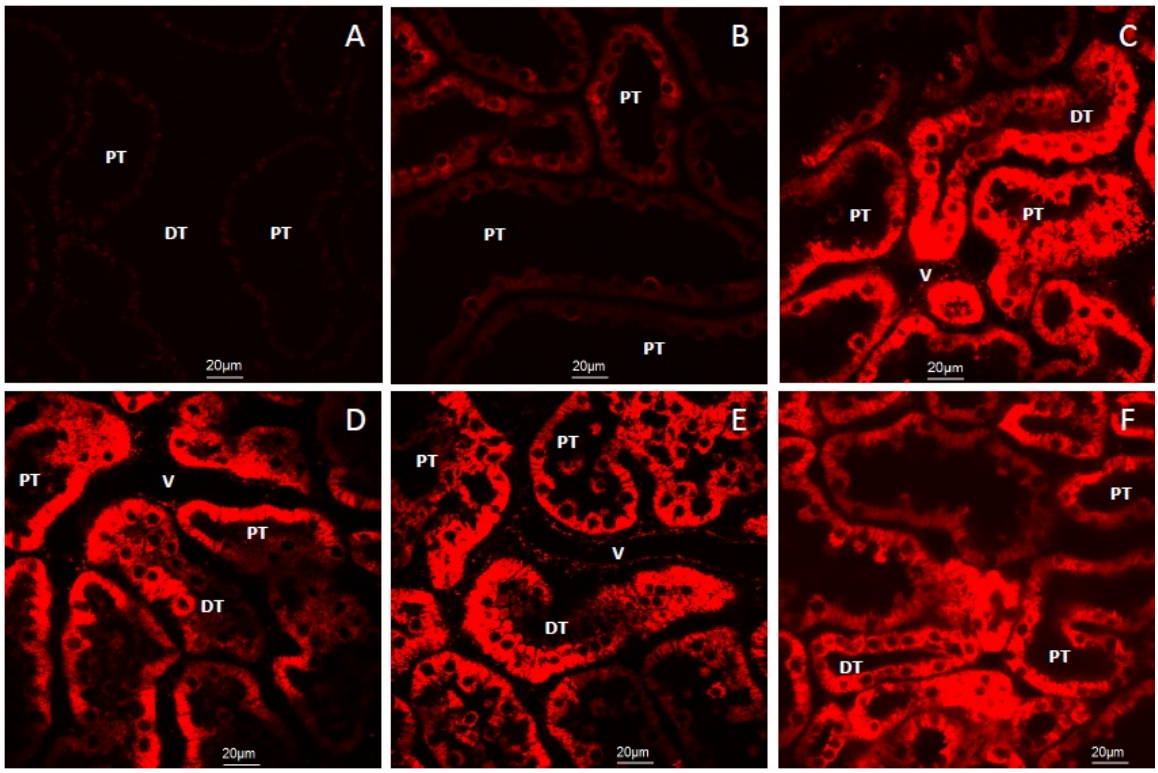

Figure 74. Mitochondria membrane potential activity was examined in nephron segments of various live rats

Image (A) represents baseline autofluorescence in a normal rat that did not receive the TMRM dye. In the other cases live rats received hydrodynamic injections of (B) saline; (C) IDH2 plasmids; (D) SULT1C1 plasmids; (E) SULT1C1 plasmids in the uninephrectomized rats. The rat imaged in (E) was subjected to ischemic-preconditioning and did not receive a hydrodynamic injection. Rats (B) through (F) were given TMRM via jugular vein after being exposed to 30 minutes of ischemia one week after receiving hydrodynamic injections or ischemic preconditioning, and were imaged approximately 15-20 minutes after receiving jugular vein infusions of TMRM and renal blood flow was restored.

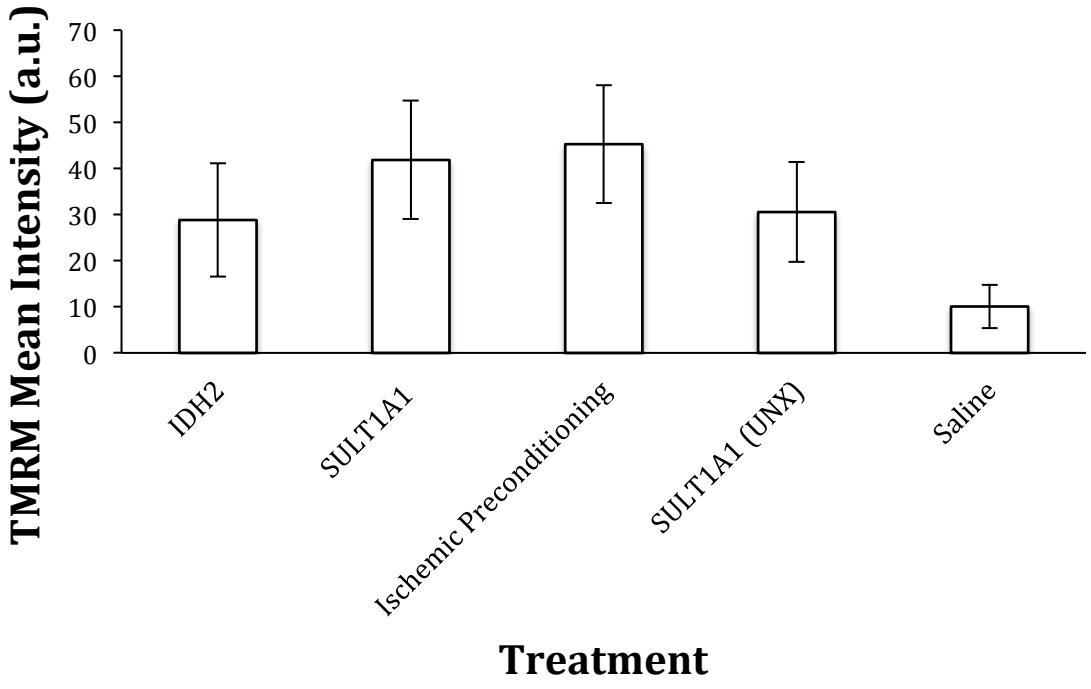

Figure 75. Comparison of mean TMRM fluorescence signal intensities recorded from live kidneys subjected to ischemic preconditioning and hydrodynamic gene delivery

TMRM fluorescence signal intensities were measured in rats that received ischemic preconditioning and hydrodynamic injections of saline; and mitochondrial plasmids (IDH2 and SULT1C1). SULT1C1 (UNX) = group of right nephrectomized rats that received hydrodynamic injections of SULT1C1 plasmids into their left renal veins.

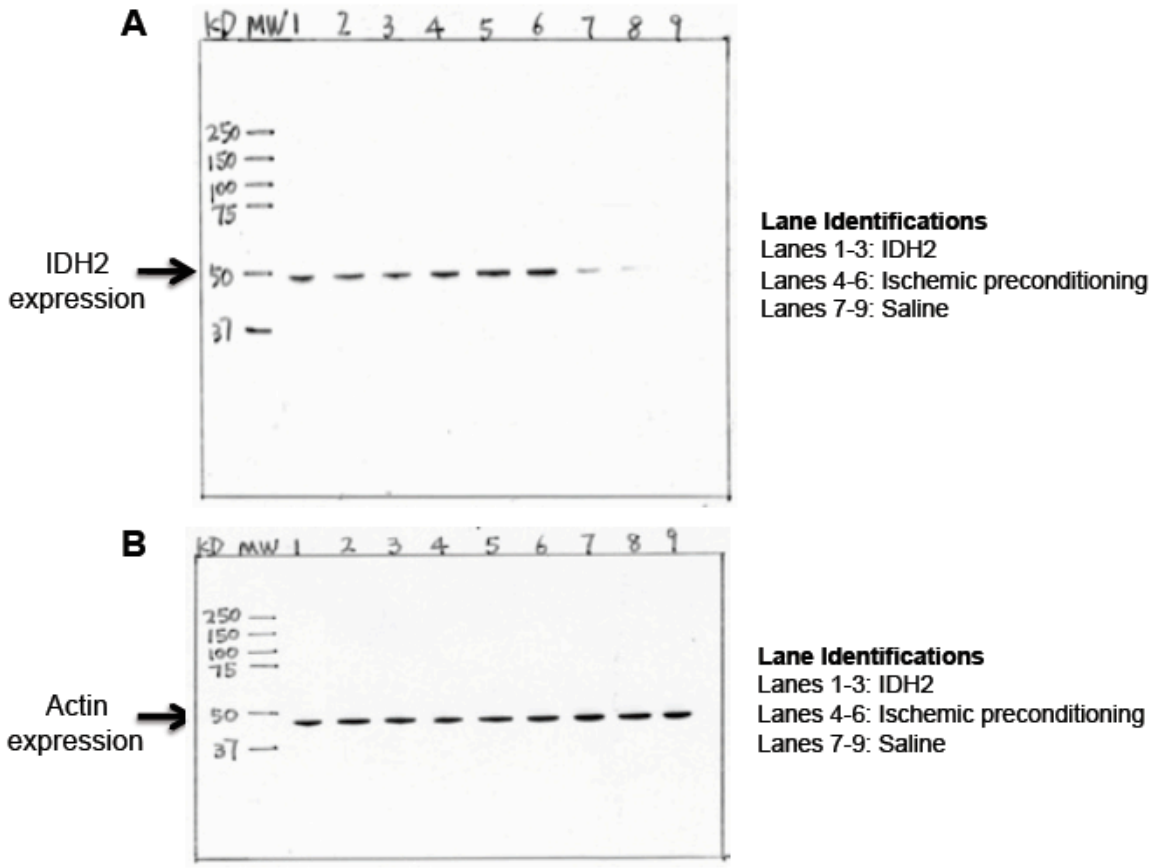

Figure 76. Western blot analysis identifying the varied levels of IDH2 protein expression in rat kidneys

Western blot analysis was conducted on tissue sections obtained from rats after various treatments presented in (A): hydrodynamic injection of IDH2 (lanes 1 through 3) and saline (lanes 7 through 9), and rats that were subjected to ischemic preconditioning (lanes 4 through 6). The molecular weight of the IDH2 and the actin molecules are approximately 47 kDa and 42 kDa respectively. These data illustrate the upregulation of IDH2 expression in rats that received hydrodynamic delivery and ischemic pre-conditioning as compared to the exogenous levels presented in the control rats. These data also illustrate the relatively homogenous level of actin expression in rats that received IDH2 hydrodynamic delivery and ischemic pre-conditioning as compared to the exogenous levels presented in the saline-treated control rats (B).

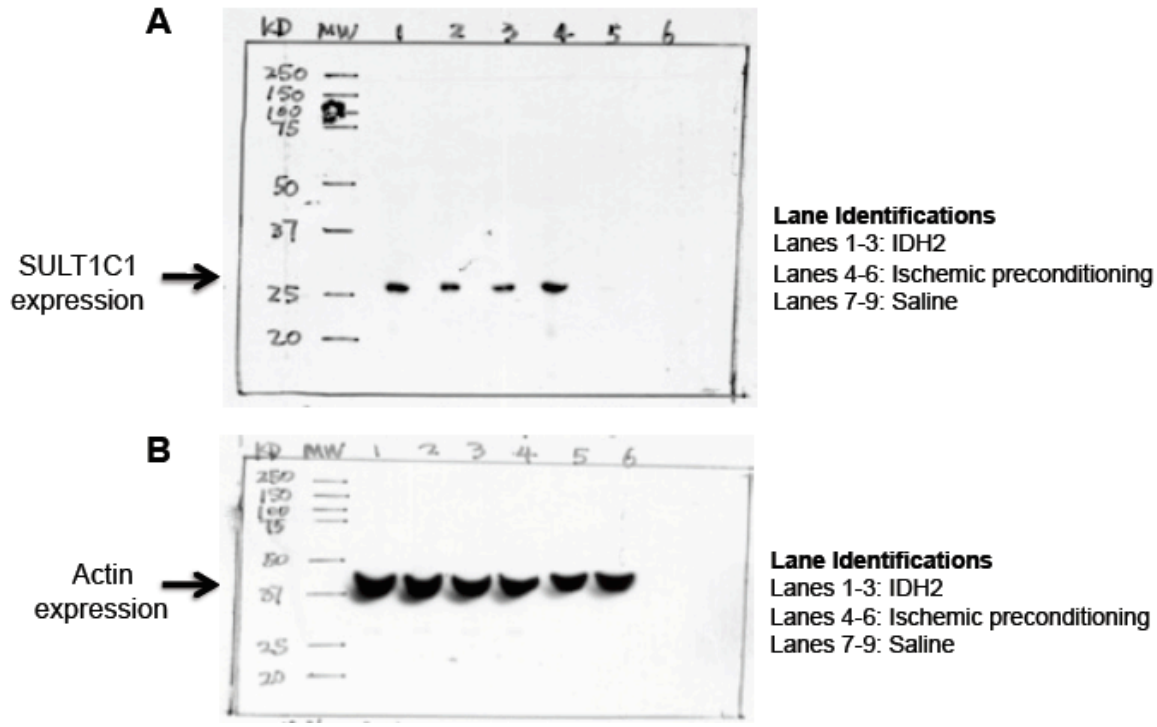

Figure 77. Western blot analysis identifying the varied levels of SULT1C1 protein expression in rat kidneys

Western blot analysis was conducted on tissue sections obtained from rats after various treatments presented in (A): hydrodynamic injection of SULT1C1 (lanes 1 and 3) and saline (lanes 4 and 6), and rats that were subjected to ischemic preconditioning (lanes 4 and 5). Similar to the IDH2 data, these data also illustrate the upregulation of SULT1C1 expression in rats that received hydrodynamic delivery and ischemic pre-conditioning as compared to the exogenous levels presented in the control rats. Again, these data also illustrate the relatively homogenous level of actin expression in rats that received SULT1C1 hydrodynamic delivery and ischemic pre-conditioning as compared to the exogenous levels presented in the saline-treated control rats (B).

From these data we observed the upregulation of IDH2 and SULT1C1 gene expression in rats that received hydrodynamic delivery and ischemic pre-conditioning, as compared to the exogenous levels presented in the control rats, which support the previously described TMRM data.

Chapter 6. Hydrodynamic fluid delivery facilitates efficient exogenous macromolecule uptake in large animals

A. Fluid delivery into live normal Ossabaw swine kidneys

1. Low rate renal vein infusions are unable to facilitate the efficient delivery of exogenous macromolecules to Ossabaw swine kidneys

In order to investigate whether low rate renal vein infusion could adequately deliver exogenous substances to live pig kidneys, we relied on angiography to visualse the delviery of these substance in real-time. Ossabaw swine received catheter-guided infusions of 50 ml of 0.9% saline containing toluidine blue dye and PET/CT contrast agent into either the renal vein. During that time, angiograms were collected across a 5-second period so that we could outline rapid filling and draining of the renal vein (Figure 78). From these angiograms we observed that thee low rate infusions were incapable of redirecting renal flow and introducing dye into the kidney. Renal venous output inhibited entry of these macromolecules into the kidney, thus nullifying its utility for our purposes.

2. Low rate renal artery infusions facilitates off-target delivery of exogenous macromolecules in various organs of Ossabaw swine

Live images acquired from a pig during a catheter-guided infusion of 50 ml of 0.9% saline containing toluidine blue dye and PET/CT contrast agent into the right renal artery outlined successful uptake and expulsion of exogenous fluid throughout various renal arterial branches (Figure 79). Exogenous uptake was not limited to the right kidney,

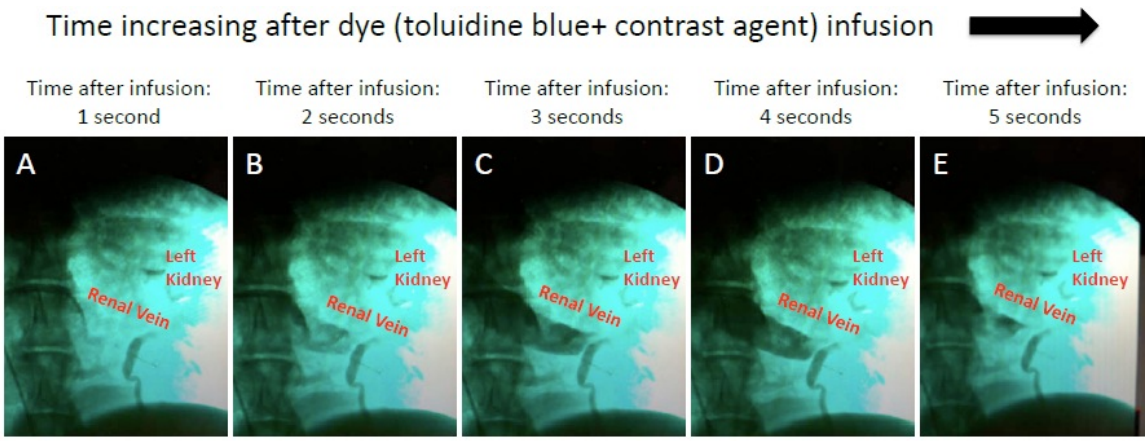

Figure 78. Live images acquired from a live pig during a catheter-guided infusion of 50 ml of 0.9% saline containing toluidine blue dye and PET/CT contrast agent into the left renal vein

Images (A) through (E), which were taken across a 5-second period, outline the rapid filling and draining of the vein. The low pressure infusion was incapable of redirecting renal flow and introducing the dye into the kidney.

as the toluidine dye was ultimately transported to the contralateral left kidney (Figure 80), and other organs that receive a large fraction of the cardiac output such as the heart, liver and spleen. Even though this was a local infusion into the kidney, these results mimic those obtained from systemic fluid delivery and hydrodynamic injections conducted without vascular cross-clamps in rats, which does not limit deivery to targeted kidneys.

B. Critical parameters and mechanisms to support effective renal transgene delivery in live pigs

1. Pig vital signs are unaffected by retrograde hydrodynamic renal vein injections

During hydrodynamic retrograde injections into the renal vein of live Ossabaw swine, we recorded animal vital signs. As with the rat, these showed the hydrodynamic injection process did not alter pig's blood pressure, heart rate and temperature.

2. Hydrodynamic retrograde renal vein delivery facilitates the atypical internalization of macromolecules in live pigs

As previously observed in the rat, hydrodynamic renal vein injections facilitated robust and widespread uptake of low and large molecular weight fluorescent dextrans in live Ossabaw pigs. Two-photon micrographs of fixed kidney sections obtained from these pigs revelaed the uncharacteristic apical and basolateral uptake of large molecular weight dextran molecules with proximal tubule epithelial cells within the renal cortex and medulla (Figures 81-83), similar to that observed in the rat (Figures 19-21).

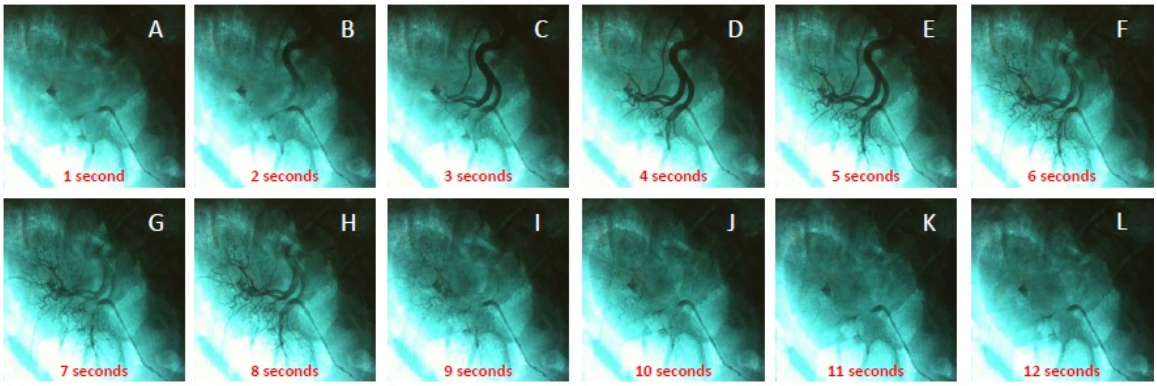

Figure 79. Live images acquired from a live pig during a catheter-guided infusion of 50 ml of 0.9% saline containing toluidine blue dye and PET/CT contrast agent into the right renal artery

Images (A) through (L), illustrate, in chronological order, the right kidney before infusion of the dye, and the subsequent filling and passage of the mixture of dyes through various renal arterial branches.

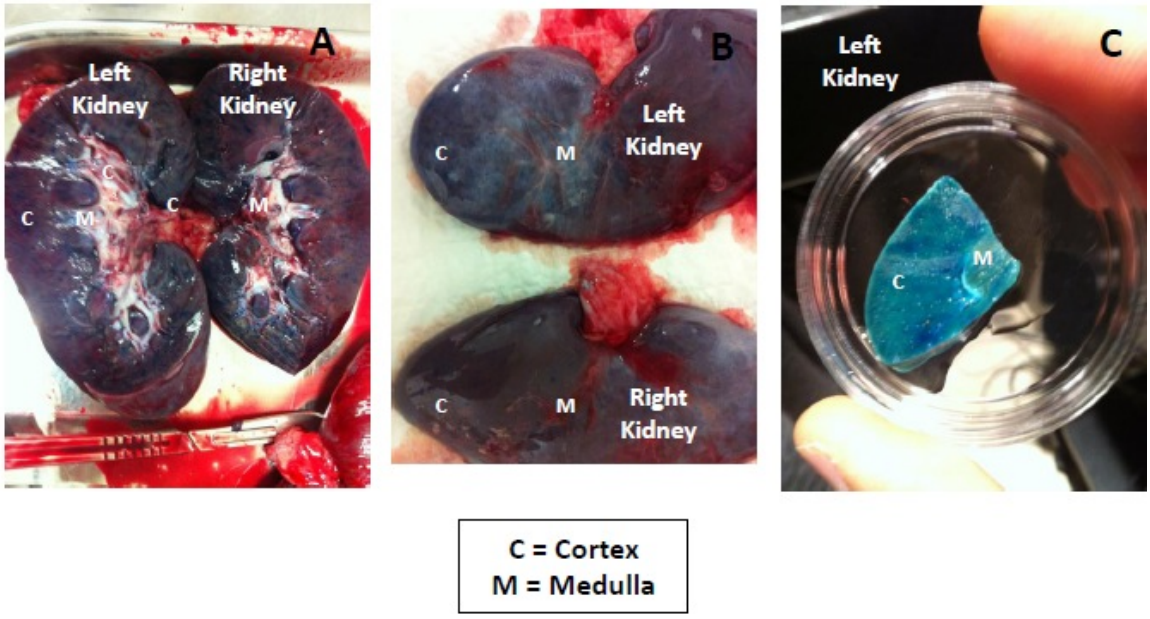

Figure 80. Whole kidneys harvested from an Ossabaw swine that received a low rate a catheter-guided infusion of 50 ml of 0.9% saline containing toluidine blue dye and PET/CT contrast agent into the right renal artery that was presented in the angiograms data in Figure 3.19

Images (A) and (B) whole sections of both left and right kidneys showing widespread uptake of the toluidine dye throughout these organs; and (C) a section highlighting cortical and medullary compartments that are filled with the toluidine dye. These data compare well with those presented in Figure 3.19 regarding the substantial passage of the dye mixture across the kidney. These kidneys were harvested and sectioned within 2 hours of delivering the dyes.

It should also be noted that during these initial attempts to deliver exogenous substance to the pig kidney, it was difficult to adequately restrict blood flow within the many bifurications of the renal vein and artery. We believe the anatomy permitted leakage of probes to the contralateral kidney. Nevertheless, 150 KDa TRITC molecules that were observed in the contralateral kidney remained restricted to the vasculature (Figure 81), indicating the need for hydrodynamic injection to facilitate the uptake of the high molecular weight dextran molecules by the tubular epithelia.

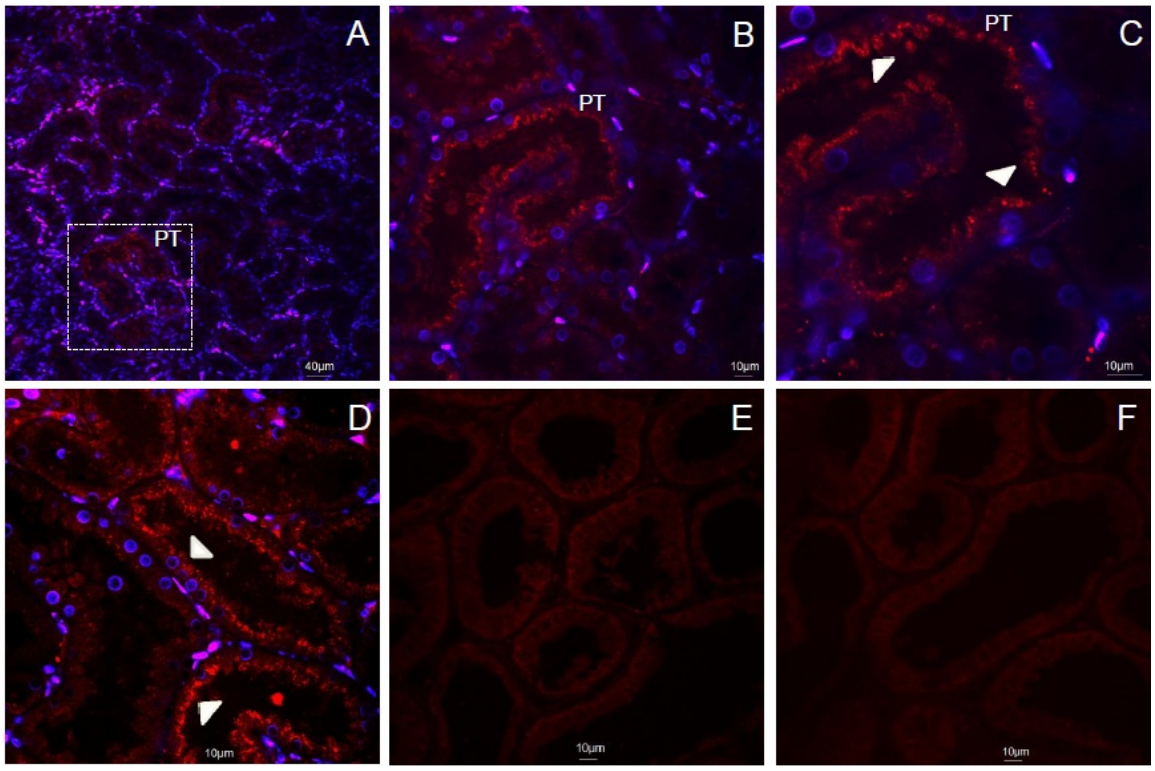

Figure 81. Additional e*x vivo* two-photon fluorescent investigation of kidney tissues harvested from an Ossabaw swine that received a hydrodynamic retrograde injection of 50 ml solution containing 400 µg of 150 kDa FITC dextran molecules
These images were taken after the tissues were fixed with 4% paraformaldehyde and counterstained with Hoechst 33342 to label nuclei: (A) widefield 20x objective image; (B) 60x objective image of the region outlined in image A; (C) 60x objective image with 2X digital zoom of the region outlined in image A; (D) 60x objective image of an alternate microscopic region; and images (E and F) autofluorescence . Arrowheads identify regions with significant concentrations of 150 kDa dextran molecules that have been internalized within proximal tubule epithelial cells.

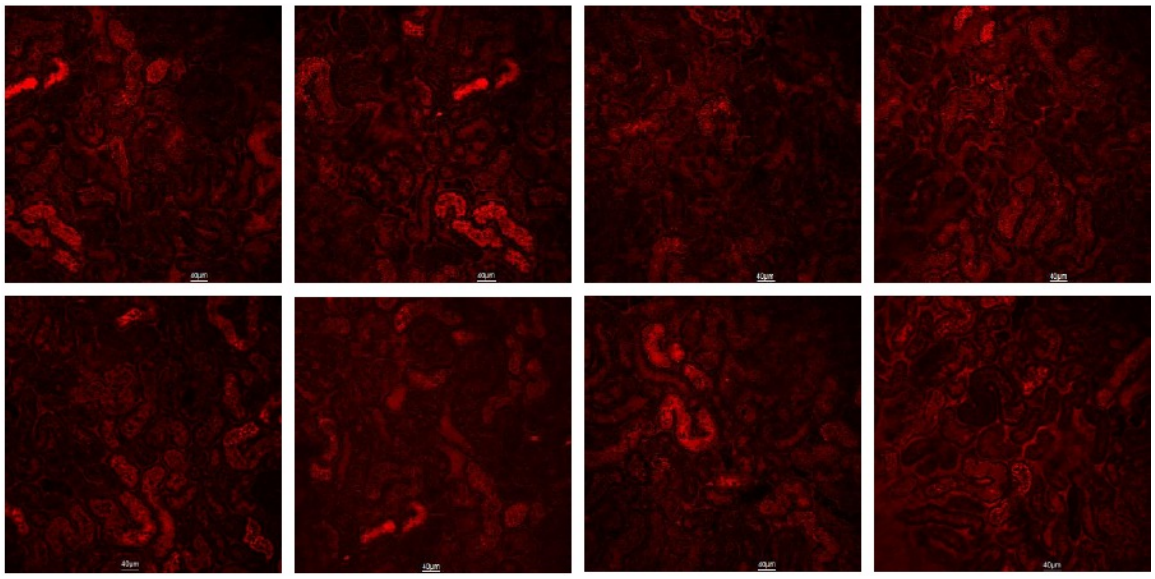

Figure 82. *Ex vivo* two-photon fluorescent investigation of kidney tissues harvested from an Ossabaw swine that received a hydrodynamic retrograde injection of 50 ml solution containing 400 µg of 150 kDa TRITC dextran molecules
These images were taken prior to fixation to examine the degree of renal dextran uptake by collecting 10 adjacent microscopic fields using widefield 20x objective.

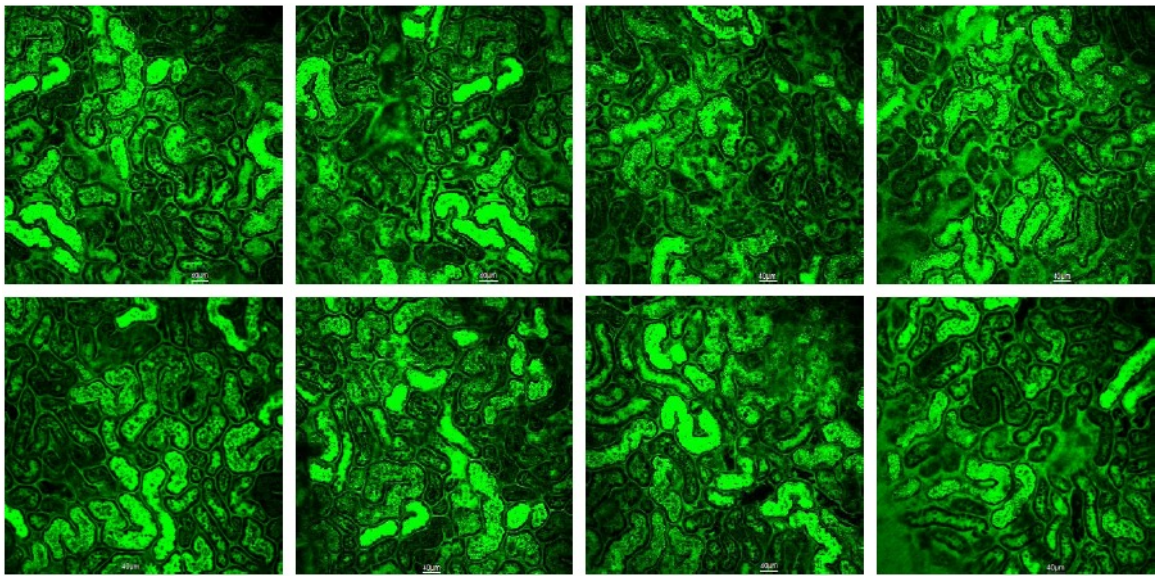

Figure 83. *Ex vivo two-photon* fluorescent investigation of kidney tissues harvested from an Ossabaw swine that received a hydrodynamic retrograde injection of 50 ml solution containing 400 µg of 4 kDa FITC dextran molecules
These images were taken prior to fixation to examine the degree of renal dextran uptake by collecting 10 adjacent microscopic fields using widefield 20x objective. These microscopic fields are paired to those presented in Figure 3.20.

IV. DISCUSSION

A. Summary

In Chapter 1, we presented results obtained from the various experiments that were conducted to optimize the design and characterization of a method to facilitate and monitor transgene delivery in the rat kidney. We determined that relatively low-volume, fine-needle, hydrodynamic delivery provided optimal delivery characteristics. This method provided widespread delivery of low, intermediate and large molecular weight molecules, and transgenes in live rat kidneys with minimal injury. Our hydrodynamic method facilitated widespread organ-specific non-viral/viral transgene expression, while not adversely affecting renal morphology, serum creatinine levels and vital signs.

In Chapter 2, we investigated the utility of hydrodynamic transgene delivery for the study of IRI. This technique allowed us to track live changes in the actin cytoskeleton, which is among the most abundant proteins within eukaryotic cells. Rats that expressed hydrodynamic-derived fluorescent actin were subjected to moderate and severe ischemia-reperfusion injury (IRI) via unilateral/bilateral renal pedicle clamps. Using intravital two-photon microscopy we recorded live cytoskeletal dynamics, in real-time, during reperfusion. This technique provided a reliable means to observe changes in proximal tubule (major site of damage during IRI).

In Chapter 3, we extended our transgene delivery investigations to consider rats with forms of mild and moderate IRI. Using this technique, we found that hydrodynamic

fluid delivery also facilitates robust delivery of low and high molecular weight molecules and reliable plasmid expression in live rats with mild and moderate IRI.

In Chapter 4, another application of hydrodynamic isotonic fluid delivery was identified. In this case we showed that this form of fluid therapy could be useful in treating IRI, as it ameliorated serum creatinine changes during IRI. In particular, this technique blunted rises in serum creatinine levels within 24 hours of its application in rats with moderate IRI. This therapeutic effect was observed with injections delivered as early as 1 hour after injury was established, as well as those administered at the time of maximal damage (24 hours after the injury was established).

In Chapter 5, we again investigated the therapeutic benefit that may be obtained from this injection process, and identified a method that protected rat kidneys against moderate IRI. In these studies we delivered supraphysiological doses of two types of mitochondrial genes to Sprague Dawley rat kidneys, using hydrodynamic retrograde venous injections. These genes were previously identified to have been upregulated in Sprague Dawley rats subjected to ischemic preconditioning. Sprague Dawley rats that received hydrodynamic injections of plasmids encoding these genes were exposed to moderate IRI. Strikingly these rats appeared to be resistant to this injury, as their serum creatinine levels normal. Western blot analysis confirmed upregulation of mitochondria enzyme expression in rats that received hydrodynamic injections of mitochondrial-expressing plasmids. Moreover, mitochondrial membrane potential analyses revealed enhanced mitochondria activity in these rats and those with ischemic preconditioning.

In Chapter 6, we again extended the utility of our hydrodynamic delivery technique for studies in large animals. For this phase of experimentation, we conducted low-rate and rapid infusions in Ossabaw swine (the Ossabaw swine has been used to develop a well established model for human vascular studies[230]). As previously observed in the rat, low-rate renal vein infusions were also incapable of efficiently deliver exogenous macromolecules to Ossabaw swine kidneys, while low rate renal artery infusions facilitates off-target delivery of exogenous macromolecules in various organs of Ossabaw swine. However, hydrodynamic retrograde renal vein injections facilitated targeted apical and basolateral macromolecule cellular internalization of in live pig proximal tubules, without affecting vital signs and generating significant degree of renal injury. Overall, these results compare well with those observed in the rat.

B. The effect of hydrodynamic delivery on exogenous macromolecule uptake in normal rats

We investigated the ability of several systemic and local infusion methods to reliably transport low, intermediate and large macromolecules across various renal cell membranes in live rats, while generating minimal injury. These studies provided varied results regarding kidney-specific delivery, cellular incorporation of exogenous large molecular weight substances, and degrees of injury generated from each delivery process.

First, from the systemic delivery standpoint, both jugular and tail vein infusion techniques initially enabled the circulation of exogenous materials to the heart. Thereafter

these materials were redistributed to kidneys via the cardiac output. This phenomenon exploited the fact that the kidneys receive greater than 20% of the cardiac output[231]. As a result, this method failed to limit the distribution of delivered agents to the kidney.

It should also be noted that, systemic delivery via the jugular vein, is not necessarily best suited for survival experiments, even though there is a collateral compensation from the other jugular venous line via the dural sinuses[232]. After reviewing these results, we shifted our studies to local infusion techniques.

In comparison, fine-needle injections into the renal capsule eliminated off-target delivery to other organs. Nevertheless, delivery was also restricted to the region that extended to approximately 40 μm below the capsule, which surrounded the injection site. High molecular weight dextran molecules delivered by this method, were also not uniformly distributed within these superficial cortical zones. These facts limited our interest in this technique, as it merely provided site-specific transgene expression comparable to that which is achieved using micropuncture gene delivery[218].

We then focused on designing a delivery method that would facilitate widespread internalization of relatively large macromolecules, comparable in size to the transgene vectors, and investigated whether hydrodynamic infusions could reliably achieve this result. We utilized the full effect of the pressurized injection system, under conditions of hydrodynamic equilibrium, by inserting PE-50 catheters into the renal artery and vein, through which 150 kDa FITC dextrans were rapidly delivered.

Renal artery and vein catheterization facilitated the uptake of albumin and 150 kDa dextran molecules. Increases in vascular permeability generated from arterial and venous ligation-derived injury[233] and hydrodynamic fluid forces[234,235] were sufficient to mediate the widespread and robust internalization of intermediate and high molecular weight molecules within renal cells. Unfortunately, these PE-50 infusion processes produced significant and irreversible levels of renal injury.

We then hypothesized that forces produced by hydrodynamic injections may be sufficient to facilitate the delivery of exogenous transgenes throughout kidneys, and ultimately assist their cellular incorporation. It was also envisioned that the level of injury and disruption to regular renal function, generated from 30- gauge needle hydrodynamic injections, would be comparably less than that produced by a PE-50 catheter.

Our initial hydrodynamic retrograde fine-needle renal vein injection studies provided promising results as we investigated extent of macromolecule uptake that could be attained throughout the entire kidney. We determined that hydrodynamically injecting approximately 0.5 ml of toluidine dye solution into the left renal vein of live rats was sufficient to facilitate robust delivery throught the organ. Saggital plane sections of left and contralateral right kidneys; hearts; livers; lungs; and spleens harvested from the rats that received these injections revealed widespread distribution of the toluidine dye only within the left kidney, when injections perfomed with vascular clamps. This provided proof that this method is capable of delivering ample quantities of exogenous substances throughout the kidney, while eliminating unwanted off-target probe distribution.

Nevertheless, further investigation was required to detemine whether this process would also facilitate transepithelial passage of high molecular weight compounds in various renal cells. For these experiments we used dextran reporters, since albumin may mask disruptions to vascular structure and normal nephron function. Previous studies have demonstrated that albumin can be filtered by normal glomeruli and occupy both vasculature and tubular compartments[181]. This property can confound studies on macromolecule passage across renal cell and glomerular membranes in normal rats.

Our analyses confirmed that was also possible to use hydrodynamic fine-needle injection to facilitate renal cellular uptake of large molecular weight compounds with minimal injury. Normally, large molecular weight dextrans are unable to transit the glomerular filtration barrier. Therefore, these molecules remain restricted to the renal vasculature of normal rats[122,207]; whereas small molecules are filtered by glomeruli, and can enter proximal tubule epithelial cells, via clathrin-mediated endocytosis[117,207,236].

In contrast, we observed that the large molecular weight (150 kDa) molecules had the uncharacteristic and extraordinary ability to access tubular lumens and be internalized within vesicles in tubular epithelial cells. This effect was only observed when these large molecules were delivered to the kidney by the hydrodynamic injection process. Even though the complete mechanism(s) of hydrodynamic delivery to renal cells is not fully understood, these results suggest possible means by hydrodynamic forces generated from rapid, fine-needle injections could facilitate reliable delivery and expression of transgene vectors (which have molecular weights on the order of 150 kDa) with minimal injury.

C. The effect of hydrodynamic delivery on transgene expression in live normal rats

After determining that our renal hydrodynamic injection process was capable of reliably mediating widespread cellular uptake of large molecular weight marcomolecules, our studies progressed to gene delivery phase of the project. We then investigated the potential to induce reliable renal transgene expression using delivery techniques previously outlined. At that point we first verified the quality of our plasmid, baculovirus and adenovirus transgene vectors in cell culture before conducting *in vivo* studies.

This *in vitro* work produced anticipated genetic transformation results using untagged, and actin and tubulin fluorescent expression vectors. However, the fluorescent actin structures observed *in vitro* from cells that were incubated with baculovirus expression vectors, deviated from normal actin morphology observed with plasmid-based and adenovirus-based transgene expression vectors. This may have resulted from the fact that, unlike the plasmid and adenovirus vectors, the baculovirus vectors were designed to express actin-binding proteins and not actual actin monomers. We also considered that insect-derived baculovirions might have generated cytotoxic responses *in vivo*.

After completing these *in vitro* studies, we began our transgene delivery studies in live animals. Transgene expression was examined in live animal kidneys and in freshly excised tissues with intravital two-photon fluorescence microscopy, and in fixed tissue sections with confocal laser scanning microscopy. These studies provided results that appeared to depend on the infusion site, infusion technique and transgene vectors.

For instance, using hydrodynamic retrograde venous injections to deliver baculovirus, plasmid and adenovirus vectors, we detected fluorescent protein expression within 24 hours of delivery. With this process we observed robust and lengthy glomerular, tubular and vascular transgene expression, generated from single doses of low plasmid concentrations or virus titer delivered by the hydrodynamic injection process. However, the overall quality and transduction rate of the live baculovirus-based expression raised significant concerns. Moreover, *in vivo* baculovirus-based fluorescent expression rates observed in superficial cortical segments limited its utility for live animal-based studies.

Nevertheless, both plasmid and adenovirus derived transgene expression, generated from hydrodynamic injections coupled with vascular clamping, resulted in comparably efficient levels of fluorescent protein expression. This distinction was based on criteria presented in Chapter 1 to evaluate gene delivery techniques[67]. Widespread, stable and lengthy transformation was observed in various vascular, tubular and glomerular cell types. These expression patterns, again unlike those derived from baculovirus vectors, did not deviate from normal renal morphology. This vast improvement in superficial cellular transformation will readily facilitate live renal studies that can be directed to understanding and treating underlying causes of renal disease.

For instance, the similar levels of transgene expression obtained from both non-viral and (adeno)viral vectors, which were limited to renal tissues (no signs of expression were recorded in other organs), highlighted the utility of the gene delivery method for kidney-specific gene transfer. In addition, hydrodynamic delivery may also be used to

facilitate long-term investigations using helper-dependent or 3rd generation adenovirus systems that are able to provide prolonged transgene expression, and simultaneously inhibit the expression of capsid proteins[237].

Moreover, in cases where the potential for mutagenesis derived over a long-term may be an issue, as has been reported with recombinant adenovirus systems[169], the ability to utilize plasmid DNA for genetic transformation offers the benefit of having a potent vector with a great safety profile. Plasmids can also be used to readily generate large volumes of a wide palate of exogenous transgenes with relatively low costs and waiting periods.

Overall, this simplified method provides an ability to rapidly and reliably deliver multiple exogenous genes to various nephron segments in healthy animals with minimal injury (Figure 84). Transgene expression observed in podocytes and epithelial cells of the S1 segment of proximal tubules may provide evidence that transient increases in pressures, generated by hydrodynamic injections, are sufficient to facilitate their passage through glomeruli barriers and S1 segments of proximal tubules. This may be plausible, because other reports have described glomerular permeability as a function of blood pressure[238]. Overall renal venous pressures increased by as much as 25 mmHg. This implied that hydrodynamic injections generated significant, yet transient increases, in renal venous and peritubular capillary pressures[239]. However, the extent of such pressure changes are expected to vary across the nephron, which may be associated with changes in renal vascular compliance[240].

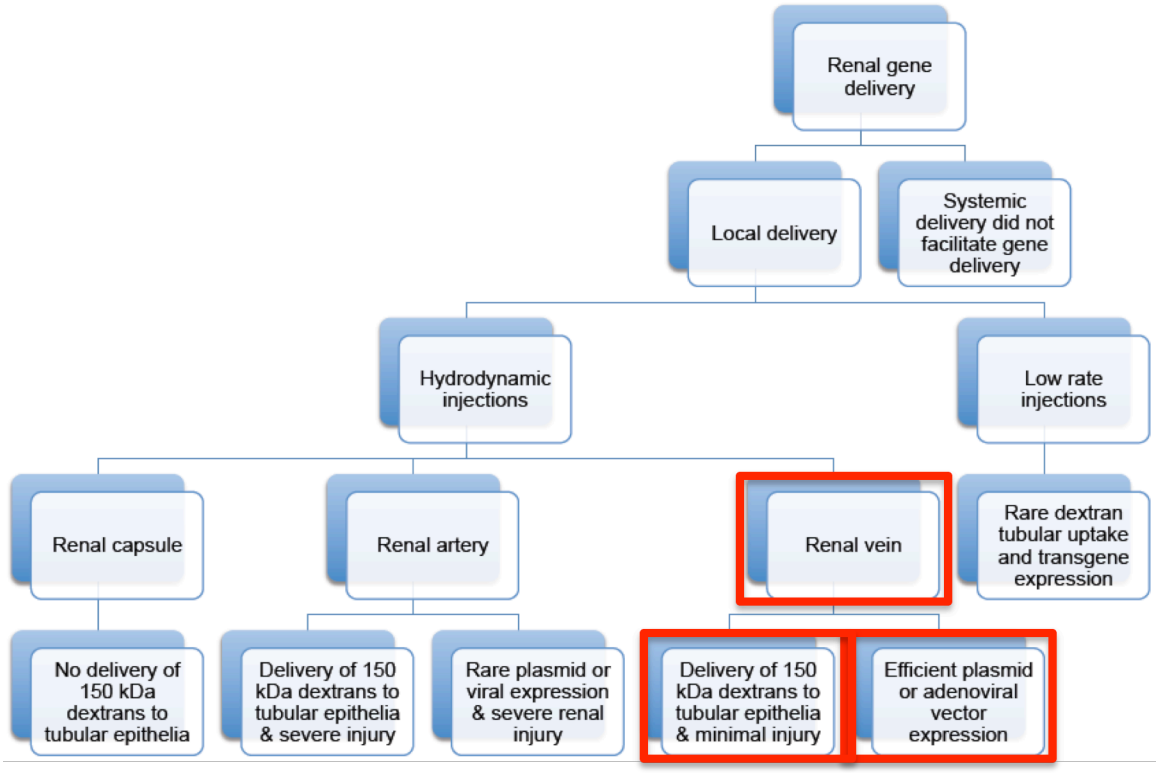

Figure 84. A summary of renal gene delivery procedures outlining the ability of each technique to facilitate transgene expression in live rats.
Efficient renal gene delivery was only facilitated with hydrodyanmic renal vein injections of either plasmid or adenoviral vectors, with minimal injury that did not appear to significantly alter normal reanl structure and function. There was a direct correlation between the delivery of large (150 kDa) molecular weight dexran molecules to tubular epithelia and trangene expression.

The data also support the claim that renal cells, which expressed hydrodynamically delivered transgenes, appear to maintain viable structural and functional capacities beyond the gene transfer process. Fluorescent protein distrubution appears to be relatively non-selective both in cell type and region of the kidney. Moreover, these results also support the possibility of mechanically induced, transient increases in vascular permeability that may facilitate atypical passage and internalization of macromolecules within the kidney, without inducing significant or long-term renal injury. If this is in fact the primary mechanism to facilitate hydrodynamic-based cell entry and gene expression, then such transient mechanical disruption of the plasma membrane may confer no advantage for viral particle uptake, and may actually be a hindrance.

Alternatively, hydrodynamic fluid delivery may aid transgene uptake by basolateral anionic transporters[241], and renal mechanotransduction via delivery of transgenes through stretch-gated ion channels[242]. Plasmid DNA and adenovirions may benefit from enhanced endocytic uptake by target cells (primarily in the tubules), triggered by rapid increases in renal fluid volume after their venous infusion. Our dextran studies supported these ideas as we observed that transient variations in fluid pressures facilitated entry of large macromolecules into tubule lumens and their internalization by the tubular epithelia. This may provide insight into the mechnism by which hydrodynamic-based transgne delivery is facilitated, as the large molecular weight dextrans are comparable in size to the transgene vectors we used.

In a separate set of experiments, we attempt to further understand the nature of transgene incorporation, we hypothesized that the hydrodynamic forces, generated by pressurized injections, were sufficient to facilitate viral endocytic uptake prior to their deactivation by the complement response. Both adenovirus[243] and baculovirus[244] entry into mammalian cells have been shown to be primarily dependent on clathrin-mediated endocytosis. This endocytic activity can be efficiently deactivated by the complement system[229,245,246]. To test this hypothesis, we conducted a series of experiments that monitored baculovirus-derived fluorescent protein expression under standard systemic and hydrodynamic renal vein delivery conditions. These studies clearly outlined the benefit obtained from the localized injection's ability to protect viral particles from the complement response and mediate the required cellular transformation *in vitro* and *in vivo*. However, future studies are needed to elucidate exact mechanisms for transgene uptake and expression relative transformation vectors, renal compartments and cell types.

It should be noted that hydrodynamic transgene delivery also has side effects, which result in brief, mild, and reversible levels of renal injury. Notably, these side effects do not appear to impair overall renal function, as serum creatinine levels are unaffected by either the delivery process or the resulting plasmid-based transgene expression. Histology has also revealed normal and intact renal morphology following transgene delivery and expression. Additionally, this process does not appear to impact the overall health of the animal as vital signs are unaffected by this injection process and the animals did not present any signs of illness during our prolonged observation.

D. Cytoskeletal dysregulation monitored in live rats with ischemia-reperfusion injury

Utilizing hydrodynamic delivery, we introduced fluorescent actin plasmid expression vectors in the kidneys of normal rats that were then subjected to IRI. With the aid of two-photon fluorescence microscopy, we then tracked structural and functional cytoskeletal changes in initiated by ischemic injury in live rats. Combing hydrodynamic delivery and intravital microscopy facilitated us to monitor loss and remodeling of actin components in live proximal tubule epithelial cells, which is the major site of IRI.

Apart from structural tissue breakdown that was noted, loss of tissue fluorescence signals may have occurred via changes pH and fluorescent quenching with continuous imaging. Therefore, as discussed by Ashworth et al.[247], these results provide an approach to potentially study in detail, the cellular and subcellular events associated with renal ischemic injury. In turn, this monitoring technique may be extended to the study of other live renal structures and nephron segments.

E. The effect of hydrodynamic delivery on transgene expression in rats with ischemia-reperfusion injury

Traditionally, the development of renal gene therapy has lagged behind other organ-directed gene therapies. This is because of reported low frequency renal gene transfer efficiencies and difficulty in targeting specific cell types[60]. But, it appears that hydrodynamic delivery may overcome this issue in either normal or injured renal states.

We arrived at this conclusion by first determining that hydrodynamic delivery could be used to successfully delivery low and large molecular weight dextrans throughout nephrons of normal rats and those with moderate IRI. Thereafter, our investigations revealed that this relatively simple technique generated efficient transgene expression in live renal segments, namely proximal tubule epithelia, which is the major site of damage in AKI. These observations made from injured rats were hallmarks of acute IRI, which can generate patchy or segmental renal damage[180,248].

Our data illustrated the fact that hydrodynamic delivery facilitated widespread distribution of low (5 KDa) and large (150 KDa) molecular weight molecules in rats with moderate renal IRI. Moreover, a substantial quantity of both low and large dextran molecules were internalized by damaged proximal tubule epitheliala. This in turn provided sufficient evidence to support the idea that retrograde hydrodynamic injections may facilitate the expression of exogenous transgenes in injured rat kidneys, and in particular, at the major site affected by AKI.

Combining these facts with our estimated transfection rates for injured rats, we believed that the combination of hydrodynamic delivery and ischemia/reperfusion injury, which is known to promote vasculature and cellular permeability, may have further mediated the passage of materials across disrupted tubular epitheial cell membranes. This phenomenon may have also directly enhanced the internalization of exogenous materials, in the possible absence or reduction in endocytic capacities, resulting from injury-derived loss of brush border components in proximal tubules. Kelley *et al*. provided similar a

rationale for transgene expression since they observed expression in rats with injured glomeruli using adenovirus vectors[66].

Interestingly, we were able to facilitate transgene expression in mammalian kidneys that had been subjected to acute injury, during both the initial phase of injury and at the maximal point of damage. Based on this, it is necessary to consider the state of the cells expressing the transgenes. There exists the probability that both injured and functional cells populations would express transgenes in some undefined ratio. Naturally, it would be of interest to shift this ratio to benefit the injured cells. Nevertheless, due to the nature of AKI and proximal tubule function, it would be of interest to target functional cells in an attempt to protect them from irreversible damage and foster their proliferation to compensate for terminal injured cells[249].

Overall, these results now provide a novel platform that may be used to address the challenges observed in generating reliable renal gene transfer to a variety of cell types within normal and injured kidneys. Moreover, from a clinical perspective, we believe that this localized delivery of transgenes might potentially maximize welcomed therapeutic benefit, by limiting offsite deleterious effects[250].

F. The effect of hydrodynamic isotonic fluid delivery on ischemia-reperfusion injury

After investigating the therapeutic potential of this delivery technique we determined that it is possible to use a relatively low volume (0.5 ml) hydrodynamic isotonic fluid delivery to the left renal vein, 1 and 24 hours after inducing moderate IRI,

to reduce the level of injury. IRI was established in rats via a bilateral pedicle cross-clamp for 30-45 minute. These rats then received hydrodynamic isotonic fluid injections in their left kidneys. It is still unclear from a mechanistic perspective the manner in which this amelioration occurs, but we hypothesize that this approach, as compared to standard renal fluid therapy, may reduce tubular blockages and physically disrupt capillary congestion and facilitate diuresis to reinstate intrinsic renal function and creatinine levels.

Moreover, these results can be compared to those presented by Molitoris et al[22]. In that study this group investigated the therapeutic potential of RNAi to ameliorate ischemia-reperfusion derived AKI in rats, using siRNAs delivered intravenously, via tail vein injections. The siRNA against p53 provided significant improvements in serum creatinine levels in injured rats. Although siRNA preferentially accumulated in the kidney, this technique still has a potential to generate unwanted protein silencing in other organs. In comparison, the delivery technique utilized for this study appears to provide more targeted delivery to the kidney. In previous experiments we verified exogenous materials delivered using this cross-clamping hydrodynamic method, restricted the uptake/expression of toluidine dye, fluorescent dextrans and EGFP-actin plasmid vectors to the injected organ. Transgene expression was absent in contralateral kidneys and other highly aerobic organs like the heart, lung, liver and spleen, suggesting this method could be useful for organ-targeted gene delivery.

Overall, this work paves the way for further investigations of fundamental events in IRI and extends the present utility of intravital imaging in renal pathophysiological

studies. The potential therapeutic benefit observed in these results also provides an exciting platform to facilitate the future management of IRI. This may in turn facilitate the development of hydrodynamic-based protection- and repair-directed interventions, albeit using in a single infusion technique, that may accommodate alternate forms of renal therapy, such as RNAi and other types of drug delivery systems.

G. Hydrodynamic-based IDH2 or SULT1C1 transgene expression enhances mitochondrial activity and blunts serum creatinine increases in rats with moderate IRI

Once we established that this delivery method could reliably facilitate efficient fluorescent protein expression in the rat kidney, we considered whether this method could be used for the management of AKI. In doing so we investigated the possibility of delivering genes encoding SULT1C1 or IDH2. The hydrodynamic delivery of plasmid vectors that encoded these proteins provided resistance against AKI in rats (in rats with two kidneys and uninephrectomized rats) that were subjected from moderate IRI, based on serum creatinine measurements. These genes have been suggested to enhance the activation of specific signaling pathways that provide protection from IRI[251].

This phenomenon was first suggested from ischemic preconditioning studies conducted in rats. Ischemic preconditioning is an experimental technique that has been applied to various tissue types, to produce resistance to reductions in blood and oxygen supplies. With specific regard to the IDH2 and SULT1C1 mitochondrial enzymes, their

observed renoprotective effect may involve mechanisms related to cell-stress pathway activation. Among the cell-stress pathways that have activated by renal ischemia, mitochondrial enzymes IDH2 and SULT1C1, have been shown to be upregulated in Sprague Dawley rats kidneys subjected to ischemic preconditioning, and aids in this animal's ability to resistant IRI[252].

Overall, from a mechanistic perspective, ischemic preconditioning has been studied for the past 50 years, during which time many ideas have been put forward to outline its organ protective role[253]. For instance, in the context of myocardial ischemia, there has been much debate about collateral vascular recruitment as a means of improving myocardial oxygenation[254]. Other studies have implicated mitochondria as key mediators of ischemic preconditioning. Specifically, the opening of a mitochondrial channel, called the mitochondrial ATP-sensitive potassium channel or mitoK_{ATP} is believed to be critical for the induction of this phenomenon, and drugs that activate this channel protect against ischemia and inhibitors of mitoK_{ATP} reverse these protective effects[253]. Ischemic preconditioning has been shown to reduce post-ischemic tissue hyper-oxygenation as it preserves NADH dehydrogenase and cytochrome c oxidase[255]. These events work to prevent oxidative stress, decrease infarction size and increase tissue viability on reperfusion[255].

Using these outlined rationales we delivered relatively large doses of plasmid vectors that expressed these genes to normal rat kidneys of Sprague Dawley. The Sprague Dawley is not genetically resistant to this form of injury as compared to, for example, the

Brown-Norway rat[256]. Ischemic preconditioning is generally done 3-7 days prior to IRI. Based on this time frame, we waited seven days after the gene delivery process and then attempted to induce AKI by subjecting these rats to 30-45 minute bilateral renal pedicle cross-clamps. Similar studies were conducted on uninephrectomized rats.

Strikingly, we determined that either IDH2 or SULT1C1 transgene treatments were sufficient to blunt the effect of IRI in these Sprague Dawley rats. Serum creatinine levels in rats that receiving hydrodynamic retrograde venous injections of either plasmid remained within normal or baseline levels despite being subjected to moderate IRI, when compared to rats that received saline injections. Upregulation of either mitochondrial enzyme appeared to have protected renal function from the IRI. These results are supported by enhanced mitochondrial membrane potential activity in rats with moderate IRI that received hydrodynamic injections of either IDH2 or SULT1C1 plasmids.

IDH2 could clearly change mitochondria function based on its role in the TCA cycle, however a potential role for Sult1c1 is not obvious from its known function. cDNA for each protein was purchased from OriGene and transfected into immortalized S3 murine proximal tubule cells. Both cDNAs increased mitochondria potential based on JC-1 fluorescence and conferred resistance to hypoxic injury in cultured S3 murine proximal tubule cells (data not shown). This set of results led us to test both cDNAs in vivo by gene delivery to the kidney.

At present, little is known about mitochondrial adaptations in experimental or genetic models of resistance. This is an important gap in our knowledge since a variety of

organisms and tissues have demonstrable adaptations to ischemia/hypoxia or anaerobic conditions by altering mitochondria protein expression. There are knowledge gaps in how mitochondria adaptations influence hemodynamics. However, proximal tubules are highly dependent on mitochondrial oxidative phosphorylation. Hypoxia or I/R injury leads to impaired mitochondrial energetic capacity and/or activation of cell death pathways. Post-hypoxic mitochondria are a source of reactive oxygen species, which represent a contributing factor toward cellular injury, and may cause vasoconstriction. For example, superoxide enhances effects of other vasoactive factors and may have direct actions in reducing renal blood flow[257,258]. As a results, we hypothesized that adaptations in mitochondrial composition confer protection to ischemia by altering baseline mitochondria function. These adaptations preserve mitochondria integrity in response to injury, leading to cytoprotection and preservation of renal hemodynamics.

H. Fast rate infusions are essential for fluid delivery to live pig kidneys

Angiograms acquired from Ossabaw swine during catheter-guided infusions of 50 ml of 0.9% saline containing toluidine blue dye and PET/CT contrast agent into the left renal vein were incapable of introducing the dye into the kidney, nullifying its viability as a reliable renal fluid infusion technique.

Similarly, live images acquired from these animals during a catheter-guided infusions of the mixture of toluidine blue dye and PET/CT contrast agents into the right renal artery, resulted in the successful uptake and expulsion of exogenous fluid

throughout various renal arterial branches. This fluid uptake was not limited to the target kidney as the toluidine dye was ultimately transported to the contralateral left kidney and other organs that received a large fraction of the cardiac output, such as the heart, liver and spleen. Even though this was a local infusion into the kidney, these results mimic those obtained from systemic fluid delivery in rats, as this method does not limit the distribution of the exogenous agents to the targeted kidney.

As observed in the rat, hydrodyanmic pressurized injections into the renal vein also facilitated the widespread delivery of exogenous susbstances throughout pig kidneys. Again, we determined that it was necessary to conduct this injection and clamp various bifurications that lead off main renal vein in order to limit delivery to the target organ.

I. Hydrodynamic delivery also facilitates widespread proximal tubule epithelial cell internalization of exogenous macromolecules in live pigs

Low and high molecular weight fluorescent dextrans can be delivered through the renal vein of live Obbabaw swine using retrograde hydrodynamic injections. This form of delivery results in the robust and widespread uptake of both exogenous probes. As with our rat studies, we again utilized two-photon fluorescent microscopy to observe atypical localization of large (150 kDa) molecular weight dextran molecules along proximal tubule brush borders and within proximal tubule epithelial cellular cytoplasms, viewing various fixed tissue sections of the renal cortex and medulla. These results indicate it may be possible to utilize hydrodynamic fluid delivery in large mammals in a manner similar

to those previously described in rats. This in turn may facilitate the development of transgene delivery systems in large animals that may aid therapeutic and protective strategies for the future management of kidney injury.

V. CONCLUSIONS

We first designed and characterized a method, using hydrodynamic fluid delivery, to facilitate and monitor transgene expression in rat kidneys. In devising this approach we hypothesized that hydrodynamic forces, generated from retrograde pressurized injections, were able to facilitate widespread delivery of exogenous reagents throughout the kidney. This hypothesis was tested by injecting fluorescent albumin and dextrans into rodent renal veins under various conditions of hydrodynamic pressure. These molecules were observed throughout live renal segments using intravital fluorescence two-photon microscopy. Thereafter plasmids, baculovirus and adenovirus vectors, which express EGFP, and EGFP-actin, EGFP-tubulin. EGFP-occludin, EGFP-ZO1, Histone H2B-tdTomato and RFP-actin fusion proteins, were also introduced into live rodent kidneys.

Fluorescent protein expression was observed in live and *ex vivo* kidney segments using two-photon microscopy, and *in vitro* with confocal laser scanning microscopy. We recorded widespread transgene expression in live glomerular, tubular and vascular segments beyond a month after the introduction of the transgenes. The plasmid and adenovirus vectors provided robust levels of fluorescent protein expression throughout the rat kidney. Moreover, this process generated low and transient levels of injury that did not alter overall kidney.

Second, after successfully designing and characterizing this method, we determined that hydrodynamic delivery used in conjunction with intravital two-photon

microscopy facilitated the real-time monitoring of actin cytoskeleton dynamics in live rat kidneys. Actin cytoskeletal deregulation was monitored on a widespread scale, at the major site of damage during ischemia-reperfusion injury. This provides a novel platform to idenfity specific renal cellular and tissue alterations during injury.

Third, we investigated the potential to use hydrodynamic fluid injection to deliver transgenes to rats with various forms of ischemia-reperfusion injury. These pressurized renal vein injections of plasmid vectors mediated efficient fluorescent protein expression in live rats with mild and moderate ischemia/reperfusion renal injury during the initial phase of injury and at the time of maximal damage.

Fourth, we recognized that a localized form of fluid therapy, administered through hydrodynamic fluid delivery, ameliorated serum creatinine changes during IRI as early as 1 hour after injury, as well as at the later time of maximal damage generated by such acute forms of kidney injury.

Fifth, we identified that hydrodynamic gene delivery could be used as a gene therapy strategy to protect rat kidneys against moderate IRI by facilitating the upregulation/overexpression of specific mitochondrial enzymes in Sprague Dawley rats. The expression of these plasmid blunted rises in serum creatinine, which is the present standard clinical marker for AKI.

Last, we extended the utility of our delivery technique to facilitate targeted, apical and basolateral macromolecule cellular internalization in live pig proximal tubules, without affecting vital signs and generating significant degree of renal injury.

Thus, with the careful selection of reporter constructs, hydrodynamic fluid delivery provides a reliable medium to simultaneously contrast and examine innate and abnormal cellular dynamics. Moreover, it enables therapeutic fluid delivery and monitoring, in small and large animals, while facilitating the widespread expression of biochemically relevant genes that can be used to prevent and treat IRI. In conclusion, our studies demonstrated that this single and relatively simple method has widespread application for the study and management of AKI.

VI. FUTURE STUDIES

We will investigate the kinetics of siRNA distribution and silencing in proximal tubule epithelial cells of live rats. Our studies will specifically examine the accumulation of fluorescently-labeled siRNA constructs and their potential potency in silencing protein expression in proximal tubular cells of live animals, generated by hydrodynamic transgene delivery. This work will be extended to an investigation on whether it would be possible to reduce or eliminate genetamicin toxocity using a combination of hydrodynamic delivery and siRNA silencing mechanisms.

We also aim to investigate renal injury by including additional functional and structural analyses such as GFR measurements, and biomarker readouts of NGAL and KIM-1. We expect that this research will facilitate the *in vivo* assessment of siRNA-mediated tubular protein silencing that may be directed towards therapeutic applications related to the inhibition of gentamicin-derived nephrotoxicity.

Simultaneously, we will focus on the design of a catheter that would facilitate minimally invasive hydrodynamic fluid delivery to the kidney. For these studies we will utilize injection parameters previously acquired and those that will be obtained from future hydrodynamic delivery injections in Ossabaw pigs.

VII. REFERENCES

1. Ferguson, M.A., Vaidya, V.S. & Bonventre, J.V. Biomarkers of nephrotoxic acute kidney injury. *Toxicology* **245**, 182-193 (2008).
2. Bellomo, R., Ronco, C., Kellum, J.A., Mehta, R.L. & Palevsky, P. Acute renal failure - definition, outcome measures, animal models, fluid therapy and information technology needs: the Second International Consensus Conference of the Acute Dialysis Quality Initiative (ADQI) Group. *Crit Care* **8**, R204-212 (2004).
3. Cerda, J.*, et al.* Epidemiology of acute kidney injury. *Clin J Am Soc Nephrol* **3**, 881-886 (2008).
4. Himmelfarb, J.*, et al.* Evaluation and initial management of acute kidney injury. *Clin J Am Soc Nephrol* **3**, 962-967 (2008).
5. Hingorani, S., Molitoris, B.A. & Himmelfarb, J. Ironing Out the Pathogenesis of Acute Kidney Injury. *American Journal of Kidney Diseases* **53**, 569-571 (2009).
6. Kinsey, G.R. & Okusa, M.D. Pathogenesis of Acute Kidney Injury: Foundation for Clinical Practice. *American Journal of Kidney Diseases* **58**, 291-301 (2011).
7. Lattanzio, M.R. & Kopyt, N.P. Acute kidney injury: new concepts in definition, diagnosis, pathophysiology, and treatment. *J Am Osteopath Assoc* **109**, 13-19 (2009).
8. Nagase, M., Aisawa, T., Honda, N. & Nihei, H. [Renal pathophysiology of hemorrhagic hypotension, acute ischemic renal failure, and obstructive nephropathy (author's transl)]. *Nihon Jinzo Gakkai shi* **19**, 254-261 (1977).
9. Thadhani, R., Pascual, M. & Bonventre, J.V. Acute renal failure. *N Engl J Med* **334**, 1448-1460 (1996).
10. Bakris, G.L. & Ritz, E. The message for World Kidney Day 2009: Hypertension and kidney disease: a marriage that should be prevented. *Nephrol Dial Transplant* **24**, 695-697 (2009).
11. Diseases, N.I.o.D.a.D.a.K. United States Renal Data System (USRDS) Annual Data Report. (National Institute of Diabetes and Digestive and Kidney Diseases, National Institutes of Health, Bethesda, MD, 2007).
12. Couser, W.G., Remuzzi, G., Mendis, S. & Tonelli, M. The contribution of chronic kidney disease to the global burden of major noncommunicable diseases. *Kidney International* **80**, 1258-1270 (2011).
13. Bakris, G.L. & Ritz, E. The message for World Kidney Day 2009: hypertension and kidney disease: a marriage that should be prevented. *Kidney Int* **75**, 449-452 (2009).
14. Gandhi, M., Olson, J.L. & Meyer, T.W. Contribution of tubular injury to loss of remnant kidney function. *Kidney Int* **54**, 1157-1165 (1998).
15. Schrier, R.W., Wang, W., Poole, B. & Mitra, A. Acute renal failure: definitions, diagnosis, pathogenesis, and therapy. *J Clin Invest* **114**, 5-14 (2004).

16. Waikar, S.S., Betensky, R.A. & Bonventre, J.V. Creatinine as the gold standard for kidney injury biomarker studies? *Nephrol Dial Transplant* **24**, 3263-3265 (2009).
17. Tonomura, Y., Uehara, T., Yamamoto, E., Torii, M. & Matsubara, M. Decrease in urinary creatinine in acute kidney injury influences diagnostic value of urinary biomarker-to-creatinine ratio in rats. *Toxicology* **290**, 241-248 (2011).
18. Excerpts from the United States Renal Data System 2001 Annual Data Report: Atlas of end-stage renal disease in the United States - Introduction. *American Journal of Kidney Diseases* **38**, S9-S16 (2001).
19. Pannu, N. & Nadim, M.K. An overview of drug-induced acute kidney injury. *Crit Care Med* **36**, S216-223 (2008).
20. Hofmann, R.M. Preventing harm during treatment of acute kidney injury: what do we really know? *Advances in chronic kidney disease* **19**, 142-148 (2012).
21. Rosen, S. & Stillman, I.E. Acute tubular necrosis is a syndrome of physiologic and pathologic dissociation. *J Am Soc Nephrol* **19**, 871-875 (2008).
22. Molitoris, B.A.*, et al.* siRNA targeted to p53 attenuates ischemic and cisplatin-induced acute kidney injury. *J Am Soc Nephrol* **20**, 1754-1764 (2009).
23. Stillman, I.E., Lima, E.Q. & Burdmann, E.A. Renal biopsies in acute kidney injury: who are we missing? *Clin J Am Soc Nephrol* **3**, 647-648 (2008).
24. Krawczeski, C.D.*, et al.* Serum cystatin C is an early predictive biomarker of acute kidney injury after pediatric cardiopulmonary bypass. *Clin J Am Soc Nephrol* **5**, 1552-1557 (2010).
25. Lameire, N., Van Biesen, W. & Vanholder, R. Acute renal failure. *Lancet* **365**, 417-430 (2005).
26. Mehta, R.L.*, et al.* Acute Kidney Injury Network: report of an initiative to improve outcomes in acute kidney injury. *Crit Care* **11**, R31 (2007).
27. Zhou, H., Hewitt, S.M., Yuen, P.S. & Star, R.A. Acute Kidney Injury Biomarkers - Needs, Present Status, and Future Promise. *Nephrology self-assessment program : NephSAP* **5**, 63-71 (2006).
28. Dharnidharka, V.R., Kwon, C. & Stevens, G. Serum cystatin C is superior to serum creatinine as a marker of kidney function: a meta-analysis. *American journal of kidney diseases : the official journal of the National Kidney Foundation* **40**, 221-226 (2002).
29. Herget-Rosenthal, S.*, et al.* Early detection of acute renal failure by serum cystatin C. *Kidney Int* **66**, 1115-1122 (2004).
30. Devarajan, P. Neutrophil gelatinase-associated lipocalin--an emerging troponin for kidney injury. *Nephrol Dial Transplant* **23**, 3737-3743 (2008).
31. Ichimura, T., Hung, C.C., Yang, S.A., Stevens, J.L. & Bonventre, J.V. Kidney injury molecule-1: a tissue and urinary biomarker for nephrotoxicant-induced renal injury. *Am J Physiol Renal Physiol* **286**, F552-563 (2004).
32. Parikh, C.R., Abraham, E., Ancukiewicz, M. & Edelstein, C.L. Urine IL-18 is an early diagnostic marker for acute kidney injury and predicts mortality in the intensive care unit. *J Am Soc Nephrol* **16**, 3046-3052 (2005).

33. Coll, E.*, et al.* Serum cystatin C as a new marker for noninvasive estimation of glomerular filtration rate and as a marker for early renal impairment. *American journal of kidney diseases : the official journal of the National Kidney Foundation* **36**, 29-34 (2000).
34. Liu, K.D.*, et al.* Serum interleukin-6 and interleukin-8 are early biomarkers of acute kidney injury and predict prolonged mechanical ventilation in children undergoing cardiac surgery: a case-control study. *Crit Care* **13**, R104 (2009).
35. Parikh, C.R.*, et al.* Urinary IL-18 is an early predictive biomarker of acute kidney injury after cardiac surgery. *Kidney Int* **70**, 199-203 (2006).
36. Martin, L.G., Casarella, W.J. & Gaylord, G.M. Azotemia caused by renal artery stenosis: treatment by percutaneous angioplasty. *AJR. American journal of roentgenology* **150**, 839-844 (1988).
37. Stapleton, F.B., Jones, D.P. & Green, R.S. Acute renal failure in neonates: incidence, etiology and outcome. *Pediatr Nephrol* **1**, 314-320 (1987).
38. Lattanzio, M.R. & Kopyt, N.P. Acute kidney injury: new concepts in definition, diagnosis, pathophysiology, and treatment. *J Am Osteopath Assoc* **109**, 13-19 (2009).
39. Kinsey, G.R. & Okusa, M.D. Pathogenesis of acute kidney injury: foundation for clinical practice. *American journal of kidney diseases : the official journal of the National Kidney Foundation* **58**, 291-301 (2011).
40. Glassford, N.J. & Bellomo, R. Acute kidney injury: Fluid therapy in acute kidney injury: the FACTTs. *Nat Rev Nephrol* **7**, 305-306 (2011).
41. Glassford, N.J. & Bellomo, R. Acute kidney injury: how can we facilitate recovery? *Curr Opin Crit Care* **17**, 562-568 (2011).
42. Uchino, S.*, et al.* Diuretics and mortality in acute renal failure. *Crit Care Med* **32**, 1669-1677 (2004).
43. Auron, A., Tal, L., Srivastava, T. & Alon, U.S. Reversal of hypercalcemic acute kidney injury by treatment with intravenous bisphosphonates. *Pediatr Nephrol* **24**, 613-617 (2009).
44. Kellum, J.A. & J, M.D. Use of dopamine in acute renal failure: a meta-analysis. *Crit Care Med* **29**, 1526-1531 (2001).
45. Galley, H.F. Can acute renal failure be prevented? *Journal of the Royal College of Surgeons of Edinburgh* **45**, 44-50 (2000).
46. Yaklin, K.M. Acute kidney injury: an overview of pathophysiology and treatments. *Nephrology nursing journal : journal of the American Nephrology Nurses' Association* **38**, 13-18; quiz 19 (2011).
47. Weisberg, L.S. Management of severe hyperkalemia. *Crit Care Med* **36**, 3246-3251 (2008).
48. Berger, A., Edelsberg, J., Inglese, G.W., Bhattacharyya, S.K. & Oster, G. Cost comparison of peritoneal dialysis versus hemodialysis in end-stage renal disease. *The American journal of managed care* **15**, 509-518 (2009).
49. Papalois, B.E.*, et al.* Long-term peritoneal dialysis before transplantation and intra-abdominal infection after simultaneous pancreas-kidney transplantations. *Arch Surg* **131**, 761-766 (1996).

50. SoRelle, R. Health Care Financing Administration wants to make kidney transplant availability equal, regardless of race. *Circulation* **101**, E37 (2000).
51. Roberts, R., Ballin, N. & Weech, M. Availability of suitable kidney transplant donors from an ICU population: a pilot study. *Transplant Proc* **21**, 3975-3976 (1989).
52. Roloff, J.S., Marshall, J.P., 2nd & Reynolds, J.O., Jr. Kidney transplant donors. Estimate of availability by autopsy survey. *Arch Surg* **103**, 359-362 (1971).
53. Miao, Y.*, et al.* [Long-term survival of high-risk kidney transplant patients]. *Zhonghua wai ke za zhi [Chinese journal of surgery]* **48**, 589-592 (2010).
54. Flechner, S.M.*, et al.* Kidney transplant rejection and tissue injury by gene profiling of biopsies and peripheral blood lymphocytes. *Am J Transplant* **4**, 1475-1489 (2004).
55. Beitland, S., Moen, H. & Os, I. Acute kidney injury with renal replacement therapy in trauma patients. *Acta anaesthesiologica Scandinavica* **54**, 833-840 (2010).
56. Friedmann, T. A brief history of gene therapy. *Nature genetics* **2**, 93-98 (1992).
57. Imai, E. Gene therapy for the treatment of renal disease: prospects for the future. *Current opinion in nephrology and hypertension* **6**, 496-503 (1997).
58. Edelstein, M.L., Abedi, M.R., Wixon, J. & Edelstein, R.M. Gene therapy clinical trials worldwide 1989-2004-an overview. *J Gene Med* **6**, 597-602 (2004).
59. Blau, H.M. & Springer, M.L. Gene therapy--a novel form of drug delivery. *N Engl J Med* **333**, 1204-1207 (1995).
60. Imai, E. Gene therapy for renal diseases: its potential and limitation. *J Am Soc Nephrol* **14**, 1102-1104 (2003).
61. Basile, D.P. Toward an effective gene therapy in renal disease. *Kidney Int* **55**, 740-741 (1999).
62. Kelley, V.R. & Sukhatme, V.P. Gene transfer in the kidney. *Am J Physiol* **276**, F1-9 (1999).
63. Lien, Y.H. & Lai, L.W. Renal gene transfer: nonviral approaches. *Mol Biotechnol* **24**, 283-294 (2003).
64. Kohn, D.B. & Candotti, F. Gene therapy fulfilling its promise. *N Engl J Med* **360**, 518-521 (2009).
65. Cavazzana-Calvo, M.*, et al.* Gene therapy of human severe combined immunodeficiency (SCID)-X1 disease. *Science* **288**, 669-672 (2000).
66. Kelley, V.R. & Sukhatme, V.P. Gene transfer in the kidney. *Am J Physiol* **276**, F1-9 (1999).
67. Lien, Y.H. & Lai, L.W. Renal gene transfer: nonviral approaches. *Mol Biotechnol* **24**, 283-294 (2003).
68. Imamura, R.*, et al.* Intravital two-photon microscopy assessment of renal protection efficacy of siRNA for p53 in experimental rat kidney transplantation models. *Cell Transplant* **19**, 1659-1670 (2010).
69. Imai, E. Gene therapy approach in renal disease in the 21st century. *Nephrol Dial Transplant* **16 Suppl 5**, 26-34 (2001).

70. Sandovici, M., Deelman, L.E., de Zeeuw, D., van Goor, H. & Henning, R.H. Immune modulation and graft protection by gene therapy in kidney transplantation. *Eur J Pharmacol* **585**, 261-269 (2008).
71. Sandovici, M., Deelman, L.E., Benigni, A. & Henning, R.H. Towards graft-specific immune suppression: Gene therapy of the transplanted kidney. *Adv Drug Deliv Rev* **62**, 1358-1368 (2010).
72. Torras, J., Cruzado, J.M., Herrero-Fresneda, I. & Grinyo, J.M. Gene therapy for acute renal failure. *Contrib Nephrol* **159**, 96-108 (2008).
73. Humes, H.D., MacKay, S.M., Funke, A.J. & Buffington, D.A. Acute renal failure: growth factors, cell therapy, and gene therapy. *Proceedings of the Association of American Physicians* **109**, 547-557 (1997).
74. Friedmann, T. & Roblin, R. Gene therapy for human genetic disease? *Science* **175**, 949-955 (1972).
75. Lien, Y.H. & Lai, L.W. Gene therapy for renal diseases. *Kidney international. Supplement* **61**, S85-88 (1997).
76. Dai, C., Yang, J. & Liu, Y. Single injection of naked plasmid encoding hepatocyte growth factor prevents cell death and ameliorates acute renal failure in mice. *J Am Soc Nephrol* **13**, 411-422 (2002).
77. Yazawa, K.*, et al.* Direct transfer of hepatocyte growth factor gene into kidney suppresses cyclosporin A nephrotoxicity in rats. *Nephrol Dial Transplant* **19**, 812-816 (2004).
78. Leonard, E.C., Friedrich, J.L. & Basile, D.P. VEGF-121 preserves renal microvessel structure and ameliorates secondary renal disease following acute kidney injury. *Am J Physiol Renal Physiol* **295**, F1648-1657 (2008).
79. Wang, J., Long, Q., Zhang, W. & Chen, N. Protective effects of exogenous interleukin 18-binding protein in a rat model of acute renal ischemia-reperfusion injury. *Shock* **37**, 333-340 (2012).
80. Lee, D.S.*, et al.* Recombinant uteroglobin prevents the experimental crescentic glomerulonephritis. *Kidney Int* **66**, 1061-1067 (2004).
81. Mizui, M.*, et al.* Electroporation-mediated HGF gene transfer ameliorated cyclosporine nephrotoxicity. *Kidney Int* **65**, 2041-2053 (2004).
82. Sandovici, M.*, et al.* Adenovirus-mediated interleukin-13 gene therapy attenuates acute kidney allograft injury. *J Gene Med* **9**, 1024-1032 (2007).
83. Vavrincova-Yaghi, D.*, et al.* Gene therapy with adenovirus-delivered indoleamine 2,3-dioxygenase improves renal function and morphology following allogeneic kidney transplantation in rat. *J Gene Med* **13**, 373-381 (2011).
84. DeYoung, M.B. & Dichek, D.A. Gene therapy for restenosis: are we ready? *Circ Res* **82**, 306-313 (1998).
85. Kay, M.A., Glorioso, J.C. & Naldini, L. Viral vectors for gene therapy: the art of turning infectious agents into vehicles of therapeutics. *Nature medicine* **7**, 33-40 (2001).
86. Cancedda, R., Bianchi, G., Derubeis, A. & Quarto, R. Cell therapy for bone disease: a review of current status. *Stem Cells* **21**, 610-619 (2003).

87. Burger, S.R. Current regulatory issues in cell and tissue therapy. *Cytotherapy* **5**, 289-298 (2003).
88. Migliaccio, A.R., Grazzini, G. & Hillyer, C.D. Ex vivo generated red cells as transfusion products. *Stem cells international* **2012**, 615412 (2012).
89. Hochedlinger, K. & Jaenisch, R. Nuclear transplantation, embryonic stem cells, and the potential for cell therapy. *N Engl J Med* **349**, 275-286 (2003).
90. Brodie, J.C. & Humes, H.D. Stem cell approaches for the treatment of renal failure. *Pharmacological reviews* **57**, 299-313 (2005).
91. Mason, C., Brindley, D.A., Culme-Seymour, E.J. & Davie, N.L. Cell therapy industry: billion dollar global business with unlimited potential. *Regenerative medicine* **6**, 265-272 (2011).
92. Semedo, P.*, et al.* Mesenchymal stem cells attenuate renal fibrosis through immune modulation and remodeling properties in a rat remnant kidney model. *Stem Cells* **27**, 3063-3073 (2009).
93. Kelly, K.J., Kluve-Beckerman, B., Zhang, J. & Dominguez, J.H. Intravenous cell therapy for acute renal failure with serum amyloid A protein-reprogrammed cells. *Am J Physiol Renal Physiol* **299**, F453-464 (2010).
94. Hekking, L.H.*, et al.* Mesothelial cell transplantation in models of acute inflammation and chronic peritoneal dialysis. *Peritoneal dialysis international : journal of the International Society for Peritoneal Dialysis* **23**, 323-330 (2003).
95. Rouskova, L., Hruska, I. & Filip, S. Issues and ethical problems of stem cell therapy--where is Hippocrates? *Acta Medica (Hradec Kralove)* **51**, 121-126 (2008).
96. Grimm, D. & Kay, M.A. Therapeutic application of RNAi: is mRNA targeting finally ready for prime time? *J Clin Invest* **117**, 3633-3641 (2007).
97. Wang, J.H., Hendry, B.M. & Sharpe, C.C. Silencing genes in the kidney: antisense or RNA interference? *Nephrol Dial Transplant* **23**, 2115-2118 (2008).
98. Obbard, D.J., Gordon, K.H., Buck, A.H. & Jiggins, F.M. The evolution of RNAi as a defence against viruses and transposable elements. *Philos Trans R Soc Lond B Biol Sci* **364**, 99-115 (2009).
99. Racz, Z. & Hamar, P. RNA interference in research and therapy of renal diseases. *Gene Therapy for Renal Diseases and Transplantation* **159**, 78-95 (2008).
100. Valadi, H.*, et al.* Exosome-mediated transfer of mRNAs and microRNAs is a novel mechanism of genetic exchange between cells. *Nature cell biology* **9**, 654-659 (2007).
101. Saal, S. & Harvey, S.J. MicroRNAs and the kidney: coming of age. *Current opinion in nephrology and hypertension* **18**, 317-323 (2009).
102. Cantaluppi, V.*, et al.* Microvesicles derived from endothelial progenitor cells protect the kidney from ischemia-reperfusion injury by microRNA-dependent reprogramming of resident renal cells. *Kidney Int* (2012).
103. Liu, Y.W., Surka, M.C., Schroeter, T., Lukiyanchuk, V. & Schmid, S.L. Isoform and splice-variant specific functions of dynamin-2 revealed by analysis of conditional knock-out cells. *Mol Biol Cell* **19**, 5347-5359 (2008).

104. Loerke, D*., et al.* Cargo and dynamin regulate clathrin-coated pit maturation. *PLoS Biol* **7**, e57 (2009).
105. Schmid, E.M. & McMahon, H.T. Integrating molecular and network biology to decode endocytosis. *Nature* **448**, 883-888 (2007).
106. Cao, H., Chen, J., Awoniyi, M., Henley, J.R. & McNiven, M.A. Dynamin 2 mediates fluid-phase micropinocytosis in epithelial cells. *J Cell Sci* **120**, 4167-4177 (2007).
107. Watanabe, A*., et al.* Targeted prevention of renal accumulation and toxicity of gentamicin by aminoglycoside binding receptor antagonists. *J Control Release* **95**, 423-433 (2004).
108. Monia, B.P. First- and second-generation antisense oligonucleotide inhibitors targeted against human c-raf kinase. *Ciba Found Symp* **209**, 107-119; discussion 119-123 (1997).
109. Bouillet, P., Robati, M., Bath, M. & Strasser, A. Polycystic kidney disease prevented by transgenic RNA interference. *Cell death and differentiation* **12**, 831-833 (2005).
110. Wise, T.G., Schafer, D.S., Lowenthal, J.W. & Doran, T.J. The use of RNAi and transgenics to develop viral disease resistant livestock. *Developments in biologicals* **132**, 377-382 (2008).
111. Vaughan, E.E., DeGiulio, J.V. & Dean, D.A. Intracellular trafficking of plasmids for gene therapy: mechanisms of cytoplasmic movement and nuclear import. *Curr Gene Ther* **6**, 671-681 (2006).
112. Forest, C. & Antras-Ferry, J. [Gene expression regulation. Principles and methods]. *Diabete Metab* **18**, 476-485 (1992).
113. Geley, S. & Muller, C. RNAi: ancient mechanism with a promising future. *Experimental gerontology* **39**, 985-998 (2004).
114. Tijsterman, M. & Plasterk, R.H. Dicers at RISC; the mechanism of RNAi. *Cell* **117**, 1-3 (2004).
115. Jose, A.M. & Hunter, C.P. Transport of sequence-specific RNA interference information between cells. *Annu Rev Genet* **41**, 305-330 (2007).
116. Chu, K., Kim, M., Jeong, S.W., Kim, S.U. & Yoon, B.W. Human neural stem cells can migrate, differentiate, and integrate after intravenous transplantation in adult rats with transient forebrain ischemia. *Neurosci Lett* **343**, 129-133 (2003).
117. Tanner, G.A., Sandoval, R.M., Molitoris, B.A., Bamburg, J.R. & Ashworth, S.L. Micropuncture gene delivery and intravital two-photon visualization of protein expression in rat kidney. *Am J Physiol Renal Physiol* **289**, F638-643 (2005).
118. Fisher, G.H*., et al.* Development of a flexible and specific gene delivery system for production of murine tumor models. *Oncogene* **18**, 5253-5260 (1999).
119. Gusella, G.L., Fedorova, E., Marras, D., Klotman, P.E. & Klotman, M.E. In vivo gene transfer to kidney by lentiviral vector. *Kidney Int* **61**, S32-36 (2002).
120. Stephan, D*., et al.* [Direct gene transfer in the rat kidney in vivo]. *Arch Mal Coeur Vaiss* **90**, 1127-1130 (1997).

121. Suda, T. & Liu, D. Hydrodynamic gene delivery: its principles and applications. *Mol Ther* **15**, 2063-2069 (2007).
122. Xing, Y., Pua, E.C., Lu, X. & Zhong, P. Low-amplitude ultrasound enhances hydrodynamic-based gene delivery to rat kidney. *Biochem Biophys Res Commun* **386**, 217-222 (2009).
123. Koike, H.*, et al.* An efficient gene transfer method mediated by ultrasound and microbubbles into the kidney. *J Gene Med* **7**, 108-116 (2005).
124. Moullier, P.*, et al.* Adenoviral-mediated gene transfer to renal tubular cells in vivo. *Kidney Int* **45**, 1220-1225 (1994).
125. Verkman, A.S. & Yang, B. Aquaporin gene delivery to kidney. *Kidney Int* **61**, S120-124 (2002).
126. Decorti, G., Malusa, N., Furlan, G., Candussio, L. & Klugmann, F.B. Endocytosis of gentamicin in a proximal tubular renal cell line. *Life Sci* **65**, 1115-1124 (1999).
127. Zhu, G., Nicolson, A.G., Cowley, B.D., Rosen, S. & Sukhatme, V.P. In vivo adenovirus-mediated gene transfer into normal and cystic rat kidneys. *Gene Ther* **3**, 298-304 (1996).
128. Ye, X., Liu, X., Li, Z. & Ray, P.E. Efficient gene transfer to rat renal glomeruli with recombinant adenoviral vectors. *Hum Gene Ther* **12**, 141-148 (2001).
129. Wang, G.*, et al.* Increasing epithelial junction permeability enhances gene transfer to airway epithelia In vivo. *Am J Respir Cell Mol Biol* **22**, 129-138 (2000).
130. Herweijer, H. & Wolff, J.A. Gene therapy progress and prospects: hydrodynamic gene delivery. *Gene Ther* **14**, 99-107 (2007).
131. Kallskog, O.*, et al.* Lymphatic vessels in pancreatic islets implanted under the renal capsule of rats. *Am J Transplant* **6**, 680-686 (2006).
132. Lecocq, M.*, et al.* Uptake by mouse liver and intracellular fate of plasmid DNA after a rapid tail vein injection of a small or a large volume. *J Gene Med* **5**, 142-156 (2003).
133. Zhou, T., Kamimura, K., Zhang, G. & Liu, D. Intracellular gene transfer in rats by tail vein injection of plasmid DNA. *AAPS J* **12**, 692-698 (2010).
134. Zhou, T., Kamimura, K., Zhang, G. & Liu, D. Intracellular gene transfer in rats by tail vein injection of plasmid DNA. *Aaps J* **12**, 692-698 (2010).
135. Fujii, N.*, et al.* Targeting of interstitial cells using a simple gene-transfer strategy. *Nephrol Dial Transplant* **21**, 2745-2753 (2006).
136. Saimura, M.*, et al.* Intraperitoneal injection of adenovirus-mediated NK4 gene suppresses peritoneal dissemination of pancreatic cancer cell line AsPC-1 in nude mice. *Cancer Gene Ther* **9**, 799-806 (2002).
137. Maruyama, H.*, et al.* Sustained transgene expression in rat kidney with naked plasmid DNA and PCR-amplified DNA fragments. *J Biochem* **137**, 373-380 (2005).
138. Kaikkonen, M.U., Maatta, A.I., Yla-Herttuala, S. & Airenne, K.J. Screening of complement inhibitors: shielded baculoviruses increase the safety and efficacy of gene delivery. *Mol Ther* **18**, 987-992 (2010).

139. van Loo, N.D.*, et al.* Baculovirus infection of nondividing mammalian cells: mechanisms of entry and nuclear transport of capsids. *J Virol* **75**, 961-970 (2001).
140. Gusella, G.L.*, et al.* Lentiviral gene transduction of kidney. *Hum Gene Ther* **13**, 407-414 (2002).
141. Nickisch-Rosenegk, M., Teschke, T. & Bier, F.F. Construction of an artificial cell membrane anchor using DARC as a fitting for artificial extracellular functionalities of eukaryotic cells. *Journal of nanobiotechnology* **10**, 1 (2012).
142. Nemerow, G.R. & Stewart, P.L. Role of alpha(v) integrins in adenovirus cell entry and gene delivery. *Microbiology and molecular biology reviews : MMBR* **63**, 725-734 (1999).
143. Clapham, P.R. & McKnight, A. Cell surface receptors, virus entry and tropism of primate lentiviruses. *J Gen Virol* **83**, 1809-1829 (2002).
144. Ray, S.D., Kamendulis, L.M., Gurule, M.W., Yorkin, R.D. & Corcoran, G.B. Ca2+ antagonists inhibit DNA fragmentation and toxic cell death induced by acetaminophen. *FASEB J* **7**, 453-463 (1993).
145. Schwartz, D.A.*, et al.* CpG motifs in bacterial DNA cause inflammation in the lower respiratory tract. *J Clin Invest* **100**, 68-73 (1997).
146. Zhou, H.S., Liu, D.P. & Liang, C.C. Challenges and strategies: the immune responses in gene therapy. *Med Res Rev* **24**, 748-761 (2004).
147. Hibbitt, O.C.*, et al.* Delivery and long-term expression of a 135 kb LDLR genomic DNA locus in vivo by hydrodynamic tail vein injection. *J Gene Med* **9**, 488-497 (2007).
148. Maruyama, H.*, et al.* High-level expression of naked DNA delivered to rat liver via tail vein injection. *J Gene Med* **4**, 333-341 (2002).
149. Camino, A.M.*, et al.* Adenovirus-mediated inhibition of SPARC attenuates liver fibrosis in rats. *J Gene Med* **10**, 993-1004 (2008).
150. Brunetti-Pierri, N.*, et al.* Pseudo-hydrodynamic delivery of helper-dependent adenoviral vectors into non-human primates for liver-directed gene therapy. *Mol Ther* **15**, 732-740 (2007).
151. Budker, V.G.*, et al.* Mechanism of plasmid delivery by hydrodynamic tail vein injection. II. Morphological studies. *J Gene Med* **8**, 874-888 (2006).
152. Herweijer, H. & Wolff, J.A. Gene therapy progress and prospects: hydrodynamic gene delivery. *Gene Ther* **14**, 99-107 (2007).
153. Li, J., Yao, Q. & Liu, D. Hydrodynamic cell delivery for simultaneous establishment of tumor growth in mouse lung, liver and kidney. *Cancer Biol Ther* **12**, 737-741 (2011).
154. Sawyer, G.J.*, et al.* Hydrodynamic gene delivery to the liver: theoretical and practical issues for clinical application. *Curr Gene Ther* **9**, 128-135 (2009).
155. Sebestyen, M.G.*, et al.* Mechanism of plasmid delivery by hydrodynamic tail vein injection. I. Hepatocyte uptake of various molecules. *J Gene Med* **8**, 852-873 (2006).

156. Zhang, L.*, et al.* [Human coagulation factor IX gene therapy in murine hemophilia B by hydrodynamic delivery and site-specific genomic integration.]. *Zhonghua Xue Ye Xue Za Zhi* **31**, 294-299 (2010).
157. Liu, F., Song, Y. & Liu, D. Hydrodynamics-based transfection in animals by systemic administration of plasmid DNA. *Gene Ther* **6**, 1258-1266 (1999).
158. Gupta, S.*, et al.* Isolation and characterization of kidney-derived stem cells. *J Am Soc Nephrol* **17**, 3028-3040 (2006).
159. Karow, M.*, et al.* Site-specific recombinase strategy to create induced pluripotent stem cells efficiently with plasmid DNA. *Stem Cells* **29**, 1696-1704 (2011).
160. Narang, A.S.*, et al.* Vascular endothelial growth factor gene delivery for revascularization in transplanted human islets. *Pharm Res* **21**, 15-25 (2004).
161. Panakanti, R. & Mahato, R.I. Bipartite vector encoding hVEGF and hIL-1Ra for ex vivo transduction into human islets. *Mol Pharm* **6**, 274-284 (2009).
162. Favre, D., Ferry, N. & Moullier, P. Critical aspects of viral vectors for gene transfer into the kidney. *J Am Soc Nephrol* **11 Suppl 16**, S149-153 (2000).
163. Gusella, G.L.*, et al.* Lentiviral gene transduction of kidney. *Hum Gene Ther* **13**, 407-414 (2002).
164. Corridon, P.R.*, et al.* A method to facilitate and monitor expression of exogenous genes in the rat kidney using plasmid and viral vectors. *Am J Physiol Renal Physiol* **304**, F1217-1229 (2013).
165. Hamar, P.*, et al.* Small interfering RNA targeting Fas protects mice against renal ischemia-reperfusion injury. *Proc Natl Acad Sci U S A* **101**, 14883-14888 (2004).
166. Maruyama, H.*, et al.* Rat kidney-targeted naked plasmid DNA transfer by retrograde injection into the renal vein. *Mol Biotechnol* **27**, 23-31 (2004).
167. Maruyama, H.*, et al.* Kidney-targeted naked DNA transfer by retrograde renal vein injection in rats. *Hum Gene Ther* **13**, 455-468 (2002).
168. Xing, Y., Pua, E.C., Lu, X. & Zhong, P. Low-amplitude ultrasound enhances hydrodynamic-based gene delivery to rat kidney. *Biochem Biophys Res Commun* **386**, 217-222 (2009).
169. Ruzsics, Z.*, et al.* Transposon-assisted cloning and traceless mutagenesis of adenoviruses: Development of a novel vector based on species D. *J Virol* **80**, 8100-8113 (2006).
170. Uren, A.G., Kool, J., Berns, A. & van Lohuizen, M. Retroviral insertional mutagenesis: past, present and future. *Oncogene* **24**, 7656-7672 (2005).
171. Mohrin, M.*, et al.* Hematopoietic stem cell quiescence promotes error-prone DNA repair and mutagenesis. *Cell stem cell* **7**, 174-185 (2010).
172. Wischnitzer, S. Current techniques in biomedical electron microscopy. *International review of cytology* **22**, 1-61 (1967).
173. Dhawan, A.P., D'Alessandro, B. & Fu, X. Optical imaging modalities for biomedical applications. *IEEE reviews in biomedical engineering* **3**, 69-92 (2010).
174. Masters, B.R. Correlation of histology and linear and nonlinear microscopy of the living human cornea. *Journal of biophotonics* **2**, 127-139 (2009).

175. Schmitt, J.M., Knuttel, A. & Yadlowsky, M. Confocal microscopy in turbid media. *Journal of the Optical Society of America. A, Optics, image science, and vision* **11**, 2226-2235 (1994).
176. Dunn, K.W.*, et al.* Functional studies of the kidney of living animals using multicolor two-photon microscopy. *Am J Physiol Cell Physiol* **283**, C905-916 (2002).
177. Helmchen, F. & Denk, W. Deep tissue two-photon microscopy. *Nature methods* **2**, 932-940 (2005).
178. Denk, W. & Svoboda, K. Photon upmanship: why multiphoton imaging is more than a gimmick. *Neuron* **18**, 351-357 (1997).
179. Dunn, K.W. & Young, P.A. Principles of multiphoton microscopy. *Nephron Exp Nephrol* **103**, e33-40 (2006).
180. Ashworth, S.L., Sandoval, R.M., Tanner, G.A. & Molitoris, B.A. Two-photon microscopy: visualization of kidney dynamics. *Kidney Int* **72**, 416-421 (2007).
181. Comper, W.D., Haraldsson, B. & Deen, W.M. Resolved: normal glomeruli filter nephrotic levels of albumin. *J Am Soc Nephrol* **19**, 427-432 (2008).
182. Kang, J.J., Toma, I., Sipos, A., McCulloch, F. & Peti-Peterdi, J. Quantitative imaging of basic functions in renal (patho)physiology. *Am J Physiol Renal Physiol* **291**, F495-502 (2006).
183. Wang, E., Sandoval, R.M., Campos, S.B. & Molitoris, B.A. Rapid diagnosis and quantification of acute kidney injury using fluorescent ratio-metric determination of glomerular filtration rate in the rat. *Am J Physiol Renal Physiol* **299**, F1048-1055 (2010).
184. Medarova, Z., Pham, W., Farrar, C., Petkova, V. & Moore, A. In vivo imaging of siRNA delivery and silencing in tumors. *Nature medicine* **13**, 372-377 (2007).
185. Moore, A. & Medarova, Z. Imaging of siRNA delivery and silencing. *Methods Mol Biol* **487**, 93-110 (2009).
186. Penuelas, I., Haberkorn, U., Yaghoubi, S. & Gambhir, S.S. Gene therapy imaging in patients for oncological applications. *European journal of nuclear medicine and molecular imaging* **32 Suppl 2**, S384-403 (2005).
187. Hebden, J.C., Arridge, S.R. & Delpy, D.T. Optical imaging in medicine: I. Experimental techniques. *Phys Med Biol* **42**, 825-840 (1997).
188. Ghiran, I.C. Introduction to fluorescence microscopy. *Methods Mol Biol* **689**, 93-136 (2011).
189. Valeur, B. & Berberan-Santos, M.N. A Brief History of Fluorescence and Phosphorescence before the Emergence of Quantum Theory. *J Chem Educ* **88**, 731-738 (2011).
190. Marsh, P., Burns, D. & Girkin, J. Practical implementation of adaptive optics in multiphoton microscopy. *Optics express* **11**, 1123-1130 (2003).
191. Lakowicz, J.R.*, et al.* Time-resolved fluorescence spectroscopy and imaging of DNA labeled with DAPI and Hoechst 33342 using three-photon excitation. *Biophys J* **72**, 567-578 (1997).

192. de Grauw, C.J., Vroom, J.M., van der Voort, H.T. & Gerritsen, H.C. Imaging properties in two-photon excitation microscopy and effects of refractive-index mismatch in thick specimens. *Applied optics* **38**, 5995-6003 (1999).
193. Young, P.A., Clendenon, S.G., Byars, J.M. & Dunn, K.W. The effects of refractive index heterogeneity within kidney tissue on multiphoton fluorescence excitation microscopy. *J Microsc* **242**, 148-156 (2011).
194. Rothman, S.S. *Lessons from the living cell: the culture of science and the limits of reductionism*, (McGraw-Hill Companies, 2001).
195. Dunn, K.W., Sandoval, R.M. & Molitoris, B.A. Intravital imaging of the kidney using multiparameter multiphoton microscopy. *Nephron Exp Nephrol* **94**, e7-11 (2003).
196. Liang, X., Graf, B.W. & Boppart, S.A. In Vivo Multiphoton Microscopy for Investigating Biomechanical Properties of Human Skin. *Cell Mol Bioeng* **4**, 231-238 (2011).
197. Masters, B. & So, P. Confocal microscopy and multi-photon excitation microscopy of human skin in vivo. *Opt Express* **8**, 2-10 (2001).
198. Masters, B.R. & So, P.T. Multi-photon Excitation Microscopy and Confocal Microscopy Imaging of In Vivo Human Skin: A Comparison. *Microsc Microanal* **5**, 282-289 (1999).
199. Stutzmann, G. Seeing the brain in action: how multiphoton imaging has advanced our understanding of neuronal function. *Microsc Microanal* **14**, 482-491 (2008).
200. Chia, T.H., Williamson, A., Spencer, D.D. & Levene, M.J. Multiphoton fluorescence lifetime imaging of intrinsic fluorescence in human and rat brain tissue reveals spatially distinct NADH binding. *Opt Express* **16**, 4237-4249 (2008).
201. Bacskai, B.J*., et al.* Four-dimensional multiphoton imaging of brain entry, amyloid binding, and clearance of an amyloid-beta ligand in transgenic mice. *Proc Natl Acad Sci U S A* **100**, 12462-12467 (2003).
202. Lin, J*., et al.* Assessment of liver steatosis and fibrosis in rats using integrated coherent anti-Stokes Raman scattering and multiphoton imaging technique. *J Biomed Opt* **16**, 116024 (2011).
203. Thorling, C.A*., et al.* Multiphoton microscopy and fluorescence lifetime imaging provide a novel method in studying drug distribution and metabolism in the rat liver in vivo. *J Biomed Opt* **16**, 086013 (2011).
204. Peti-Peterdi, J., Burford, J.L. & Hackl, M.J. The first decade of using multiphoton microscopy for high-power kidney imaging. *Am J Physiol Renal Physiol* **302**, F227-233 (2012).
205. Hall, A.M., Crawford, C., Unwin, R.J., Duchen, M.R. & Peppiatt-Wildman, C.M. Multiphoton imaging of the functioning kidney. *J Am Soc Nephrol* **22**, 1297-1304 (2011).
206. Molitoris, B.A. & Sandoval, R.M. Multiphoton imaging techniques in acute kidney injury. *Contrib Nephrol* **165**, 46-53 (2010).

207. Molitoris, B.A. & Sandoval, R.M. Intravital multiphoton microscopy of dynamic renal processes. *Am J Physiol Renal Physiol* **288**, F1084-1089 (2005).
208. Molitoris, B.A. & Sandoval, R.M. Techniques to study nephron function: microscopy and imaging. *Pflugers Arch* **458**, 203-209 (2009).
209. Dunn, K.W., Sutton, T.A. & Sandoval, R.M. Live-animal imaging of renal function by multiphoton microscopy. *Curr Protoc Cytom* **Chapter 12**, Unit12 19 (2007).
210. Meneton, P., Ichikawa, I., Inagami, T. & Schnermann, J. Renal physiology of the mouse. *Am J Physiol Renal Physiol* **278**, F339-351 (2000).
211. Kaunitz, J.D., Cummins, V.P.S., Mishler, D. & Nagami, G.T. Inhibition of Gentamicin Uptake into Cultured Mouse Proximal Tubule Epithelial-Cells by L-Lysine. *J Clin Pharmacol* **33**, 63-69 (1993).
212. von Bonsdorff, C.H., Fuller, S.D. & Simons, K. Apical and basolateral endocytosis in Madin-Darby canine kidney (MDCK) cells grown on nitrocellulose filters. *EMBO J* **4**, 2781-2792 (1985).
213. Kreutz, R.P.*, et al.* Morbid obesity and metabolic syndrome in Ossabaw miniature swine are associated with increased platelet reactivity. *Diabetes Metab Syndr Obes* **4**, 99-105 (2011).
214. Sandoval, R.M.*, et al.* A non-nephrotoxic gentamicin congener that retains antimicrobial efficacy. *J Am Soc Nephrol* **17**, 2697-2705 (2006).
215. Hall, A.M., Rhodes, G.J., Sandoval, R.M., Corridon, P.R. & Molitoris, B.A. In vivo multiphoton imaging of mitochondrial structure and function during acute kidney injury. *Kidney Int* **83**, 72-83 (2013).
216. Park, K.M., Chen, A. & Bonventre, J.V. Prevention of kidney ischemia/reperfusion-induced functional injury and JNK, p38, and MAPK kinase activation by remote ischemic pretreatment. *J Biol Chem* **276**, 11870-11876 (2001).
217. Molitoris, B.A.*, et al.* siRNA targeted to p53 attenuates ischemic and cisplatin-induced acute kidney injury. *J Am Soc Nephrol* **20**, 1754-1764 (2009).
218. Tanner, G.A., Sandoval, R.M., Molitoris, B.A., Bamburg, J.R. & Ashworth, S.L. Micropuncture gene delivery and intravital two-photon visualization of protein expression in rat kidney. *Am J Physiol Renal Physiol* **289**, F638-643 (2005).
219. Chen, X.G.*, et al.* Gene delivery to mice spermatogenic stem cells by Effectene. *Chinese medical journal* **117**, 630-632 (2004).
220. Cunnion, K.M. & Frank, M.M. Complement activation influences Staphylococcus aureus adherence to endothelial cells. *Infect Immun* **71**, 1321-1327 (2003).
221. Georgopoulos, L.J.*, et al.* Preclinical evaluation of innate immunity to baculovirus gene therapy vectors in whole human blood. *Mol Immunol* **46**, 2911-2917 (2009).
222. Basile, D.P.*, et al.* Chromosome substitution modulates resistance to ischemia reperfusion injury in Brown Norway rats. *Kidney Int* **83**, 242-250 (2013).
223. Kelly, K.J.*, et al.* Intercellular adhesion molecule-1-deficient mice are protected against ischemic renal injury. *J Clin Invest* **97**, 1056-1063 (1996).

224. Levi, M. & Cronin, R.E. Early selective effects of gentamicin on renal brush-border membrane Na-Pi cotransport and Na-H exchange. *Am J Physiol* **258**, F1379-1387 (1990).
225. Hall, A.M., Rhodes, G.J., Sandoval, R.M., Corridon, P.R. & Molitoris, B.A. In vivo multiphoton imaging of mitochondrial structure and function during acute kidney injury. *Kidney Int* **83**, 72-83 (2013).
226. Dunn, K.W.*, et al.* Functional studies of the kidney of living animals using multicolor two-photon microscopy. *Am J Physiol Cell Physiol* **283**, C905-916 (2002).
227. Molitoris, B.A. & Sandoval, R.M. Intravital multiphoton microscopy of dynamic renal processes. *Am J Physiol Renal Physiol* **288**, F1084-1089 (2005).
228. Link, C.D.*, et al.* Conversion of green fluorescent protein into a toxic, aggregation-prone protein by C-terminal addition of a short peptide. *J Biol Chem* **281**, 1808-1816 (2006).
229. Kaikkonen, M.U., Maatta, A.I., Yla-Herttuala, S. & Airenne, K.J. Screening of complement inhibitors: shielded baculoviruses increase the safety and efficacy of gene delivery. *Mol Ther* **18**, 987-992 (2010).
230. Neeb, Z.P.*, et al.* Metabolic syndrome and coronary artery disease in Ossabaw compared with Yucatan swine. *Comp Med* **60**, 300-315 (2010).
231. Middlekauff, H.R., Nitzsche, E.U., Nguyen, A.H., Hoh, C.K. & Gibbs, G.G. Modulation of renal cortical blood flow during static exercise in humans. *Circ Res* **80**, 62-68 (1997).
232. Conkbayir, I., Men, S., Yanik, B. & Hekimoglu, B. Color Doppler sonographic finding of retrograde jugular venous flow as a sign of innominate vein occlusion. *J Clin Ultrasound* **30**, 392-398 (2002).
233. Rippe, C., Rippe, A., Larsson, A., Asgeirsson, D. & Rippe, B. Nature of glomerular capillary permeability changes following acute renal ischemia-reperfusion injury in rats. *Am J Physiol Renal Physiol* **291**, F1362-1368 (2006).
234. Suda, T. & Liu, D. Hydrodynamic gene delivery: its principles and applications. *Mol Ther* **15**, 2063-2069 (2007).
235. Zhang, X., Dong, X., Sawyer, G.J., Collins, L. & Fabre, J.W. Regional hydrodynamic gene delivery to the rat liver with physiological volumes of DNA solution. *J Gene Med* **6**, 693-703 (2004).
236. Christensen, E.I. & Maunsbach, A.B. Effects of dextran on lysosomal ultrastructure and protein digestion in renal proximal tubule. *Kidney Int* **16**, 301-311 (1979).
237. Morral, N.*, et al.* Administration of helper-dependent adenoviral vectors and sequential delivery of different vector serotype for long-term liver-directed gene transfer in baboons. *Proc Natl Acad Sci U S A* **96**, 12816-12821 (1999).
238. Neal, C.R.*, et al.* Glomerular filtration into the subpodocyte space is highly restricted under physiological perfusion conditions. *Am J Physiol Renal Physiol* **293**, F1787-1798 (2007).

239. Carlsson, P.O., Jansson, L., Andersson, A. & Kallskog, O. Capillary blood pressure in syngeneic rat islets transplanted under the renal capsule is similar to that of the implantation organ. *Diabetes* **47**, 1586-1593 (1998).
240. Bude, R.O. & Rubin, J.M. Relationship between the resistive index and vascular compliance and resistance. *Radiology* **211**, 411-417 (1999).
241. Ludwig, T., Riethmuller, C., Gekle, M., Schwerdt, G. & Oberleithner, H. Nephrotoxicity of platinum complexes is related to basolateral organic cation transport. *Kidney Int* **66**, 196-202 (2004).
242. Weinbaum, S., Duan, Y., Satlin, L.M., Wang, T. & Weinstein, A.M. Mechanotransduction in the renal tubule. *Am J Physiol Renal Physiol* **299**, F1220-1236 (2010).
243. Li, E., Stupack, D., Bokoch, G.M. & Nemerow, G.R. Adenovirus endocytosis requires actin cytoskeleton reorganization mediated by Rho family GTPases. *J Virol* **72**, 8806-8812 (1998).
244. Long, G., Pan, X., Kormelink, R. & Vlak, J.M. Functional entry of baculovirus into insect and mammalian cells is dependent on clathrin-mediated endocytosis. *J Virol* **80**, 8830-8833 (2006).
245. Zaiss, A.K.*, et al.* Complement is an essential component of the immune response to adeno-associated virus vectors. *J Virol* **82**, 2727-2740 (2008).
246. Tian, J.*, et al.* Adenovirus activates complement by distinctly different mechanisms in vitro and in vivo: indirect complement activation by virions in vivo. *J Virol* **83**, 5648-5658 (2009).
247. Ashworth, S.L.*, et al.* ADF/cofilin mediates actin cytoskeletal alterations in LLC-PK cells during ATP depletion. *Am J Physiol Renal Physiol* **284**, F852-862 (2003).
248. Burne-Taney, M.J., Yokota, N. & Rabb, H. Persistent renal and extrarenal immune changes after severe ischemic injury. *Kidney Int* **67**, 1002-1009 (2005).
249. Kume, S., Thomas, M.C. & Koya, D. Nutrient sensing, autophagy, and diabetic nephropathy. *Diabetes* **61**, 23-29 (2012).
250. Singh, S., Narang, A.S. & Mahato, R.I. Subcellular fate and off-target effects of siRNA, shRNA, and miRNA. *Pharm Res* **28**, 2996-3015 (2011).
251. Basile, D.P., Donohoe, D., Cao, X. & Van Why, S.K. Resistance to ischemic acute renal failure in the Brown Norway rat: a new model to study cytoprotection. *Kidney Int* **65**, 2201-2211 (2004).
252. Nilakantan, V.*, et al.* Favorable balance of anti-oxidant/pro-oxidant systems and ablated oxidative stress in Brown Norway rats in renal ischemia-reperfusion injury. *Mol Cell Biochem* **304**, 1-11 (2007).
253. Ardehali, H. Signaling mechanisms in ischemic preconditioning: interaction of PKCepsilon and MitoK(ATP) in the inner membrane of mitochondria. *Circ Res* **99**, 798-800 (2006).
254. Murry, C.E., Jennings, R.B. & Reimer, K.A. Preconditioning with ischemia: a delay of lethal cell injury in ischemic myocardium. *Circulation* **74**, 1124-1136 (1986).

255. Kim, H.K., Thu, V.T., Heo, H.J., Kim, N. & Han, J. Cardiac proteomic responses to ischemia-reperfusion injury and ischemic preconditioning. *Expert Rev Proteomics* **8**, 241-261 (2011).
256. Basile, D.P.*, et al.* Chromosome substitution modulates resistance to ischemia reperfusion injury in Brown Norway rats. *Kidney Int* **83**, 242-250 (2013).
257. Evans, R.G. & Fitzgerald, S.M. Nitric oxide and superoxide in the renal medulla: a delicate balancing act. *Curr Opin Nephrol Hypertens* **14**, 9-15 (2005).
258. Just, A., Olson, A.J., Whitten, C.L. & Arendshorst, W.J. Superoxide mediates acute renal vasoconstriction produced by angiotensin II and catecholamines by a mechanism independent of nitric oxide. *Am J Physiol Heart Circ Physiol* **292**, H83-92 (2007).

CURRICULUM VITAE

Peter R. Corridon

EDUCATION

Ph.D. in Biomolecular Imaging and Medical Biophysics (Indiana University, Indianapolis, IN, USA)
Research Topic: Hydrodynamic Delivery for the Study, Treatment and Prevention of Acute Kidney Injury - 2013

Research Summary: Advancements in human genomics have simultaneously enhanced our basic understanding of the human body and ability to combat debilitating diseases. Historically, research has shown that there have been many hindrances to realizing this medicinal revolution. One hindrance, with particular regard to the kidney, has been our inability to effectively and routinely delivery genes to various loci, without inducing significant injury. However, we have recently developed a method using hydrodynamic fluid delivery that has shown substantial promise in addressing aforesaid issues. We optimized our approach and designed a method that utilizes retrograde renal vein injections to facilitate widespread and persistent plasmid and adenoviral based transgene expression in rat kidneys. Exogenous gene expression extended throughout the cortex and medulla, lasting over 1 month within comparable expression profiles, in various renal cell types without considerably impacting normal organ function. As a proof of its utility we by attempted to prevent ischemic AKI, which is a leading cause of morbidity and mortality across among global populations, by altering the mitochondrial proteome. Specifically, our hydrodynamic delivery process facilitated an upregulated expression of mitochondrial enzymes that have been suggested to provide mediation from renal ischemic injury. Remarkably, this protein upregulation significantly enhanced mitochondrial membrane potential activity, comparable to that observed from ischemic preconditioning, and provided protection against moderate ischemia-reperfusion injury, based on serum creatinine and histology analyses. Strikingly, we also determined that hydrodynamic delivery of isotonic fluid alone, given as long as 24 hours after AKI is induced, is similarly capable of blunting the extent of injury. Altogether, these results indicate the development of novel and exciting platform for the future study and management of renal injury.

M.Eng. in Biomedical Engineering (Rensselaer Polytechnic Institute, Troy, NY, USA)
Research Topic: Time-domain Terahertz Spectroscopy for Non-invasive Skin Diagnostics – 2008

Research Summary: Time-domain Terahertz (THz) spectroscopy and imaging are currently being evaluated as innovative tools for medical diagnostics. Overall such focus is justified as present medical standards warrant enhanced techniques that can provide greater sensitivity and specificity as the unique challenges related to cancer and thermal injury persist. The application of THz-pulse imaging of human skin tissues and associated cancers has been demonstrated recently in vitro and in vivo. In vivo studies of basal cell carcinoma have underscored the potential of THz technology as an early clinical screening tool. Research has also been directed towards the development of THz-based systems for imaging burn injury and evaluating the quality of treatments. THz pulsed imaging has been used to differentiate burnt from healthy tissue models. Such work analogously illustrates the potential clinical utility of THz technology for burn injury management. Nevertheless, before such systems can be introduced into clinical settings, it is believed that further fundamental insight related to the THz radiation propagation in biological media is required. This dissertation seeks to contribute to this objective. Herein we present a series of novel and systematic studies related to a controlled experimental model comprising of the major constituents of human skin. We determined relationships that quantified tissue optical properties for a series of physiological states that mimic healthy and diseased conditions at THz frequencies. Additionally, we characterized specific molecular markers to investigate the capacity in which THz techniques can be used for the enhanced skin cancer and burn diagnostics.

M.S. in Applied Mathematics (Rensselaer Polytechnic Institute, Troy, NY, USA)
Research Topic: Electrical Impedance Tomography for Myocardial Infarction Diagnosis and Treatment – 2006

Research Summary: Myocardial infarctions, heart attacks, remain one of the leading causes of death and most expensive disease to treat worldwide. Generally this form of cardiovascular disease results from interruptions of blood supply. Such events have direct correlations to cardiac electrical properties. Electrical impedance tomography (EIT) has been proposed to diagnose early settings of this form of cardiac injury non-invasively and in real time. Specifically, EIT is a technique used for determining the electrical conductivity and permittivity distributions in the interior of a body from measurements made on its surface. Typically, currents are applied through electrodes placed on the surface of the body and the resulting voltages are measured. Using this technique, we investigated the feasibility of detecting and removing scarred myocardial tissue by designing a 3D EIT-based catheter-navigation algorithm, capable of precisely guiding a series of electrodes for cardiac ablation treatment.

M.S. in Electrical Engineering (Tuskegee University. Tuskegee, AL, USA)
Research Topic: The Fabrication and Characterization of a Phosphosilicate Membrane Electrode Assembly – 2003

Research Summary: A biocompatible pacemaker that neither requires recharging nor replacement, unless it's malfunctioning, would be a huge benefit to the medical industry. Several groups have tried to create such devices in the past, but the harsh chemical and biological environment inside the body rendered them unworkable. However, our novel battery system, which is powered by variations between body and ambient temperatures, is a solid-state heat engine that works on the Ericsson cycle. This system provides the same efficiency as that provided by the Carnot cycle for an engine operating between two different temperatures, while capable of withstanding the body's internal environment. This system, which is based on the backbone of fuel cell technology, uses the electrochemical potential of the hydrogen pressure that is applied throughout a membrane electrode assembly (MEA). Herein, we present a characterization of the MEA that may be used to drive this heat engine and power small, surgically implanted internal devices to potentially enhance the quality of human life.

B.A. in Mathematics, Hons. (University of the West Indies, St. Augustine, Trinidad & Tobago)
Minor Concentrations: Linguistics and Sociology
Research Topic: The Harvest of the Trinidad & Tobago Red Brocket Deer – 1999

Research Summary: The Caribbean is well known for its unique and diverse fauna, however habitat loss and extensive gaming have significant impact on this natural phenomenon. To this end, we attempted to define a guideline that would describe an appropriate balance between current rates of harvesting and associated extinction. We achieved this aim by utilizing differential (predator-prey) models to describe species populations like the red brocket deer, quenk and lappe. Such models may aid conversation efforts to safeguard these endangered species and maintain our natural habitat.

RESEARCH EXPERIENCES

US and International Patents: Nucleic Acid Molecule Delivery Methods & Materials, **May 2013**
Indiana University School of Medicine, Indiana

Summary of Inventions: The present inventions provide a simplified technique to rapidly induce and monitor transgene delivery and expression in live mammalian kidneys. To achieve this aim the inventors utilized two-photon excitation and confocal laser scanning microscopy techniques to investigate the hydrodynamic venous delivery of transgene vectors, including plasmids, baculovirions and adenovirions. The present invention therefore provides methods of delivering nucleic acid molecule into a kidney cell of a subject, comprising: administering at least one isolated nucleic acid molecule

into the renal vein of a mammalian subject. Included in the present methods are those methods wherein the at least one isolated nucleic acid molecule is administered in a manner selected from the group consisting of: using the renal vein as a guide; applying retrograde pressure; augmented hydrodynamic delivery; blood vessel clamping; injection. Moreover, we have identified specific genes that can be introduced by our delivery technique to protect kidneys from acute forms of injury.

Graduate Research Fellow, Indiana University School of Medicine, IN
Quantitative Confocal and Multiphoton Microscopy Laboratory, Division of Nephrology, Indiana Center for Biological Microscopy
(Group Leader – Simon Atkinson, Ph.D.), 2009 - 2013

- Acquired training in fundamental wet laboratory techniques
- Acquired training in Immunofluorescence techniques
- Research focused on the investigation of the actin cytoskeleton structure as a function of renal disease

Graduate Research Fellow, Indiana University School of Medicine, IN
Department of Cellular and Integrative Physiology
(Group Leader – David Basile, Ph.D.), 2009

- Acquired training in rodent animal surgical techniques
- Acquired training in Immunihistochemistry and Histology
- Conducted experiments to understand the role of Angiotensin II in renal kidney function post ischemia, in relation to acute and chronic kidney disease

Graduate Research Fellow, Indiana University School of Medicine, IN
Quantitative Confocal and Multiphoton Microscopy Laboratory, Division of Nephrology, Indiana Center for Biological Microscopy
(Group Leader – Kenneth Dunn, Ph.D.), 2009

- Developed of transient transgenic animal models
- Animal microsurgery
- Acquired training in Clinical Ultrasonography
- Acquired training in confocal, multiphoton and intravital microscopy and associated quantitative analyses

Undergraduate Research Advisor and Mentor, Rensselaer Polytechnic Institute, NY
Terahertz and Ultrafast Spectroscopy Laboratory, Center for Terahertz Radiation
(Program Advisor – Gwo-Ching Wang), 2005 - 2007

- Instructed undergraduate students in the areas of biomedical applications of Terahertz Wave Science including measuring optical properties of the head
- Mentored student in academic pursuits by providing career and academic counseling, planning, and advising
- Prepared funded proposal with undergraduate student for summer 2006 research support
- Participated in collaborative efforts with Centre for Biomedical Engineering, School of Electronic Engineering at University of Adelaide, Australia

Undergraduate Abstract Reviewer and Presentation Judge, ABRCMS Conference

Annual Biomedical Research Conference for Minority Students (ABRCMS) Atlanta, GA, 2005

Annual Biomedical Research Conference for Minority Students (ABRCMS) Anaheim, CA, 2006

- Reviewed 30 abstracts for conference submission in the area of Biomedical Quantitative Sciences
- Conducted on-site poster and podium presentation judging
- Gained invaluable insight into the conference submission and peer review process

NSF-IGERT Summer Undergraduate Research Advisor and Mentor, Rensselaer Polytechnic Institute, NY

Dept. of Physics / Center for Terahertz Radiation (Program Advisor – Gwo-Ching, Ph.D.), 2005

- Instructed an undergraduate student from St. John Fisher College, NY on biomedical applications of Terahertz Wave Science
- Conducted novel experiments on artificial and human skin samples using Terahertz techniques
- Provided career and academic counseling, planning, and advising to students
- Assisted students in the development of testing strategies, writing skills through seminars and workshops
- Assisted mentee in acquiring first published conference and journal proceedings

Graduate Research Assistant, Rensselaer Polytechnic Institute, NY

Terahertz and Ultrafast Spectroscopy Laboratory, Center for Terahertz Radiation (Group Leader – Xi-Cheng Zhang, Ph.D.), 2004 - 2007

- Operated as the primary student investigator for biomedical applications of Terahertz Wave Science
- Was responsible for primary Biomedical Terahertz and Ultrafast Spectroscopy Laboratory, Center for Terahertz Radiation
- Conducted experiments to characterize terahertz radiation propagation through biological tissues
- Primary research focused in the area of medical diagnostics, and biomedical spectroscopy and sensing

Graduate Research Assistant, Rensselaer Polytechnic Institute, NY

Electrical Impedance Tomography Laboratory (Group Advisor – David Isaacson, Ph.D.), Summer 2003

- Developed mathematical models of the electrical impedance distributions in the female breast for early cancer detection
- Constructed medical phantoms and conducted experiments to verify mathematical models and computer simulations

Research Intern, Johnson Research and Development, GA
Electrical Engineering Design, 2001 - 2003 (Group Advisor – Lonnie Johnson, Ph.D.)

- Designed and characterized a system for the development of novel fuel cells
- Constructed and tested phosphosilicate electrode membrane assembly to power bio-implants
- Collaborated with Professor Meilin Lui, Center for Fuel Cell and Battery Technologies, Georgia Institute Technology

TEACHING EXPERIENCES

Instructor, Division of Diversity and Upward Bound Program, Indiana University-Purdue University, IN

- Courses: Biology, Chemistry, Mathematics, Physics and Spanish
- Provided training and education to under-represented students at regional high schools and at the IUPUI campus

Graduate Teaching Assistant, Rensselaer Polytechnic Institute, NY
TA in the Department of Biomedical Engineering, 2003 - 2004 for the following courses (faculty supervisors listed)

- Course: Tissue-Biomaterial Interactions, under supervisor - Rena Bizios, Ph.D.
- Course: Tissue Biomechanics and Biomedical Engineering Design, under supervisor - Jan Stegemann, Ph.D.

Graduate Teaching Assistant, Tuskegee University, AL
TA in the Department of Electrical Engineering, 2000 - 2002 for the following courses (faculty supervisors listed)

- Signals and Design, under supervisor - Daryl Padget, Ph.D.
- Digital Design, under supervisor - Farud Touati Ph.D.
- Introduction to Electrical Circuits, under supervisor – Kaylan Das, Ph.D.
- General Physics II, sunder supervisor – Indulal Kothari, Ph.D.
- Supervised classes of approximately 30 students in each course, graded course work and provided tutorials and lectures

Middle High and High School Teacher, Holy Name Convent, Trinidad & Tobago
Department of Mathematics, 1999 - 2000

- Taught 3 courses: Introductory and Advanced Mathematics, and Introductory Physics
- Students age ranged from 12 to 19 years
- Prepared daily lessons for classes of approximately 40 students
- Participated in student mentoring council
- Provided career and academic counseling, planning, and advising to students
- Assisted students in the development of testing strategies, writing skills, and completing college applications
- Coordinated a special project that provided individual after hours tutoring for both disadvantaged and gifted students

ADDITONAL WORK EXPERIENCES

Resident Assistant, Rensselaer Polytechnic Institute, NY

- Residence Life Program (Supervisors – Amanda Bingel and Lamaar Walker), 2005 - 2008
- Was responsible for the safety, integration and general welfare of 80 graduate and undergraduate students in residence halls
- Promoted a comfortable, academically nurturing and recreational environment through the development of individualized activities to match the needs of the residents in the campus halls

Student Recruiting Officer, Rensselaer Polytechnic Institute, NY

The Office of Institute Diversity and The Office of Graduate Admission (supervisors – George Robbins, Senior Associate Dean and Kenneth B. Durgans, Vice Provost, Institute Diversity), 2003 - present

- Represented the institution at national conferences/ graduate recruitment fairs
- Provided campus tours
- Spearhead a team for international undergraduate recruitment – prepared funded proposal for recruitment programs
- Liaised with faculty and administrative representatives at The University of Puerto Rico – Mayaguez, The University of the West Indies – St. Augustine, Tuskegee University, Morehouse College, Grown University, Syracuse University and Cornell University

Director and Founder, Corridon's Tutoring Services, Trinidad & Tobago

Corridon Tutoring Services, Trincity, Trinidad and Tobago, 1998 – 2000

- Headed a private tutoring firm that was focused on the development of high school students
- Specialized in Mathematics and Physics tutoring services

Operations Supervisor, Little Medford & Associates Limited, Trinidad & Tobago

Statistical Analysis Division, Summer 1998

- Supervised a staff of 10 members
- Collected and analyzed census data on Trinidad & Tobago for various governmental projects

Accounting Clerk, Ministry of Energy and Energy Resources, Trinidad & Tobago

Accounts Division, Summer 1997

- Studied basic accounting principles and prepared ministerial reviews

PUBLICATIONS A N D PRESENTATIONS

Proceedings:

1. Corridon, P., Rhodes, G., Gattone, V., Leonard, E., Basile, D., Bacallao, R., Atkinson, S. *A Method to Facilitate and Monitor Expression of Exogenous Genes in the Rat Kidney Using Plasmid and Viral Vectors,* American Journal of Physiology, Renal Physiology, March, 2013
2. Corridon, P., Rhodes, G., Bacallao, R., Atkinson, S. *Monitoring Live Actin Cytoskeleton Alterations in the Setting of Ischemia-Reperfusion Injury, Kidney Week 2011, American Society of Nephrology, San Diego, CA, November, 2012*
3. Hall, A., Rhodes, G., Sandoval, R., Corridon, P., Molitoris, B. *In Vivo Multiphoton Imaging of Mitochondrial Structure and Function During Acute Kidney Injury*, Kidney International, September 2012
4. Corridon, P., Rhodes, G., Leonard, E., Basile, D., Gattone, V., Bacallao, R., Atkinson. *Visualizing Hydrodynamic Transgene Delivery and Expression in Live Mammalian Kidney*s, Biophysical Society 56th Annual Meeting, San Diego, CA, February, 2012
5. Corridon, P., Rhodes, G., Bacallao, R., Atkinson, S. *Hydrodynamic-mediated Transgene Expression of Baculovirus Vectors in Live Mammalian Kidneys,* Indiana Physiological Society Annual Meeting, Ball State University, Muncie, IN, February, 2012
6. Corridon, P., Rhodes, G., Bacallao, R., Atkinson, S. *Hydrodynamic-mediated Transgene Expression of Baculovirus Vectors in Live Mammalian Kidneys, Kidney Week 2011, American Society of Nephrology, Philadelphia, PA, October, 2011*
7. Corridon, P., Rhodes, G., Bacallao, R., Atkinson, S. *Efficient Transgene Delivery in Live Mammalian Kidneys,* Indiana Physiological Society Annual Meeting, Indiana University School of Medicine, Indianapolis, IN, February, 2011
8. Corridon, P. *Advanced Technologies for Managing Burn Injuries*. 3rd International Conference on Appropriate Technology, Kigali, Rwanda, November, 2008
9. Corridon, P., Jackson, J., Hosein, A. *A Telehealth Network to Support the National Myocardium Infarction Center of Trinidad & Tobago*. 3rd International Conference on Appropriate Technology, Kigali, Rwanda, November, 2008
10. Corridon, P., Claudio, D., Wilke, I. *Does Human Hair Impose a Significant Effect on the Propagation of Terahertz Radiation?* Optical Terahertz Science and Technology Topical Meeting, Optical Society of America (OSA), Orlando, FL, USA, March, 2007
11. Corridon, P., Wilke, I. *Monitoring the Dehydration of Artificial Skin by Time-Domain Terahertz Transmission Measurements.* Optical Terahertz Science and Technology Topical Meeting, Optical Society of America (OSA), Orlando, FL, USA, March, 2007

12. Corridon, P., Krest , C., Ascazubi, R., Wilke, I. *A Characterization of the Optical Properties of Artificial Skin Using Time-Domain Terahertz Spectroscopy.* 2nd Annual Tech Valley Engineering Symposium, Albany, NY, USA, April, 2006
13. Corridon, P., Krest , C., Ascazubi, R., Wilke, I. *Time-Domain Terahertz Spectroscopy of Artificial Skin*. Proc. SPIE Vol. 6080, San Jose, CA, USA, January, 2006. Pp 608007
14. Corridon, P. Isaacson, D., Newel, J. *A 2-D Analytic Description of the Forward Problem for the Female Breast in the Mammography Geometry using Electrical Impedance Tomography.* Proc. Walter Lincoln Hawkins Graduate Research Conference, Troy, NY, USA, October, 2004. Pp 3-8
15. Corridon P., Isaacson, D., Kao, T., Newell, J., Saulnier, G. *A 2-D Forward Model for Early Breast Cancer Detection Using Electrical Impedance Tomography.* NSF Conference, CenSSIS, Northeaster University, Boston, MA, USA, April, 2004
16. Corridon, P. Burge, L. Johnson, L. *The Fabrication of a Low-Temperature Phosphosilicate Membrane Electrode Assembly,* Proc. Walter Lincoln Hawkins Graduate Research Conference, Troy, NY, USA, October, 2003. Pp 6-9

Invited Talks & Presentations:

1. Corridon, P*., In Vivo Imaging of Transgene Expression in Rodent Kidney Models of Acute Kidney Injury*. Anatomisches Institut & Swiss National Centre of Competence in Research, University of Zurich, Switzerland, March, 2013
2. Corridon, P., Roysam, B., Wilke, I. *An Experimental Model Characterizing the Interactions between Terahertz Radiation and Biological Tissues.* Department of Dermatology, The University of Puerto Rico, San Juan, Puerto Rico, October, 2006
2. Corridon, P., Roysam, B., Wilke, I. *The Potential Applications for Skin Diagnostics Using Time-Domain Terahertz Spectroscopy.* The University of Trinidad and Tobago, Trinidad and Tobago, October, 2006
3. Corridon, P., Roysam, B., Wilke, I. *Towards Advances in Disease Diagnosis using Time-Domain Terahertz Spectroscopy*. Medical School, Medical Center, Manati, Puerto Rico, July, 2006
4. Corridon, P., Roysam, B., Wilke, I. *Terahertz Wave Spectroscopy of Artificial Skin.* Institute of Physics, Clarendon Laboratory, Oxford University, Oxford, United Kingdom, June, 2006
5. Corridon, P., Roysam, B., Wilke, I. *Suitable Skin Models for Terahertz Wave Propagation Medical Research*, University of Nottingham, Nottingham, United Kingdom, June, 2006
6. Corridon, P., Roysam, B., Wilke, I. *Terahertz Wave Propagation in Dermal Constructs.* Institute of Physics, University of Leeds, Leeds, United Kingdom June, 2006
7. Corridon, P., Roysam, B., Wilke, I. *Time-Domain Terahertz Spectroscopy of Artificial Skin Structures.* Dept. Physics, Durham University, Durham, United Kingdom, June, 2006

8. Corridon, P., Roysam, B., Wilke, I. *Artificial Skin Structures for Time-Domain Terahertz Spectroscopy Medical Phantoms*.
   Dept. Physics, Johann Wolfgang Goethe-Universität, Frankfurt, Germany, June, 2006
9. Corridon, P., Roysam, B., Wilke, I. *Terahertz Wave Propagation in Dermal Constructs*, College of Engineering, University of Puerto Rico, Mayaguez, Puerto Rico, May, 2006
10. Corridon, P., Krest, C., Ascazubi, R., Wilke, I. *Viable Terahertz Tissue Phantoms*. NSF-AGEP Institutions Seminar Series, Rensselaer Polytechnic Institute, Troy, NY, February, 2006

Newspaper, Magazine, Books Articles:

1. Corridon, P. Diabetes: An Outsider's Look on a Growing Problem in Kuwait. The City Magazine, May, 2012
2. Corridon, P. *Breast Cancer: Do I need to be Aware?* Ocean Style Magazine, September, 2005
3. Corridon, P. *Facts about Skin Cancer*. Features Article, The Trinidad Express, January 24th, 2005

HONORS, GRANTS AND AWARDS

1. Research presentation and travel grant/award, Indiana Physiological Society Annual Meeting, Ball State University, Muncie, IN, February, 2013
2. Fellow, SREB-State Doctoral Scholars Program, Southern Regional Education Board (SREB), October 2012
3. Research presentation award, Indiana Physiological Society Annual Meeting, Ball State University, Muncie, IN, February, 2012
4. Research travel award, Indiana University School of Medicine, Graduate Division, August, 2010-2011
5. NIH George M. O'Brien Award (P30 DK079312-01), 2010-2013
6. University Fellowship, Indiana University School of Medicine, Graduate Division, August, 2009-2010
7. Travel award, Annual Biomedical Research Conference for Minority Students (ABRCMS), November, 2006
8. Rensselaer funded proposal to diversify research intensive efforts in developing institutions in Trinidad and Tobago, 2006
9. NSF-AGEP Funded Proposal to develop and implement the Graduate Student Seminar Series, 2006-2007
10. NSF-AGEP Travel Award, 2006, International Society for Optical Engineering Annual Meeting, January 2006
11. COMPACT for Faculty Diversity Program Graduate Award, 2005
12. NEBHE Doctoral Award, 2005
13. NSF-AGEP Graduate Travel Award, 2005
14. Rensselaer Polytechnic Institute Graduate Student Travel Award, 2005
15. Doctoral Research Award, Integra LifeSciences Corporation, NY, 2005

16. Top Research Paper Award, Walter Hawkins Graduate Student Conference, Rensselaer Polytechnic Institute, 2004
17. Rensselaer Polytechnic Institute Graduate Student Travel Award, 2004
18. Outstanding Poet, Famous American Poet Society, 2004
19. Tuskegee University Graduate Travel Award, 2002
20. Fellow of Eta Kappa Nu, National Electrical & Computer Engineering Honor Society, 2002
21. Inaugural BP Student Mentorship Award, Tuskegee University, 2002